THE
PHYSICAL REVIEW
A Journal of Experimental and Theoretical Physics Established by E. L. Nichols in 1893

VOL. 53, NO. 5 MARCH 1, 1938 SECOND SERIES

Cosmic-Ray Intensities at Great Depths

VOLNEY C. WILSON
University of Chicago, Chicago, Illinois
(Received January 13, 1938)

A fourfold Geiger-Müller tube telescope was employed to count the relative number of cosmic rays under different thicknesses of rock. Each Geiger-Müller tube consisted of a 0.125 mm tungsten wire anode and a cylindrical copper cathode 9 cm in diameter and 71 cm in length sealed in a glass envelope filled with hydrogen to a pressure of 9.6 cm of mercury. The experiment was performed in a mine whose shaft was inclined at an angle of 34° from the horizontal. Counts were made at thirty-nine different stations at depths from zero to 1408 meters of water equivalent, where the rate was 5.7×10^{-5} as great as at the surface. When the intensity is plotted against the depth, the resulting curve shows no points of inflection. The effective absorption coefficient decreases from 0.07 per meter of water at the surface to 0.0025 at the greatest depth. If the logarithm of the intensity is plotted against the logarithm of the depth, two straight lines, one from 20 to 250 and the other from 250 to 1418 meters water equivalent from the top of the atmosphere, represent the data well. Shower counts were also made at ten of the stations. These also show a bend at 250 meters. This suggests that there may be two types of very penetrating rays both capable of producing showers. It may be that one of these consists of "heavy electrons" and the other of "neutrinos."

INTRODUCTION

THE famous experiments of Millikan and Cameron[1] on the intensity of cosmic rays in mountain lakes showed a continuous decrease of intensity with depth, which is typical of nearly all cosmic-ray absorption experiments since the early work of Hess and Kolhörster.[2] In 1934, however, J. Clay[2(e)] reported that when he lowered his ionization chamber into the Red Sea, the intensity increased with depth from 200 to 250 meters of sea water, and then decreased rapidly to zero with increasing depth. In the same year, A. Corlin[2] reported a similar increase in the Kiirunavaara mine in northern Sweden. However, this increase appeared between 430 and 520 meters water equivalent. It seems improbable that the number of rays increases, but rather, as suggested by Clay[2(e)] and W. F. G. Swann[3] that the specific ionization may increase by some unknown mechanism. Primarily to test this point, a new experiment has been performed, in which a Geiger-Müller tube telescope was used to count the rays at different depths in a mine.

[1] R. A. Millikan, Nature **116**, 823 (1925); **121**, 19 (1928); Nat. Acad. Sci. Proc. **12**, 48 (1926). R. A. Millikan and G. H. Cameron, Phys. Rev. **28**, 851 (1926); **31**, 163, 921 (1928); **37**, 235 (1931).

[2] For bibliography of these experiments up to 1934, cf. e.g., A. Corlin, "Cosmic Ultraradiation in Northern Sweden," Annals of the Observatory of Lund **4**, (1934). Papers published since that time include: (a) E. Regener, Zeits. f. Physik **100**, 286 (1936). (b) W. Kolhörster, Zeits. f. Physik **88**, 536 (1934). (c) J. Clay, Physica **1**, 363 (1934). (d) J. Clay, Physica **3**, 646 (1936). (e) J. Clay and C. G. t'Hooft, Physica **2**, 1039, 1042 (1935). (f) J. Clay, J. T. Wiersma and G. H. Graaff, Physica **1**, 659 (1934). (g) J. Clay, J. T. Wiersma and C. G. t'Hooft, Physica **1**, 1077 (1934). (h) J. Clay, C. G. t'Hooft, J. L. Dey and J. T. Wiersma, Physica **4**, 121 (1937). (i) D. H. Follett and J. D. Crawshaw, Nature **136**, 1026 (1935); Proc. Roy. Soc. London **A155**, 546 (1936). (j) Auger and Rosenbar, Comptes rendus **201**, 1116 (1935); **202**, 1923 (1936). (k) H. Maass, Ann. d. Physik **27**, 507 (1936). (l) F. Weischedel, Zeits. f. Physik **101**, 732 (1936). (m) J. Barnothy and M. Forró, Zeits. f. Physik **104**, 744 (1937). (n) A. Ehmert, Zeits. f. Physik **106**, 751 (1937). (o) W. H. Pickering, Phys. Rev. **52**, 1131 (1937).

[3] W. F. G. Swann, Phys. Rev. **46**, 432 (1934).

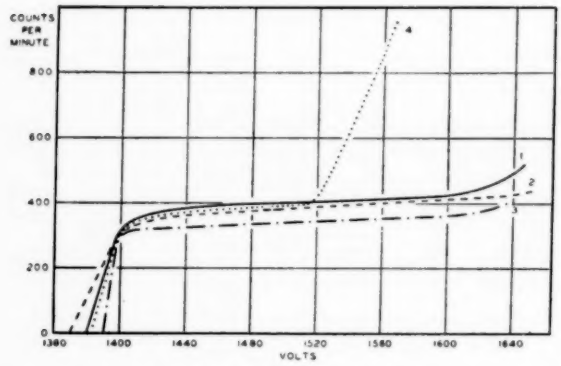

Fig. 1. Geiger-Müller tube counting rates *versus* applied voltage.

The Apparatus

Four Geiger-Müller tubes were arranged for fourfold vertical coincidence. The copper cathodes of these tubes were cylinders 9 cm in diameter and 71 cm long, and the anodes were of 0.125 mm (5 mil) tungsten wire stretched along the axes of the copper cylinders. These electrodes were sealed in glass envelopes, and after thorough cleaning, the tubes were filled with hydrogen to a pressure of 9.6 cm of mercury. The residual counts per minute as taken in the mine are plotted against the voltage in Fig. 1. These curves show the unusually low residual counting rates for such large tubes, the broad operating plateaus, and the degree to which the tubes were matched. Unfortunately, a tube with characteristics similar to number two was broken during the trip from Chicago to Mohawk, Michigan. The tubes were operated at 1480 volts; however, voltage fluctuations in the 110-volt primary, in one instance, caused the secondary voltage to go to 1520 volts, and in another, to drop to 1440 volts. It may be seen from the curves that these voltages are within the working range of all the tubes. The efficiencies at 1480 volts, as determined by the method of Street and Woodward,[4] were No. 1, 97.6 percent; No. 2, 97.8 percent; No. 3, 98.5 percent. These efficiencies were determined in the laboratory where the individual counting rates were approximately 1500 per minute. In the mine where the experiment was performed, the individual counts were consistently 500 per minute or less; thus, the efficiencies were probably higher than indicated above, and were assumed to be constant.

The circuit employed is shown in Fig. 2. One 57 tube was connected directly to the Geiger-Müller tube according to the Neher-Harper circuit.[5] This was done to obtain a quick recovery of the Geiger-Müller tube. The high voltage was supplied by a power pack built according to the Gingrich[6] modification of the Evans[7] type circuit. The grid bias and screen voltage of the Neher-Harper 57 tube and the grid bias of the thyratron were supplied by dry batteries. The other voltages were supplied by a common power pack, equipped with a 350-volt transformer and a type 80 rectifier. The output pulse from the thyratron was put through an impulse counter similar to the type developed by F. Shonka. The assembled apparatus is shown in Fig. 3.

The Experiment

The experiment was performed at Mohawk, Michigan, in the No. 2 shaft of the Seneca Copper Corporation. This mine is especially

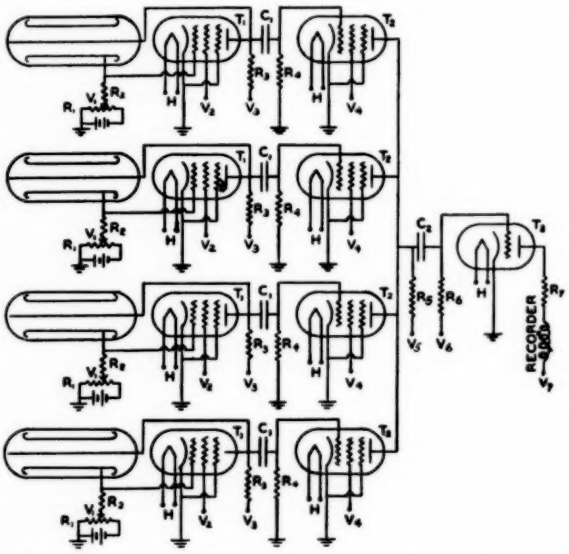

Fig. 2. Diagram of circuit used. T_1 and T_2 are type 57 tubes; T_3 is a type 885 thyratron; $R_1=R_2=R_3=2\times10^6$ ohms; $R_4=5\times10^5$ ohms; $R_5=1\times10^5$ ohms; $R_6=5\times10^4$ ohms; $R_7=6\times10^3$ ohms; $V_1=-4$ volts (about); $V_2=+45$ volts; $V_3=+1480$ volts; $V_4=+90$ volts; $V_5=+250$ volts; $V_6=-47$ volts; $V_7=+300$ volts; $C_1=50$ $\mu\mu$f; $C_2=0.02$ μf; $H=2.5$ volts a.c.

[4] J. C. Street and R. H. Woodward, Phys. Rev. **46**, 1029 (1934).

[5] H. V. Neher and W. W. Harper, Phys. Rev. **49**, 940 (1936).

[6] N. S. Gingrich, R. S. I. **7**, 207 (1936).

[7] R. D. Evans, R. S. I. **5**, 371 (1934).

suitable for such an experiment for five reasons: first, the shaft is inclined at an angle of 34° from the horizontal, thus the Geiger-Müller tube telescope could be set up in the shaft under any desired thickness of rock; second, the density of the overlying rock is uniform and well known; third, the surrounding rock is comparatively free from radioactive material; fourth, since the surface of the ground is nearly level, the thickness of the rock could be determined accurately; and fifth, the mine was not in operation, thus permitting ample time for the experiment.

The Geiger-Müller tubes were placed with their axes parallel and 11.5 cm from center to center. In this position, a ray coming down the shaft could not pass through more than one tube, and hence could not be recorded, since the instrument recorded only the simultaneous discharge of all four tubes. Readings were taken with the telescope in the vertical and in the horizontal position, and the horizontal counts, assumed to be due to showers, were subtracted from the vertical counts to give the number of vertical rays. Actually near the surface this correction is too great, since some of the horizontal counts there are caused by penetrating rays traveling nearly horizontally. No attempt was made to correct for the possibiilty of a cosmic ray passing through tubes 1 and 2 simultaneously with another ray passing through tubes 3 and 4, etc. Since this correction will remain very nearly a constant factor, its omission will not change the shape of the absorption curve. The radioactivity of the rock was very low and surprisingly uniform. The accidental counts were one in fourteen days. This was determined by measuring the individual and the twofold counting rates in the mine. The coincidence time of the circuit τ, was calculated from the equation $A_{1,2}=2N_1N_2\tau$, where $A_{1,2}$ is the twofold accidental rate for tubes 1 and 2; and N_1 and N_2 are the individual counting rates. The fourfold accidental counting rate, $A_{1,2,3,4}$, was then found from the equation $A_{1,2,3,4}=4N_1N_2N_3N_4\tau^3$.[8]

[8] Recent theoretical and experimental studies soon to be published by Carl Eckart and Francis Shonka show that the general equation for the accidental counting rate with n counters, each having its characteristic coincidence time τ, is

$$A_{1,2,\ldots,n}=(N_1N_2\cdots N_n)(\tau_1\tau_2\cdots\tau_n)\left(\frac{1}{\tau_1}+\frac{1}{\tau_2}+\frac{1}{\tau_3}\cdots\frac{1}{\tau_n}\right).$$

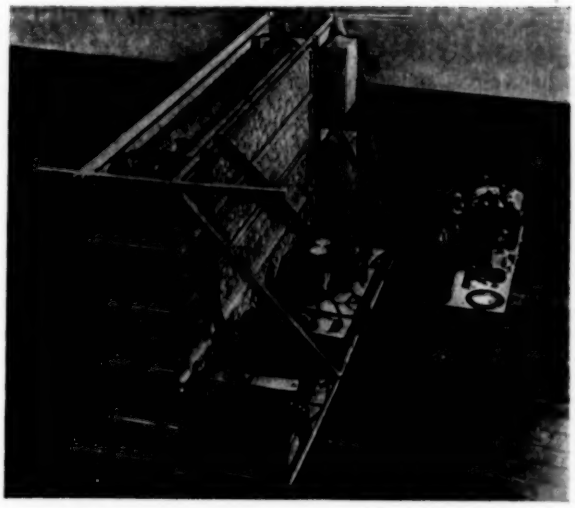

FIG. 3. The apparatus, showing *A*, the top Geiger-Müller tube; *B*, the first two stages of amplification; *C*, the high voltage pack; and *D*, the recorder.

In order to determine the amount of rock through which the rays must penetrate, the slope of the skipway rails was determined every 100 ft., and the distance of the apparatus from the surface was measured along the rails by a steel tape. A level of the surface ground over the shaft was run, and the vertical distance was corrected for this and for the variation in the ceiling height in the shaft. To express the absorbing material in equivalent depths of water, the rock thickness was multiplied by the density of the rock. The density and thickness of the overlying lava flows, obtained from diamond core drillings, was kindly furnished by T. M. Broderick, geologist for the Calumet and Hecla Consolidated Copper Company. The average density of the rock was 2.875 grams per cc.

DATA AND RESULTS

The main part of the data is given in Table I. The second column, depth in meters water equivalent, was obtained as explained above. The next three columns need no explanation. Column six, counts per minute in the horizontal position, was taken from Table II, to be explained later. In computing the last column, I_0 was taken as 81.4 counts per minute. The probable errors were obtained from the statistical errors in counting ($\epsilon=0.6745N^{\frac{1}{2}}$). Reading number 15 was taken at a depth of 274.6 meters,

with the apparatus tipped at an angle of 18° from the horizontal. Similarly, readings 27 and 28 were taken at angles of 60° and 45° from the horizontal at a depth of 652.3 meters, and readings 34 and 35 were taken at 45° and 23° from the horizontal at 1106.7 meters. It was possible for a ray traveling at an angle of 14° 30′ from the center line of the four tubes to pass through all the tubes. When the apparatus was tipped, the difference between the minimum and maximum thickness of rock through which a ray might travel was great. Most of the rays counted probably came through less material than would be indicated by dividing the vertical thickness by the sine of the angle between the horizontal and the line through the center of the tubes. If 7° 15′ was added to this angle, points 15, 27, and 28 would best fit the rest of the data; therefore, 7° 15′ was also added to the corresponding angles to get the effective depths for points 34 and 35. At 398.7 meters, reading 19, it was discovered that the apparatus was slightly out of line in the box. It was assumed that this occurred while tipping the apparatus to 18°. On this assumption, readings 16, 17, and 18 would be slightly low; therefore, on the upward trip reading 36 was taken in this region.

When the apparatus was tipped at 23° from the horizontal at 1106.7 meters (effective depth 2220 meters) only 2 counts were recorded in 2.5 days. This is approximately the shower intensity expected at 1106.7 meters; therefore, it is impossible to say whether these counts were due to showers or to rays coming through 2220

TABLE I. *Cosmic-ray intensities from fourfold vertical coincidence counts.*

Station No.	Depth Meters Water Equiv.	Counts Vertical	Time Min.	Counts per Min. Vertical	Counts per Min. Horizontal	Difference	I/I_0
1	0	11666	140	83.3 ±0.5	2.32	81.0	0.995 ±0.006
2	4.62	3642	67	54.3 ±0.6	1.76	52.54	0.646 ±0.007
3	11.3	3599	101.5	35.4 ±0.4	1.22	34.18	0.420 ±0.005
4	17.0	1791	79	22.7 ±0.36	0.85	21.85	0.269 ±0.005
5	25.4	8818	636	13.85 ±0.10	0.58	13.27	0.163 ±0.0016
6	23.6	15627	1025	15.24 ±0.08	0.63	14.61	0.180 ±0.0010
7	89.1	997	402	2.48 ±0.05	0.17	2.31	0.0284 ±0.0006
8	112.0	1211	720	1.68 ±0.03	0.11	1.57	0.0193 ±0.0004
9	138.7	604	489	1.23 ±0.03	0.08	1.15	0.0141 ±0.0004
10	163.2	673	740	0.909 ±0.02	0.068	0.841	0.0104 ±0.0003
11	186.4	744	1020	0.729 ±0.015	0.055	0.674	0.0083 ±0.0002
12	214.8	628	1128	0.557 ±0.015	0.045	0.512	0.0063 ±0.0002
13	245.4	399	964	0.414 ±0.014	0.032	0.382	0.0047 ±0.0002
14	274.6	267	803	0.332 ±0.014	0.022	0.310	0.00381 ±0.00017
15	645 *	75	1216	0.0617 ±0.005	0.022	0.040	0.00049 ±0.00006
16	304.5	416	1510	0.275 ±0.009	0.017	0.258	0.00317 ±0.00012
17	323.3	268	1246	0.215 ±0.009	0.015	0.200	0.00246 ±0.00011
18	347.0	212	1128	0.188 ±0.009	0.014	0.174	0.00214 ±0.00011
19	398.7	187	1248	0.150 ±0.007	0.012	0.138	0.00170 ±0.00009
20	398.7	179	1196	0.150 ±0.007	0.012	0.138	0.00170 ±0.00009
21	440.8	181	1716	0.106 ±0.005	0.010	0.096	0.00118 ±0.00006
22	497.2	183	2138	0.086 ±0.004	0.009	0.075	0.00092 ±0.00005
23	545.5	216	2955	0.073 ±0.003	0.008	0.065	0.00080 ±0.00004
24	601.8	148	2690	0.055 ±0.003	0.0065	0.0485	0.00060 ±0.00004
25	647.9	116	2474	0.047 ±0.003	0.0054	0.0414	0.00051 ±0.00004
26	652.3	149	3220	0.046 ±0.002	0.0054	0.0409	0.00050 ±0.00003
27	703 *	91	2830	0.0322 ±0.002	0.0054	0.0268	0.00033 ±0.00003
28	820 *	129	4131	0.0312 ±0.002	0.0054	0.0258	0.00032 ±0.00003
29	748.3	105	3304	0.0318 ±0.002	0.0040	0.028	0.00034 ±0.00003
30	840.0	71	2835	0.025 ±0.002	0.0030	0.022	0.00027 ±0.00003
31	940.2	43	2201	0.0195 ±0.002	0.0025	0.017	0.00021 ±0.00003
32	1034.5	34	2791	0.0122 ±0.0014	0.0021	0.0101	0.00013 ±0.00002
33	1106.7	38	3625	0.0105 ±0.0013	0.0006	0.0099	0.00012 ±0.00002
34	1408 *	16	3040	0.00526±0.0009	0.0006	0.00466	0.000057±0.00001
35	2220 *	2	3532	0.0006 ±0.0003	0.0006	0.0	0
36	336.1	317	1315	0.241 ±0.009	0.0015	0.226	0.00278 ±0.00010
37	72.7	2612	741	3.52 ±0.05	0.18	3.34	0.0410 ±0.0005
38	50.5	3852	612	6.30 ±0.07	0.44	5.96	0.0733 ±0.0008
39	0	115377	1380	83.60 ±0.17	2.17	81.4	1.000 ±0.002

* These points were obtained with the apparatus tipped at various angles.

meters water equivalent. It was assumed that they were showers and that no rays were detected at an effective depth of 2220 meters water equivalent.

As explained above, a ray coming down the shaft could not pass through more than one Geiger-Müller tube; however, to be sure that there was no error introduced by working in the shaft, reading 26 was taken at a position 65 feet into a side drift. There is no detectable difference between the shaft and the drift readings. Points number 34 and number 35 were also taken in a drift.

In Fig. 4, I/I_0 is plotted on a logarithmic scale against the depth below the surface of the ground. For comparison, the points are numbered to correspond to the numbers in column 1 of Table I. The points inside the rectangles represent the readings taken with the apparatus tipped. Apparently, these points are not as accurate as the vertical readings. The fact that there appears to be no systematic difference between these readings and the vertical readings seems to mean that no large part of the rays is diffusely scattered.

The readings with the tubes in horizontal position are given in Table II. These values were plotted against the depth and the figures in column 6 of Table I were taken from this curve.

Discussion

Curve *A* of Fig. 5 is a plot on a double logarithmic scale of I/I_0 against the depth measured from the top of the atmosphere. These points may be represented either by a curve which is slightly concave downward or by three straight lines. One straight line from 20 to 250 meters

Table II. *Counts per minute with the tubes in horizontal position.*

Station Number	Depths in Meters Water Equivalent	Counts per Minute Horizontal
1	0	2.32 ±0.15
5	25.4	0.58 ±0.02
8	112.0	0.109 ±0.002
10	163.2	0.068 ±0.007
12	214.8	0.045 ±0.005
14	274.6	0.019 ±0.003
18	347.0	0.014 ±0.003
22	497.2	0.010 ±0.002
25	647.9	0.0054±0.0009
32	1034.5	0.0021±0.0006
39	0	2.17 ±0.04

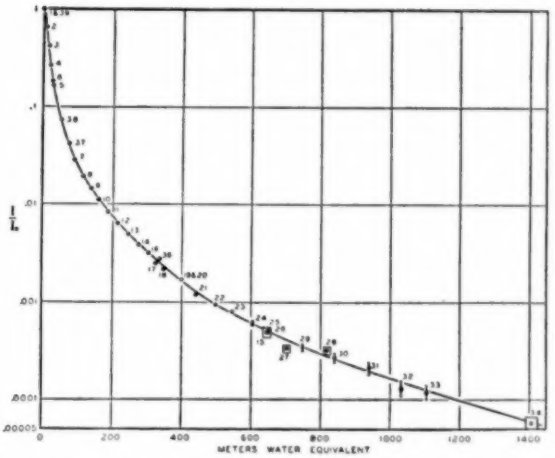

Fig. 4. Cosmic-ray intensity on a logarithmic scale plotted against the depth from the surface of the earth.

and another from 250 to 1420 meters seem to represent the data very well over this wide range. Assuming the validity of such a straight line relation, the analytical expression for the cosmic-ray intensity as a function of the depth is:

$$20 \leq h \leq 250m, \quad I/I_0 = 95.37 \times h^{-1.77},$$
$$250 \leq h \leq 1420m, \quad I/I_0 = 6058 \times h^{-2.82},$$

where h is the thickness in meters water equivalent from the top of the atmosphere.

It is evident from Fig. 4 that the data may also be represented by a group of exponentials. The corresponding absorption coefficients (taken from the slope of the curve) vary from 0.07 per meter of water at the surface to 0.0025 per meter at the greatest depth.

Comparison with Data of Other Observers

While this experiment was in progress, A. Ehmert[2(n)] published a report of a similar experiment performed with threefold Geiger-Müller tube coincidences in water. His values are shown by curve *B* in Fig. 5. Although his data extend only to one-sixth of the depth of the present measurements, it is interesting to notice how closely the two curves agree to a depth of 240 meters. In making the comparison, the two values obtained at the surface of the earth were equated. Possibly the separation below this point is due to the different transition effects in going from air into water, and from air into rock. The exponent of h for Ehmert's curve is -1.87 as compared with -1.77 above. This may represent

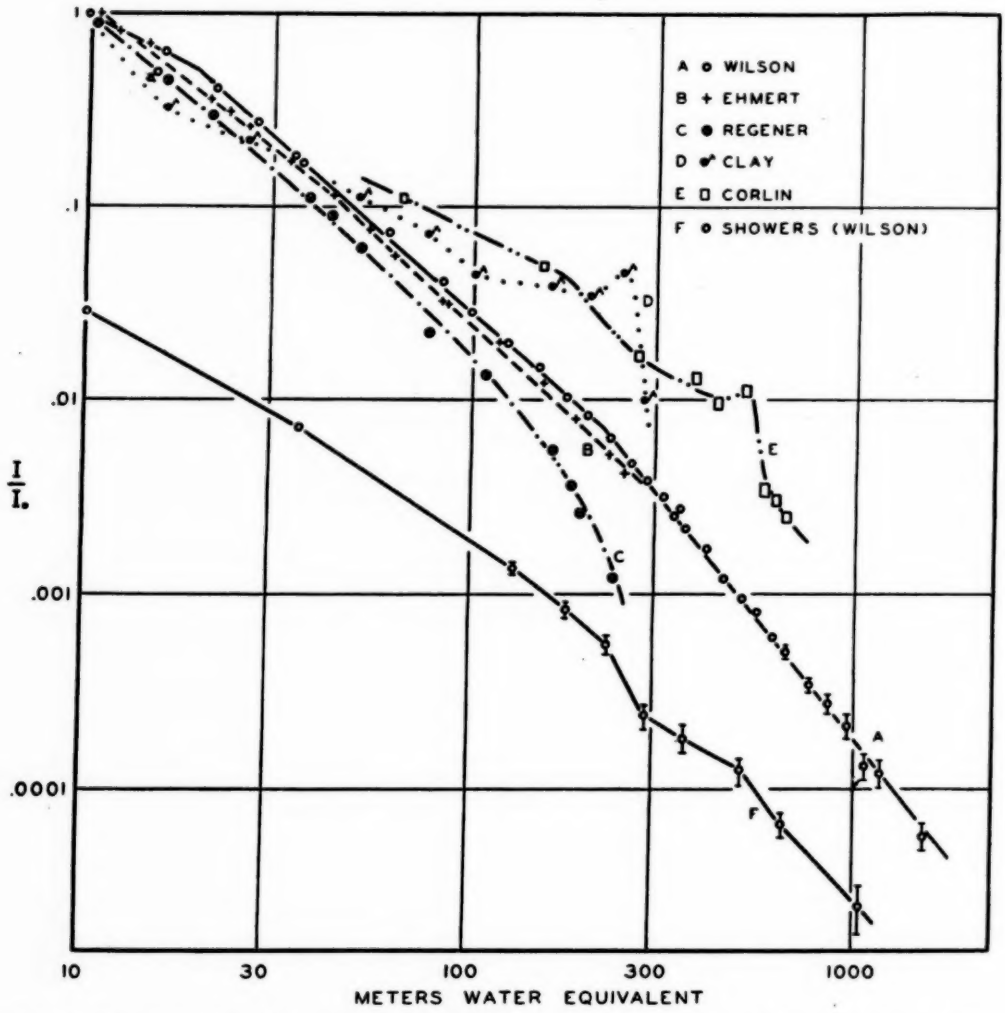

FIG. 5. Cosmic-ray intensity plotted on a logarithmic scale *versus* the depth from the top of the atmosphere plotted on a logarithmic scale.

a real difference, arising because of the different absorbing media or because of the difference in the solid angles subtended by the two telescopes. Ehmert has shown that his values agree closely with those from previous counter tube coincidence experiments. The ionization data of E. Regener,[9] J. Clay,[2(c)] and A. Corlin,[2] equated at the surface of the earth, are shown by curves *C*, *D*, and *E* of Fig. 5. One would not expect the ionization measurements and the coincidence measurements to agree perfectly because an ionization chamber records rays from all directions including showers, whereas a coincidence apparatus records rays from a limited solid angle. The coincidence measurements, however, appear to be more consistent than the ionization measurements, probably because the coincidence apparatus is much less affected by radioactivity in the surrounding medium.

The horizontal counts as given in Table II (assumed to be showers) are plotted in curve *F* of Fig. 5. The apparatus was not designed to record showers, and readings were taken only long enough to obtain sufficient accuracy for correcting the vertical coincidences. Nevertheless, it will be seen that apparent decreases occur in the shower intensity at just the depths at which Clay and Corlin find sharp decreases in ionization. In view of the magnitude of the probable errors of these shower counts, the sig-

[9] E. Regener, Physik. Zeits. **34**, 306 (1933).

nificance of this coincidence is questionable. Curve *A*, however, also shows a bend at about the same depth. Perhaps this bend at about 250 meters marks the end of one shower producing component.

Ehmert attributes the bend in his curve at 45 meters to a transition effect caused by secondaries which have a range of 35 meters, and are considerably more abundant in water than in air. Similarly, the bend in the absorption curve under rock at 20 meters water equivalent may be attributed to a transition effect. Point "*a*" of Fig. 5 was taken in air with the apparatus tipped. This indicates that there is no bend in the intensity curve in air alone; thus further substantiating the transition hypothesis. In this case, the secondaries have a range of only about 10 meters of water equivalent. This comparison suggests that the secondaries are much more rapidly absorbed in the rock than in water. Since the curve in rock is slightly above that for water, if the secondaries are more readily absorbed in the rock, they must also be even more rapidly produced in the rock.

Nature of the Rays

W. Heitler[10] has pointed out that if the Bethe-Heitler theory for the absorption of β-rays is valid to infinite energy, then the β-rays (both + and −) "with any reasonable energy" must be absorbed in about 10 to 15 meters of water equivalent from the top of the atmosphere. Also it has been shown[11] that for very high energies the absorption of photons is about the same as the absorption of β-rays. Thus one concludes from theoretical considerations that probably the very penetrating rays are not β-rays (+ or −) or photons. Experiment shows that neutrons are rapidly absorbed by water; therefore, if the penetrating rays are neutrons, one would expect the absorption to be much greater in water than in rock. This is not the case; therefore, the rays are probably not neutrons. According to the theory of Bethe and Heitler, protons should not excite appreciable radiation, and would thus not be expected to produce showers at great depths such as has been observed in this experiment. Heisenberg has suggested that the penetrating rays are "neutrinos" present in the primary rays and also produced as shower secondaries. Also it is very probable that the newly discovered "heavy electrons" could penetrate to the great depth.

Since the penetrating cosmic rays seem to show a new type of absorption, and since they show such great penetration, it seems reasonable to assume that the very penetrating cosmic rays are rays of which at the present time we have little knowledge. One cannot now say whether these rays are "neutrinos," "heavy electrons," protons (if they can produce showers), or some new type of ray. However, since the curves for both the vertical and the horizontal coincidences show a bend at about 250 meters water equivalent, one is led to suggest that there may be two types of very penetrating rays both capable of producing showers. It is not impossible that one of these consists of "heavy electrons" and the other of "neutrinos."

In conclusion, the writer wishes to express his sincere appreciation to Professor Arthur H. Compton for his inspiring direction and generous assistance with this experiment. It is also a pleasure to thank Mr. William F. Hartman, manager, and Mr. J. Ralph Abramson, assistant manager, of the Seneca Copper Corporation for their cooperation in the use of the Gratiot mine and its equipment; Mr. Francis R. Shonka for his assistance in building the Geiger-Müller tubes; and Messrs Haydn Jones, George E. Boyd, John F. Gall, and George G. Wright, Jr. for their help in taking the data.

[10] W. Heitler, Proc. Roy. Soc. London **A161**, 261 (1937).
[11] H. Bethe and W. Heitler, Proc. Roy. Soc. London **A146**, 83 (1934).

Photoelectric Ionization in the Ionosphere

E. O. HULBURT
Naval Research Laboratory, Anacostia Station, Washington, D. C.
(Received November 6, 1937)

The ionization equilibrium in the various atmospheric gases is calculated from the Saha theory on the assumption that the spectral energy curve of sunlight for ultraviolet frequencies above the limits of the principal series is that of a black body at 6000°K. A calculated region of ionization due mainly to oxygen and partly to nitrogen is found at about 200 km with maximum electron density 1.6×10^6, in agreement with F_2 observation in winter temperate latitudes. The assumption of an expansion of the high atmosphere under the sun, with resulting winds and diffusion, leads to a partly quantitative explanation of the observed seasonal changes in F_2, and to a qualitative explanation of F_1. In the case of E region the equations do not indicate what radiation causes the ionization nor what gases are ionized. This may be due to the omission in the theory of the possibility of ionization by frequencies below the series limits. Calculation suggests that E ionization is mainly ionic resulting from two processes, the first being the formation by the ionizing radiation of positive ions and free electrons, and the second being the formation of negative ions by the attachment of the electrons to oxygen molecules.

IN the early stage of ionospheric research two theoretical papers appeared which reached similar conclusions, namely, that the upper atmospheric ionization could reasonably be attributed to the ultraviolet light of the sun. In one paper[1] the recombination of electrons was calculated from the Saha theory of photoelectric equilibrium and in the other paper[2] from oxygen attachment and the three-body encounter theory of Sir J. J. Thomson. Experimental knowledge of the ionosphere has been greatly increased by the investigations[3] of the National Bureau of Standards, the Department of Terrestrial Magnetism of the Carnegie Institution and the Bell Telephone Laboratories, with observing stations at Washington, D. C., U. S. A., New York, N. Y., U. S. A., Huancayo, Peru, and Watheroo, Western Australia. Additional experimental data have become available concerning the attachment of free electrons to oxygen molecules. In the following paragraphs the photoelectric theory is worked out in detail and is compared with experiment with greater rigor than has been possible hitherto. The conclusion is reached that F_2 arises from the ionization of oxygen and nitrogen and that F_1 may be due to the modification of F_2 by winds and expansion of the atmosphere. No quantitative explanation of the origin of the E region emerges from the equations.

Certain important facts of the ionosphere may be briefly stated. We deal only with the more prominent regions of ionization and present numerical data averaged over at least a month, thereby eliminating from discussion daily, or other short time, irregularities and disturbances in the ionosphere. During the years of sunspot minimum 1933 and 1934 for the sun overhead the equivalent electron density y for E, F_1 and F_2 was about 1.5, 3 and 6×10^5 at virtual heights of about 100, 200 and 400 km, respectively. The ionization below, between and above these apparent levels is not known except that the values at the levels are not exceeded. On the assumption, as yet unchallenged, that the upper atmosphere is approximately electrically neutral, the densities of positively and negatively charged particles are equal. With increased sunspots in 1935, 1936 and 1937 y for all regions experienced a general augmentation. At Washington in 1937 the summer noon values of y were about 2, 4 and 8×10^5 for E, F_1 and F_2, respectively; the winter noon value for F_2 was 2×10^6. During daylight hours not too near sunrise and sunset y of E varied with the zenith angle ζ of the sun closely according to

$$y=y_0(\cos\zeta)^{\frac{1}{2}}, \qquad (1)$$

where y_0 is the value of y for $\zeta=0°$, i.e., the sun overhead.[3, 4] In the case of F_1 y obeyed (1) only

[1] Pannekoek, Proc. K. Akad. Amsterdam **29**, 1165 (1926).
[2] Hulburt, Phys. Rev. **31**, 1018 (1928).
[3] Gilliland, Kirby, Smith and Reyner, Nat. Bur. Stand. J. Research **18**, 645 (1937); Berkner, Wells and Seaton, Terr. Mag. and Atmos. Elect. **41**, 173 (1936); Schafer and Goodall, Proc. Inst. Rad. Eng. **23**, 1670 (1935); each paper being the latest of a series.
[4] Hulburt, Phys. Rev. **46**, 822 (1934); Terr. Mag. **40**, 193 (1935).

approximately. For F_2 y departed considerably from (1) but a reasonable theory[4] based on expansion of the atmosphere, winds and the rotation of the earth was proposed to account for the departures.

Observations of the magnetic double refraction of radio echoes returned from the ionosphere indicate that F, F_1 and F_2 are predominately electronic as far as the refraction of radio waves is concerned. In the case of E the double refraction is rarely observed. The fact is open to two interpretations, (1) that E is always predominately electronic and that the nonappearance of the extraordinary component is due to absorption, (2) that E is usually predominately ionic, hence yielding no extraordinary component within the accessible radio spectrum, but may at times be electronic. The two views are equally acceptable to the echo experiments. (2) is preferable to E layer theory, as explained later, and to theories of terrestrial magnetic variations.[5]

From measurements[3] at various latitudes and hours of the day in 1933 and 1934 the virtual heights of E were about 100, 120, and 140 km, and of F_1 were about 210, 230 and 240 km, for $\zeta=0°$, 60° and 70° to 80°, respectively. F_1 does not usualy appear in winter temperate latitudes. The virtual heights of F_2 were, within 30 km, 400, 380, 330, 280, 260 and 250 km for $\zeta=0°$, 20°, 40°, 60°, 80° and 90°, respectively. At night F_2 and F_1 coalesce to form a single F layer which remains at a virtual height of 250 to 300 km during the nocturnal hours. There were no important changes in the virtual heights during the years of increasing sunspots 1935, 1936 and 1937.

In general the virtual heights are always greater than the true heights, and the virtual height curve may give a very deceiving impression of the true distribution of ionization above sea level. For example, Murray and Hoag[6] have worked out a method for determining within limits the true heights from the virtual heights. When the method was applied to the Washington ionosphere observations of August 31, 1933, it turned out that whereas the virtual height of F_2 increased with decreasing ζ, the true height decreased with decreasing ζ. Thus, although F_2 appeared to rise during the morning to a midday maximum height and to descend in the afternoon, it actually descended during the morning to a midday minimum height and rose again in the afternoon.

We use the tables of Maris[7] of the densities of the various gases of the atmosphere to great heights based on a day temperature of 360°K above 80 km with complete mixing from sea level to about 110 km and isothermal equilibrium above 110 km. The density n of the molecules or atoms of each gas is expressed as a function of the height z by

$$n=n_0\epsilon^{-pz}, \tag{2}$$

where z is measured from the level where $n=n_0$.

$$p=mg/kt, \tag{3}$$

m being the mass of the gas particle, g the acceleration due to gravity at the height z, $k=1.372\times10^{-16}$ the Boltzman constant and t the temperature Kelvin. For $z=140$ km n is 3.45×10^{12}, 9.29×10^{11}, 4.20×10^{10}, 4.42×10^{8}, 4.29×10^{8} and 1.77×10^{7}, and above 140 km p is 0.810, 0.925, 1.12, 2.36 and 0.116×10^{-6}, for molecular nitrogen, molecular oxygen, argon, krypton and helium, respectively. For atomic nitrogen and oxygen p is 0.405 and 0.462×10^{-6}, respectively. From these values the average percentages by volume of the gases in the atmosphere from 200 to 280 km are about 88, 10 and 1 for nitrogen, oxygen and argon, respectively; the proportion of helium increases from about 0.1 at 200 km to 30 percent at 300 km. Above 300 km helium predominates if the extrapolation to such high levels is valid. Hydrogen and water vapor are left out of consideration on the basis that if they were present hydrogen lines should appear in spectra of the night sky and the aurorae; no such lines are observed. However, the presence or absence of hydrogen and water vapor in the high atmosphere can not be said to be settled at the present time.

It is assumed that the atmospheric gases are ionized by the absorption of solar ultraviolet light of frequencies above ν_0, where $h\nu_0=\chi$, χ being the ionizing energy. If $i_\nu d\nu$ is the intensity of the ionizing sunlight in the range from ν to $\nu+d\nu$ and β_ν the molecular or atomic absorption

[5] Hulburt, Rev. Mod. Phys. **9**, 44 (1937).
[6] Murray and Hoag, Phys. Rev. **51**, 333 (1937).
[7] Maris, Terr. Mag. **33**, 233 (1928); **34**, 45 (1929).

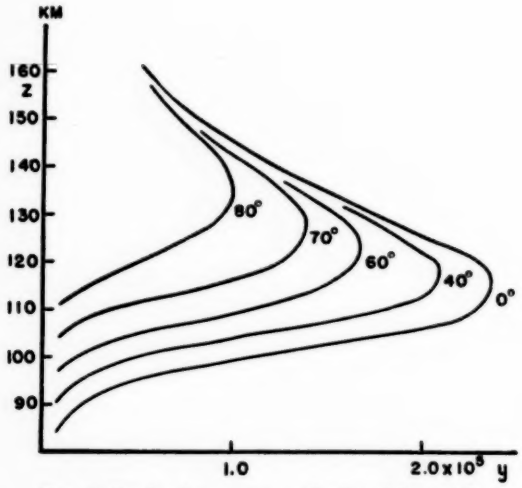

FIG. 1. Ionization curves calculated from (6).

coefficient of the gas, the rate cm^{-3} of absorption of energy is $n\beta_\nu i_\nu d\nu$. If one assumes that all of the absorbed energy causes ionization one finds that the number $q_\nu d\nu$ cm^{-3} $sec.^{-1}$ of electron ion pairs produced is

$$q_\nu d\nu = n\beta_\nu i_\nu d\nu/\chi. \tag{4}$$

The total ionization production is equal to $\int q_\nu d\nu$ taken over all regions of the spectrum which cause ionization. An exact evaluation of the integral is unprofitable at present and sufficient accuracy is secured by dealing with average values. Therefore we drop the subscript ν, denoting the intensity of the total ionizing light by i and the average absorption coefficient by β. (4) becomes

$$q = n\beta i/\chi. \tag{4.1}$$

Recombination of electrons and positive ions is assumed to take place at the rate of

$$\alpha y^2, \tag{4.2}$$

where α is the recombination coefficient and y the electron density. For equilibrium $q = \alpha y^2$ and from (4.1)

$$y^2 = n\beta i/\alpha\chi. \tag{4.3}$$

Let i be the intensity at a height z in the terrestrial atmosphere and ζ the zenith angle of the sun. Then

$$di = n\beta i\, dz/\cos\zeta. \tag{4.4}$$

On substituting (2) into (4.4) and integrating one obtains

$$i = i_0 \epsilon^{-\beta n/p \cos\zeta}, \tag{5}$$

where i_0 is the intensity outside of the atmosphere. From (4.3) and (5).

$$y^2 = (n\beta i_0/\alpha\chi)\epsilon^{-\beta n/p \cos\zeta}. \tag{6}$$

This is the general expression for the ionization in any region for equilibrium conditions. Equilibrium requires that for a sufficient period of time the sun be approximately stationary with reference to the earth, the atmosphere be free from winds and mass motions and there be no diffusion of the ionization. None of these conditions are exactly true but some may be approximately true. Further, (5) and hence (6) is derived on the assumptions that the earth is flat and that the rays of ionizing light traverse the atmosphere in straight lines. For $\zeta < 80°$ the errors arising from the assumptions are less than 15 percent, but as ζ nears 90° the errors may be large.

With arbitrary values of the constants β, i_0, α and χ the y, z curves calculated from (6), (2) and (3) are plotted in Fig. 1 for various values of ζ. From (6) y reaches a maximum value given by

$$y = [(pi_0 \cos\zeta)/(\epsilon^{\alpha\chi})]^{\frac{1}{2}}, \tag{7}$$

ϵ being the Naperian base. Eq. (7) is of the same form as (1) and therefore is in agreement with observation insofar as (1) represents facts.

The virtual height z' of a radio ray passing vertically into a region of ionization is given by

$$z' = \int dz/\mu, \tag{8}$$

where μ is the refractive index of the region at a height z and the integral is taken along the ray. Because of the magnetic field of the earth the ionosphere is doubly refracting and for the ordinary component

$$\mu^2 = 1 - ye^2c^2/\pi mf^2, \tag{9}$$

where f is the frequency of the radio wave, e and m refer to the electron, and c is the velocity of light. C.g.s.e.m. units are used throughout this paper.

In Fig. 2 are plotted the values of z' from (8) and (9) corresponding to the y, z curves of Fig. 1. If the curves of Figs. 1 and 2 were worked out for values of z 100 km higher, they would be little changed; in such a case, for example, z'

for $\zeta=80°$ would be about 35 km above z' for $\zeta=0°$, as in Fig. 2. The variations of z' with latitude and time of day given by the f, z' curves of Fig. 2 agree fairly well with observation in the case of E region and moderately well in the case of F_1 region. This agreement together with that of (7) constitutes the main evidence in favor of the supposition that E and F_1 are largely due to photoelectric effects of sunlight, and that the effects reach approximate equilibrium in a time short in comparison with possible modifications due to the relative motions of earth and sun, and to diffusion and winds in the upper atmosphere. Ionosphere changes[3] during eclipses of the sun offer corroborative evidence.

In order to work out quantitatively by means of (6) the ionization in the various gases of the atmosphere, we proceed to explicit formulation of i_0, β and α. We consider first the intensity i_0. The spectral energy curve of solar radiation is assumed to be that of a black body at temperature $t_1=6000°$K. The total energy cm^{-2} radiated in the frequency range from ∞ to ν_0 is

$$\int_{\infty}^{\nu_0}(8\pi h\nu^3/c^2)(\epsilon^{a\nu}-1)^{-1}d\nu, \qquad (10)$$

where $a=h/kt_1$. Integration of (10) yields approximately

$$(8\pi h/c^2)(\nu_0^3/a+3\nu_0^2/a^2+6\nu_0/a^3+6/a^4)e^{-a\nu_0}. \qquad (10.1)$$

For ν_0 in the ultraviolet the first term only of (10.1) may be retained without causing an error greater than 15 percent. Then the solar energy i_0 erg cm^{-2} sec.$^{-1}$ falling vertically on the top of the atmosphere is

$$i_0=f(8\pi\nu_0^3kt_1/c^2)\epsilon^{-h\nu_0/kt_1}, \qquad (11)$$

where $f=1/184{,}000$ is the fraction of the total sphere subtended at the earth by the sun.

The absorption coefficient β for light in the continuum below the series limit usually used is that deduced by Kramers[8] from classical electromagnetic theory assuming a special law of electron capture. Kramers' theory gives, neglecting terms of unit order,

$$\beta=\frac{16\pi^2}{3(3)^{\frac{1}{2}}}\frac{Z^2e^6c^5}{h}\frac{h\nu_0}{(h\nu)^3}, \qquad (12)$$

[8] Kramers, Phil. Mag. **46**, 836 (1923).

where Z is the atomic number. β has values only for $\nu\geqq\nu_0$. (12) was derived for atoms but may be used approximately for molecules. From quantum theory Gaunt[9] derived a slightly different expression. There appear to be no direct experimental tests of (12) in the optical range; the formula can scarcely claim an accuracy better than an order of magnitude. Rosseland[10] has commented, "One sometimes has the feeling that the applicability of this formula has been strained beyond the breaking point." For He, A, N and O the first ionization potential is 24.46, 15.69, 14.48 and 13.55 volts,[11] and at ν_0 from (12) β is 4.75×10^{-18}, 9.46×10^{-16}, 1.69×10^{-16} and 2.52×10^{-16}, respectively.

The recombination coefficient α is derived from the Saha theory[12] of the ionization of a gas in photoelectric, thermodynamic equilibrium with radiation. The reaction isobar of a gas at temperature t_1 ionized by and in equilibrium with radiation at temperature t_1 is

$$x^2P/(1-x^2)=(2\pi mh^{-2})^{3/2}(kt_1)^{5/2}\epsilon^{-h\nu_0/kt_1}, \qquad (13)$$

where x is the fraction of atoms ionized and P is the total pressure. For a gas at temperature t and radiation at a temperature t_1, Pannekoek[1] showed that the right-hand side of (13) must be multiplied by $t^{\frac{1}{2}}/2t_1^{\frac{1}{2}}$. Then noting that $P=nkt$ and $x=y/n\ll1$, (13) becomes

$$y^2=n2^{\frac{1}{2}}(\pi mkh^{-2})^{\frac{1}{4}}t_1t^{\frac{1}{2}}\epsilon^{-h\nu_0/kt}\equiv nA, \qquad (13.1)$$

which is of the same form as (4.3). Comparison

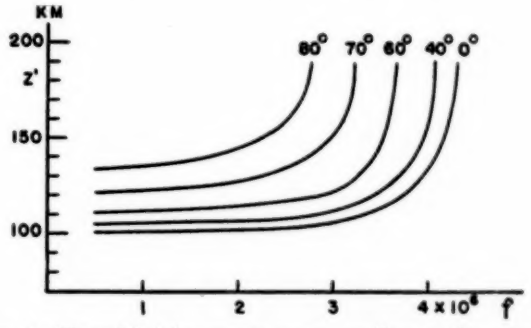

FIG. 2. Virtual height curves corresponding to the curves of Fig. 1.

[9] Gaunt, Phil. Trans. Roy. Soc. **229A**, 163 (1929–1930), also gives a critical discussion of the opacity formulae of Milne, Eddington, Oppenheimer and Rosseland.

[10] Rosseland, *Theoretical Astrophysics*, (1936) p. 194.

[11] Bacher and Goudsmit, *Atomic Energy States* (1932).

[12] Saha, Phil. Mag. **40**, 472 (1920); Woltjer, ibid. **47**, 209 (1924); Fowler, ibid. **45**, 1 (1923).

of (13.1) and (4.3) gives $\alpha=\beta i_0/A\chi$. Substitution of β from (12), i_0 from (11) and A from (13.1) leads to

$$\alpha=32\pi(2\pi m/27k)^{\frac{1}{2}}(Z^2e^6c^3/m^2)(\nu_0^3/h\nu^3t^{\frac{1}{2}}). \quad (14)$$

If some other formula for β than (12) were used a value of α different from (14) would result. Since α has been derived directly from β it contains the errors and uncertainties of β. The substitution of ν_0 for ν in (14) and the introduction of numerical values yield an average value of α in the continuum near to and ending with ν_0,

$$\alpha=1.02\times10^{-11}Z^2/t^{\frac{1}{2}}. \quad (14.1)$$

For $t=360°$K, α is 3.4×10^{-11} and 2.6×10^{-11} for atomic oxygen and nitrogen, respectively.

Mohler[13] has recently determined α to be 2×10^{-10} for mercury vapor at pressures below 10^{-1} mm and an electron temperature of about 2000°K, and 3×10^{-10} for caesium vapor at a pressure below 10^{-2} mm and temperature 1200°K. The corresponding values from (14.1) are 1.5×10^{-9} and 8.9×10^{-11}. The agreement is perhaps as good as could be expected in view of the fact that (14) contains no correction due to screening of the nuclear charge Z or additional terms to include effects of line absorption at frequencies below ν_0.

The three-body collision theory of Sir J. J. Thomson[14] led to a recombination rate αy^2 in agreement with (4.2), and yielded an expression for α which for pressures below 10^{-2} atmosphere reduced to

$$\alpha=2\pi(u^2+u'^2)^{\frac{1}{2}}(2e^2/3kt)^3(1/\gamma+1/\gamma'), \quad (15)$$

where u and u' are the velocities of thermal agitation of negative and positive particles, respectively, and γ and γ' their free paths among the molecules of the gas. For $t=360°$K (15) becomes

$$\alpha=\tau n, \quad (15.1)$$

where τ is 1.6×10^{-23} for electrons and positive ions and 2.4×10^{-25} for positive and negative ions. Eq. (15) was derived on the assumption that a positively and negatively charged particle combine only upon simultaneous encounter with a third body, as a neutral atom or molecule, which absorbs the energy of recombination. The formula does not include the possibility of recombination by "direct encounter" of the charged particles. Loeb[15] pointed out that this effect will add a term to (15) which may be important at low pressures; however, lack of potential barrier data precluded exact evaluation of the term. Since α of (15.1) varies with the molecular density it is greater than α of (14) for $n>10^{12}$ or $z<150$ km. Therefore the ionization equilibrium in F region is controlled by (14) and in E region by (15).

According to laboratory experiment free electrons become attached to oxygen molecules to form relatively stable negative ions; they do not become attached appreciably to the other particles of the high atmosphere. The rate of attachment is

$$by. \quad (16)$$

The attachment is usually stated in terms of h, the probability of electron capture at a collision. Then

$$b=uh/\gamma, \quad (16.1)$$

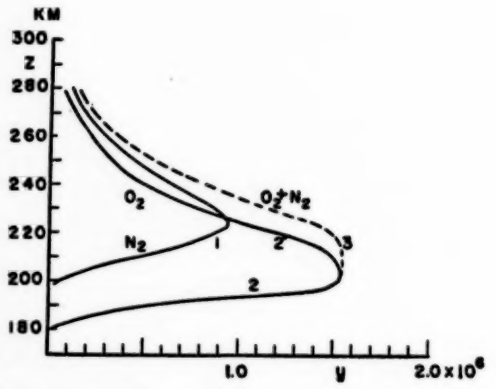

FIG. 3. Theoretical ionization curves for winter noon.

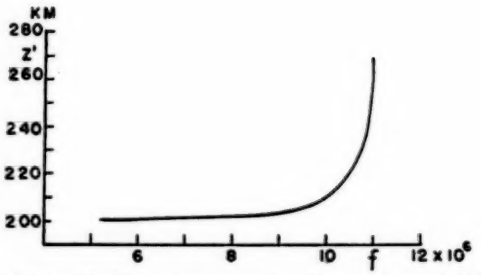

FIG. 4. Virtual height curve corresponding to curve 2, Fig. 3.

[13] Mohler, Phys. Rev. **51**, 1008 (1937).
[14] Thomson, Phil. Mag. **47**, 337 (1924).
[15] Loeb, Phys. Rev. **51**, 1110 (1937); **52**, 40 and 136 (1937).

where u is the temperature velocity of the electron and γ the free path among the oxygen molecules. From Bradbury's[16] measurements h increased rapidly with the decrease of electron energy for energies below 1 electron volt. At 0.2 electron volt, the lowest energy at which observations were made, corresponding to a temperature of 770°K, h was 2.5×10^{-4}. This in (16.1) with $t=360°$K gives $b=2\times10^{-12}\ n'$, where n' is the density of oxygen molecules, which is nearly two orders of magnitude above the value of the former paper[2] based on earlier experimental data.

Now (16) with $b=2\times10^{-12}n'$ gives a loss of electrons much more rapid than that due to the recombination of (14) or (15) and therefore would be expected to control the ionization equilibrium. However for F_1 and F_2 regions (16) gives very low values of y, a very rapid decrease of y at night, and leads to $y=y_0\cos\zeta$ instead of to (1). These results conflict with observation and force the conclusion that (16) does not hold in the F regions, either because all the oxygen there is atomic, or because for some unknown reason the laboratory value is not applicable to the conditions at great heights. As discussed later similar difficulties with (16) in E region are not so acute.

The atmospheric ionization is now calculated by means of (6) with i_0, β and α given by (11), (12) and (14), respectively. Assume that for winter midday in temperate latitudes the temperature t of the high atmosphere is 360°K and ζ is 60°. Assume that oxygen and nitrogen are molecular and that the values of β and α derived from atomic constants are true for molecules. The y, z curve from (6) for N_2 is drawn in curve 1, Fig. 3. For O_2 the values of y given by (6) were reduced by $\frac{1}{8}$ because of the reduction of i_0 for O_2 due to the absorption by nitrogen of frequencies below the series limit 850A; the reduced y, z values for O_2 are plotted in curve 2, Fig. 3. Similar calculations for He, A and Kr yielded regions of ionization with maximum values of y of 0.06, 1.3 and 4.8×10^5 at heights of 55, 172 and 140 km, respectively. However, these regions probably do not exist in theory, for the light which causes them is totally extinguished by

[16] Bradbury, Phys. Rev. **44**, 883 (1933).

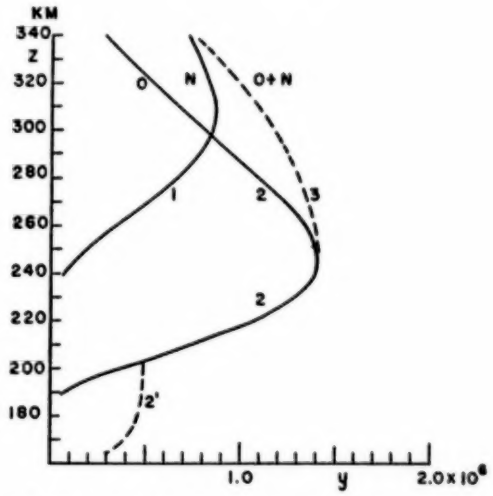

FIG. 5. Theoretical ionization curves for summer noon.

superincumbent oxygen and nitrogen, if the variation of β with ν indicated by (12) is anywhere near correct. Therefore, the total ionization is the summation of curves 1 and 2, Fig. 3, obtained approximately by taking the square root of the sum of the squares of the abscissas of curves 1 and 2. This gives curve 3, Fig. 3, with a maximum $y=1.55\times10^6$ in fair agreement with the Washington winter noon values for F_2 which have increased from about 0.5×10^6 in 1934 to 2×10^6 in 1937. The f, z' curve corresponding to curve 2 (or 3), Fig. 3, is drawn in Fig. 4 and indicates a virtual height of 205 km. This value is increased by effects of ionization below 180 km, and would appear to be in accord with the observed virtual heights 230 to 270 km. Calculation shows that diffusion[2] of the ionization in a vertical direction will not modify the y, z curves of Fig. 3 very much and therefore will not disturb the conclusion just stated.

For noon in the tropics and in summer temperate latitudes we give numerical expression to the expansion hypothesis[4] and assume that above 200 km oxygen and nitrogen are atomic and that the temperature is 500°K. The y, z curves, determined on these assumptions, from (6) for $\zeta=0°$, are shown in curves 1 and 2, Fig. 5, for O and N, and the curve of total ionization in curve 3. The maximum value 1.4×10^6 of curve 3 is somewhat above the summer noon values for F_2 at Washington, Watheroo (Australia) and Huancayo (Peru), which were about

0.5, 0.6 and 0.9×10^6 in 1934, 1935 and 1936, respectively. The f, z' curve, given in curve 2, Fig. 6, corresponding to curve 2, Fig. 5, indicates a virtual height of 220 km, which is below the observed values of 300 to 400 km for $\zeta<25°$. Furthermore, the curves of Fig. 5 do not account for F_1 region. However, a relatively minor bulge in lower part of curve 2, Fig. 5, will yield F_1. In illustration, the bulge 2′ gives rise to an f, z' curve shown in curve 2′, Fig. 6, which is similar to the observed curves, the lower branch referring to F_1 and the upper to F_2. In the main, the several discrepancies between observation and theory would seem to be reasonably attributable to effects of diffusion and winds which have not been included in the theoretical calculations. Such effects follow necessarily from the expansion hypothesis, for expansion of the atmospheric reaches under the sun must give rise to winds blowing in all directions away from the subsolar regions. Spreading of the ionization in vertical and horizontal directions by winds and diffusion will reduce the calculated values of y, increase the virtual heights, and might produce the F_1 bulge in the y, z curves.

The foregoing calculations have been based on the assumption of upper atmospheric temperatures of 360° and 500°K for winter and summer days, respectively. The conclusions do not depend critically on the assumption but would hold equally well for a lower selection of temperatures, say, 260° and 400°K. Appleton's[17]

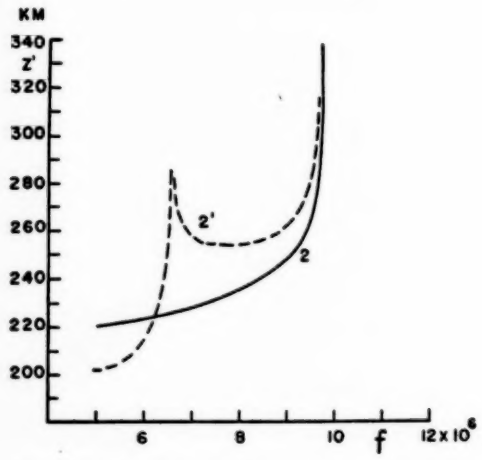

FIG. 6. Virtual height curves corresponding to curves 2 and 2′, Fig. 5.

[17] Appleton, Nature **136**, 52 (1935).

extension of the expansion hypothesis[4] to indicate summer noon temperatures of at least 1200°K appears extreme and uncalled for by the experimental facts.

If the degradation of y in the night is assumed to be due to recombination unaffected by other factors, an assumption open to discussion, we may write

$$dy=-\alpha y^2 dt,$$

or

$$y=1/(1/y_0+\alpha t), \tag{17}$$

where y_0 is the value at sunset and y the value t seconds later. For F region at Washington in December, 1936, the average value of y_0 at sunset, or 5 P.M., was 1.25×10^6 and at 11 P.M. y was 0.25×10^6. With $\alpha=3.4\times10^{-11}$, calculated from (14) for oxygen, and with $t=6$ hours (17) gives $y=0.59\times10^6$, which is larger than the observed value. Similar calculations with the data of other times and places gave similar results, namely, that the recombination coefficient α of (14) was of the correct order of magnitude but was too small by a factor of 2 to 4. Therefore (14) yields agreement with F region observation which, although not precise, is perhaps unexpectedly good.

The theory provides no explanation of the E region ionization since no light in the continuum above ν_0 can reach E levels in effective amount, if the absorption coefficients given by (12) are correct. For example, the total number of molecules in a vertical column of the atmosphere above 100 km is 1.8×10^{20}, which is equivalent to 6.4 cm of air at N.T.P. Accordingly, in order for the ionization to reach 100 km levels β cannot be much greater than 10^{-20}; this is several orders of magnitude below β of (12). The fact that y of E conforms closely with (1) indeed more closely than y of any other region of ionization, is strong evidence that E is caused by a moderately penetrating solar radiation which approximately travels in straight lines into the terrestrial atmosphere and is absorbed exponentially. The radiation might be ultraviolet light, x-rays or particles of zero average charge; the first seems the most probable, the light being of frequency less than ν_0, as the lines of the principal series.

The high value of the attachment of electrons

to oxygen molecules gives support to the view[18] that in E region a twofold reaction occurs, namely, the ionizing radiation first produces positive ions and free electrons and the free electrons become rapidly attached to form negative oxygen ions. If the ratio of the rate of electron attachment to the rate of ionic recombination were sufficiently great the ionization of E region would be predominately ionic, rather than electronic as far as the refraction of radio waves is concerned, the disappearance of ions would be by the recombination formula (15.1), and y of E would agree with (1) and hence with observation. Numerically, however, the ratio of b/α should be about 3 times greater than the value given by (15.1) and (16.1). This would occur either if α of (15.1) were a little less, or if Bradbury's[16] curve of h against electron energy continued to increase with decreasing energy in the domain below 0.2 electron volts. Further experimental knowledge of attachment and recombination coefficients might contribute to the question in an important manner.

[18] Hulburt, Phys. Rev. **34**, 1167 (1929); **35**, 240 (1930).

MARCH 1, 1938 PHYSICAL REVIEW VOLUME 53

Emission of Neutrons from Argon, Chlorine, Aluminum and Some Heavier Elements Under Alpha-Particle Bombardment

ERNEST POLLARD, HOWARD L. SCHULTZ AND GORDON BRUBAKER
Sloane Physics Laboratory, Yale University, New Haven, Connecticut

(Received January 5, 1938)

The emission of neutrons from chlorine, argon, scandium, titanium, manganese and iron under alpha-particle bombardment was established. The yield from argon is considerable and enabled a measurement of the energy of the neutrons to be made: the majority are associated with a group of energy change -5.6 ± 1.0 Mev, but two groups must be present. The excitation curve for these neutrons was plotted for alpha-particle energies between 3.5 and 9.0 Mev and varies smoothly in agreement with penetration through a barrier of radius 7.6×10^{-13} cm. This smooth variation means that the total neutron yield does not change rapidly as a new group is excited, from which it is deduced that observations on single groups would show apparent resonance effects. The excitation curve for chlorine fits a theoretically derived function for a nuclear radius of 6.0×10^{-13} cm and a similarly plotted curve for aluminum agrees with a radius of 5.8×10^{-13} cm. These last elements have radii approximately fitting the formula $R=R_0A^{\frac{1}{3}}$ with $R_0=1.94\times10^{-13}$, while argon has a radius which is definitely too large to fit the above relation. This abnormally large radius is linked with the large neutron content of the argon nucleus.

INTRODUCTION

THE use of a boron trifluoride filled ionization chamber surrounded by paraffin is so sensitive a neutron detector that neutron emission can be detected even with weak alpha-particle sources. Using an arrangement of this kind we have subjected a number of elements to bombardment by Th C′ alpha-particles and looked for the emission of neutrons. It was found that a slight yield could be detected from scandium, titanium, manganese and iron, indicating that the absorption of an alpha-particle with emission of a neutron is a general occurrence in this section of the periodic table. The yields from these elements were, however, roughly equal to the background of the detecting apparatus and therefore not suitable for detailed study. On the other hand argon and chlorine were found to give considerable yields of neutrons (in the case of argon the yield is second only to that from beryllium if Th C′ alpha-particles are used) and the nature of the neutron yield from these two elements was therefore further studied. An estimate of the energy of a neutron group was made for argon and excitation curves for both elements plotted. As a check an excitation curve for the neutrons from aluminum was also determined: from these three excitation curves values for the nuclear radii of the three elements can be found. A preliminary report of the experiments on argon and chlorine appeared early in 1937.[1]

[1] E. Pollard, H. L. Schultz and G. Brubaker, Phys. Rev. **51**, 140 (1937).

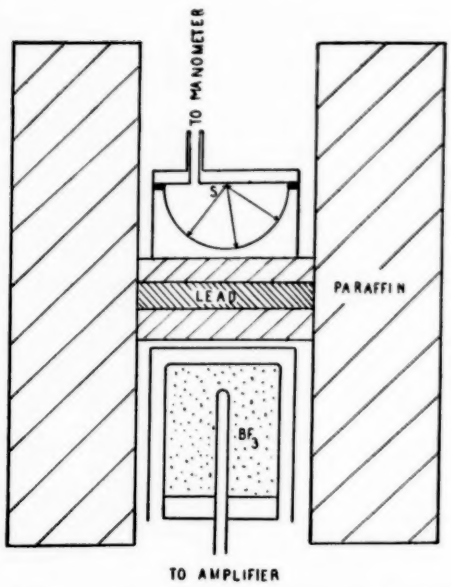

FIG. 1. The arrangement of source, ionization chamber and surrounding paraffin.

EXPERIMENTAL ARRANGEMENT

The essentials of the arrangement for bombardment and detection are shown in Fig. 1. The radioactive source *S* was placed at the center of a hemisphere of four centimeters radius cut in a brass block. Targets of various materials mounted on hemispherical bases could be placed inside the block, or gases could be bombarded with a silver hemisphere as backing. For preliminary experiments a smaller bombardment arrangement was used in which the material bombarded was placed in a brass tray and exposed to, or shielded from, the source, by rotating a small copper plate over the source button. The ionization chamber was of the shape drawn: it was filled with boron trifluoride at atmospheric pressure and a potential of a thousand volts applied to the outer electrode; the collection electrode was connected to the input of a conventional linear amplifier. The source box and ionization chamber were placed in a cylinder of paraffin of outside diameter 30 cm and inside diameter 12 cm; varying thicknesses of paraffin could be placed between box and chamber. A block of lead was interposed to diminish the gamma-ray background from the source. No difficulty was experienced in separating the kicks produced by the neutrons from the background due to gamma-rays except when sources larger than fifty millicuries were employed.

For general trial experiments different targets were used and the yield measured with target alternately exposed to, or shielded from, the alpha-particles: for gaseous targets the yield was compared with the yield when the box was evacuated. Excitation curves for the two solid targets were plotted by varying the pressure of oxygen in the hemispherical container and measuring the neutron yield; and for argon by varying the pressure of argon itself. Sources of thorium and radium active deposits and polonium were used, deposited on buttons of either nine or ten millimeters in diameter: both silver and monel metal buttons were used for Th C′ and Ra C, while the polonium source was deposited on palladium.[2]

EXPERIMENTAL RESULTS

General survey

The first result of general survey experiments was an apparent yield of neutrons from the source itself. This phenomenon has been mentioned by Szilard.[3] It appears to be greater for Th C′ sources than for Ra C sources of equal strength and is not observed for polonium: the probable explanation is that it is partly due to the transmutation of the material of the source button and partly to the nuclear photoeffect on the deuterium present in the paraffin. Whatever the cause, the presence of a yield of roughly two counts per minute above the background (also roughly two per minute) rendered it difficult to study the properties of neutron yields from elements except where this yield is large. The data in Table I are the results of experiments intended to test the presence or absence of neutron emission when an element is bombarded by Th C′ alpha-particles. Only relative yields should be considered as the counting level was not always the same. The limits of error given are not to be regarded as rigorous: they merely serve to give some indication of the extent of the counting in each determination. Following a somewhat arbitrary convention, we have divided

[2] The polonium source was kindly supplied by Professor Bearden and Dr. Kanne of Johns Hopkins University.
[3] L. Szilard, Nature **136**, 950 (1935).

the value by the square root of the number of particles counted to give the limits above. We consider that where a yield is claimed to exist no impurity in the material could account for the observed emission. This general survey shows clearly that elements of moderately high atomic number will emit neutrons when bombarded by alpha particles of roughly 9 Mev energy. The experiments of Ridenour and Henderson[4] in which induced radioactivity has been observed in a wide variety of elements also indicate this. Since the yields we observe with natural sources are so small it is clearly preferable to use artificial alpha-particles for further study in this field and we therefore contented ourselves with the above data except for the two elements argon and chlorine where the yields are large enough to enable the plotting of excitation curves, and in the case of argon to determine the energy of the emitted neutrons.

Argon

Energy of neutrons.—In order to obtain a large yield of neutrons a brass cylinder was filled with a mixture of argon and fifty millicuries of radon and recoil protons from paraffin looked for with a proportional counter as used in experiments on proton emission. A lead block was interposed between the neutron "bomb" and the counter to diminish the effect of the gamma-radiation and a paraffin layer was placed on the counter side of the block. A source of Th C′+Be giving roughly one third as many neutrons as the argon-radon bomb gave a yield of recoil protons equal to three times the counter background. The argon radon mixture gave no detectable effect (one-third the background) with counters having foils of greater than 2.0 cm air equivalent over their opening so that very few neutrons of energies greater than one Mev can be emitted from this mixture. The counter was then filled with hydrogen at 47 cm pressure which would be capable of detecting recoil protons of range less than six millimeters air equivalent. A rise in counts from twelve per hour to seventy per hour was observed when the argon-radon mixture was brought near, indicating the presence of a yield of relatively low energy neutrons. From estimates of the size of oscillograph deflections compared with protons of known energy, we estimated that the majority of the neutrons gave recoil protons of ranges between four and six millimeters air equivalent. The neutrons from the $A+\alpha$ reaction, using radon and its products for bombarding are therefore *mainly confined to less than 500,000 electron volts energy*. This conclusion has been verified by the more satisfactory work of McCarthy of this laboratory who measured the lengths of sixty recoil tracks in a cloud chamber filled with hydrogen and found the majority of tracks to lie between 6 and 8 millimeters air equivalent with no tracks greater than eighteen millimeters air equivalent. If we suppose, as a simplifying assumption that the neutrons are due to bombardment by 6.5 Mev alpha-particles and that they are emitted with 0.5 Mev energy, then the nuclear energy in the reaction:

$$A^{40}+He^{4}\rightarrow Ca^{43}+n^{1}+Q$$

is $$Q=-5.6\pm1.0 \text{ Mev.}$$

[4] L. N. Ridenour and W. J. Henderson, Phys. Rev. **52**, 889 (1937).

TABLE I. *Results of alpha-particle bombardment.*

ELEMENT	TARGET	YIELD PER MINUTE	BACKGROUND PER MINUTE	CONCLUSION	REACTION
Titanium	Metal	4.4±0.4	3.5±0.4	True yield[a]	$Ti[\alpha, n]Cr$
Chlorine	"arochlor" gas	6.3±0.6	3.9±0.4	True yield	$Cl[\alpha, n]K$
		5.0±0.5	1.6±0.3	" "	
Scandium	Sc_2O_3	5.4±0.6	4.4±0.5	Probable yield[b]	$Sc^{45}[\alpha, n]V^{48}$
Iron	Filings	3.1±0.3	2.4±0.2	True yield	$Fe^{56}[\alpha, n]Ni^{59}$
Manganese	MnO_2	3.8±0.5	2.3±0.3	True yield	$Mn^{55}[\alpha, n]Co^{58}$
Carbon	Lamp black	3.8±0.2	3.5±0.2	No yield	
Oxygen	Tank gas	3.7±0.2	3.5±0.2	No yield	
Nitrogen	Air	6.0±0.5	2.2±0.3	Yield	$N^{14}[\alpha, n]F^{17}$
Argon	Gas	7.0±0.9	1.9±0.3	Large yield	$A^{40}[\alpha, n]Ca^{43}$

[a] Walke (Phys. Rev. **52**, 784 (1937)) obtained two radioactive products from the activation of Ti with alpha-particles which he suggests may be due to this type of reaction.
[b] This reaction has been definitely established by Walke (Phys. Rev. **52**, 671 (1937)) who observed the artificial radioactivity of V^{48}.

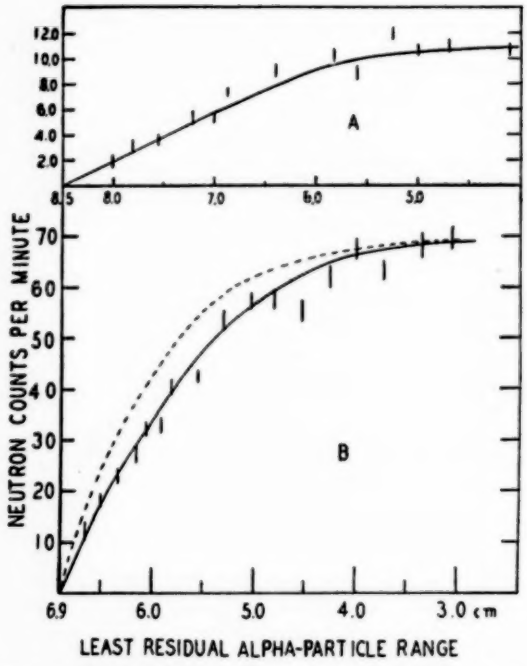

FIG. 2. Graph showing the neutron yield from argon bombarded by alpha-particles from Th C′ (*A*) and Ra C (*B*) as the gas pressure in the hemispherical chamber is varied. The line drawn through the points in *A* is the theoretically expected yield if the nuclear radius is 7.3×10^{-13} cm; that in *B* for a radius of 7.6×10^{-13} cm. The dotted line in *B* is the theoretical curve for a radius of 6.8×10^{-13} cm which is close to the value expected from the relation $R=R_0A^{\frac{1}{3}}$.

Excitation curves.—A gaseous target is not suitable for plotting an excitation curve directly as it must be confined between walls of a material which is both thin and vacuum tight. If, however, the stopping power of the gas is known it is quite possible to derive an excitation curve from a set of data giving the variation of yield with pressure in the hemispherical bombardment chamber as described already. Thus, when the hemisphere is evacuated, only alpha-particles of full residual range traverse the space. As gas is admitted a band of energies from maximum down to a value governed by the gas pressure is effective in the space until at high pressures the alpha-particles are fully stopped in the gas and do not reach the limits of the container. The increase in yield corresponding to an increase in pressure is therefore the yield due to the increased absorption and if desired the excitation curve for a thin layer of gas may be derived from the yield-pressure curve by differentiation. Or preferably, a theoretical excitation function may be integrated for progressively widening limits and compared with the experimental results. This procedure was followed in a number of runs made with Th C′, Ra C and polonium sources with the results given in Fig. 2. The yield is plotted against the lower limit of alpha-particle range corresponding to the pressure. It can be seen that for Th C′ particles (curve *A*) the yield rises linearly until alpha-particles of less than 6.5 cm range are present after which it falls away indicating that alpha-particles with residual ranges between 6.5 and 8.6 cm are equally effective in causing transmutation while those below 6.5 cm are progressively less effective. The Ra C curve *B* shows the lower energy portion in more detail and indicates that alpha-particles of as low as 3.0 cm continue to cause transmutation. The results with polonium verify this last deduction since a definite yield was observed for alpha-particles of less than 3.0 cm range. In curve *A* 500 particles were counted at each point; in curve *B*, 1000.

The lines drawn in Fig. 2 are derived from the Gamow penetration formula ($l=0$) assuming radii of 7.3 and 7.6×10^{-13} for the argon nucleus. The theoretical curve for a thin layer has been integrated to compare with the experimental results. It can be seen that the fit is quite good and we suggest the value $7.6\pm0.3\times10^{-13}$ for the nuclear radius of argon. We give greater weight to the results with Ra C on account of the larger number counted and the fact that a single alpha-particle group is present.

Presence of two groups of neutrons.—A point of some interest arises from the fact that alpha-particles of relatively low energy can cause the emission of neutrons. It was definitely established that alpha-particles of three centimeters range can set free neutrons and if it be assumed as a limiting case that at this range the emitted neutrons have zero energy the nuclear energy change cannot be less than -4.0 Mev, which is 1.6 Mev greater than found from the measured neutron energies.[5] This discrepancy means that some explanation other than the simple reaction with a single nuclear energy change must be sought and two reasonable possibilities present

[5] With this nuclear energy change the average range of projected protons due to neutrons from Rn+A as in our experiments would be expected to be 7 cm air equivalent as against 0.7 cm found.

themselves. The first is that the emission of two neutrons may occur according to $A^{40}[\alpha, 2n]Ca^{42}$; the second that at high alpha-particle energies an excited state of Ca^{43} is formed which reverts to the ground state with emission of gamma-radiation. The first process requires a considerable energy change in going from A^{40} to Ca^{42} and for that reason, we think, is improbable. The second process, the formation of Ca^{43} in an excited state is normally to be expected and is much more probably the true explanation. On this view the neutrons emitted would have energies corresponding to two "Q" values, the one the value -5.6 Mev already found and a more energetic group of relatively low yield of Q value certainly exceeding -4.0 Mev (which just permits the release of neutrons by 3.0 cm alpha-particles). The presence of this second group could not be established with certainty by direct experiments as the available yields were not large enough. It is, of course, possible that several groups are present. If this view is accepted there is an interesting deduction to be made from the excitation curve. We find a smooth fit to the Gamow formula for the *total* neutron emission, whereas it would be expected that a sharp drop in yield would occur at the critical alpha-particle energy below which the -5.6 Mev group could not be emitted. Since this group is the more prominent this drop in yield should be very definite, whereas Fig. 2 shows no sign of a clear discontinuity. If, then, the *total* emission is governed only by the penetrability of the barrier, the yield of any one group must be affected by

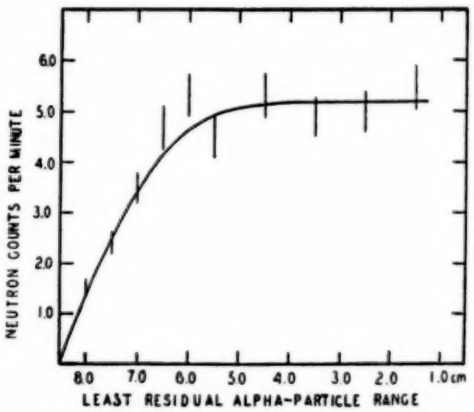

FIG. 3. Neutron yield from chlorine gas at varying pressures in a hemispherical chamber. The line is the theoretical curve for a nuclear radius of 6.0×10^{-13} cm.

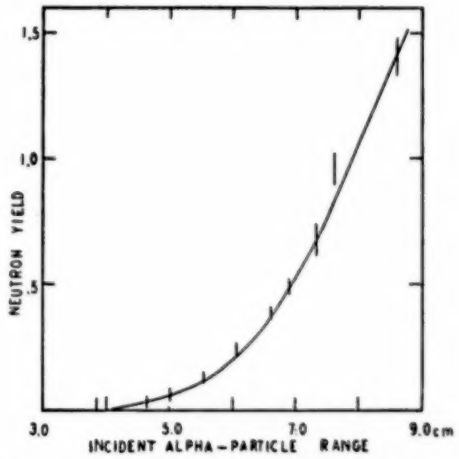

FIG. 4. Neutron yield from a thick layer of "Arochlor" (containing chlorine, carbon and hydrogen) as the range of the bombarding alpha-particles is varied by introducing oxygen at different pressures between source and target. The line is the theoretical curve for a nuclear radius of 6.0×10^{-13} cm.

the presence or absence of other groups and in particular the yield of the "Q" greater than 4.0 Mev group must fall when the 5.6 Mev group appears, thus giving the appearance of resonance. This explanation of "resonance" effects has been proposed by Waring and Chang[6] and Chang and Szalay[7] to explain the variations in the yield of induced radioactivity from the reactions $Al^{27}[\alpha, n]P^{30}$ and $Mg^{24}[\alpha, n]Si^{27}$. Our experiments lend confirmation to their views.

Chlorine

The majority of the experiments were conducted with "Arochlor" (a chlorinated diphenyl) as a target and our work was confined to plotting an excitation curve. Two runs were made with chlorine gas following the procedure used for argon, with the results shown in Fig. 3. Only the general behavior should be inferred from this curve as the number of particles counted to a point was between one hundred and two hundred: the great chemical activity of chlorine gas renders this type of experiment unpleasant. The curve through the points is the thoretical function for penetration through a barrier of radius 6.0×10^{-13} cm integrated as for argon; it can be seen that although the points are rather scattered,

[6] J. R. S. Waring and W. Y. Chang, Proc. Roy. Soc. **157**, 652 (1936).

[7] W. Y. Chang and A. Szalay, Proc. Roy. Soc. **159**, 72 (1937).

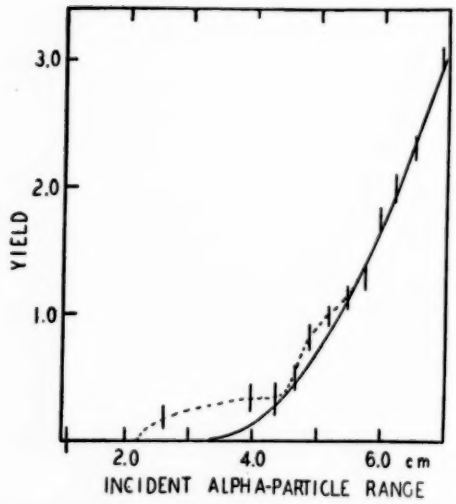

FIG. 5. Excitation curve for a thick layer of aluminum. The full line is the theoretical relation for a nuclear radius of 5.8×10^{-13} cm. The dotted line indicates possible resonance effects at 4.8 cm and 2.3 cm alpha-particle range.

the fit is good. In Fig. 4 is shown the results of bombarding a thick layer of "Arochlor" with both Th C′ and Ra C sources. The curve below 6.9 cm alpha-particle range is more accurately known although the certainty is considerably less than that for argon. A net count of between three and five hundred particles was made at each point. The curve through the points is the theoretical curve for a nuclear radius of 6.0×10^{-13} cm: the agreement is good and the fact that this is the same radius as found in Fig. 3 justifies the method of plotting excitation curves for gaseous targets. We suggest the value $6.0\pm0.5\times10^{-13}$ cm for the nuclear radius of chlorine.

The interpretation we originally gave for this process was the reaction:

TABLE II. *Nuclear radii.*

ELEMENT	NUMBER OF NUCLEAR PARTICLES (A)	$A^{\frac{1}{3}}\times1.94\times10^{-13}$	FOUND RADII (cm)
Al	27	5.80×10^{-13}	$5.80\pm0.3\times10^{-13}$
Cl	35	6.30×10^{-13}	$6.00\pm0.5\times10^{-13}$
A	40	6.63×10^{-13}	$7.60\pm0.3\times10^{-13}$

$$Cl^{37}+He^{4}\rightarrow K^{40}+n^{1}.$$

In view of the experiments of Hurst and Walke[3] and Ridenour and Henderson[4] it is certain that part of the neutrons are due to the reaction:

$$Cl^{35}+He^{4}\rightarrow K^{38}+n^{1}.$$

It is most probable that both processes occur.

Aluminum

A thick hemispherical target was bombarded at various alpha-particle ranges with the results shown in Fig. 5. Roughly four hundred particles were counted at each point. It can be seen that while no striking resonance effects are present, yet there may be small irregularities present as suggested by Waring and Chang.[6] The smooth curve drawn through the points is derived from the Gamow penetration formula for a nuclear radius of 5.8×10^{-13} cm. The agreement is satisfactory. We suggest limits of error of 0.3×10^{-13} cm.

Nuclear radii of light elements

Our results give us the values of the nuclear radii for aluminum, chlorine and argon. These should vary proportionally to the cube root of the number of particles (A) in the nucleus. The values found, are given in Table II together with the values of the expression $A^{\frac{1}{3}}\times1.94\times10^{-13}$ which fits the value for aluminum. It can be seen that the values found vary with respect to the calculated value; this is in part to be expected by reason of the possible errors: we feel, however, that the large value for argon lies beyond the limits of error and represents a real anomaly. This can be linked with the fact that argon has an unusually large excess of neutrons over protons.

It is a pleasure to thank Professor A. F. Kovarik for his interest and encouragement, and Mr. R. M. Ryder for assisting with the calculations of barrier penetration.

[3] D. G. Hurst and H. Walke, Phys. Rev. **51**, 1033 (1937).

An Improved Method for the Determination of the Specific Charge of Beta-Particles

C. T. ZAHN AND A. H. SPEES
Department of Physics, University of Michigan, Ann Arbor, Michigan
(Received January 15, 1938)

In the following article is described a method for the determination of the ratio e/m of beta-particles. The method represents a modification of the experiments of Bucherer and of Neumann in which the positions of the source and the detector are effectively interchanged and the photographic plate is replaced by a Geiger counter in a fixed position. A general discussion is given for the behavior of electrons in crossed fields inside a shallow condenser, and application is made to the special case here described. A semi-graphical procedure is then outlined for the determination of the shape and the intensity of the peaks to be observed by the Geiger counter as the voltage on the condenser is varied. The effect of scattering on such experiments and the importance of resolution calculations are then pointed out. In this latter regard the modified experiment appears to have considerable advantage over the original method of Bucherer. In fact, as a result of these considerations, doubts are raised as to the validity of the usually accepted interpretation of Neumann's experimental data at the higher velocities. A more complete discussion of the interpretations of the classical experiments of Neumann is promised for a later date. The possibilities of the method for measurements on electrons of very high velocities are discussed. Experimental results obtained by application of the present method to the determination of the specific charge of pure disintegration electrons will be given in the paper immediately following.

THE method here described was developed for the purpose of determining the ratio e/m for pure disintegration electrons as distinguished from the secondary, or discrete beta-particles.[1] As is well known, Bucherer's classical experiment consisted in placing a source of beta-rays at the center between the plane plates of a circular condenser in vacuum and then superimposing a uniform magnetic field parallel to the condenser plates. The crossed fields and the condenser plates form a velocity filter with a resolving power depending on the plate separation and on the length of path in the condenser. The filtered velocity depends on the ratio of the electric and the magnetic field intensities, E/H, and on the angle θ between the magnetic field and the radius of projection into the condenser ($v=cE/H \sin\theta$). After leaving the condenser the electrons are deflected in the magnetic field alone and finally produce a trace on a photographic plate. Each point on the trace corresponds to a different angle θ and hence to a different filtered velocity v. The deflection depends on the momentum of the electron, and the ratio e/m can be calculated very simply from the measured values of E, $H \sin\theta$, and the deflection. Neumann's modification consisted in working with only one velocity at a time, with the magnetic field and the electron path mutually perpendicular ($\theta=\pi/2$). Hence he placed a source at the end of a rectangular condenser.

For the above-mentioned purpose it was thought that the use of a Geiger counter as detector might eliminate the inconveniences and the inaccuracies of the photographic method as well as permit the use of weak sources. A Geiger counter, used simply in Neumann's arrangement to replace the photographic plate, would have to be moved about to explore the region covered by the plate. This would cause considerable inconvenience, particularly if it were necessary to use the counter in vacuum, as in the case of beta-rays of low energy. It will, however, be seen in the sequel that these difficulties, as well as other serious limitations of the Bucherer-Neumann method, can be successfully eliminated by the use of the following modification. The method consists essentially in interchanging the positions of the source and the detector. The source S, Fig. 1, is placed some distance from the first end of the condenser plates and somewhat below the central plane; and the rays transmitted are detected by means of a Geiger counter G placed at the other end, or at any distance along the appropriate circular arc drawn from the condenser. The electrons will be transmitted only when, on their arrival at the entrance to the condenser, they are directed approximately

[1] For preliminary results see C. T. Zahn and A. H. Spees, Phys. Rev. **52**, 524 (1937).

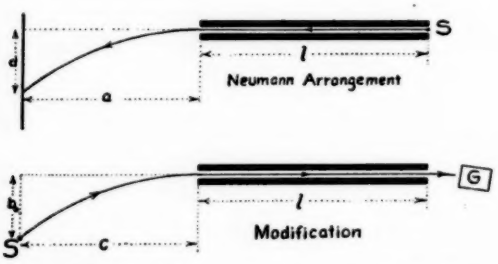

FIG. 1. Arrangement of source and detector in the Neumann experiment and in the present modification.

along the central plane and when at the same time the electric field is so adjusted that their velocity $v=cE/H$. The relative geometry of the source and the condenser specifies within a certain small tolerance a momentum $H\rho$, and the observed value of E permitting transmission serves to determine the velocity associated with this momentum. Here the momentum is selected first, and then the velocity is measured; whereas in the Bucherer experiment the velocity is selected first and then the momentum is measured.

With this modification the geometry is kept fixed, and all the geometrical calibrations can be made once for all, after which all subsequent measurements can be made exclusively by the use of electric meters and the Geiger counter. With this fixed geometrical arrangement one can then obtain extremely accurate *relative* measurements independent of all geometrical factors; whereas in the photographic method all individual results are subject to errors in the microphotometric measurements on rather poorly resolved lines. Electrons of various values of the momentum $H\rho$ can be studied simply by varying H. A further simplification is provided by the fact that an experiment may be repeated at will without the necessity of opening the vacuum chamber as in the photographic method.

Other advantages are to be seen in connection with certain objections which have been raised from time to time against the interpretations of the Bucherer-Neumann data. As will be remembered, a long discussion between Bestelmeyer and Bucherer centered around the question as to whether the limited resolving power of the condenser could cause a dissymmetry in the line density on the photographic plate, sufficient to displace the observed maximum appreciably from the theoretical position corresponding to perfect resolution. Bucherer made some calculations for the case $\beta=0.3$ and found no serious dissymmetry, but he does not seem to have made similar calculations for the higher velocities—although it is just at the higher velocities that one would expect such difficulties, and although in fact he (as did Neumann later) found it impossible to obtain sharp traces for $\beta>0.8$, because of a spreading and fogging of the photographic line! It is clear that the resolution should become poorer as the velocity increases and that one should expect just such a limitation as was observed. Therefore the question raised by Bestelmeyer still seems pertinent, at least for the higher velocities; that is, for velocities near the region where the resolution becomes poor. It is of further interest to note that Neumann, after repeating Bucherer's measurements with slight alterations, stated that: for $\beta<0.7$ the agreement with the relativity theory was satisfactory, but that for $\beta>0.7$ the data showed a definite trend from the theory, it not being quite clear whether or not the discrepancy was within the limits of experimental error. Later Schaeffer, after remeasuring Neumann's plates with an improved microphotometer, seemed satisfied that the small systematic discrepancies could be explained by imperfections in the original photometric measurements. Nevertheless, not until a thorough theoretical investigation of the system of rays in such an experiment is made, will it be possible to state definitely within what limits of error and over what region of velocities the theory of relativity has been verified experimentally by Neumann's results. It is desired here simply to point out the difficulties in interpretation associated with Neumann's data and the improvement achieved in this regard by the use of the present modification. A complete analysis of the electron "optics" of the *modified* experiment will be given in the following. A similar treatment of the Bucherer-Neumann apparatus will, however, be deferred to a later article, in which it is planned to give a critical discussion and interpretation of Neumann's results.

In the interpretation of Neumann's data an idealized theory was used, which takes into account neither the imperfect resolution of the apparatus nor the possibility of scattering from the condenser plates. The possibility of scattering

has been mentioned, but it was assumed, with questionable justification, that the scattering is of negligible amount, or at least that it is so spread out after reaching the photographic plate as to be of negligible, or of uniform density in the region of the line. Now it is well known that a considerable number of electrons is scattered diffusely from material surfaces. The coefficient of diffuse back-scattering may, in fact, vary from 10→80 percent, depending on the incident energy and roughly on the density of the scatterer. For silver it is of the order of 40→60 percent, and for aluminum or glass, 10→40 percent. With such high reflection coefficients it seems possible, in an arrangement like that of Bucherer, that a very considerable amount of multiply scattered radiation could emerge from the condenser in addition to that expected on the idealized theory in which it is assumed that all electrons are absorbed after impinging on the condenser plates. In fact, it does not seem impossible that for heavy scatterers the multiple reflections could produce a scattered component much greater than the direct component. It might at first seem that scattering would not cause serious difficulty, since, even after scattering and the accompanying energy reduction due to range depth in the scatterer, the particles would still not escape from the condenser unless they had the proper velocity for compensation. But it should be remembered that the scattering will occur at all points along the condenser plates, and that for points near the exit the resolution becomes very poor, since the effective path length is small. Hence, while the intensity of the beam may be considerably enhanced by the presence of scattering, the effective resolving power may be greatly reduced. Scattering would then tend to aggravate the difficulties associated with limited resolving power, and to a degree that is difficult to estimate.

This resolution difficulty will exist for any actual experiment; and, if one should wish to extend the region of experimental verification of the theory of relativity to higher velocities, one would finally be limited accordingly. It is therefore of importance first to increase the ideal resolving power to the greatest possible value consistent with intensity requirements, and then to eliminate scattering insofar as is possible. In view of these considerations it will be seen that the present modification offers considerable advantage over the original method. First, by the use of the Geiger counter it should be possible to work with lower intensities (neglecting the undesirable increase due to scattering) and therefore with higher resolving power. Further, it may be noted that in Neumann's experiment, for example, about one-half the total radiation from the source enters the condenser space, while only about *one ten-thousandth* of this can possibly be transmitted directly to the photographic plate, the rest being absorbed or scattered. On the other hand, with the present modification, since the source is some distance from the condenser opening, the amount of radiation entering the condenser may be of the same order of magnitude as that which can be transmitted when the electric field is adjusted for a peak; and in fact, by the use of auxiliary slits any desired momentum resolution can be obtained. Also by placing the counter at some distance along the circular arc from the condenser and using further defining slits at the proper points, one can obtain a double momentum resolution and at the same time reduce the scattered component of radiation entering the counter. Scattering will, of course, not be entirely eliminated even here; for when the electric field is not adjusted for a peak, the electrons will impinge on the condenser plates; but the effect of scattering will obviously be greatly reduced when compared to that in the Bucherer experiment. Further, it is possible by the use of the auxiliary slits to restrict the momentum interval of the electrons so that when the condenser voltage is adjusted for a peak, there will be no scattering at all, since all the beam will pass freely through the condenser. Under these circumstances the chief effect of scattering will occur at voltages some distance on either side of the peak. On the other hand, in the Bucherer experiment, the scattered radiation is distributed all over the peak; and, in fact, it is possible that the peak intensity itself may be largely due to scattered radiation of various degrees of resolution.

Electrons in Crossed Fields

In studying electron paths in crossed fields it is a simple matter to obtain certain general rela-

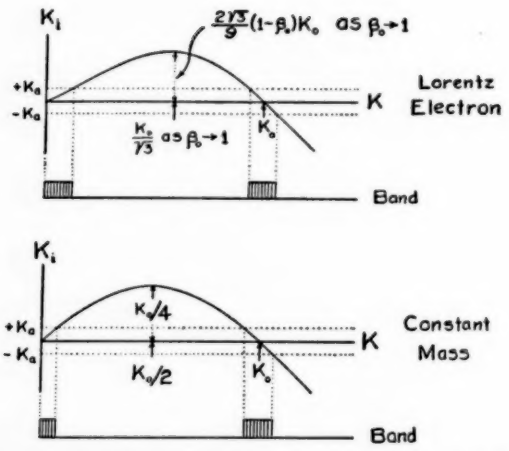

FIG. 2. The curvature of the electron path inside the condenser for constant electric and magnetic field but for various values of the curvature of the electron path in the magnetic field alone.

tions which apply to cases where the condenser separation is small compared with its length. The force is then always very nearly perpendicular to the direction of motion, *for those electrons* which eventually pass all the way through the condenser; and therefore the velocity and the mass are invariant under the motion. The equation of motion may then be written:

$$mv^2k_i = Hev - ceE, \tag{1}$$

where m is the mass of the electron; v, its velocity; and k_i, the curvature of the trajectory inside the condenser. To a close approximation the electrons in question will describe circular paths of curvature k_i. One may further write:

$$mv^2k = Hev, \tag{2}$$

where k is the curvature the electron path would have in the magnetic field alone, and therefore a measure of the reciprocal of the momentum of the electron. If one further writes $cE/H \equiv v_0$, which is the velocity for which (1) vanishes, or the velocity for which the forces are compensated, it then follows from (1) and (2) that:

$$k_i/k = 1 - v_0/v \tag{3}$$

If the relation between the mass and the velocity is known, it will be possible in general to express k_i as a function of k and k_0 alone. For Lorentz electrons, for which $m = m_0/(1-\beta^2)^{\frac{1}{2}}$, it follows that:

$$k_i = k[1 - ((A^2+k^2)/(A^2+k_0^2))^{\frac{1}{2}}], \tag{4}$$

where $A = eH/m_0c$. For electrons of constant mass it would follow that:

$$k_i = k[1 - k/k_0]. \tag{5}$$

(The latter case was of special interest in connection with certain speculations mentioned in a previous Letter to the Editor, and to be discussed in the paper immediately following.)

It will therefore be seen that the resolution characteristics will depend on the particular type of variation of mass with velocity, and that a relativity distribution of electrons, with constant rest mass, may have a different resolution width from that of a distribution of constant actual mass.

Qualitative considerations: The general behavior of a shallow condenser in crossed fields may be understood by considering the relation (4), or (5). Two special cases are of interest: (*a*) k_0 fixed and k variable, as in the Bucherer experiment, and (*b*) k fixed and k_0 variable, as is approximately the case for the modified experiment.

Case (*a*) k_0 *fixed.*—With k_0 fixed; that is, with E and H fixed, one can determine the behavior of the velocity filter for a distribution of varying k. The relations (4) and (5) will have the general characteristics shown in Fig. 2. As the velocity increases beyond v_0 (i.e., $k < k_0$) a maximum value of k_i is reached, after which k_i falls to zero, for $v = c$ in the case of Lorentz electrons, and for $v = \infty$ in the case of constant mass. A simple consideration of the geometry of the condenser will show that there is a maximum value of $|k_i| \equiv k_a$, for which electrons could be transmitted at all. This maximum value will correspond to the special initial conditions indicated in Fig. 3. Whenever $|k_i| > k_a$ the electron can definitely *not* be transmitted; but if $|k_i| \lesssim k_a$ the electron has a possibility of being transmitted, provided that the initial conditions at entrance

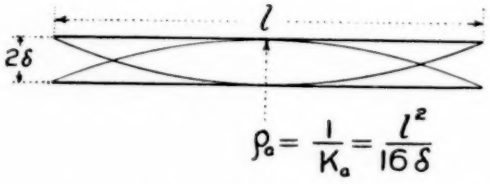

FIG. 3. Geometrical conditions which show that there is a maximum value of $|k_i| = k_a$ for which electrons can be transmitted.

to the condenser be suitable. If $k_a \ll k_0$ one sees from Fig. 2 that the condenser may transmit electrons only in two small bands, one around $k=k_0$, and another around $k=0$ (i.e., high velocity). The latter band around $k=0$ will usually be of no importance, unless it becomes very wide. As k_a is made smaller, by proper choice of the condenser geometry (see Fig. 3), the band narrows down and the resolution improves. But if k_a becomes larger one may reach the condition shown in Fig. 4, where the condenser behaves as a "by-pass" filter for all velocities greater than a velocity slightly less than v_0. Under these conditions the condenser cannot be regarded as a filter for a small band around $k=k_0$. It may also be noted that as k_a is decreased it requires smaller k_0 for a given required resolution; that is, for higher velocities the resolution becomes poorer with a given k_a.

From these considerations of the case (*a*) one sees clearly the imitations of the Bucherer experiment. In fact, when either k_a becomes too large, or v_0 becomes too large, the band around $k=k_0$ spreads out to meet the band around $k=0$, and the resolution becomes infinitely bad on the side of the higher velocities, while remaining only fairly good on the lower side.

Case (*b*) *k fixed.*—In the case of the modified experiment one may regard k as approximately fixed within the small limits defined by the narrow momentum interval. Then one is interested in the variation of k_i with k_0 where k_0 is varied by varying the electric field E. This variation is shown in Fig. 5 for two neighboring values of k, corresponding to the limits of the momentum selection before reaching the condenser. The shaded rectangle represents the band in k_0 for which transmission is potentially possible (*but further* contingent upon the proper choice

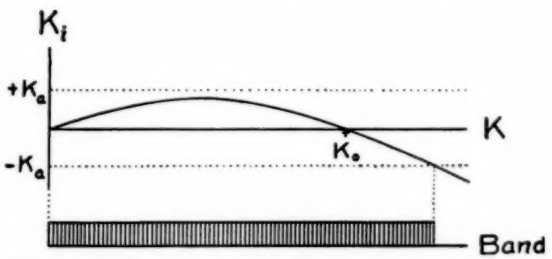

FIG. 4. Conditions under which the condenser system behaves as a "by-pass" filter for velocities greater than a velocity slightly less than v_0.

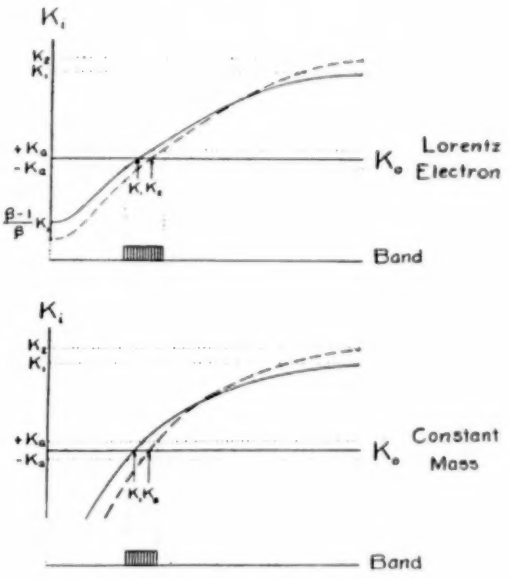

FIG. 5. Variation of k_i with k_0.

of initial conditions at entrance into the condenser). A comparison of these curves with those of Fig. 2 shows the decided advantages of the modified arrangement as regards resolution. Whereas in the Bucherer experiment k_i has a definite maximum in the interval $k=0 \rightarrow k_0$; in the present case k_i increases steadily with k_0 and approaches the value k assymptotically. Nothing appears here corresponding to the high velocity band around $k=0$ in the former case. Besides, the over-all spread in k_i, for example, in the simple case of constant mass is $-\infty \rightarrow k_0/4$ in the former case; and $-\infty \rightarrow k$ in the latter, which indicates that k_a may be much larger in the latter case and still give good resolution. The same is true of the case with Lorentz electrons. In addition, here the behavior around $k_0=k$ will be much more nearly symmetrical than that around $k=k_0$ in the Bucherer experiment.

CONDITIONS FOR CUT-OFF

Up to the present one has considered simply the overall limits of k, or of k_0 permitted by the geometry of the condenser alone; but transmission will be further contingent on the actual initial conditions at entrance into the condenser. The position of the source will in general determine these initial conditions, but it will be of more general use to determine the cut-off conditions in terms of the initial conditions them-

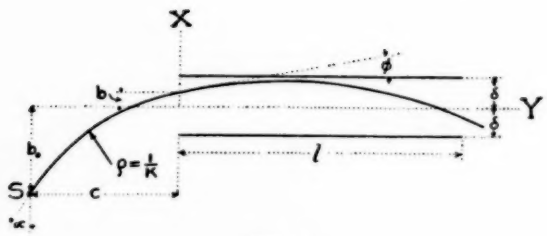

FIG. 6.

selves, regardless of how the source may give rise to them. One can specify the initial conditions in terms of b and ϕ (of Fig. 6), where b represents the distance of the point of entrance above the central plane of the condenser; and ϕ, the angle between the initial direction of motion and the same plane. The equation of the trajectory of the electron may be written, for small deflections and in the interval inside the condenser space, as:

$$x=b+\phi y-k_i y^2/2 \quad \text{for} \quad 0\leqq y\leqq l.$$

It is then easy to show that the conditions for cut-off may be written:

(I) $+\delta\leqq b\leqq -\delta$ (cut-off at entrance),
(II) $+\delta\leqq b+\phi l-l^2k_i/2\leqq -\delta$ (end cut-off),
(III) simultaneously: $0\leqq \phi/lk_i\leqq l$ and
$+\delta\leqq b+\phi^2/2k_i\leqq -\delta$,

which latter pair of simultaneous conditions expresses the fact that there is an extremal value of x between the two ends of the condenser and that at the same time this extremal value itself is outside the interval of the condenser space, or outside the interval $+\delta\leqq x\leqq -\delta$.

These conditions involve the three variables b, ϕ, and k_i; and, if one uses the previous relation between k_i and k, they may be expressed in terms of b, ϕ, and k. They are generally applicable, and if one specifies the position of the source at $y=0$ and $x=b$, they refer to the conditions of the Bucherer-Neumann experiment. If, on the other hand, one places a source in front of the condenser, as in the modified arrangement of Fig. 1, the variables b, ϕ, and k are no longer independent. In fact, for small variations around the central ray it is easily seen that;

$$\phi=-k'c-\alpha'(1-b_0k_{00}), \tag{6}$$

$$b=-k'b_0/k_{00}-\alpha'c, \tag{7}$$

where $\alpha'\equiv\alpha-\alpha_{00}$ and $k'\equiv k-k_{00}$; whence also:

$$\phi=b(1-b_0k_{00})/c-k'b_0/k_{00}c. \tag{8}$$

Any two of the four variables ϕ, b, α', and k' will suffice to specify the trajectory completely; but since b and k' enter rather simply into the cut-off conditions, it is convenient to choose these as the independent variables. Now, for any given value of k', or for any given momentum, there will be a definite interval in b for which rays are transmitted; and because of the linear relationship (7) this interval in b will be proportional to the corresponding interval in α'; that is:

$$\Delta b=-c\Delta\alpha', \text{ for constant } k'. \tag{9}$$

But the interval $\Delta\alpha'$ is a measure of the relative intensity of rays transmitted with momentum specified by k', if one assumes that the source is isotropic and its distribution function is practically constant throughout the small interval in k' permitted by the apparatus. According to (9) then, so also is Δb a measure of the relative intensity of the same rays. The problem of determining the actual intensity-momentum band transmitted for given values of E and H resolves itself into determining Δb as a function of k'.

In order to apply the cut-off conditions it is necessary to specify k_i in terms of k. For Lorentz electrons the relation (4) holds; and for electrons of constant mass, relation (5). (It may be recalled that k_{00} refers to the central ray defined by the position of the source relative to the condenser; and k_0, to the compensated value of k specified by the ratio E/H.) In either of the above two cases, since the interval in k' is assumed small, one may write:

$$k_i=B(k-k_0), \quad \text{where } B=(\partial k_i/\partial k)_{k=k_0}.$$

Then, if $k_0-k_{00}\equiv\Delta$, it follows from the definition of k' that $k_i=B(k'-\Delta)$. Δ is then a measure of the amount that the condenser voltage is off adjustment for the peak of transmission. For Lorentz electrons it can be shown that $B=-(1-\beta_0^2)$; while for the case of constant mass, $B=-1$.

These relations, taken together with the cut-off conditions and the source conditions, should suffice to determine the momentum distribution of electrons for given values of Δ, and hence one can determine the value of Δ at which absolute cut-off occurs. For this purpose the cut-off con-

ditions may be rewritten as follows:

$$\text{(I)}\quad +\delta \lessdot b \gtrless -\delta,$$

$$\text{(II)}\quad +\delta \gtrless b[1+(1-b_0k_{00})l/c] - k'[lb_0/k_{00}c+l^2B/2]+l^2B\Delta/2 \gtrless -\delta,$$

$$\text{(III)}\quad (a)\ 0 \lessdot \{b(1-b_0k_{00})/c - k'(b_0/k_{00}c)\}/B(k'-\Delta) \gtrless l,$$

$$(b)\ +\delta \gtrless b+[b(1-b_0k_{00})/c - k'(b_0/k_{00}c]^2/2B(k'-\Delta) \gtrless -\delta.$$

Conditions (I) and (II) restrict transmission to a parallelogram in the b, k' plane, and (III) further restricts it to a space lying inside two hyperbolae unless at the same time outside two wedgeshaped spaces defined by the two straight lines implied by (III) (*a*). An example of this restricted area is shown in Fig. 7 for $\Delta=0$. The allowed values of b, k' are those contained inside the heavy closed curve, and the spread Δb for any given k' is given by the section of the line, $k'=$constant, lying within the restricted area. The total intensity of radiation transmitted for the given value of Δ is proportional to the area inside the same curve. As Δ varies the restricted area decreases until finally for a certain value $\pm\Delta_m$ the whole region is excluded and no transmission is further possible. The values of this integrated area, plotted against the value of Δ show the shape of the peak to be observed by the Geiger counter as the voltage on the condenser is varied. (From the form of the cut-off conditions it is easily seen that in general this curve will be symmetrical around $\Delta=0$.) In the particular case shown in Fig. 7 the restricted area departs from the parallelogram only very slightly, and the extremal type of cut-off plays an unimportant role; but for other values of Δ the extremal cut-off may play the predominant role.

The particular type of cut-off which predominates for the value of Δ at which absolute cut-off occurs may depend on the particular problem, so that further generalizations become difficult to express in concise form; but *for particular cases* it is not too laborious a task to carry out graphically the method outlined above. (The integrated restricted areas can be conveniently obtained by the use of a planimeter.)

In this way one can determine whether the resolution width in k' is really sufficiently small to prevent shifts in the peak due either to the k_i,

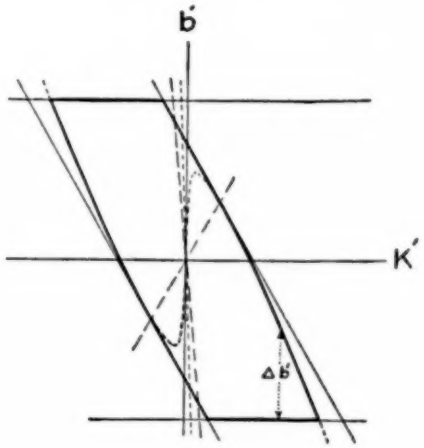

FIG. 7.

k relationship or to variations in the source intensity with k. Considerations of the latter type are of much greater importance in connection with the Bucherer experiment, where (as will be pointed out in a future discussion) it is possible to obtain focusing effects which may conceal a very poor resolving power, indeed, and permit large shifts in the density maximum of the photographic line. Such a determination of the expected shape of the observed peaks should also serve to distinguish between effects due to the direct and the scattered components of the radiation detected.

FOCUSING EFFECTS

The equation of the trajectory inside the condenser, expressed in terms of b and k', becomes for the modified experiment:

$$x=b[1+(1-b_0k_{00})y/c] - k'[b_0y/k_{00}c+By^2/2]+B\Delta y^2/2.$$

From this one sees that if

$$y=y_1\equiv -c/(1-b_0k_{00}),$$

then x is independent of b, which means that all rays of the same energy, if continued backward with the same curvature k_i, will be congruent at a point on the line $y=y_1$ and of ordinate varying linearly with k' and Δ.

On the other hand, if

$$y=y_2\equiv 2b_0/(-Bk_{00}c),$$

then x is independent of k' and varies linearly with b and Δ, which means that an image of the front end of the condenser is projected on the

plane $y=y_2$, provided $l \leq y_2$, and with a magnification given by the coefficient of b and a shift proportional to Δ. These relations suggest graphical methods, but in order to obtain reasonable accuracy it would require apparatus of unwieldy proportions.

Resolution Limits at High Velocities

The actual spreads in k' and Δ can be obtained by the above method; but one can obtain an approximate idea of the behavior of the apparatus with increasing velocity β by considering the absolute over-all limits $k_i = \pm k_a$, *defined by the geometry of the condenser alone.* In general the actual resolution width will be somewhat smaller than that estimated in this way, so that such considerations will give an upper limit to the resolution width (since the source conditions further restrict the spreads involved). If one assumes that all the increments around the central compensated ray are small, then in general:

$$dk_i = (\partial k_i/\partial k_0)_{k_0=k} dk_0 + (\partial k_i/\partial k)_{k=k} dk = \pm k_a,$$

where one can set $k_0 = k_{00} = k$. (See Fig. 5.) If one remembers that also dk is limited by the same values $k_i = \pm k_a$; that is, $dk = \pm k_a/(\partial k_i/\partial k)_{k=k}$ then one sees that

$$(\partial k_i/\partial k_0)_{k_0=k} dk_0 = \pm 2k_a$$

or $dk_0 = \pm 2k_a/(\partial k_i/\partial k_0)_{k_0=k} = \pm 2k_a/(1-\beta_{00}^2)$

or the over-all spread $\Delta k_0 = 4k_a/(1-\beta_{00}^2)$. This provides an upper limit to the spread Δk_0 in terms of k_a and β, and for the case of Lorentz electrons.

One can also show, for Lorentz electrons, that

$$\Delta E/E = (1-\beta_0^2)\Delta k_0/k_0 = (1-\beta^2)\Delta k_0/k$$

and from the preceding relation that

$$\Delta E/E = 4k_a/k,$$

which shows that this absolute upper limit of the resolution width is independent of β. But it must be remembered that $\partial k_i/\partial k_0$ and $\partial k_i/\partial k$ were assumed constant over the intervals in question. In order that this be true β cannot be too near unity, since with increasing velocity the negative intercept of the curve of Fig. 5 approaches zero. From the figure one sees that the positive limit of k_i is always equal to $+k$; and the negative limit, to $-k(1-\beta)/\beta$. Therefore, in order to insure fairly small resolution width, as well as approximate symmetry around k, it will suffice to have $k(1-\beta)/\beta$ considerably larger than k_a. As a practical expression of this fact one might choose the limiting ratio between the negative intercept and k_a to be some number p which may be regarded as a "factor of safety:"

$$k(1-\beta)/\beta k_a = p$$

or $$\beta = 1/(1+pk_a/k) \underset{\beta \to 1}{\rightarrow} (1-pk_a/k).$$

In this way the limiting value of β is expressed simply in terms of k_a and k, both of which quantities are limited by practical geometrical considerations. k is limited by the fact that the source has a finite extension relative to which b_0 must be large; whereas $k_a = 16\delta/l^2$ and hence is simply related to the geometry of the condenser. In Table I are shown the limiting values of β for different values of k/k_a, and for the two cases $p=5$ and $p=2$. In addition, the corresponding values of $H\rho$ and the kinetic energy of the electron are given. (For $p=2$ one should expect a rather large resolution width, but even for such a case one could probably calculate the errors caused by the resulting dissymmetry and the momentum distribution of the source,—if one wished to extend such experiments to the extreme limit of high velocities.)

In a particular application of the present method (to be described in the following experimental paper) the value of k/k_a was approximately 25, and with this arrangement one millicurie of radium E was found more than sufficient to locate the peak for $\beta = 0.75$. It therefore seems definitely possible that an extension of the method to considerably higher velocities could be achieved by increasing the ratio k/k_a and using sources of greater intensity. There will, however, be various practical limita-

Table I. *Limiting values of β for different values of k/k_a for $p=5$ and $p=2$.*

	$p=5$			$p=2$		
k/k_a	β	$H\rho$	(Mev)	β	$H\rho$	(Mev)
25	0.83	2550	0.4	0.93	4350	0.9
50	0.91	3750	0.7	0.96	5850	1.3
100	0.95	5100	1.1	0.98	8450	1.8
250	0.98	7450	1.8	0.992	13400	3.5

tions. For example, as $\beta_0 \rightarrow 1$

$$H\rho_0 \rightarrow 1705/(1-\beta_0^2)^{\frac{1}{2}}.$$

Hence, for a given value of $\rho_0 = 1/k_0$, H increases rather rapidly. On the other hand, since $\beta_0 = E/H$, one sees that, as $\beta_0 \rightarrow 1$, E becomes proportional to H, approximately. Therefore, for a given value of ρ_0, E and H will increase approximately in the same ratio. In addition to the latter conditions there are also intensity requirements, which will probably be the final practical factor in such experiments. While it is at present difficult to predict how far it would be feasible to extend these experiments, it is quite clear that the present method offers the possibility of carrying the study of the variation of electron mass to higher energies of the order of ten times those used in the Bucherer-Neumann experiments.

In conclusion the authors wish to acknowledge support from the Horace H. Rackham School of Graduate Studies of the University of Michigan.

MARCH 1, 1938 PHYSICAL REVIEW VOLUME 53

The Specific Charge of Disintegration Electrons from Radium E

C. T. ZAHN AND A. H. SPEES
Department of Physics, University of Michigan, Ann Arbor, Michigan

(Received January 15, 1938)

Rough preliminary measurements of the ratio e/m for the pure primary beta-particles from radium E and of momentum about 2000 $H\rho$ were described in a recent Letter to the Editor. The present article includes a more detailed description of these results as well as of more accurate results obtained with an improved experimental arrangement. In order to ascertain the origin of the side-peaks observed by the former measurements, in the new apparatus the resolving power was increased by doubling the length of the electric condenser, and the scattering was reduced by the use of aluminum for the construction of the condenser. In addition several auxiliary defining slits were inserted at points along the electron path, and all calibrations were rechecked so that the central peak could be located with moderate accuracy. In the preliminary measurements no special attempt had been made toward great accuracy, since the apparatus was designed primarily to distinguish between ordinary Lorentz electrons and the widely differing special type of heavy electrons required by the *speculation* that the well-known beta-ray paradox might be explained by variations, with velocity, of the rest mass of the electrons created in the nucleus, rather than by the neutrino hypothesis. With the improved apparatus extremely sharp peaks were observed by means of the Geiger counter, showing that the method described in the preceding article offers the possibility of very accurate determinations of the ratio e/m. The side-peaks were greatly reduced in height and separation, as compared with those in the preliminary experiments; and with variations in the slits behaved in such a way as to indicate that they are due to scattering from the condenser plates, as previously suspected, or possibly to small nonuniformities in the magnetic field. In any case the latter variations in the side-peaks were found to have no appreciable influence on the position of the central peak, and the side-peaks are therefore of no serious consequence. Further, an analysis along the lines indicated in the preceding article was carried out for the detailed resolution characteristics in this particular case, and it was found that no side-peaks should be expected in the absence of scattering, although second degree equations do occur in the cut-off conditions for the source-condenser system. The central peak was found to be so sharp that it was possible to locate it without difficulty to within 1/10 percent of the voltage at the peak. In fact, the accuracy in determining the peak voltage was limited, in the present arrangement, rather by fluctuations in the magnetic field and in the battery voltage. Similarly, the absolute determination of e/m was limited rather by the accuracy of calibrations, both electromagnetic and geometrical. In the present arrangement no special aim was made toward accurate absolute results to better than one or two percent, but the method offers the possibility of considerably greater accuracy; and if one requires only relative values of e/m, the same accuracy could be obtained without special precautions as to the calibrations. In addition, one is here free from the grave uncertainties (to be discussed in a later article) associated with the possibility of scattering in the Bucherer-Neumann experiments. The final corrected value of e/m was found to be in agreement with the theory of relativity to within 1½ percent, which is well within the limits of experimental error. *The above-mentioned speculations as regards the special type of heavy electron are therefore untenable.*

IN a previous Letter to the Editor[1] a brief description was given of a method for the determination of the ratio e/m for beta-particles, and at the same time preliminary results obtained by the use of this method were reported

[1] C. T. Zahn and A. H. Spees, Phys. Rev. **52**, 524 (1937).

for the beta-rays of radium E of momentum about 2000 Hρ. It was there mentioned that cloud chamber experiments of H. R. Crane and J. J. Turin[2] had suggested the possibility that primary beta-particles may have greater energy than that conventionally indicated by the curvature of their paths in a magnetic field, or by their momentum. This would require that their masses be different from the conventional mass $m_0/(1-\beta^2)^{\frac{1}{2}}$. An examination of the literature showed that Bucherer's and Neumann's classical experiments[3] for the determination of the ratio e/m of beta-particles had been made at a time when the differences in origin of the primary and the secondary particles had not yet been understood; and that the rays studied by these experimenters consisted chiefly of the secondary, or discrete beta-particles from radium and its equilibrium products. It then appeared that no actual experiments on the specific charge of the actual disintegration electrons had ever been made, after the identification of the latter with the continuous beta-rays.

The question of a possibly different rest mass for the primary beta-rays is closely connected with the well-known beta-ray paradox which led to the hypothesis of the neutrino. Lacking any definite experimental evidence to the contrary, one is tempted to make the speculation, that after all the neutrino hypothesis may not be necessary if the rest mass of the beta-particle were different from the conventional m_0. If one gives up the neutrino and still insists on the conservation of energy and a definite disintegration energy W, then by Einstein's principle of equivalence the *actual* masses of the electrons would all have the same value $W/c^2 \equiv M = M_0/(1-\beta^2)^{\frac{1}{2}}$, no matter what the velocity of emission of the particle. This would require that the beta-particle be a very special kind of electron, whose rest mass depended on the velocity of emission in such a way that $M_0=(W/c^2)(1-\beta^2)^{\frac{1}{2}}$; that is, the rest mass of the slower electrons would be greater than that of the faster ones. If it further be assumed that the upper limit of the beta-ray energy, as *conventionally* calculated from the upper limit of the experimental momentum distribution, really represents the disintegration energy, and hence at the limiting energy there is no mass anomaly, then $M_0=m_0$ at the upper limit and $M_0>m_0$ for all other particles of the spectrum. Hence the electrons required by these speculations would be "heavy."

It need not be pointed out that there would be no violation of the theory of relativity involved here. It would simply mean that in the particular process of creation of beta-particles these particles would be created with such values of rest mass as to give them always the same actual mass, independent of their velocities at creation. The effect on certain experiments, however, would be the same as if one had a velocity distribution of particles of constant mass M, and the theory of relativity were not applicable. For example, this would be the case in experiments where the velocity remains constant in magnitude, as for electrons in magnetic fields or in electric fields which are perpendicular to the direction of motion. These latter conditions hold approximately for the case of electrons inside a condenser of small plate separation compared to the length, provided that one consider only such electrons as can pass all the way through the condenser. These same conditions are precisely the conditions which obtain for the Bucherer experiment and for the modification described in the preceding article.

It was also thought not impossible that the extra rest mass here involved might in some way be associated with abnormal values of the spin coordinate; and that the heavy electron might be created in metastable states, so that they need not return to normal until after a long time or after infrequent processes of "nuclear proportions;" and that therefore the extra energy might not be observable in the classical calorimeter experiment.

Inasmuch as no observations on the specific charge of actual disintegration electrons seemed to have been made, it was thought of importance to make at least a few observations of this kind and at the same time to keep in mind the values of e/m to be expected both in the case of conventional Lorentz electrons and in the case of

[2] See reference to Crane's report on the possible difference between nuclear beta-particles and electrons, G. Breit, Third Washington Conference on Theoretical Physics, Rev. Sci. Inst. **8**, 141 (1937).

[3] A. H. Bucherer, Ann. d. Physik, **28**, 513 (1909), G. Neumann, Ann. d. Physik, **45**, 529 (1914).

the above-mentioned speculations. In the latter of the two cases one would expect the greater departures from the ordinary value of e/m to occur at the lowest velocities of the spectrum. Therefore it would be desirable to measure e/m at the lowest velocity consistent with limitations of the apparatus due to absorption in windows, etc.

Preliminary measurements were made, applying a method fully described in the preceding paper, on the beta-rays from radium E and of momentum approximately 2000 $H\rho$. The latter momentum is sufficiently far from the upper limit of the spectrum that the observed heavy mass should have been about twice the value for normal electrons, if the above speculations were valid. For this purpose a carefully machined brass condenser, of 6 cm length and 0.5 mm plate separation and with quartz separators was used. The source was in the form of a nickel wire 1 cm long and 0.5 mm thick and covered with a radium E deposit of approximately 1 millicurie strength. This source was placed about 5.5 cm from the front end of the condenser and 1 cm below the central plane, corresponding to the value $\rho_{00}=16$ cm. (See preceding article for definition of constants.) The condenser and the source were placed in a vacuum chamber inside a pair of 18-inch water-cooled Helmholtz coils providing a magnetic field of 125 gauss (that is $H\rho_{00}=2000$). These coils were calibrated and tested for uniformity of field in the usual manner by means of a carefully wound exploring coil, a standard mutual inductance, and a ballistic galvanometer. A supply of voltages up to 2000 was provided for the condenser by small B batteries, and the voltage was measured by means of a carefully calibrated Jewell voltmeter with extra resistances. After leaving the condenser the rays passed through an aluminum window (of thickness 2 mils) on leaving the vacuum chamber, and then into a bubble counter provided with a scale-of-eight thyratron recording circuit.

Measurements with this preliminary arrangement were briefly described in the above-mentioned letter.[1] An example of the latter measurements is shown in Fig. 1, where the number of electrons recorded per minute by the Geiger counter is plotted against the condenser voltage V. The two arrows on the voltage axis

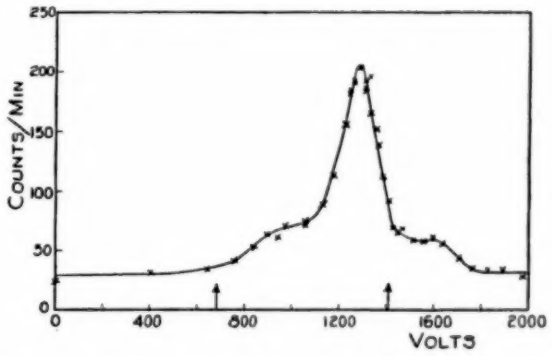

FIG. 1. Preliminary results showing number of electrons recorded per minute as a function of the condenser voltage.

indicate roughly the expected value of "peak" voltage for the two cases in question.

The latter values are calculated as follows. Assuming conventional mass at the upper limit of the spectrum, one obtains the disintegration energy W from the ordinary relativity relation between total energy and momentum:

$$W^2=c^2P_m^2+m_0^2c^4$$

or

$$W^2=c^2e^2(H\rho)_m^2+m_0^2c^4,$$

where P_m and $(H\rho)_m$ refer to the upper limit of momentum. For radium E the total energy at the upper limit is taken as 1.66 Mev; or the kinetic energy, as 1.15 Mev.[4]

Now the apparatus specifies a definite $H\rho_{00}$ independently of the values of mass and velocity. Hence the ratio of the masses in the two cases will be given by the inverse ratio of the observed velocities. For ordinary electrons one would have:

$$\beta_1=H\rho/[(H\rho)^2+(m_0c/e)^2]^{\frac{1}{2}}$$

and for the special type of heavy electron:

$$\beta_2=H\rho e/cM=H\rho ce/W$$

whence it is easily seen that

$$(\beta_1/\beta_2)^2=[(H\rho)_m^2+(m_0c/e)^2]/[(H\rho)^2+(m_0c/e)^2].$$

With $H\rho=2000$ and $(H\rho)_m=5280$ one obtains: $\beta_1=0.74$; $\beta_2=0.35$; and $\beta_1/\beta_2=2.1=M/m_1$. Since for a constant magnetic field H the velocity for the compensated electrons is proportional to the electric field E, the value of the condenser voltage at which one should expect a peak is inversely proportional to the mass of the electron of the given momentum $H\rho$.

[4] E. M. Lyman, Phys. Rev. 51, 1 (1937).

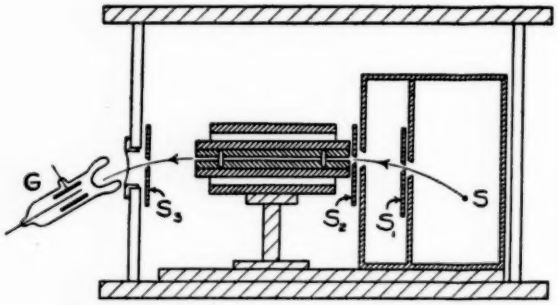

FIG. 2. Schematic diagram of the apparatus.

As was previously pointed out these preliminary data indicated a main peak near the value corresponding to the ordinary Lorentz electron and also two side peaks, the origin of which was not definitely understood. A rough estimate of the expected resolution of the condenser indicated that these side peaks probably must be due either to a bona fide mass effect or to scattering from the condenser plates. While these same results showed quite definitely that the assumption of the previously mentioned type of heavy electron is untenable, the main central peak seemed to be displaced from the expected value for the Lorentz electron by an amount possibly beyond the limits of experimental error. It was therefore decided to repeat the experiment with various improvements of such a nature as to enable one to distinguish between instrumental effects and bona fide mass effects. In this new arrangement it was also planned to aim at greater accuracy by recalibrating all the apparatus.

A schematic diagram of the improved arrangement is shown in Fig. 2. The distance from the source to the condenser was increased over that in the preliminary apparatus, so as to obtain both greater accuracy in establishing the geometrical ρ_{00} and at the same time greater effective momentum resolution. Because of limitations in machining the condenser plates it was not deemed advisable to reduce the plate separation, but the resolving power was further increased by doubling the length of the condenser. The condenser plates were made of aluminum 1 cm thick. Three 1-cm quartz interferometer separators were available to be used as separators for the condenser. The plates were carefully milled down on the sides by an amount sufficient to leave the plates separated by approximately $\frac{1}{2}$ mm. It was found possible in this way to obtain a uniform separation to considerably better than one percent of the separation. The plates were insulated by means of two pieces of plate glass, and the condenser was held rigid by three clamps (not shown) placed just over the quartz posts.

For the purpose of obtaining information concerning the nature of the side peaks the condenser was made of aluminum rather than brass, so as to reduce the scattering coefficient. In addition, adjustable slit systems S_1, S_2, and S_3 were inserted, chiefly to limit the radiation entering the condenser approximately to that momentum interval that could be transmitted by the condenser, and thus further to cut down the scattered component. The slit S_3 serves the same purpose by favoring the direct radiation and giving further momentum resolution. These slit systems could be raised or lowered by means of screws operated outside the vacuum chamber; and each system consisted of three interchangeable slits of widths approximately $\frac{1}{4}$, $\frac{1}{2}$ and 1 cm. Variations in the slit width enable one to ascertain whether scattering from the slits themselves plays an important rôle. The slit S_2 was placed about 1 mm from the front end of the condenser so as to confine the stray field of the condenser to small distances from the end of the plates, as well as to permit further definition of the momentum interval of the electrons reaching the condenser.

The source was enclosed in an aluminum box $\frac{1}{8}$ inch thick to absorb extraneous radiations, including the gamma-radiation; and, in order to avoid distortions in the magnetic field near the source, the latter was deposited on a nickel-plated, rather than a solid nickel wire. The wire itself was mounted on an aluminum frame. Further shielding with lead sheet between the counter and the condenser (with a small opening to allow the beam to pass through) considerably cut down the background of the counter.

TABLE I. *Constants of the apparatus.*

$2\delta = 0.04663$ cm	$H\rho_{00} = 1926.5$
$l = 12$ cm	$\beta_1 = 0.7487$
$b_0 = 2.992$ cm	$W = 1.66$ Mev
$(b_0^2+c^2)^{\frac{1}{2}} = 9.77$ cm	$\beta_2 = 0.3481$
$\rho_{00} = 15.94$ cm	$\beta_1/\beta_2 = M/m_1 = 2.15$
$H = 120.85$ gauss	

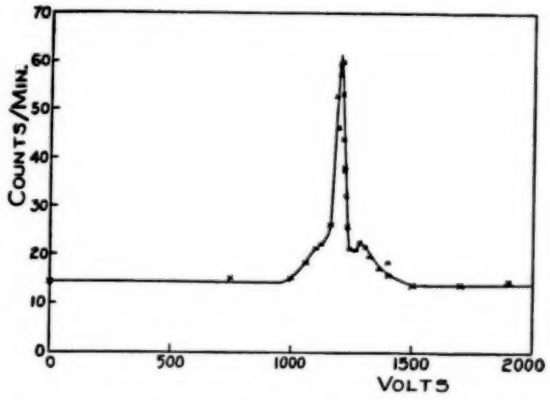

FIG. 3. Electron counts per minute as a function of condenser voltage when slits S_1, S_2, and S_3 of Fig. 2 are omitted.

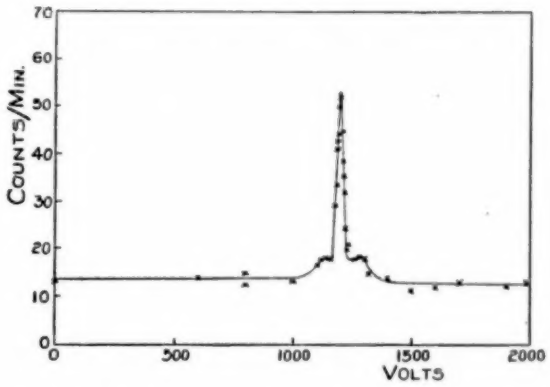

FIG. 4. Electron counts per minute as a function of condenser voltage when the slits S_1, S_2, and S_3 of Fig. 2 are inserted.

The vacuum chamber consisted of a Pyrex tube, of diameter 12 inches and length 8 inches, placed between two brass plates, 14 inches square and $\frac{1}{2}$ inch thick. In the Pyrex tube was ground a 1 inch hole over which the aluminum window could be sealed.

The constants of the final apparatus are given in Table I, with the notation of the preceding article on the theory of the method.

With this arrangement a number of observations were made on the transmitted radiation for condenser voltages from zero up to 2000 volts. Counts were observed for time intervals of ten minutes at each voltage, and the total number of counts observed for voltages on the peak was about 600. It was found that variations of slit width produced negligible, if any shifts in the peak voltage. The curve in Fig. 3 corresponds to a case where the slits were all left out; and that in Fig. 4, to a case where all the slits were in position. All three slits were electrically grounded, and in order to prevent dissymmetries or shifts due to the grounding of the slit S_2 the condenser voltage was supplied in such a way as to permit grounding at the center of the battery, or at any other point. Variations in the position of this ground, however, were found to produce no appreciable effect.

These results, when compared with the preliminary results shown in Fig. 1 show clearly that the side peaks are of an instrumental origin, rather than due to a mass effect. Their separation and height are considerably reduced as compared to those in the previous case. Also the introduction of slits produces the same type of reduction. These facts suggest very strongly that the subsidiary peaks are really due to scattering from the condenser plates. One might, in fact, expect that scattering could produce the observed type of side peaks; for as one adjusts the voltage just off the peak value there will be scattering from the plates near the exit of the condenser, but under these conditions the scattered radiation will immediately escape from the condenser and be greatly dispersed because of the very poor resolution for rays originating near the exit from the condenser. Now as the voltage is adjusted farther off the peak the scattering occurs farther back in the condenser, and consequently there is a greater chance for multiple scattering and at the same time a greater resolution for the scattered radiation. On the other hand the probability for escape decreases as compared to that for absorption, because of the decreasing angular aperture. With these two opposing effects it seems likely that such side maxima might occur.

In order to be able to interpret intelligently the results obtained by this method a careful analysis was carried out for the resolution and intensity characteristics of the method used. Since part of the conditions for cut-off by the condenser plates involve second degree equations in the small variations assumed, it was thought possible that side peaks might be characteristic of the instrument itself, quite apart from scattering. For this reason it was considered advisable to complete the analysis outlined in the

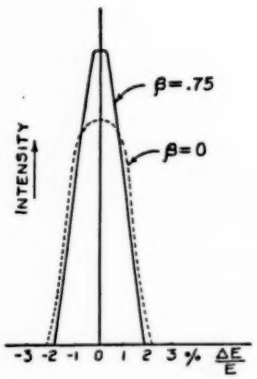

FIG. 5.

preceding article before attempting to interpret the data. Besides, it is always necessary to know the actual momentum spread of the transmitted electrons in order to insure that it is small enough that variations in the source intensity with momentum may be neglected, as well as variations of the slope of the k_i, k curve.

Resolution calculations were then carried out for the case $\rho_{00}=16$ cm, $b_0=3$ cm or $c=9.33$ cm, $l=12$ cm, and $\delta=0.025$ cm, which case approximates satisfactorily the conditions of the experimental arrangement. Since, as has been pointed out, the resolution depends on the particular type of variation of the mass with the velocity, the calculations were performed for the two cases: (1) Lorentz electrons around 2000 $H\rho$, or $\beta=0.75$ approximately; and (2) electrons of constant mass, and around the same momentum.

The results of these calculations are shown graphically in Fig. 5. In the notation of the previous article Δ really represents an increment in k_0, so that one can conveniently express the resolving power as $\Delta k_0/k_0=\Delta/k_{00}$. But one is interested more directly in the resolving power in terms of E, or in terms of the observed voltage V; that is, in $\Delta E/E=\Delta V/V$. Now it has also been shown that:

$$\Delta E/E=(1-\beta^2)\Delta k/k, \text{ for Lorentz electrons.}$$

For this reason the curves of Fig. 5 are plotted against $\Delta E/E$. It may be recalled from the previous article, that the over-all absolute half-width allowed by the condenser alone $\Delta E/E=2k_a/k$, which in the present case amounts to about 8.9 percent; and also that this limiting value was found to be independent of β. It is of interest to note, that, even though the position of the source improves the resolution by more than a factor of 4 : 1, nevertheless, in this case at least, also the *actual* voltage resolution for the two cases is about the same; namely, about 2 percent.

Figure 6(a) and Fig. 6(b) show the intensity-momentum distributions of the electron beams transmitted for different values of Δ, and for the two cases $\beta=0$ and $\beta=0.75$, respectively. The difference in the behavior shown in the two cases is related to the fact that the predominant type of cut-off, as Δ approaches its cut-off value, is different. One sees also from these figures that the expected half-widths, due to both the source and the condenser, have about the same value, 5 percent for *both cases;* whereas the over-all absolute limits of the half-widths defined by the condenser alone should be $\Delta k/k=k_a/(1-\beta^2)k$, or about 5 percent and 10 percent for the two cases, respectively. Hence the source does not further restrict the spread Δk appreciably for the case

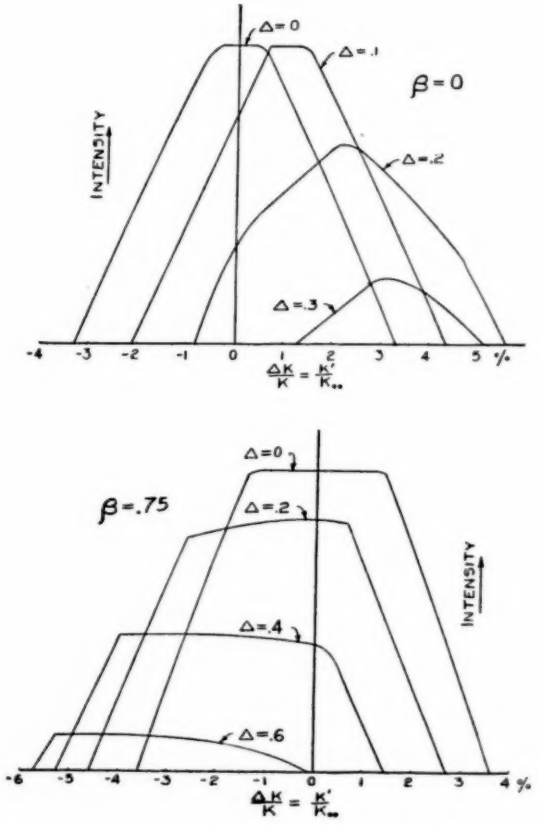

FIG. 6a AND 6b. Intensity-momentum distributions of electron beams transmitted for different values of Δ and for the two cases $\beta=0$ and $\beta=0.75$.

$\beta=0$; but for the case $\beta=0.75$, by a factor of about 1 : 2.

It is then clear that the voltage resolution obtained by the present method should be extremely good (2 percent half-width) as compared with that obtainable with the photographic method. As regards the effect of nonuniformities in the intensity-momentum distribution of the source, one must consider the above spreads in k itself. These spreads were found to be about 5 percent half-width, but because of the extreme sharpness of the voltage resolution effects of the source distribution will be very much minimized.

These results also show clearly that one should not expect side peaks for the direct, or unscattered radiation, and therefore further suggest that the latter are really due to scattering. It should, however, be noted that the effect of the finite extension of the source over the cylindrical wire has been tacitly neglected. The effect of this distribution would be to broaden the observed peak. To a close approximation one may regard this effect as due chiefly to a shift in the resolution curve without a change in width, which shift would be given by the change in k_{00} as the source position changes. In the present arrangement, with a $\frac{1}{2}$ mm source wire, one estimates the shift in k_{00} from points at the top to points at bottom of the wire to correspond to a half-width in k_{00} of about 0.7 percent or 0.4 percent in V. Now, if the source material is distributed uniformly over the cylindrical wire, the source intensity for small equal increments of k_{00} will be much greater for the values of k_{00} corresponding to the top and bottom of the wire than for the other points, since the electrons in question leave these points in directions tangent to the surface. Hence one might expect, under conditions where the "natural width" due to a line source is smaller than the extra width due to the source extension, that the integrated effect of the whole source could give rise to a double peak, between which one would expect a flat central portion, unless the peaks are not resolved, in which case one would expect simply a somewhat broadened central peak.

Since the natural resolution width was calculated as 2 percent half-width approximately; and the extra half-width due to the source, 0.4 percent, one would hardly expect the source distribution to produce resolved double peaks. At least, one would expect such peaks, if resolved, to appear only in the "fine structure" of the central peak, since the actual observed side peaks are separated by 13 percent in the case of no slits (see Fig. 3), or about ten times the separation estimated for the effect of the source distribution. This is further borne out by the preliminary data of Fig. 1, for which one would expect the source extension to be equivalent to a half-width of 1.3 percent in V, whereas the observed half-separation of the side peaks was about 20 percent.

Finally, it seems most probable that the side-peaks are due either to scattering from the condenser plates, as previously suggested, or to some other instrumental cause such as nonuniformity of the magnetic field (see later). In any case the presence of these peaks seems to be of no consequence as regards the position of the central peak, since variations in the separation and intensity of the side peaks, produced by slits and variations of the condenser resolution, caused no appreciable shifts in the central maximum. In fact, the observed half-widths of Fig. 3 and Fig. 4, 3.8 percent and 2.7 percent, respectively, when compared with the total theoretical half-width in the absence of scattering, $2.0+0.4=2.4$ percent, show that, at least *with* the auxiliary defining slits, the scattering does not even cause much broadening of the central peak.

Observed Value of e/m

In the preliminary experiments with the short brass condenser no special attempt was made toward great accuracy, since the apparatus was designed primarily to distinguish only semi-quantitatively between two cases of widely differing mass. Therefore no importance is to be attached to the previously mentioned possibility of a discrepancy of about 10 percent from the theory of relativity, particularly since it was later discovered that some of the rough calibrations were sufficiently at fault to explain away a large part of the discrepancy, and since in calculating the expected position of the central peak of Fig. 1 no correction was made for the stray field of the electric condenser and none for the effect of nonuniformity of the magnetic field of the Helmholtz coils.

End effect of the condenser: In order to take account of the attenuation of the electric field of the condenser, which in the idealized theory is assumed to occur abruptly at the end, Bucherer has pointed out that the effect is as if the ideal condenser were extended a distance p beyond the end of the plates; and he made some estimates based on Coffin's mathematical solutions of the end effect for certain types of condenser, which, however, do not approximate his own experimental conditions very well. For thin condenser plates an accurate solution is well known, but for thick plates like those of Bucherer the stray field may extend considerably farther than in the case of thin plates. Besides, in order to make the correction as Bucherer made it, it is necessary to be able to assume that the end effect extends only a short distance beyond the condenser plates, so that it may be treated as giving rise to a sudden impulse over a short distance. Since Bucherer's method of estimating p does not strictly apply to the actual conditions, Neumann attempted to treat the extra length p as a further constant to be determined from sets of data taken with two different values of the distance from the condenser to the photographic plate. But he found that his values of p, as calculated from his various sets of data, varied all the way from positive to negative values. Finally he had to satisfy himself that these fluctuations were due to the experimental difficulties associated with the determination of a small difference, and to take an average of all his values of p. (As will be seen in a later article on the interpretation of Neumann's data, there may have been other reasons for his difficulty in determining a constant value of p.)

In the present apparatus thick aluminum plates were used, for obvious mechanical reasons; and, as previously mentioned, in order to reduce the stray field suddenly to zero, a grounded slit was placed just in front of, and about 1 mm from the entrance to the condenser space. Hence a mathematical calculation for the stray field becomes impractical, but the effect may in no sense be negligible, if one aims at reasonable accuracy. Consequently measurements of the field attenuation were made by the well-known electric trough method on a large-scale model of the slit-condenser system. When the slit and the center tap of the battery are grounded, the central plane of the condenser becomes a plane of symmetry at zero potential. By the theory of images in a conductor this permits halving the model and placing a conducting surface of zero potential at the plane of symmetry. Further, in order to obtain the conditions of the approximate two-dimensional problem, it is necessary to construct only a shallow trough; since, as is well known, the effect of the insulating surfaces at the top and bottom of the electrolyte is the same as if the problem were a simple electrostatic problem with *insulating* dielectrics, but with the insulating surfaces of the air and the bottom of the trough replaced by surfaces of dielectric of specific inductive capacity zero (i.e. of negative polarizability). Under these conditions the latter surfaces of equivalent dielectric behave as perfect reflectors with *unchanged* sign of electric charge, in contradistinction to the case of reflections in conducting surfaces, where the sign of the charge is changed. The net effect of all the multiple reflections thus brought into play is such as to extend the model effectively to infinity, simulating a two-dimensional problem. (A more rigorous explanation in terms of boundary conditions is obvious.)

By this method the effective extra length p of the condenser was found to be $p=0.29$ mm, or about half the condenser separation. By a simple calculation it can be shown that the end effect is equivalent to a reduction in ρ_{00} of amount $(c/b_0)p$, which in the present case is $9.31\times.029/2.992=0.09$ cm, or $0.09/15.94=0.56$ percent of ρ_{00}.

Correction for nonuniformities in the magnetic field: The value $H=120.85$ gauss, given in Table I, refers to the value of the magnetic field intensity measured at the center of the Helmholtz coils. By exploring with a small coil it was found that the magnetic field dropped off by an amount of the order of a percent as one moved the coil from the center of the field to the extreme positions of the source and of the exit end of the condenser. Because of this nonuniformity it is necessary to make two small corrections when calculating the expected peak voltage for Lorentz electrons:

(I) In the space between the source and the condenser, since the average field will be less

than the above-mentioned value of H, the momentum $H\rho$ of the electrons reaching the condenser with their velocity directed along the central plane will be smaller than the value given in Table I. One may take this effect into account by calculating the effective reduction in ρ_{00} corresponding to the value of H at the center of the field space. This correction may be made approximately by assuming that the field drops off linearly between the condenser and the source. (It would, of course, be more accurate to integrate over the region in question.) In this way one finds that the effect is equivalent to a reduction in ρ_{00} of 0.72 percent.

This reduction of 0.72 percent, taken together with the 0.56 percent due to the end effect of the condenser, gives a total reduction of 1.28 percent, whence the effective

$$\rho_{00}=15.94(1-0.0128)=15.72,$$

which corresponds to an effective momentum of $15.72\times120.8=1898$ $H\rho$, or to an effective velocity $\beta_1=0.745$, instead of 0.749 as given in Table I.

(II) Similarly one must correct for the small drop in magnetic field in the condenser space. For this correction one may again assume approximate linearity of the field variation with y. By making use of the original equations of the theory of the preceding paper, and replacing H by a field varying linearly with y, one may calculate the change in k necessary to compensate for the change in deflection at the exit of the condenser due to the small attenuation in the magnetic field. When this is done for the central ray ($b=0$ and $\phi=0$) at $k_0=k$, one finds that the effect is equivalent to a reduction in the expected peak voltage E_0 of amount 1.46 percent.

Final corrected value of expected peak voltage E_0: With the ideal values of Table I one calculates for the expected, but uncorrected value of the peak voltage E_0 the value 1266 volts; whereas the observed value 1222 volts differs from the uncorrected theoretical value by 3.5 percent. With the corrected value $\beta_1=0.745$ and the corrected value of k_0 one calculates the corrected value of the expected peak voltage as 1240 volts. This leaves a final discrepancy of about $\frac{3}{4}$ percent on the side of heavy electrons, but this corresponds only to about the estimated limit of experimental error, and on the basis of the present experiments cannot be considered as definite evidence for a bona fide anomalous mass effect. Besides, the corrections made for the nonuniformity in magnetic field are only rough approximations, since the field does not actually drop off linearly along the electron path; and no correction was made for the small effect of the earth's magnetic field. (It is also worth mentioning here that, while the shift in the central peak voltage due to the nonuniformity of the magnetic field, as given roughly by the latter calculations, is small; on the other hand the shape of the peak may possibly be considerably altered, and possibly in such a way as to give rise to small side peaks like those observed. In fact, a more detailed consideration of the maximum possible order of magnitude to be expected for the scattered component of the transmitted radiation makes it difficult to believe that the observed side peaks could be caused by scattering. In any case, since the side peaks have been shown to have no appreciable effect on the position of the central peak, they are of no further consequence in this connection.)

In conclusion the authors wish again to acknowledge their indebtedness to Dr. J. A. Bearden and Mr. C. M. Herget of the Johns Hopkins University for their continued generosity in supplying another radium E source for the final experiments. The authors are also indebted to Dr. O. S. Duffendack and Mr. Harold Lifschutz for the loan of some of the excellent Geiger counters which they have developed in this laboratory; to Mr. J. L. Lawson for the loan of a scale-of-eight recording circuit and for assistance with the same; to Mr. W. C. Parkinson, especially for assistance with the experiments by the electric trough method; and to various other members of the department mentioned more specifically in the preliminary Letter to the Editor. Finally the authors gratefully acknowledge support from the Horace H. Rackham School of Graduate Studies of the University of Michigan.

Further Observations on the Production of N^{13}

R. B. ROBERTS* AND N. P. HEYDENBURG
Department of Terrestrial Magnetism, Carnegie Institution of Washington, Washington, D. C.

(Received January 5, 1938)

The reactions $C^{12}+H^1 \rightarrow N^{13}+h\nu$ and $C^{12}+H^2 \rightarrow N^{13}+n^1$ have been studied and the absolute yield of positrons measured for various voltages. The proton-capture reaction shows a single resonance of 30 kv half-width at 450 kv. This resonance has been compared with the similar lithium resonance to fit it into the voltage scale of the lithium and fluorine resonances. Comparison of the positron yields of the two reactions permits a calculation of the yield of N^{13} in the proton reaction from the yield of neutrons in the deuteron reaction as measured by Amaldi, Hafstad, and Tuve. The yield thus determined is approximately 7.5 times higher than the previously accepted value based on positron measurements, and corresponds to a total reaction cross section of about 8.4×10^{-24} volt cm². However, the observed number of positrons from the deuteron reaction, obtained by comparison with uranium, is 2.5 times less than the number of neutrons from the same reaction. This discrepancy could be explained by K electron capture by the N^{13} nucleus, but the errors involved are too uncertain to say definitely that this process does occur. An unsuccessful attempt was made to observe scattering of protons by carbon at the resonance voltage.

INTRODUCTION

SEVERAL problems of considerable interest and theoretical importance are connected with the production of N^{13} by proton and deuteron bombardment of carbon ($C^{12}+H^1 \rightarrow N^{13}+h\nu$, $C^{12}+H^2 \rightarrow N^{13}+n^1$). The early work of Hafstad and Tuve[1] indicated a possible doublet-structure in the resonance capture of protons, but the scatter of their points was such that its existence was doubtful. Their work on carbon was done prior to the installation of the high resistance voltmeter. It seemed desirable to repeat the measurement of the carbon resonance for proton capture to fit it into the voltage scale established by the lithium and fluorine resonances.[2] An anomalous scattering of protons at the resonance energy is expected in elements having a broad resonance for radiative capture, and carbon seemed a favorable element for the detection of this anomaly because of its availability in a gaseous form, its low atomic number, and the large resonance-width established by our measurements as reported below.

The production of N^{13} by deuteron bombardment of carbon brings up another interesting problem. In this reaction each N^{13} atom produced is accompanied by a neutron, but the absolute yield of neutrons measured by Amaldi, Hafstad, and Tuve[3] is approximately seven times larger than the yield of positrons reported by Hafstad and Tuve. If these figures were sufficiently accurate, they would constitute evidence for K electron capture with a high probability by the N^{13} nucleus, but, while the neutron yield has an estimated error of 20 percent, the early measurements of the positron yield may be in error by a rather large unknown factor due to the former uncertainties regarding voltage measurements. We have therefore tried to improve the measurement of the yield of positrons to such a degree that if any large discrepancy exists between the yield of neutrons and positrons it should be attributed definitely to K electron capture.

PROCEDURE

Carbon targets, consisting of one-inch disks of Acheson graphite, were activated by two-minute exposure to the ion beam in vacuum. The activity was measured by observing the initial and final times for a standard deflection of a string electrometer connected to an ionization chamber of the Amaldi-Fermi type[4] containing oxygen at a pressure of three atmospheres and having a window of 0.1 mm aluminum. Immediately after each measurement the sensitivity of the electrometer was checked by observing the time required for the same deflection to be produced by a calibrated uranium beta-ray source. A

* Carnegie Institution Fellow.
[1] Hafstad and Tuve, Phys. Rev. **48**, 306–315 (1935).
[2] Hafstad, Heydenburg and Tuve, Phys. Rev. **50**, 504–514 (1936).
[3] Amaldi, Hafstad and Tuve, Phys. Rev. **51**, 896–912 (1937).
[4] Amaldi and Fermi, Phys. Rev. **50**, 899–928 (1936).

nomogram calculated from the period of radionitrogen (taken to be 620 seconds) was used to compute what fraction of the total activity had been observed. Each observation then gave the activity in terms of the intensity of the uranium source and independent of the sensitivity of the electrometer. Drift corrections were negligible except for the lowest voltage points.

The accuracy of the nomogram, that is, the correctness of the period selected, was determined by making two such observations with each of a group of ten targets. The activities calculated from the two sets of data agreed to within one percent although the initial times of the observations were roughly one and six minutes after activation. As the initial time for each subsequent observation was very close to one minute and the sensitivity of electrometer was adjusted to give approximately constant deflection time, in spite of large variations of target activity, the error arising in the use of the nomogram was negligible.

For the determination of the absolute yield, the electrometer was calibrated in terms of uranium beta-particles per division by the standardized uranium source, which had been previously used by Amaldi, Hafstad, and Tuve for measurement of neutron intensities.[3] The beta-particles from this source had to penetrate 0.2 mm of aluminum before reaching the ionization chamber, so the ionization was produced solely by the beta-particles from UX_2. In converting the calibration to positrons per division no correction was made for any difference in ionizing power as the beta-ray spectrum of UX_2 is similar to that of N^{13}.[5-7] Neither was any correction made for reflection of the beta-rays, as the target and the uranium standard had approximately the same atomic number and mass per square centimeter, the standard consisting of a small mass of UNO_3 embedded in a much larger mass of paraffin and wrapped in 0.1 mm of aluminum. It is reasonable to believe that the neglect of these factors does not introduce an error as great as 50 percent.

Two other sources of error occur, one in the measurement of the ion current and one in the loss of the radioactive gas from the target. From previous experience the error in ion-current measurement (due to secondary electron effects and contamination of the magnetically analyzed ion beam) is known to be less than five percent. The loss of radioactive gas while the target was in the air was shown to be negligible by the appearance of the decay curve. The loss of gas while the target was in the vacuum was estimated by evacuating a target of known activity. After four minutes of evacuation the activity was 10 percent less than would be expected from the normal decay. In the ordinary procedure the targets remained in the vacuum for two minutes during activation and approximately 20 seconds after activation. Consequently a reasonable estimate of the loss would be five percent. Variations in these two errors are believed to be mainly responsible for the scatter of the points shown in Fig. 1. A correction was made for the decay of the target during bombardment.

Voltage Determination

The high resistance voltmeter was originally calibrated in 1935.[2] Last April the rubber tubing in which the resistors were enclosed was replaced by varnished cambric tubing, about one dozen of the individual resistors which differed from 10 megohms by as much as 10 percent being renewed at the same time. It was also uncertain whether high humidity (early part of October) might have an appreciable effect on the calibration. It therefore seemed necessary to make a recalibration of the voltmeter before we could establish accurately the voltage of the proton-capture resonance in carbon. This was done by observing the lithium gamma-ray resonance at 440 kv. Since this voltage for the lithium resonance was obtained immediately after the original calibration of the voltmeter and has been checked in other laboratories,[8, 9] it is thought to be essentially correct.[10] A repetition of this gamma-ray

[5] Kurie, Richardson and Paxton, Phys. Rev. **49**, 368–381 (1936).
[6] Froler, Delsasso and Lauritsen, Phys. Rev. **49**, 561–574 (1936).
[7] Sargent, Proc. Roy. Soc. **A139**, 659–673 (1933).
[8] Bothe and Gentner, Zeits. f. Physik **104**, 685–693 (1937).
[9] Herb, Kerst and McKibben, Phys. Rev. **51**, 691–698 (1937).
[10] Measurements of the Coulomb scattering of protons by nitrogen in this laboratory provide an independent absolute scale of voltage which agrees with the lithium calibration within less than two percent, the limit of accuracy originally ascribed to the absolute values on the lithium-fluorine resonance scale.

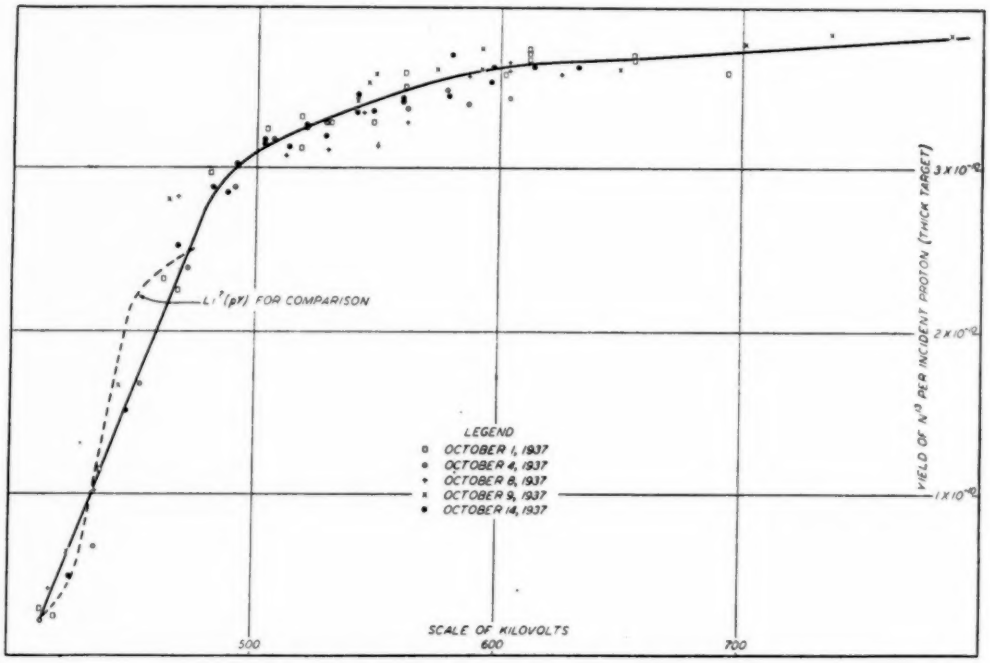

FIG. 1. Production of N^{13} by protons. $C^{12}+H^1\rightarrow N^{13}+h\nu$.

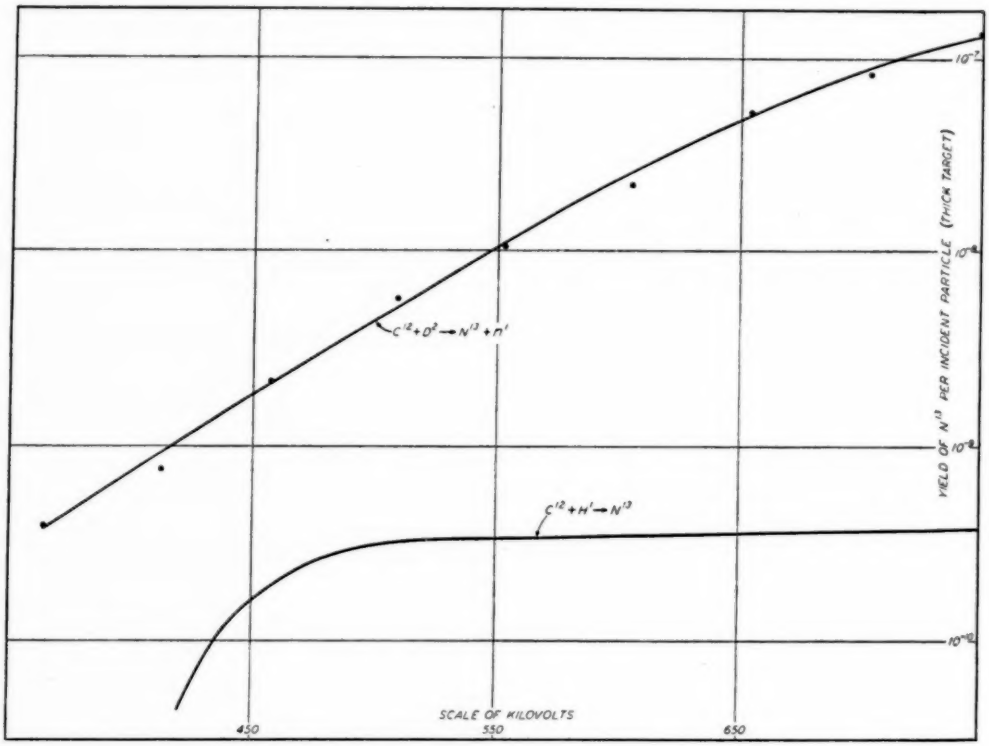

FIG. 2. Production of N^{13} by protons and deuterons.

measurement gave a reading of 452 kv for the resonance voltage. The difference of about three percent was attributed to changes in the voltmeter and a compensating change was accordingly made in the calibration. The carbon resonance was then measured and the lithium resonance measurement repeated, thus comparing the carbon resonance directly with the nearby lithium resonance. The voltage of the sharp rise in the carbon resonance, thus established, furnished a convenient check on the voltmeter for later experiments concerned with the possible existence of higher resonances in carbon. Also the lithium measurement was repeated from time to time as a further precaution. As the humidity decreased the calibration correction also decreased, coming to a final and steady value of approximately one percent at the end of October. The voltages of all points have been multiplied by a factor ranging from 0.97 to 0.99 chosen to place the lithium resonance at 440 kv.

To check the calibration of the voltmeter at higher voltages, the lithium gamma-rays were produced by bombardment with molecular hydrogen ions, giving an accurate point for calibration at 880 kv. This point, with the points at 440 and 0 kv, gave a new calibration curve which showed less departure from linearity (possibly due to heating of the resistors) than the original curve. As this calibration technique using the molecular beam had not been used previously, we repeated the measurements of Hafstad, Heydenburg, and Tuve on the fluorine resonances near 900 kv and found that the resonances occurred at voltages approximately one percent lower than the previously published values.[2] The present measurements give 880 kv and 930 kv for the doublet instead of 892 kv and 942 kv. These new values are almost certainly more accurate than the original values as they are directly compared with the 880-kv point established by the lithium resonance.

Results

Figure 1 shows the yield curve for a thick carbon target bombarded by protons. Every observation is shown on the curve with no adjustments except for the corrections to the voltage scale described above. The curve shows a single resonance of 30-kv half-width at 450 kv. The absolute yield, determined by the uranium comparison as described above, is indicated on the figure and is 3.5×10^{-10} at 560 kv.

Figure 2 shows the thick-target yield curve for the reaction $C^{12}+H^{2}\rightarrow N^{13}+n^{1}$ measured by the uranium comparison and relative values checked by a simultaneous count of the neutrons produced. The absolute yield indicated was determined by uranium comparison, and is less by a factor of 2.5 than the neutron yield from the same reaction measured by Amaldi, Hafstad, and Tuve.

Our attempt to observe the scattering of protons by carbon at the resonance voltage was unsuccessful, but in view of the theoretical importance of such an experiment we believe it advisable to include a brief account of the difficulties encountered. Anomalous scattering of protons is to be expected when a radiative capture resonance is too broad to be accounted for by the width of the gamma-ray level. The resonance-scattering anomaly must be observed with thin scatterers and at large angles (135–180°) to reduce the background of Coulomb scattering. Bethe[11] has pointed out that one would expect an increase by a factor of three in the backward scattering (180°) of protons by lithium at a proton energy of 440 kv where the lithium gamm-ray resonance occurs. However, it is practically impossible to obtain a thin film of lithium for the scatterer. For carbon, however, we might hope to observe a scattering anomaly at the energy of the broad proton-capture resonance as there are several carbon compounds in the gaseous state suitable for use as the scatterer. Acetylene, C_2H_2, is especially good, as the hydrogen would give no back scattering.

We have attempted to observe the large angle scattering of protons by C_2H_2 at the resonance voltage by use of the scattering chamber shown in Fig. 3. With the annular-ring construction we were able to obtain adequate counting rates even at the large angle selected, but in this chamber protons of less than 550-kv energy would not register reliably. At the resonance energy (450 kv) the range of the proton after collision and after passing through the window (1-mm stopping power) was too short to give reliable counts

[11] Bethe and Placzek, Phys. Rev. **51**, 450–484 (1937).

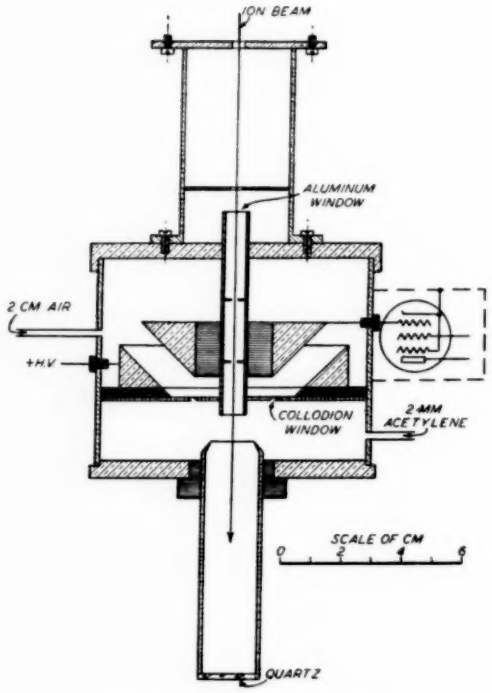

FIG. 3. Scattering chamber.

because of the large input capacity of the amplifier introduced by the annular collecting ring. We therefore concluded that this experiment requires the use of point counters for the detection of the scattered protons, although such a technique would encounter serious difficulties in obtaining adequate counting rates.

DISCUSSION OF RESULTS

The addition of the carbon resonance to the voltage scale established by the lithium and fluorine resonances furnishes another convenient voltage-calibration point. On account of its width the carbon resonance is somewhat less definite than the 440-kv lithium resonance, but this is perhaps balanced by the ease of preparation of carbon targets and their freedom from carbon contamination. The voltage of the carbon resonance is believed to be accurate to within two percent on an absolute scale, and somewhat better relative to the lithium and fluorine points. No indication of a fine structure of the carbon proton-resonance with respect to voltage appears in the present work.

The absolute yield of this proton reaction as given by the positron emission (based on our comparison with uranium) is approximately three times higher than that previously reported by Hafstad and Tuve, and gives a total reaction cross section of 3.35×10^{-24} volt cm^2. However, a more accurate method of determining the yield of N^{13} under proton bombardment is to accept the value for the yield of neutrons from carbon under deuteron bombardment published by Amaldi, Hafstad and Tuve as correct and equal to the yield of N^{13}. Then the yield of N^{13} from the proton reaction follows from the comparison of the number of positrons observed in the two reactions. This method gives a yield 2.5 times greater than the uranium comparison, corresponding to a total reaction cross section of 8.4×10^{-24} volt cm^2. The width of the gamma-ray level calculated from this value of the yield is then 0.6 volt, the lithium width being 4 volts.[12]

The yield of neutrons reported by Amaldi, Hafstad, and Tuve from the reaction $C^{12}+H^2\rightarrow N^{13}+n^1$ is believed to give a good value of the number of N^{13} atoms produced. Their method of determining neutron yields has been checked for the neutrons from deuterium bombarded by deuterium using an entirely different method, with agreement within 15 percent.[13] Moreover, there are no other reactions which could contribute appreciably to the neutron yield from the carbon. The reaction $C^{12}+H^2\rightarrow C^{12}+H^1+n^1$ is endothermic by 2.2 Mev and the reaction $C^{13}+H^2\rightarrow N^{14}+n^1$ is known to contribute only one percent to the number of neutrons observed.[14] The number of positrons observed from the reactions $C^{12}+H^2\rightarrow N^{13}+n^1$ as determined by the uranium comparison described above is less than the number of neutrons by a factor of 2.5. This discrepancy must be attributed either to estimating the number of positrons to be only 40 percent of the true number or to the conversion of N^{13} to C^{13} by K electron capture. In view of the errors involved in determining the number of positrons emitted, it would be unwise to offer this as definite evidence for K electron capture.

[12] Bethe, Rev. Mod. Phys. **9**, 207 (1937).
[13] Ladenburg and Kanner, Phys. Rev. **52**, 911–919 (1937).
[14] Bonner and Brubaker, Phys. Rev. **50**, 308–314 (1936).

Rotational Energy Distribution of OH Molecules from the λ3064 Band

ELISABETH REED LYMAN
Department of Physics, University of California, Berkeley, California

(Received December 27, 1937)

The rotational energy distribution of the OH molecules has been studied by photometric measurement of the λ3064 band. The band excited in the oxy-hydrogen flame and in the copper arc shows a thermal distribution of intensities from which temperatures of 3275°K and 6350°K, respectively, are calculated. The spectrum excited in vacuum tube discharges shows abnormal rotational energy which varies with the pressure of the water vapor in the tube. At current densities used in the experiment, no reduction of rotational energy could be obtained by addition of excess foreign gas.

THE distribution of rotational energy in an emission band spectrum depends upon the conditions of excitation of the emitting molecules, but the distribution does not always indicate the thermal energy or temperature of the gas in which the molecules are excited. Gaviola and Wood[1] were the first to observe that the high rotational temperature derived from the sensitized fluorescence spectrum of HgH was not the true gas temperature. Rieke[2] has made an extensive study of the abnormal rotation of the HgH molecule in sensitized fluorescence in the presence of N_2 and the more normal rotation when the fluorescence takes place in the presence of OH molecules. Abnormal rotation appears in the negative bands of CO^+ and the negative N_2 bands excited in a low voltage arc,[3] whereas the distribution of energy is much more normal for the same bands in an electrodeless discharge and in the neon transformer glow discharge. Among other bands showing abnormal rotation are the C_2 bands in an acetylene discharge and some He_2 bands. The emission spectrum of the OH molecule excited in an electric discharge also shows an energy distribution greatly in excess of the thermal energy of the emitting gas. Bonhoeffer and Pearson[4] stated that the abnormal rotation of OH arises from the simultaneous dissociation of H_2O and excitation of OH by electric impact. Oldenberg[5] showed that the absorption spectrum of OH shows normal rotation and that the abnormal emission spectrum may be reduced to normal rotation by the addition of large amounts of helium. In some cases, therefore, excess rotational energy can be reduced by collisions during the lifetime of the excited state of the molecules.

The following investigation is a study of the rotational energy distribution of the OH molecules by measurements of the λ3064 band excited in electrode and electrodeless discharge tubes in the presence of water vapor alone, and with additions of helium and argon. Measurements have also been made of the band excited in an oxy-hydrogen flame and in a copper arc. Excess rotational energy is found in all cases for the discharge tube spectra, although the amount varies with the conditions in the discharge. On the other hand, the flame and arc spectra both show a normal thermal distribution of rotational energy.

EXPERIMENTAL

Quartz tubes were used for both the electrode and electrodeless discharges. The capillaries were $\frac{1}{4}''$ inside diameter and 2″ long. Cylinders of coiled sheet aluminum were used as electrodes and the electrode discharge was excited by a Thordarsen 2.5 kv transformer. The high frequency excitation for the electrodeless discharge was provided by a Sloan[6] oscillator. The tubes were baked out before being filled with gas. The water vapor pressure in the discharge tubes was controlled by cold alcohol baths surrounding a small sidearm containing a few drops of water.

[1] E. Gaviola and R. W. Wood, Phil. Mag. **6**, 1191 (1928).
[2] F. F. Rieke, J. Chem. Phys. **4**, 513 (1936); **5**, 831 (1937).
[3] O. S. Duffendack, R. W. Revans and A. S. Roy, Phys. Rev. **45**, 807 (1934).
[4] K. F. Bonhoeffer and T. G. Pearson, Zeits. f. physik. Chemie **14**, 1 (1931).
[5] O. Oldenberg, Phys. Rev. **46**, 210 (1934).
[6] D. H. Sloan, R. L. Thornton and F. A. Jenkins, Rev. Sci. Inst. **6**, 75 (1935).

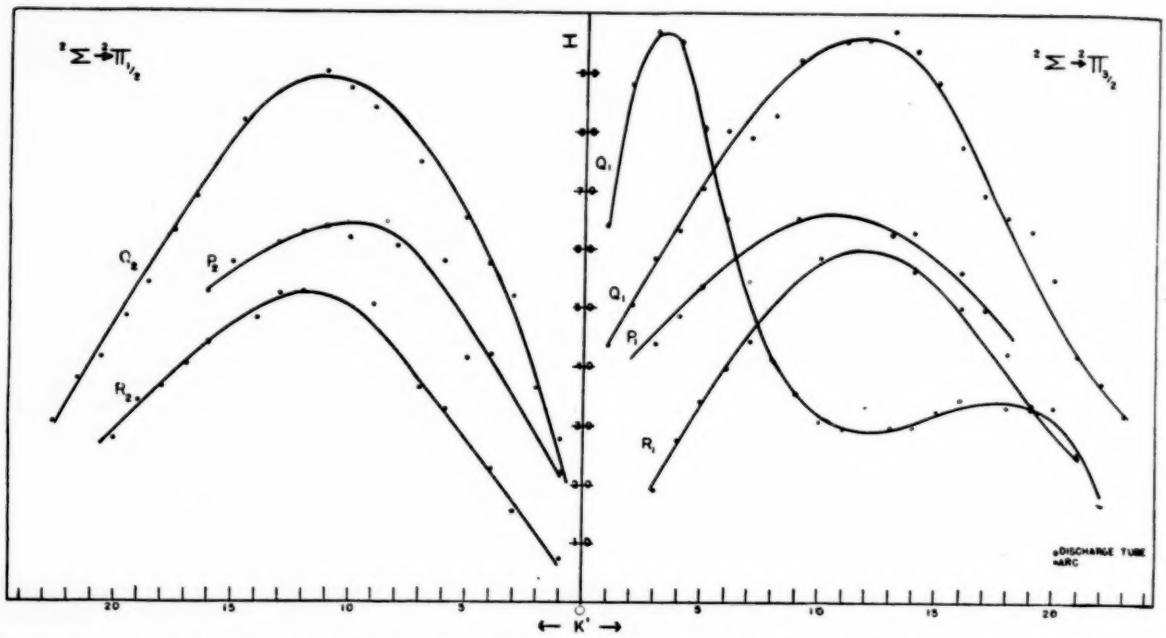

FIG. 1. Intensities of lines of the 6 principal branches of the λ3064 band of the OH arc spectrum as a function of the rotational quantum number. One branch of the band excited in a discharge through 2×10^{-2} mm H_2O.

Ordinary distilled water, which was subsequently vacuum distilled several times by means of liquid air, was used. The alcohol baths were made by cooling ethyl alcohol with liquid air to the desired temperature. The baths provided a range of temperatures from −120°C to room temperature. Before each exposure the water vapor was frozen out of the tube by liquid air and the foreign gas added. Then the appropriate alcohol bath replaced the liquid air around the water tube. The foreign gases, helium and argon, were procured spectroscopically pure. A series of spectra was photographed using a constant pressure of helium (7 mm) and varying amounts of water vapor (from 10^{-5} mm to 7 mm) in the electrode discharge tube. A similar series with argon and water vapor in the tube, and a series with water vapor alone in the electrodeless discharge tube was photographed. The latter discharge was used in preference to the inner electrode discharge for the water vapor alone in order to ensure a discharge at very low pressures without overheating the thin electrodes, and to compare the two methods of excitation. Finally a group of photographs was obtained with the electrode discharge through a trace of water vapor and increasing pressures of helium up to 50 cm. In connection with this set of experiments, varying current densities in the discharge tube were also used

The flame spectrum was obtained from the part of an oxy-hydrogen flame just above the cone. The arc spectrum was produced in an arc in air between copper electrodes around which a jet of steam was continuously rising. The arc was really run, therefore, in water vapor at atmospheric pressure contaminated with air.

The photographs were taken in the first order of a 21-foot grating. Eastman 40 plates were used with exposure times of around 5 minutes for the arc, 15 minutes to 2 hours for the discharges, and 1 hour for the flame. The plates were developed in Rodinal. A step weakener was placed directly in front of the photographic plate so that calibration marks were made on the plate at the same time and on some of the same lines whose intensities were to be measured. The transmission of the steps of the weakener as a function of wavelength was measured by means of a quartz photo-cell and a Wynn-Williams amplifier.[7] The plates were photometered with a Zeiss microphotometer. A calibration curve was obtained for each plate from the photometer trace of the steps

[7] C. E. Wynn-Williams, Phil. Mag. **6**, 324 (1928).

of the weakener and the intensities of the lines were then read directly from the curve. A plot of the measured relative intensities of the lines of the six principal branches of the band, excited in the copper arc, against the corresponding rotational quantum numbers, K', is given in Fig. 1. The intensity distribution in the arc spectrum is thermal. A curve typical of the nonthermal distribution in the discharge tube spectrum is also shown.

Results

If thermal equilibrium exists among the excited molecules, there is a linear relationship according to the Maxwell-Boltzmann theory between the logarithms of I/i and the corresponding rotational term values, where I is the measured intensity of each line and i the theoretical intensity factor. The intensity factors were calculated from formulas of Earls[8] which are specializations for the $^2\Sigma$, $^2\Pi$ transitions of the general Hill and Van Vleck[9] formulas. The term values, $T(K')$, were calculated from the wave numbers for the OH band, λ3064, of Heurlinger.[10] Curves were plotted of log I/i *vs.* $T(K')$ for each spectrum. Since the curves for each branch of the same band were similar, it was considered necessary in all further work to plot curves only of the Q_1 branch since it was the branch least perturbed by overlapping lines. None of the plots from the discharge tube spectra were straight lines, and all of the curves indicated rotational distributions with energies greater than thermal energies. Fig. 2 shows curves for the water vapor and helium (7 mm) mixtures. There is an excess of energy among the low rotational levels and a more striking excess among high levels. An inhomogeneity of temperature in a carbon arc has been shown by Lochte-Holtgreven and Maeker[11] to make the intensities of the low rotational lines in the CN bands too high. Thus temperature inhomogeneity in the discharge could account for the first few high points on the OH curves. The presence of more molecules than expected in the high rotational levels has been found also by Rieke[2] in the HgH spectrum, and to a less extent in the same spectrum by Kapuscinski and Eymers.[12] In spite of the non-Maxwellian distribution of energy in the discharge tube spectra, the curves for the different pressures of water vapor are compared by means of the slope in the middle or straight line portion of the curve. In Fig. 2 it is noticeable that the lower the water vapor pressure, the steeper the slope of the curve which indicates that the average rotational energy is lower for lower pressure. Exactly the same effect of variation of average rotational energy with water vapor pressure was found for water vapor and argon (7 mm) and for water vapor alone. Fig. 3 compares data obtained with the same water vapor pressure in the discharge tube for water-helium, water-argon, and water alone. There is agreement among the low rotational levels for the three cases, although the rotational energies differ for the high levels. The argon-water vapor mixtures usually showed the lowest energy for the high rotational levels. From the similarity of the effects with water vapor with and without small amounts of foreign gases, the conclusion

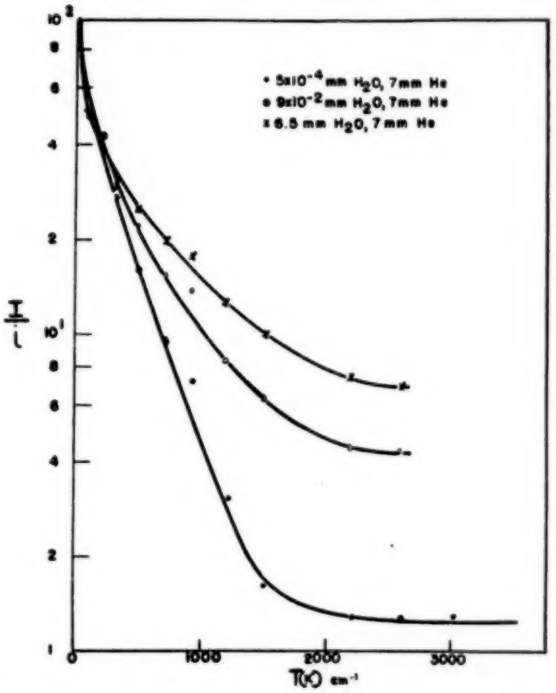

FIG. 2. Rotational term values as a function of log I/i for constant helium, varying water vapor pressure mixtures.

[8] L. T. Earls, Phys. Rev. **48**, 423 (1935).
[9] E. Hill and J. H. Van Vleck, Phys. Rev. **32**, 250 (1928).
[10] T. Heurlinger, *Dissertation* (Lund, 1918).
[11] W. Lochte-Holtgreven and H. Maeker, Zeits. f. Physik **105**, 1 (1937).
[12] W. Kapuscinski and J. G. Eymers, Zeits. f. Physik **54**, 246 (1929).

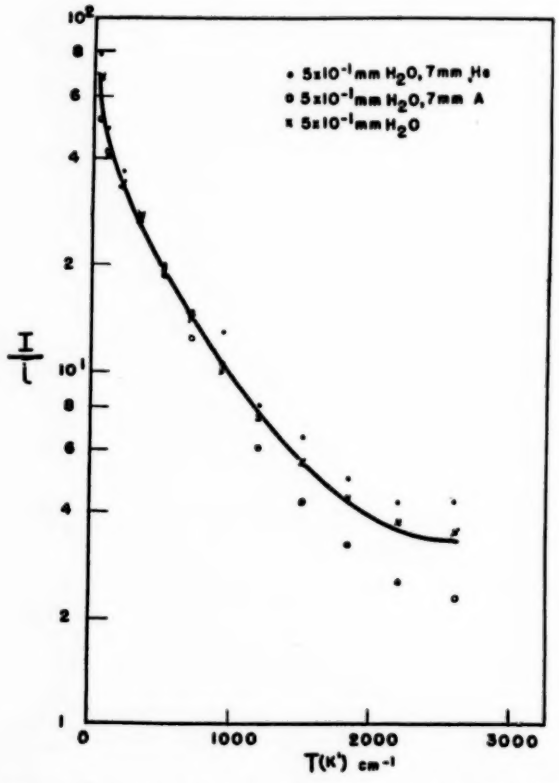

FIG. 3. Rotational term values as a function of log I/i for constant water vapor pressures in the presence of foreign gases.

may be drawn that the effect of collisions between OH molecules and comparatively small numbers of foreign gas molecules is negligible. The average rotational energy seems to depend only upon the number of OH molecules present in the discharge.

The slope of the middle portion of every curve was determined, and an effective rotational temperature calculated from the slope in order to compare the steepness of the curves. The temperature itself is meaningless because of the absence of thermal equilibrium among the molecules and is used only as a measure of the average rotational energy. In Fig. 4, the effective temperature is plotted as a function of the logarithm of the corresponding water vapor pressure in the discharge. The change in average rotational energy with water vapor pressure was gradual, but not a linear change. Under the conditions of these experiments when the pressure of helium was increased a great deal (up to 50 cm) in the presence of only a trace of water vapor, no change in the rotational distribution was noted. This is in contradiction to the effect of excess foreign gas found by others.[3, 5] When the current density in the discharge tube was greatly reduced, however, some evidence was obtained from low dispersion spectra that the head of the band was definitely weakened showing a reduction in energy among the molecules. The discharge was so weak that a grating photograph was not feasible. In Oldenberg's photograph of the same effect the head had disappeared completely. Oldenberg did not include data to show whether the distribution of energy in either the pure water or water and helium case was one representing thermal equilibrium.

In the flame spectrum of OH, the expected

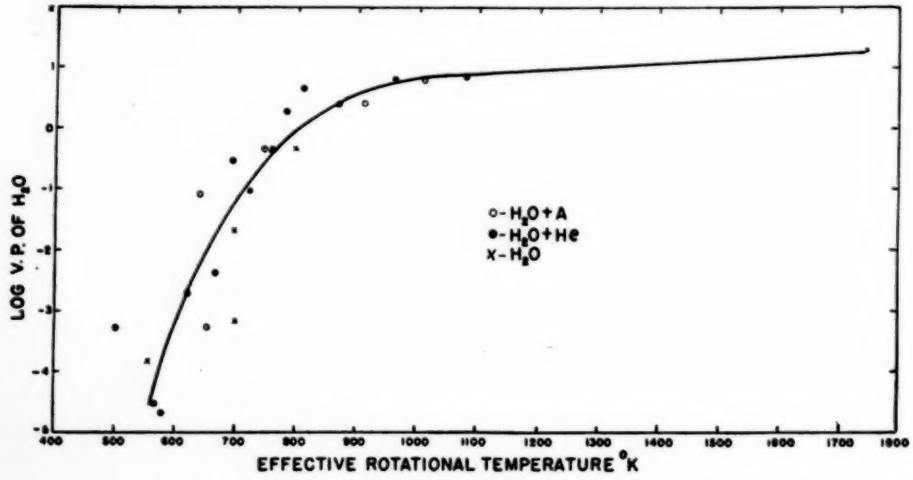

FIG. 4. Effective rotational temperatures as a function of the logarithm of the water vapor pressure in the discharge tube.

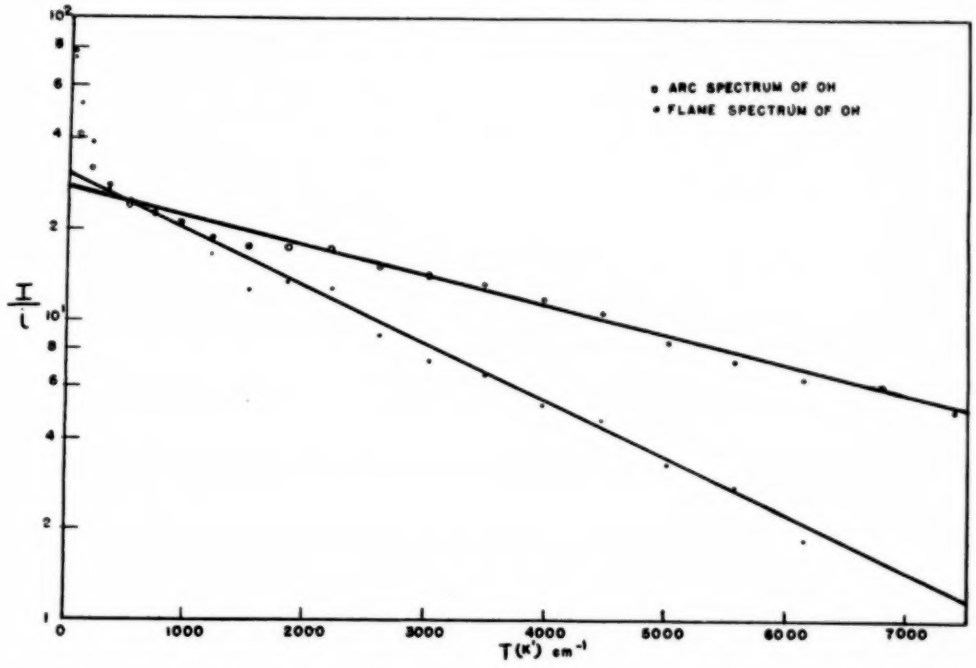

FIG. 5. Rotational term values as a function of log I/i for the arc and flame excited OH band.

thermal equilibrium among the molecules exists except among these in the lowest rotational levels (Fig. 5). The deviation may be accounted for also as caused by temperature inhomogeneity in the flame. The temperature of the flame was calculated from the slope of the straight line in Fig. 5 as 3275°K, a value in good agreement with the temperature of the oxy-hydrogen flame determined by other methods.

The arc spectrum of OH also showed a Boltzmann distribution of rotational energy with the exception of the temperature inhomogeneity deviation at the low rotational end of the spectrum (Fig. 5). The calculated temperature was 6350°K. The temperature is lower than that found for nitrogen arcs, but the result is consistent with the fact that Jenkins and Ornstein[13] found that a hydrogen arc was cooler than a nitrogen arc.

DISCUSSION OF RESULTS

The photometric study of the intensity distribution in the OH band, λ3064, leads to the conclusions that the rotational energy of the OH molecules excited in electric discharges may be reduced by decreasing the water vapor pressure in the discharge, or by adding a large excess of foreign gas provided the current density in the discharge is low, but no evidence is found for a Boltzmann distribution even at the highest pressures used. The distribution of rotational energy among the OH molecules in the flame and in the arc is found to represent thermal equilibrium.

Since the process of excitation in an electric discharge is so complicated, it would be advantageous to study the distribution of energy among the OH molecules excited under more simple conditions. Plans have been made, therefore, to measure the rotational energy distribution among the OH molecules excited by sensitized fluorescence.

In conclusion the author wishes to express her thanks and appreciation to Professor F. A. Jenkins who suggested the problem and gave constructive criticism during the course of the research, and to Professor O. Oldenberg for several helpful discussions.

[13] F. A. Jenkins and L. S. Ornstein, Proc. K. Akad. Amsterdam, **35**, 10 (1932).

On the Nuclear Moments of Indium*

S. MILLMAN, I. I. RABI, *Columbia University, New York, N. Y.*
AND
J. R. ZACHARIAS, *Hunter College, New York, N. Y.*

(Received January 11, 1938)

The atomic beam method of zero moments has been applied to measure the nuclear spin, the h.f.s. $\Delta\nu$ of the normal $^2P_{1/2}$ state and the absolute magnetic moment of In 115. The spin was found to be 9/2 and the $\Delta\nu = 0.381$ cm^{-1} in agreement with spectroscopic results. The resolving power which was attained was sufficiently high to allow a measurement of the fine structure of the zero moment peaks. From the separation of the two $m = -3$ peaks and the diamagnetic susceptibility, we calculate the moment of indium 115 to be 6.40 ± 0.20 nuclear magnetons. From the theory of this effect which is given below, it is clear that this value does not depend on any assumption with regard to the interaction between the nuclear spin and the electron configuration. Peaks arising from the metastable $^2P_{3/2}$ state, lying 2212.6 cm^{-1} above the $^2P_{1/2}$ state were found. The intensity of these peaks is in good agreement with what is expected from quantum statistics. Their exact location will permit an evaluation of the nuclear quadrupole moment.

OUR knowledge of the nuclear magnetic moments of all nuclei other than the isotopes of hydrogen has been derived solely from a study of the hyperfine structure of atomic levels. This is as true of the atomic beam methods as of the optical methods. The experimental result has always been the numerical value of some hyperfine splitting of an atomic energy state. The nuclear moment is derived on the assumption that the interaction between the nuclear angular momentum vector and the extranuclear results from an intrinsic magnetic moment of the nucleus and, in addition, some quadrupole moment. The evaluation of these moments involves a calculation of the energy of interaction of the electronic configuration with the nucleus.[1] Although the combined results reveal the existence of nuclear magnetic moment to be quite certain, its evaluation is very difficult. When results for the hyperfine structure of different levels exist, the spread in values is seldom less than 20 percent. In addition, there remains a possibility that other modes of interaction not contemplated in the theory may contribute to the hyperfine separation.[2]

In this paper there will be presented some experimental results obtained with the method of "zero moments"[3] applied to atomic beams of indium under conditions of very high resolution. From the results it is possible to calculate the nuclear moment of indium directly, i.e., the assumptions regarding the nature of the interaction between the nucleus and the electronic configuration do not influence the result. We have in addition redetermined the h.f.s. separation of the normal $^2P_{1/2}$ state of In 115, as well as the angular momentum of this nucleus.

At the high temperatures necessary to produce sufficient beam intensities for these expierments, about 19 percent of the indium atoms in the oven should be in the $^2P_{3/2}$ state which lies 2212.6 wave numbers above the normal $^2P_{1/2}$ state. Since the beam is collision-free, and the radiation transition $^2P_{3/2} - {}^2P_{1/2}$ has an expected lifetime[4] of about one second, these atoms should be present in the beam to the same extent as in the oven.

We have observed "zero moment" peaks arising from these metastable atoms. From their intensity we can verify the predictions of the quantum statistics, and their location yields information about the hyperfine structure of this state. This is the first atomic beam experiment in which it has been possible to locate zero moment peaks from a metastable state or one in which the electronic angular momentum, J, is other

* Publication assisted by the Ernest Kempton Adams Fund for Physical Research of Columbia University.

[1] The work in the field is summarized by Bethe and Bacher, Rev. Mod. Phys. 8, 82 (1936).

[2] Breit, Phys. Rev. 51, 248 (1937); Young, Phys. Rev. 52, 138 (1937).

[3] Cohen, Phys. Rev. 46, 713 (1934).

[4] The radiation emitted is mostly pure magnetic dipole radiation.

than $\frac{1}{2}$. The higher J value makes it possible to observe departures from the interval rule and consequently to study nuclear quadrupole moment.

The application of the method of zero moments to the study of absolute moments depends on the refinement of the theory of the behavior of an atom in an external magnetic field.

The magnetic moment of an atom with electronic angular momentum $J=\frac{1}{2}$ and nuclear spin i in a magnetic field H is, in units of the Bohr magneton μ_0,

$$\mu_m=-g_i m\mp\frac{x+(2m/2i+1)}{2[1+(4mx/2i+1)+x^2]^{\frac{1}{2}}}(g_J-g_i). \quad (1)$$

(The derivation is given in the appendix.) In this formula, m is the total magnetic quantum number, g_i and g_J are the usual g factors, defined as the negative of the ratio of the magnetic moment expressed in Bohr magnetons to the angular momentum expressed in units of $h/2\pi$, and x is defined by

$$x=\frac{(g_J-g_i)\mu_0 H}{hc\Delta\nu}, \quad (2)$$

where $\Delta\nu$ is the experimental separation in wave numbers between the hyperfine structure levels $F=i+\frac{1}{2}$ and $F=i-\frac{1}{2}$. The basis of the older zero moment experiment was the less refined formula of Breit and Rabi[5] which is obtained from Eq. (1) and Eq. (2) by setting $g_i=0$. In this approximation, it is evident that for negative values of m there are certain values of x for which the value of μ_m is zero in two of the $2(2i+1)$ magnetic levels. These values of x are at $-2m/(2i+1)$, $m=-\frac{1}{2}, -\frac{3}{2}, \cdots -(i-\frac{1}{2})$ if the spin is integral, and $-1, -2, \cdots -(i-\frac{1}{2})$ if the spin is a half-integer.

If a beam of atoms in a state $J=\frac{1}{2}$ with nuclear spin i passes through an inhomogeneous magnetic field, it will suffer deflection according to the law of force $F_y=\mu_m\partial H/\partial y$. A plot of the beam intensity which reaches the detector fixed at the center of the beam against the field or magnet current shows initially a rapidly decreasing intensity, since $\partial H/\partial y$ is proportional to H and the increasing deflecting force deviates more and more atoms out of the beam. When the value of the field reaches the region where x is at the lowest value of $-2m/(2i+1)$, the intensity increases, comes to a peak at this point, and then decreases to repeat (Fig. 3) the same course at each of the critical values of x. The zero moment peaks have a maximum intensity under ideal conditions equal to $1/(2i+1)$ of that of the original beam intensity.

The new feature of this experiment is the fact that the resolution is so high that the more exact Eqs. (1) and (2) must be applied. These equations show that the atoms in each of the two states with the same negative m value have their zero μ_m at two slightly different values of x and therefore of magnetic field H. The difference is such that to a high degree of approximation

$$\frac{\Delta H}{H}=\frac{2i+1}{i}\frac{\mu_i}{\mu_J}\left\{1-\left(\frac{2m}{2i+1}\right)^2\right\}^{\frac{1}{2}}, \quad (3)$$

where ΔH is the interval between the two zero moment values of the field and H is the average of the two values, μ_i and μ_J are respectively nuclear and extranuclear moments. The fraction of the atom in each of these two states is $1/(4i+2)$.

It is clear that Eq. (3) involves the nuclear moment directly and does not involve at all the nature of the interaction between the nuclear and extranuclear angular momentum which causes the hyperfine structure of the atomic level. Experimentally, the problem reduces to one of resolution, which means that the deflecting power of the apparatus must be sufficiently great that atoms with moments only slightly different from zero are deflected completely away from the detector.

Indium possesses many features which make it suitable for a first attempt at an accurate measure of absolute nuclear moment. Firstly, the moment indicated from its h.f.s. is large; secondly, the fact that the normal state is $^2P_{1/2}$ with the consequent value of $\mu_J=\frac{1}{3}\mu_0$ makes the ratio $\Delta H/H$ of Eq. (3) a much more favorable one than with the alkalis. Furthermore, there was the hope that with sufficient resolution one could observe the peaks arising from the isotope In^{113}. A preliminary investigation showed that it

[5] Breit and Rabi, Phys. Rev. **38**, 2082 (1931).

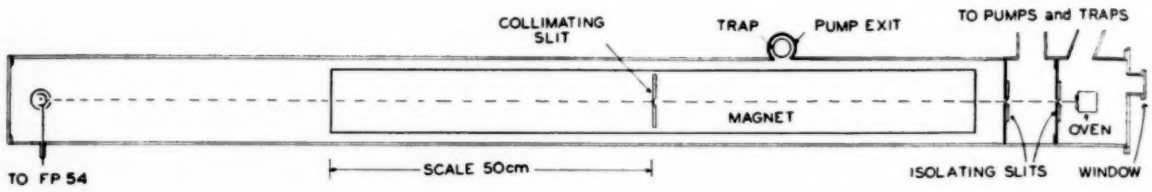

FIG. 1. Diagram of the apparatus.

is possible to detect indium with an oxide coated tungsten wire prepared in a manner[6] similar to that used for Li, even though the ionization potential is much higher (5.76 volts).

The requirements of high resolution were met by making the beam long and narrow. The total beam length was 161 cm; the defining slits were set at about 0.01 mm and the path in the deflecting field was 1 meter long. Since $\Delta\nu$ for the $^2P_{1/2}$ state of indium is 0.38 cm^{-1} and the value of g_J only $\frac{2}{3}$ high fields of the order of 10,000 gauss must be produced to reach the appropriate value of x (Eq. (2)). This circumstance made it necessary to use an iron magnet to produce the deflecting field, rather than a system of wires carrying current, which has been the previous practice.

APPARATUS

A top view of the apparatus is given in Fig. 1. It consists of a long brass tube 5″ inside diameter and $\frac{1}{8}$″ wall thickness, separated by partitions into three chambers, each pumped separately. Two narrow separating slits mounted on the partition and movable by means of screws which pass through the side of the tube permit the passage of the beam, and yet provide sufficient flow resistance to isolate effectively the oven chamber, where the vacuum is poor, from the main beam chamber.

The source is an oven which consists of a molybdenum block, with a well drilled diagonally down, in which the indium is placed. Molybdenum slit jaws with about 0.01 mm separation cover the well. The slit jaws have to be removed to reload. This design was found to be superior to the type with a separate opening for loading, because it is easier to make one exit tight to indium vapor than two. A set of tungsten heating spirals, insulated by quartz tube and grouped around the slit, serve to heat the oven. The oven itself is mounted on three tungsten pegs set in a slide. An invar screw on the side of the tube allows lateral motion of the oven while the experiment is in progress. The power supply to the oven is about 800 watts to attain a temperature of 1500°K. The oven chamber is thoroughly water-cooled.

The magnet is of a very accurate and convenient construction. A cross section is shown in Fig. 2. It is essentially a tube 1 meter long with a longitudinal gap, and is completely inside the beam chamber. It is made in two parts of Armco iron and is of the form shown in the shaded area of Fig. 2. The form of the gap is such that the boundaries are the equipotentials corresponding to the field produced by two parallel wires carrying current in opposite directions and 6.2 mm apart. The advantages of such a field have already been described.[7] The internal windings consist of four copper tubes insulated by mica and the external windings were the four segments of a hollow copper cylinder, each provided with a copper tube soldered to it. The windings are thus completely water-cooled. The magnet is

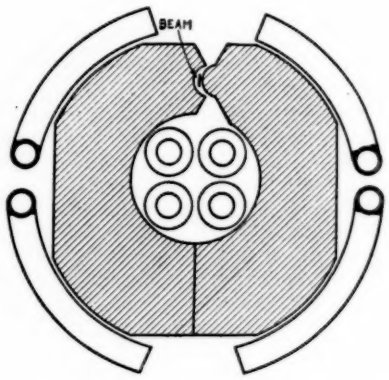

FIG. 2. Cross section of magnet and windings. The beam runs through the curved gap. This diagram is $\frac{3}{4}$ full size.

[6] Manley and Millman, Phys. Rev. **51**, 19 (1937).

[7] Rabi, Kellogg and Zacharias, Phys. Rev. **46**, 157 (1934).

excited by a bank of 2-volt storage cells connected in parallel. A field of 10,000 gauss is attained with 250 amperes. The current was measured by means of a calibrated shunt and a Leeds and Northrup type K potentiometer. It was necessary to be able to vary the current in steps of 0.01 percent and continuously in one direction in order to remain on the same hysteresis loop. The rheostat was of a simple slide wire type and could vary the current from 0 to 250 amperes. The value of the field as a function of the current was measured roughly by means of a flip coil inserted in the gap. The fine measurement was made with the beam itself in a manner to be described.

The collimating slits were mounted on a plate which set in a groove cut transversely through the magnet. The slit mount could be displaced any desired distance by means of a screw. One of the slit jaws had a vertical slot cut through it wider than the gap in the magnet. The detector was the usual oxide-coated tungsten filament, 0.025 mm in diameter, eccentrically mounted on a ground joint and provided with a microscope for very accurate setting of position. In addition, the apparatus was provided with vertical beam stops not shown in the diagram, which limited the height of the beam and were adjustable during the course of a run not only in vertical position but also in height.

Adjustment

The slits were made parallel by setting each slit and the detecting wire separately, parallel to a plumb line. A rough alignment of the slits was effected optically; all finer adjustments were made with the beam itself. These adjustments consist in setting all the slits and the detector filament in the same plane, and in setting this plane parallel to the pole face of the magnet and at a known distance from it. There is a certain optimum position where the magnitude of the field is constant over the greatest height.

The adjustments were usually made with a beam of KCl molecules which is not as difficult to handle as In. The oven is heated to an appropriate temperature and the collimating slit is pulled out of position to allow a broad beam to come down the apparatus through a slot in the slit jaw. The filament is moved until it detects this broad beam. The separating slits are made wide enough to permit this without any very accurate aim. The collimating slit is then moved in. When the slit is in line with the filament and oven slit, a beam comes through to the detector. The beam is then moved by moving the oven, separating slits and filament in step until it is cut off by an edge placed at a known distance from the convex edge of the pole piece nearest the oven. The position of the detecting filament is then read on the telemicroscope focused on the filament. The oven is then moved back, pivoting the beam about the collimating slit as a center, until it is cut off by another edge on the end of the pole face nearest the filament. From the interval between these two filament positions, the length of the beam and the length and location of the magnet, the position of the collimating slit can be calculated. The beam is then made parallel to the pole face by moving the filament back the proper distance from the cut-off point and setting the oven for the maximum intensity. The collimating slit can be moved a known interval by setting the filament at the proper point and pivoting the beam about the oven. After the collimating slit is set, the parallelism to pole face is restored by displacing the filament the proper amount and correspondingly resetting the oven. After this setting, the isolating slits are centered with respect to the beam by cutting the beam off first with one jaw and then the other, and setting the slit at the midpoint between the two positions.

It is important for the experiment that the detecting filament is accurately centered with respect to the beam; an error of 0.0004 mm represents a 1 percent error in the final value of the moment. The centering is effected by placing the filament midway between two points of equal intensity on the side of the beam. This method is very sensitive and corresponds to the center better than the point of maximum intensity which cannot be read as precisely. Although it may seem that the long apparatus would not be rigid enough to the extent desired, it was found that if it is shielded from drafts and from direct radiation and convection from the pump heaters, the average shift of the filament with respect to the beam center was less

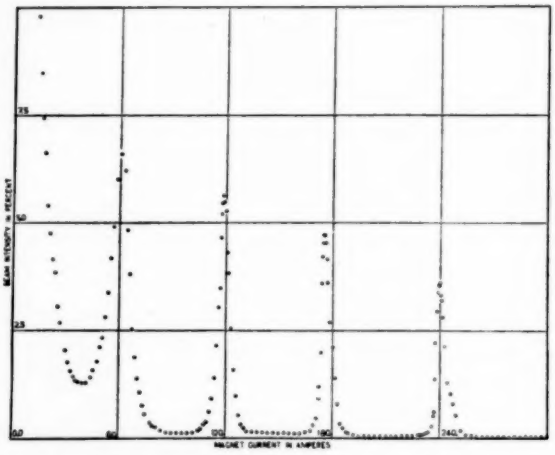

FIG. 3. Plot of the beam intensity against magnet current with detector fixed at the center of the beam.

than 0.001 mm in a period of about fifteen minutes. This is about the time consumed in the measurement of the fine structure of a peak.

Another serious difficulty was the possibility of a shift in the position of the beam when the field is turned on, because of warping of the magnet which is attached to the main tube. Such warping would not be detected with the indium beam itself. However, the effect could be investigated with a KCl beam, which is not magnetic except for nuclear and rotational moment. It was found that there was indeed a beam shift, but not much different from the expected shift of 0.0025 mm at 7500 gauss calculated from the known diamagnetic susceptibility of KCl. The apparatus itself stayed practically fixed. Had there been a shift, its effect could have been neutralized by displacing the filament beforehand by the same amount.

RESULTS

(a) The spin

In Fig. 3 is shown a plot of the indium beam intensity against magnet current. It was verified that the four approximately equidistant peaks were the only peaks from atoms in the $^2P_{1/2}$ state. The spin is therefore an odd half-integer and equal to 9/2.

(b) The h.f.s. separation

From Eq. (2) it is apparent that the h.f.s. $\Delta\nu$ can be evaluated when the field at any of the peaks is known because there x is $-2m/(2i+1)$. Since the ordinary experimental methods of measuring an inhomogeneous field in a small confined region lack precision, recourse was had to atomic beam methods. The last peak of Cs′, of which the $\Delta\nu$ is known[8, 9] to 0.2 percent, lies very close (within 1 percent) in magnet current to the first peak of In. Since the intervals in current between the first and second, and second and third peaks of In are equal (Fig. 3), and since these intervals must be equal in field, we know that the magnetization curve of field against current is linear in this region. The extrapolation from the last Cs peak to the first In peak is therefore very accurate. The experimental field ratio H(3rd peak of Cs)/H(1st peak of In) is 1.007. This yields 0.381 cm^{-1} for the $\Delta\nu$ of the $P_{1/2}$ state of In 115, as compared with the spectroscopic result of 0.380. This result is important for the absolute moment measurements because the value of g_J enters the calculation for $\Delta\nu$. The agreement between the two values shows that g_J is accurately $\frac{2}{3}$, as is to be expected from a pure $^2P_{1/2}$ term.

(c) The absolute moment

Figure 4 shows a detailed plot of the fourth peak. It differs from Fig. 3 in that much lower beam stops were used (0.7 mm instead of 2.5 mm), and smaller and more accurately measured steps in current were taken. Fig. 5 is a similar curve for the third peak, and Fig. 6 for the second. The fine structure is very easily measurable. The position of the beam was always rechecked after a complete curve of the type of Figs. 4, 5, 6 was taken to see if any accidental shift had occurred. When small shifts occurred, corrections were made by introducing a known

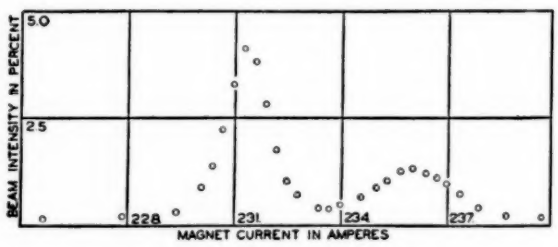

FIG. 4. Detail of fourth peak.

[8] Millman and Fox, Phys. Rev. **50**, 220 (1936).
[9] Granath and Stranathan, Phys. Rev. **48**, 725 (1935).

shift and measuring the effect on ΔI. A large number of curves were taken to diminish the effect of accidental errors.

The difference in intensity between the low and high field components of the double peak noticeable on all these curves arises from the fact that the field is necessarily inhomogeneous, and therefore varies across the width of the beam. The low field component represents atoms, the moments of which decrease with increasing field, while the high field peak comes from atoms for which the reverse is true. In the inhomogeneous field, this circumstance results in a slight focusing of the beam in the former case and a spreading in the latter.

Only the second and third peaks are suitable for the calculation of final results. The fourth peak occurs at a value of the field (9830 gauss) where the slope of the magnetization curve is changing and it is difficult to evaluate ΔH, the separation in field, from ΔI, the separation in current. At the third peak, the linearity is very good, and ΔH can be obtained accurately from ΔI by comparing it with the known field and current separation between the second and third peaks. The second peak is not as clearly resolved as the third, but the results from the two are in agreement and afford a check on the procedure.

The value of $\Delta H/H$ for the third peak, obtained by averaging 35 curves, is 0.0193; the average deviation from this mean is 0.0004. Substituted in Eq. (3) with $m=-3$ and $\mu_J=\frac{1}{2}\mu_0$ we obtain the value $\mu_i=6.65$ nuclear magnetons ($\mu_0/1838$). This value has to be corrected for the diamagnetic moment induced in the indium atom by the field. The magnitude of correction is easily evaluated by adding this moment to Eq. (1) which becomes, after setting $\mu_i=-g_i i$ and adding the diamagnetic moment $\mu_a=-\alpha H$,

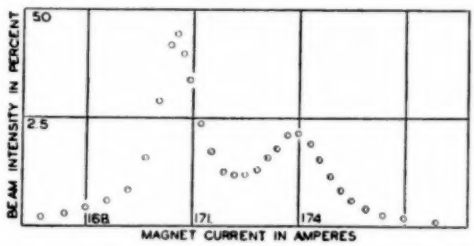

FIG. 5. Detail of third peak.

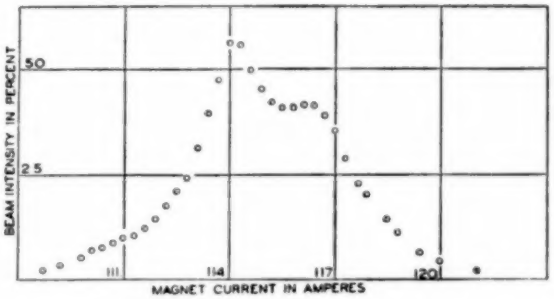

FIG. 6. Detail of second peak.

$$\mu_m=\frac{m}{i}\left(\mu_i-\alpha H\frac{i}{m}\right)$$

$$\mp\frac{g_J-g_i}{2}\,\frac{x+(2m/2i+1)}{\{1+(4mx/2i+1)+x^2\}^{\frac{1}{2}}}.$$

Since the value of m for these zero moment peaks is negative, the effect is that the value for μ_i which we obtain is too large by the amount $\alpha Hi/m$, which for the third peak is $1.5\alpha H$. If we assume a reasonable value for the molar diamagnetic susceptibility of indium 66×10^{-6}, we have a correction to the moment of about 0.25, leaving it at 6.40. This value should be correct to about 3 percent, including the error in estimating the diamagnetic contribution.

The evidence of the second peak strongly supports these values. The value of $\Delta H/H$ from 14 curves is 0.0210. The value of m is (-2). This leads to a moment of 6.31. The diamagnetic correction is the same as for the third peak, since the ratio of H/m is the same. The final value is 6.06 nuclear magnetons. This result should not be considered as a disagreement with the value obtained from the third peak, but rather as a support, since any systematic error in reading the interval between two peaks when they overlap is in the direction of making the interval smaller. The precision of the determination is naturally much less than that of the third peak.

We therefore consider the value of the moment of In^{115} to be 6.40 nuclear magnetons.

THE METASTABLE $^2P_{3/2}$ STATE

The ratio of the number of atoms in the $^2P_{3/2}$ state to those in the normal state is given by the Boltzmann factor multiplied by the ratio of the statistical weights, and is equal to 2 exp

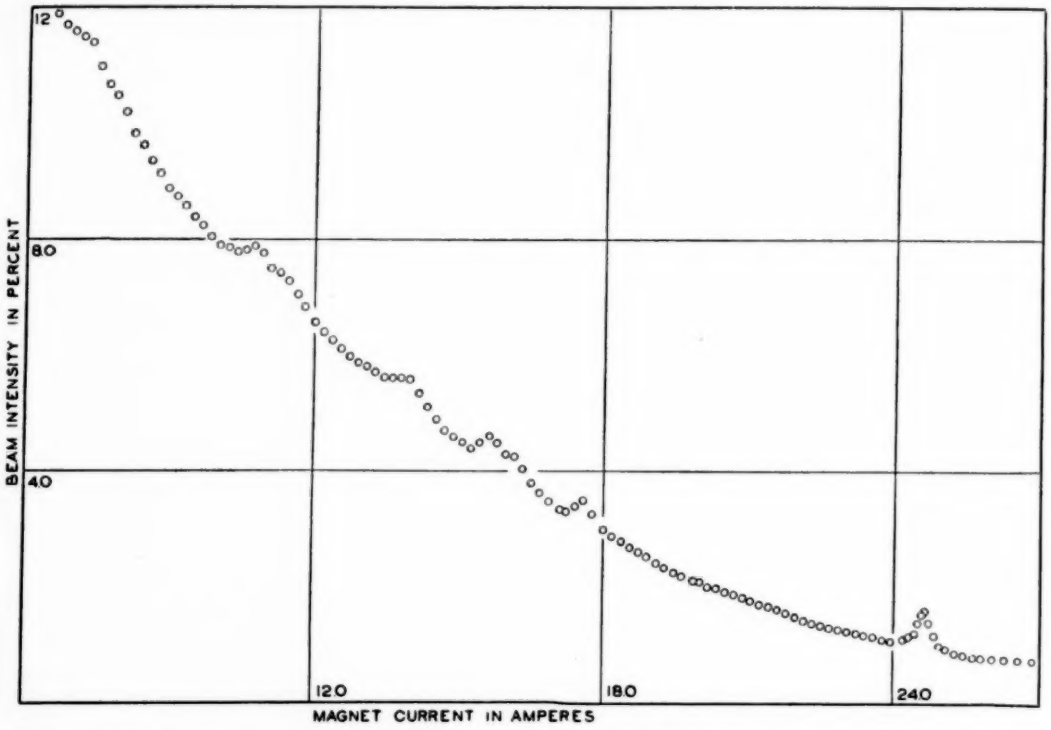

FIG. 7. Detail of the low current part of Fig. 3 showing the peaks arising from the metastable $^2P_{3/2}$ atoms against the background of undeviated $^2P_{1/2}$ atoms.

$-hc\Delta\nu/kT$. The absolute temperature was about 1500°K. At this temperature the excitation of other states may be neglected. The abundance of atoms in the higher state should be about 19 percent.

The expression for the magnetic moment as a function of the field can no longer be given as a simple quadratic function, but comes from a solution of a set of quartic equations, because the secular equation is of the fourth order. Each value of m results in a different quartic, the roots of which have been obtained by numerical methods. There are 40 such roots, but only the roots of the equations which come from negative values of m give "zero moment crossing." There are fourteen of these and in general the values of the field at which these zero moments occur are different for the different states. The fraction of atoms in a zero moment state should therefore be 0.19/40 of the total number, or about 0.5 percent.

In Fig. 7 we have a plot of the intensity against magnet current for the very early part of the curve in Fig. 3. The small peaks arise from the metastable atoms, and after subtracting the background of atoms in the normal state, we find the fraction of atoms to be 0.5 percent.

The reason they occur at such low field values is firstly the fact that the value of g_J is $\frac{4}{3}$ rather than $\frac{2}{3}$, and secondly the fact that the value of the h.f.s. separation for this state is about $\frac{1}{5}$ that of the $^2P_{1/2}$ state. This results in a very much larger value of x for a given field H.

The location of each of these peaks is a function of g_J, g_i and the value of the energy of each of the four h.f.s. levels of the h.f.s. multiplet. Since there are fourteen peaks to determine these quantities, it will be possible to ascertain any departures from the interval rule with great accuracy, and hence to study the quadrupole or higher moments of this nucleus. These experiments are being continued in this laboratory with an apparatus more suitable for low fields and high resolution.

DISCUSSION

A comparison of our result with the moment calculated from the h.f.s. of various states is given in Table I.

Our value is in fair agreement with the value calculated from the h.f.s. of the normal $^2P_{1/2}$ state. It is, however, impossible to decide from present knowledge whether the marked deviations from the true value of the moments, obtained from the s states, arise from an error in the theory of Fermi and Segrè or whether there is a specific electronic interaction with the nucleus not contemplated in the theory. It would be of great value in this connection to have a more precise theoretical calculation of the moments from these s states. The low value obtained from the $^2P_{3/2}$ state may perhaps be explained by some perturbation as in the case of thallium.

In these experiments, a careful search was made for small peaks arising from the isotope In 113, which has an abundance of 4.5 percent. Although our resolution was high enough to detect such peaks even if the spins of the two isotopes were the same and the moments differed by as little as 1 percent, we observe no such peaks. If we conclude from the work of Bacher and Tomboulian,[10] who failed to detect any lines from In 113, that the h.f.s. separations of the two isotopes are of approximately equal magnitude, we can be certain that the spin of In 113 is certainly 9/2.

In conclusion, we wish to thank Mr. Sam Cooey, chief mechanician of the physics department, whose remarkable skill in the construction of the magnet and other vital portions of this apparatus made the whole experiment feasible. The research has been aided by a grant from the Research Corporation.

Appendix

The derivation of the moment formula for $J=\frac{1}{2}$, i arbitrary, is best obtained from the F representation in which we take the Z axis as the direction of the field H.

Table I

In I	$6s$	5.02
	$5p\ ^2P_{\frac{3}{2}}$	3.8
	$5p\ ^2P_{\frac{1}{2}}$	6.1
In II	$5s$	5.46
Atomic beam		6.40

[10] Bacher and Tomboulian, Phys. Rev. **52**, 836 (1937).

The Hamiltonian of the interaction is

$$H=g(j)\mu_0 J_z H+g(i)\mu_0 i_z H. \tag{1}$$

The well-known matrix elements of J_z and i_z are given by Condon and Shortley.[11] They are

$$\begin{aligned} J_z(F\,m;\,Fm)&=(1/2F(F+1))\\ &\quad\times[F(F+1)-i(i+1)+J(J+1)]m \\ i_z(F\,m;\,Fm)&=(1/2F(F+1))\\ &\quad\times[F(F+1)-J(J+1)+i(i+1)]m \end{aligned} \tag{2}$$

$$J_z(F\,m;\,F-1\,m)=J_z(F-1\,m;\,Fm)=f$$

$$i_z(F\,m;\,F-1\,m)=i_z(F-1\,m;\,Fm)=-f \tag{3}$$

$$f=\left\{\frac{(F+J+i+1)(i+J+1-F)(F+i-J)\times(F+J-i)(F^2-m^2)}{4F^2(2F-1)(2F+1)}\right\}^{\frac{1}{2}}.$$

The secular equation for almost degenerate states is

$$|W^0_{F',F'}\delta_{F',F''}+H'_{F'',F'}-\delta_{F',F''}W|=0. \tag{4}$$

In this equation $W^0_{F'}-W^0_{F''}$ is the observed separation between the two h.f.s. levels F and $F-1$, W is the eigenvalue of the energy in the field and H' is as in Eq. (1). When these quantities are inserted we obtain

$$W_m=\frac{W^0_{i+\frac{1}{2}}+W^0_{i-\frac{1}{2}}}{2}+g(i)\mu_0 H\pm\frac{\Delta W}{2}\left(1+\frac{4m}{2i+1}x+x^2\right)^{\frac{1}{2}}, \tag{5}$$

where x is $\dfrac{(g_j-g_i)\mu_0 H}{\Delta W}$ and $\Delta W=W^0_{i+\frac{1}{2}}-W^0_{i-\frac{1}{2}}$.

The moment of the atom in a state m is given by $\mu_m=-\partial W_m/\partial H$. This differentiation leads to Eq. (1) of the text, since the first term on the right-hand side of Eq. (5) is a constant. For values of J larger than 1/2 the procedure is identical, but the secular equation is of higher degree and the solution is best obtained with numerical methods.

Equation (3) of the text is obtained by setting for negative values of m

$$\begin{aligned} g(i)m+\frac{x_1-((2|m|)/(2i+1))}{(1-((4|m|)/(2i+1))x+x^2)^{\frac{1}{2}}}\frac{g_j-g_i}{2}&=0, \\ g(i)m-\frac{x_2-((2|m|)/(2i+1))}{(1-((4|m|)/(2i+1))x+x^2)^{\frac{1}{2}}}\frac{g_j-g_i}{2}&=0. \end{aligned} \tag{6}$$

From the definition of x we have

$$\frac{x_1-x_2}{\frac{1}{2}(x_1+x_2)}=\frac{2(H_1-H_2)}{H_1+H_2}=\frac{\Delta H}{H}. \tag{7}$$

The value of x_1-x_2 and x_1+x_2 from Eq. (6) yields the desired formula if one neglects quantities of the order of $(g_i/g_j)^2$ and also drops g_i in the second term on the left-hand side of Eq. (6). This introduces an error of only about 0.1 percent. It is apparent that all reference to the nature of the interaction between the nuclear spin and the extranuclear J is eliminated from the final formula 7.

[11] *Theory of Spectra.*

Focusing and Maximum Energy of Ions in the Cyclotron

M. E. Rose
Cornell University, Ithaca, New York
(Received December 20, 1937)

The effect on the motion of the ions of the inhomogeneities of the electric and magnetic fields in the cyclotron has been investigated. It is shown that both fields exert a focusing action on the ions, the electric focusing predominating over the first part of the path and the magnetic focusing over the remaining part. For the magnetic fields hitherto used, magnetic focusing, in its domain, is more efficient and the boundary between electric and magnetic focusing lies at a radius of about half the exit slit radius. The most important factor in the electric focusing is the relative change of the radiofrequency field during the acceleration of the ion. If the electric field decreases during the time of acceleration the ion will oscillate slowly about the median plane, the amplitude of these oscillations increasing as the square root of the distance from the center of the cyclotron. For an increase of the electric field during the acceleration the ions are defocused except in the case of acceleration very near the peak dee voltage. Thus somewhat more than half of the radiofrequency cycle will be effective in producing obtainable ions. The usual magnetic fields give a strong focusing of the ions resulting in a decreasing amplitude—convergence of the beam. The only requirement for magnetic focusing is that the magnetic field near the median plane decrease radially outwards from the center of the cyclotron chamber. The effect of the deviation of the ions from resonance with the electric field oscillations is discussed. The magnetic field must be of such a form that the ions (or at least some of them) do not encounter a retarding electric field. This "resonance condition" on the magnetic field is in some conflict with the requirement of good focusing. The necessity of finding a compromise between these two effects explains the very great sensitivity of the beam intensity on "shimming." Magnetic fields are described which give the greatest energy with measurable beam intensities. The main feature of these fields is that they are greater than the field required for exact resonance near the center, and become smaller than the resonance field near the exit slit. Satisfactory results are obtained with a field which is, at the center, 0.9 percent larger than the resonance field and behaves as $1-4\times10^{-3}(r/R)^2$ with increasing distance r (R the radius of the exit slit). This field will give protons of 13.9 Mev, deuterons of 19.7 Mev and α-particles of 39.4 Mev energy if the peak voltage on the dees is 50 kv. With increasing dee voltage, $2V_0$, the maximum energies increase as $V_0^{\frac{1}{2}}$. A somewhat more complicated field is derived which gives protons of 14.9 Mev, deuterons of 21.1 Mev and α-particles of 42.2 Mev with intensities as high as one-quarter of the intensities obtained at low energies. The absolute maximum energies obtainable are about 5 percent higher than these values. It is pointed out that these high energies can only be obtained with extremely careful "shimming."

I. Introduction

ONE of the most important factors governing the intensity and energy of ions obtained from the cyclotron is the focusing action of the electric and magnetic fields. This focusing action arises, of course, from the inhomogeneities which are present in these fields. Under the ordinary operating conditions, these inhomogeneities are such as to provide a force deflecting the ions toward the median plane (central horizontal plane) of the acceleration chamber, thus preventing the ions from spreading unduly. In the case of homogeneous fields, the distance of the ions from the median plane would increase as the time spent in the cyclotron, i.e., as the number ν of accelerations. Hence an electric or magnetic field which provides a force component directed towards the median plane will result in a less rapid spread of the ions and a consequent improvement in the intensity of the emergent beam. Such an effect will constitute a focusing action. The most desirable effect would be a focusing action strong enough to produce an actual convergence of the beam. As will be shown below (Section III) such a convergent beam is indeed produced by the focusing action of the usual type of magnetic field, in accord with observations.

In the following we shall consider the focusing of ions by electric and magnetic fields which may be described as follows: The electric field is produced between two dees of the same size and shape (semi-cylinders) symmetrically placed with respect to the median plane of the cyclotron chamber. Otherwise the shape of the dees is arbitrary; e.g. the height of each dee and the dee separation may vary in any manner with the distance from the center. The magnetic field is produced by pole pieces which are axially symmetrical about the center of the cyclotron

chamber.[1] Further, the magnetic field will be very homogeneous out to a considerable distance from the center.

It may be emphasized that the assumption of symmetry about the median plane is the only assumption which we shall make concerning the electric and magnetic fields; and, of course, this property of symmetry corresponds quite accurately to the situation realized in actual practice.

II. Focusing by the Electric Field

To describe the electric field quantitatively we introduce a system of rectangular coordinates with origin at the center of the cyclotron chamber. The z axis is taken in the vertical direction and the x axis in the direction of the electric field at the center (cf. Fig. 2).

As we shall show below, the electric focusing is important only in the inner region of the cyclotron, i.e., for distances from the source considerably less than the radius of the dees. In this region there is no component of the electric field normal to the x–z plane in the acceleration, region, i.e. $\mathcal{E}_y=0$ for $x\sim 0$. In addition the x and z components of the electric field in the acceleration region are to a high degree of accuracy independent of y. Thus the electric potential will depend only on x, z and the time t. The time dependent potential encountered by an ion will be

$$V_t(x, z, t)=V(x, z)\cos(\omega t+\theta), \tag{1}$$

where ω is the circular frequency of the oscillating electric field, t the time measured from the moment when the ion passes the center ($x=0$) of the acceleration region and θ the phase of the electric field at $t=0$. ($\theta=0$ corresponds to maximum acceleration.)

The space part of the potential has the following properties:

$$V(x, -z)=V(x, z), \tag{1a}$$

$$V(\pm\infty, z)=\mp V_0, \tag{1b}$$

where $2V_0$ is the peak potential across the dees. The dependence of V on x is quite arbitrary; e.g., it is permissible to assume that the dee from which the ions enter the acceleration region has a greater height than the other dee. Such an arrangement may at first sight seem to give better electric focusing than dees of equal height; however, it will turn out that the focusing changes very little with the geometry.

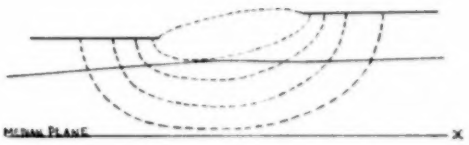

FIG. 1. Diagrammatic representation of the lines of force and path above the median plane for dees asymmetrical about the plane $x=0$.

We introduce the function U conjugate to V. U is defined by the Cauchy-Riemann relations,

$$\frac{\partial U}{\partial x}=\frac{\partial V}{\partial z}, \quad \frac{\partial U}{\partial z}=-\frac{\partial V}{\partial x}. \tag{2}$$

(These relations are the conditions for orthogonality between the equipotential lines, $V=$ const. and the lines of force, $U=$const.) From (2) it follows that U and V satisfy a Laplace equation

$$\Delta U=0, \quad \Delta V=0, \tag{3}$$

$$\Delta\equiv\partial^2/\partial x^2+\partial^2/\partial z^2. \tag{3a}$$

For the time dependent function U_t we have

$$U_t(x, z, t)=U(x, z)\cos(\omega t+\theta) \tag{4}$$

and for the symmetry properties of the space part U,

$$U(x, -z)=-U(x, z), \tag{4a}$$

$$U(\pm\infty, z)=0 \tag{4b}$$

and from (4a)

$$U(x, 0)=0. \tag{4c}$$

The boundary condition (4b) simply means that any path from far inside one dee to far inside the other will cross each line of force twice, if at all (cf. Fig. 1) (4b is actually implied by 4c).

Finally, all derivatives of V and U vanish at $x=\pm\infty$. In particular the electric field components $\mathcal{E}_z=-\partial V/\partial x$ and $\mathcal{E}_x=-\partial V/\partial z$ decrease rapidly with increasing x.

From the above discussion it is evident that the ion encounters a field whose space dependence is the same at each acceleration. The time dependence of the field will usually differ slightly from one acceleration region to the next because

[1] The importance of symmetrical position of the dees and of axially symmetrical pole pieces has been emphasized by E. O. Lawrence and D. Cooksey, Phys. Rev. 50, 113 (1936).

the Larmor rotation of the ion and the electric field oscillations will in general not be in exact resonance. Therefore the phase of the electric field at the time of acceleration will undergo a secular variation. This has no effect on the electric focusing during an individual acceleration but will change the combined focusing effect of many successive accelerations.

In the region where the electric focusing is important the magnetic field is very highly homogeneous and merely serves to give the ions a uniform circular motion, which introduces no complication into our problem. We may think of the actual "spiral" path of the ion as having been rolled out into a plane and then we have to consider a two-dimensional problem in which the magnetic field no longer plays any role. The ion in traversing its path encounters a series of acceleration regions which act as electric lenses. We shall, in the following, refer to each such acceleration region as a lens.

It will be convenient in our treatment of the electric focusing to consider separately the motion near the source and the motion after the ion has been accelerated a few times ($\nu >$ about 4, say). Of these two, the latter motion is the most important. In this case we first consider the motion of the ion in the neighborhood of a single lens and then obtain the secular variation of the motion from lens to lens. For the motion near the source, this procedure will not be valid and a numerical solution of the equations of motion is necessary.

Motion of the ion in the neighborhood of a single lens

We introduce a set of coordinates x, z with origin at the center of the lens. Since we are primarily interested in the motion of the ion with respect to the median plane we consider the equation of motion.

$$Md^2z/dt^2 = -e\partial V_i/\partial z, \tag{5}$$

where e and M are the charge and mass of the ion, respectively. Now the motion of the ion during the acceleration will be very nearly parallel to the electric field as will be apparent from our discussion of the deflections undergone by the ion (cf. below). Thus we set

$$d/dt = vd/dx, \tag{6}$$

where v is the velocity of the ion. If E is the energy at the center of the acceleration region we may write

$$v^2 = 2(E - eV(x, z)\cos\theta)/M. \tag{7}$$

Here we have disregarded the change of the electric field during the time of acceleration which is justified because the term involving V is only a small correction[2] compared to the main term E. We have from (4) (5) (6) (7) and (2)

$$2(E - eV\cos\theta)^{\frac{1}{2}}\frac{d}{dx}\left[(E - eV\cos\theta)^{\frac{1}{2}}\frac{dz}{dx}\right] = -e\frac{\partial U}{\partial x}\cos(\theta + \omega t). \tag{8}$$

In first approximation, we may be tempted to neglect the time dependence of the force on the right-hand side and the term involving V on the left. Then we would have

$$\frac{d^2z}{dx^2} = -\frac{e}{2E}\frac{dU}{dx}\cos\theta \tag{9}$$

and integrating across the acceleration region, we obtain for the deflection in the lens,

$$\Delta\alpha = \left(\frac{dz}{dx}\right)_{x=\infty} - \left(\frac{dz}{dx}\right)_{x=-\infty} = -\frac{e}{2E}\cos\theta(U_\infty - U_{-\infty}) = 0 \tag{9a}$$

by (4b). This result can be interpreted as follows: When the ion is approaching the lens it is deflected toward the median plane as we see from the direction of the lines of force (Fig. 2). This is a focusing deflection. When the ion is receding from the lens it is deflected away from the median plane (defocusing). If we neglect the time variation of the electric field and the change of the particle energy, the focusing and defocusing deflections will exactly cancel. This result is true for any shape of the dees since it follows directly from (4b) which was shown to be independent of the geometry.

Therefore we have to consider the time variation of the field and the variation of the particle

[2] Of course, it would not be justified to neglect the time dependence of the force on the right-hand side of (5).

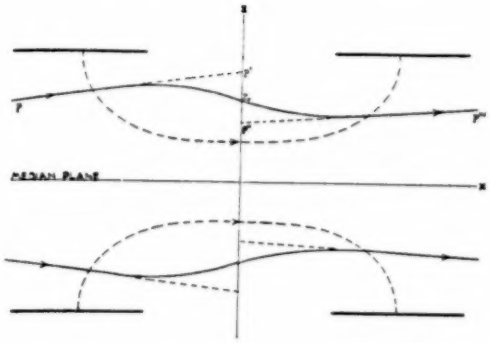

FIG. 2. Cross section of dees near acceleration region (x–z plane) showing schematically the mechanism of electric focusing. The path through the lens is represented by pz_0p''', the extrapolations of the path outside the lens by pp' and $p''p'''$. The deflection in the lens has been greatly exaggerated in the figure. The path and lines of force below the median plane are the reflections of the path and lines of force above.

energy. Taking only the former, we obtain

$$\frac{d^2z}{dx^2}=-\frac{e}{2E}\frac{dU}{dx}(\cos\theta-\omega t\sin\theta) \qquad (10)$$

and, since the first term was shown to give zero deflection, we have from (6)

$$\left(\frac{d^2z}{dx^2}\right)_{\text{field variation}}=\frac{e\sin\theta}{2E}\frac{\omega}{v}\frac{dU}{dx}x, \qquad (10a)$$

which gives upon integration

$$(\Delta\alpha)_{t.v.}=\frac{e\sin\theta}{2E}\frac{\omega}{v}\left(Ux\Big|_{-\infty}^{\infty}-\int_{-\infty}^{\infty}Udx\right) \qquad (11)$$

for the net deflection $\Delta\alpha$ in passing through the lens. The integrated term vanishes by (4b). The integral is to be extended along a parallel to the x axis[3] and will be a function of z. We have

$$\frac{\partial}{\partial z}\int_{-\infty}^{\infty}Udx=\int_{-\infty}^{\infty}\frac{\partial U}{\partial z}dx=-\int_{-\infty}^{\infty}\frac{\partial V}{\partial x}dx=2V_0. \qquad (12)$$

By (4c), $\int Udx=0$ for $z=0$, so that

$$\int_{-\infty}^{\infty}Udx=2V_0z, \qquad (12a)$$

$$(\Delta\alpha)_{t.v.}=-\frac{eV_0\sin\theta}{E}\frac{\omega}{v}z. \qquad (13)$$

[3] Actually the integral should be extended along the path of the ion, but the z component of the velocity is always small. It can be shown (cf. reference 4) that the error is only of the relative order $(dz/dx)^2$.

This result is again independent of geometry.

The variation of the particle energy is given by the terms involving V in (8). Disregarding for this calculation the time variation of the electric force, we have[4]

$$2(E-eV\cos\theta)\frac{d^2z}{dx^2}=-e\frac{dU}{dx}\cos\theta. \qquad (14)$$

Expanding in powers of eV/E, and retaining only the first term (since the constant term gives no deflection, cf. (9a)), we have

$$(\Delta\alpha)_{\text{energy change}}=-\frac{e^2}{2E^2}\cos^2\theta\int_{-\infty}^{\infty}\frac{dU}{dx}Vdx. \qquad (15)$$

The integral is obviously proportional to V_0^2 and depends also on the special geometry of the dees. It is discussed in more detail in the appendix where it is shown to be approximately equal to a positive constant times z. The ratio of the two contributions to the focusing is, according to (13) (15)

$$(\Delta\alpha)_{\text{en. ch.}}/(\Delta\alpha)_{t.v.}=b\left(\frac{eV_0}{E}\right)^{\frac{1}{2}}\frac{\cos^2\theta}{\sin\theta}, \qquad (16)$$

where b is a constant depending on the geometry. For the customary geometries, b is of the order unity (cf. appendix); it is large only if the dee separation is very small. Except for the first few revolutions, E will be very much larger than the accelerating potential eV_0; therefore, the deflection will be primarily due to the time variation of the field except: (a) during the first few revolutions and (b) for very small phases θ, of the order of $(eV_0/E)^{\frac{1}{2}}$.

[4] Strictly speaking, we obtain by carrying out the differentiation in (8) and neglecting t

$$2(E-eV\cos\theta)\frac{d^2z}{dx^2}-e\cos\theta\frac{dV}{dx}\frac{dz}{dx}=-e\cos\theta\frac{\partial U}{\partial x}. \qquad (a)$$

On the right-hand side, we have a partial derivative, on the left, total derivatives, i.e., derivatives along the path of the ion. The partial derivative is connected to the total derivative by

$$\frac{\partial U}{\partial x}=\frac{dU}{dx}-\frac{\partial U}{\partial z}\frac{dz}{dx}. \qquad (b)$$

Using this and a similar equation for $\partial V/\partial x$ we find from the Cauchy-Riemann relations

$$\frac{\partial U}{\partial x}=\left(\frac{dU}{dx}+\frac{dV}{dx}\frac{dz}{dx}\right)\Big/\left(1+\left(\frac{dz}{dx}\right)^2\right). \qquad (c)$$

Neglecting the very small term $(dz/dx)^2$, (cf. remarks preceding Eq. (6), (a) becomes identical with (14).

The deflection (13) is towards the median plane for positive θ and away from the median plane for negative θ. The first case leads to focusing and is realized if the electric field decreases during the acceleration. It is obvious that a decreasing field must lead to a net focusing because then the focusing during the entrance of the ion into the lens will be stronger than the defocusing upon leaving the lens. By the same reasoning, an electric field which increases during the acceleration (negative θ) must result in a net defocusing. The additional deflection due to the energy change, (15), always gives focusing. Formally, this comes about because the right-hand side of (15) is a negative constant times z; physically, the reason is that the ions are faster upon leaving the lens than upon entering it so that the defocusing field acts over a shorter time than the focusing field. Practically, as we have seen, the focusing due to energy change is relatively unimportant; it serves, however, to give a net focusing for small negative phases θ. Therefore slightly more than half of the radio-frequency cycle is effective in producing focused ions.

From this discussion, it appears that the electric focusing is only a differential effect, the deflection in each case being a difference between a focusing and a defocusing deflection. Therefore the deflections are very small as is borne out by the results. Even the larger deflection, (13) is the product of two small factors, *viz.* eV_0/E and $\omega z/v = z/r$ where r is the radius of the path.

We have shown that the largest part of the electric focusing is independent of the geometry and that the geometry-dependent part decreases rapidly with increasing energy. This shows that nothing can be gained for the focusing by making the dee height nonuniform such as is indicated in Fig. 1, and actually, intensity would be *lost* by such an arrangement because some of the ions coming from the higher dee would pass over the top of the lower dee and thus be lost from the beam. The considerations given above do not apply when grids are inserted in the dee openings because then the Laplace equation is not valid at the grid. This was pointed out in a private communication from Dr. E. M. McMillan. With a grid in the opening of the dee into which the ion is entering the electric focusing can indeed be increased considerably. However, in order to avoid serious obstruction of the ion beam, the ratio of the diameter of the grid wires to their spacing should not be larger than one over the total number of accelerations (200–500). The use of such thin wires would seem to offer serious practical difficulties. We shall therefore assume in the following that the geometry is as simple as possible, i.e., no grids and both dees of equal height at all points.

Motion through a combination of lenses

The motion through a combination of lenses may be described by the following two quantities: (1) The slope of the path between the $(\nu-1)$st and νth lens, $\alpha_{\nu-\frac{1}{2}}=(dz/dx)_{x=-\infty}$, and (2) the distance of the ion from the median plane at the center of the νth lens, $z_\nu=z_{(x=0)}$. The change of α in passing through a lens, $\alpha_{\nu+\frac{1}{2}}-\alpha_{\nu-\frac{1}{2}}=d\alpha/d\nu$ has been calculated in the preceding paragraph with the result given in (13) and (15).

The change of z_ν in passing from one lens to the next is composed of two parts. The first, $\Delta_1 z_\nu$, arises from the fact that the motion of the ion is not in general exactly parallel to the median plane. This gives a chance of z_ν by the amount

$$\Delta_1 z_\nu = \alpha_{\nu-\frac{1}{2}}\sigma_\nu, \tag{17}$$

where σ_ν is the distance between the $(\nu-1)$st and νth lens, *viz.*

$$\sigma_\nu = \pi v/\omega. \tag{18}$$

The second part of the change of z_ν, $\Delta_2 z_\nu$, arises from the two separate deflections of the ion in passing through the lens.[5] As may be seen from the schematic representation of the path in Fig. 2, the successive focusing and defocusing deflections of the ion result in a net shift of the path towards the median plane by an amount $p'p''$. This shift is the difference between the intercepts, at the center of the lens, of the extrapolated paths far to the right and far to the left of the lens.

From (9) we have by integrating from $-\infty$ to x

$$\frac{dz}{dx}-\alpha_{\nu-\frac{1}{2}}=-\frac{e}{2E}\cos\theta\ U. \tag{19}$$

[5] This represents the deviation of the lens from ideal thinness. In fact, the distance of the principal points from the center of the lens is $\Delta_2 z_\nu/\Delta\alpha \sim r$ (cf. Eqs. (13) and (22) below).

Thus the path at the left of the lens (pz_ν in Fig. 2) is given by

$$z_L(x)=z_\nu+\alpha_{\nu-\frac{1}{2}}x-(e\cos\theta/2E)\int_0^x Udx. \tag{20}$$

Similarly the path at the right of the lens ($z_\nu p'''$) is given by

$$z_R(x)=z_\nu+\alpha_{\nu+\frac{1}{2}}x-(e\cos\theta/2E)\int_0^x Udx. \tag{21}$$

The extrapolated straight line paths are obtained by setting the upper limit of the integrals in (20) and (21) equal to $-\infty$ and $+\infty$, respectively. Then we obtain for the difference in intercepts

$$\Delta_2 z_\nu=-(e\cos\theta/2E)\int_{-\infty}^{\infty} Udx. \tag{22}$$

The integral has already been evaluated (cf. (12a)). With this result and (17) we have for the total change of z_ν per lens

$$\Delta z_\nu=\frac{dz_\nu}{d\nu}=\alpha_{\nu-\frac{1}{2}}\sigma_\nu-\frac{eV_0\cos\theta}{E}z_\nu, \tag{23}$$

in which we have passed over to the differential equation. It is apparent that Δz_ν is also independent of the geometry.

Since (13) gives the derivative $d\alpha/d\nu$, we differentiate (23) to eliminate α and obtain, dropping the subscript ν

$$\begin{aligned}\frac{d^2z}{d\nu^2}&=\sigma\frac{d\alpha}{d\nu}+\alpha\frac{d\sigma}{d\nu}-\frac{eV_0\cos\theta}{E}\frac{dz}{d\nu}+\frac{eV_0\cos\theta}{E^2}\frac{dE}{d\nu}z\\&=\sigma\frac{d\alpha}{d\nu}+\frac{dz}{d\nu}\left(\frac{1}{\sigma}\frac{d\sigma}{d\nu}-\frac{eV_0\cos\theta}{E}\right)\\&\quad+z\frac{eV_0\cos\theta}{E}\left(\frac{1}{\sigma}\frac{d\sigma}{d\nu}+\frac{1}{E}\frac{dE}{d\nu}\right).\end{aligned} \tag{24}$$

According to (18)

$$\frac{1}{\sigma}\frac{d\sigma}{d\nu}=\frac{1}{v}\frac{dv}{d\nu}=\frac{1}{2E}\frac{dE}{d\nu}=\frac{eV_0\cos\theta}{E}. \tag{24a}$$

Therefore the coefficient of $dz/d\nu$ vanishes. The last term becomes of the order $z(eV_0\cos\theta/E)^2$ which is small compared to the first term.

Inserting (13) in (24) we obtain for the differential equation governing the electric focusing

$$\frac{d^2z}{d\nu^2}+\frac{\pi eV_0\sin\theta}{E}z=0. \tag{25}$$

If desirable, and if the phase is constant (accurate resonance maintained), E may be expressed in terms of the number ν of accelerations, *viz.*

$$E=2eV_0\cos\theta\,\nu, \tag{26}$$

$$\frac{d^2z}{d\nu^2}+\frac{\pi\tan\theta}{2\nu}z=0. \tag{26a}$$

The factor of z is a rather slowly varying function of the independent variable ν. Therefore it is permitted to apply the WKB (Debye,[6] Wentzel-Kramers-Brillouin) method of solution. For positive[7] θ, the solution of (25) is

$$z=c(E/\sin\theta)^{\frac{1}{4}}\times\sin\left[\pi^{\frac{1}{2}}\int^{\nu}d\nu(eV_0\sin\theta/E)^{\frac{1}{2}}+\delta\right], \tag{27}$$

where c and δ are integration constants. This represents an oscillation of the ions about the median plane. The envelope of the oscillations diverges slowly with increasing energy as $E^{\frac{1}{4}}$ which is a considerable improvement over the homogeneous field case ($z\sim E$).

For negative θ, the motion is no longer an oscillation but is of exponential (increasing or decreasing) type. Regardless of the initial conditions, after a few revolutions the increasing exponential will predominate resulting in a rapid increase of the distance of the ion from the median plane. If the phase θ is constant, we have in this case

$$z\sim\nu^{\frac{1}{4}}\exp\left(2\pi\nu|\tan\theta|\right)^{\frac{1}{2}}. \tag{28}$$

Thus the ions are strongly defocused in this case.

Therefore, for the favorable phases, $0<\theta<\pi/2$, the electric field results in a focusing action, although a rather weak one. The reason for the failure of the electric field to produce a stronger focusing (e.g., convergence of the beam) is due primarily to the very small deflections which take place in the lens, (cf. (13) and subsequent remarks.) This means that the lenses have a very long focal length ($\sim\nu^{\frac{1}{2}}$) and that the oscillations are of very long wave-length ($\sim\nu$).

III. Focusing by the Magnetic Field

We now describe the motion of the ion by introducing a system of cylindrical coordinates r (radius), z (distance from median plane) and φ (azimuth). The origin is taken at the center of the cyclotron chamber. Then from our assumption of symmetry (cf. introduction) it follows that the azimuthal component of the magnetic field is everywhere zero and that the radial and vertical components are independent of the

[6] P. Debye, Math. Ann. **67**, 535 (1909).

[7] $\theta<\pi/2$. We consider half the effective part of the radio-frequency cycle. Similar considerations apply to ions emitted in the other half, i.e., with initial phase between π and $3\pi/2$.

azimuth. The magnetic field is therefore described by components

$$H_r(r, z), \quad H_z(r, z); \quad H_\varphi = 0. \tag{29}$$

Again from symmetry it is evident that the magnetic lines of force are symmetrical about the median plane. That is

$$H_r(r, -z) = -H_r(r, z), \tag{30}$$

$$H_r(r, 0) = 0, \tag{30a}$$

$$H_z(r, -z) = H_z(r, z). \tag{31}$$

We shall consider a magnetic field whose inhomogeneity is very small (as is the case in the cyclotron), at maximum perhaps of the order of or less than one percent at the exit slit.[8] Therefore, it may, at first sight, seem unlikely that the magnetic field can appreciably affect the motion of the ions. However, in contrast to the electric field, the magnetic field acts over the whole path, and its focusing action is not a differential effect. Moreover, the focusing (Lorentz) force increases as the velocity of the particle. Thus we may expect the motion to be sensitive to even a small inhomogeneity in the magnetic field.

As before we are interested in the displacement of the ion from the median plane. Therefore we consider the equation of motion

$$d^2z/dt^2 = (e/Mc)[\mathbf{v}\times\mathbf{H}]_z, \tag{32}$$

which by (29) becomes

$$d^2z/dt^2 = -(e/Mc)rH_r d\varphi/dt. \tag{33}$$

Since the motion is very nearly circular we set

$$d/dt = (d\varphi/dt)d/d\varphi \tag{34}$$

and with the angular velocity given by

$$d\varphi/dt = -eH_z/Mc \tag{35}$$

we obtain

$$\frac{d^2z}{d\varphi^2} + \frac{d\log H_z}{d\varphi}\frac{dz}{d\varphi} - r\frac{H_r}{H_z} = 0. \tag{36}$$

To obtain z as a function of the number of accelerations we use

$$\pi d/d\varphi = d/d\nu, \tag{37}$$

so that we have

$$\frac{d^2z}{d\nu^2} + \frac{d\log H_z}{d\nu}\frac{dz}{d\nu} - \pi^2\frac{rH_r}{H_z} = 0. \tag{38}$$

The second term can be shown to have a negligible effect owing to the fact that the magnetic field H_z must be very homogeneous inside the acceleration chamber. In order to see this we introduce

$$\zeta = z(H_z/H_z^0)^{\frac{1}{2}},$$

where H_z^0 is the magnetic field at the center. For the actual fields, ζ differs from z by about half a percent at the most. The differential equation for ζ becomes

$$\frac{d^2\zeta}{d\nu^2} - \pi^2\frac{rH_r}{H_z}\left(\frac{H_z}{H_z^0}\right)^{\frac{1}{2}} + \zeta\left[\frac{1}{4H_z^2}\left(\frac{dH_z}{d\nu}\right)^2 - \frac{1}{2H_z}\frac{d^2H_z}{d\nu^2}\right] = 0. \tag{39}$$

The second (predominant) term is approximately (cf. (45))

$$\pi^2\zeta d\log H_z/d\log r. \tag{40}$$

In the two last terms, we also introduce the radial gradient of the field. It is sufficient for this purpose to assume the energy to be proportional to the number of accelerations ν so that

$$r\sim E^{\frac{1}{2}}\sim\nu^{\frac{1}{2}}.$$

Then the two last terms become

$$\zeta\left[\frac{1}{16\nu^2}\left(\frac{d\log H_z}{d\log r}\right)^2 - \frac{1}{8\nu^2}\frac{1}{H_z}\frac{d^2H_z}{(d\log r)^2} + \frac{1}{4\nu^2}\frac{d\log H_z}{d\log r}\right]. \tag{39a}$$

Because of the small field inhomogeneity, and because of the large number of accelerations, this expression will be very much smaller (at least by a factor 10^{-5}) than (40).

Thus our equation of motion (39) reduces to

$$d^2z/d\nu^2 - \pi^2 rH_r/H_z = 0. \tag{41}$$

Now since the motion of the ions will be confined to the vicinity of the median plane ($z\sim 0$) only the value of the Lorentz force in this neighborhood will be of importance.[9] Therefore, from (30a) we have

$$H_r(z\sim 0) = z(\partial H_r/\partial z)_0. \tag{42}$$

According to Maxwell's equation,

$$\partial H_r/\partial z = \partial H_z/\partial r \tag{43}$$

since there are no currents in the cyclotron chamber. Therefore

$$H_r = z(\partial H_z/\partial r)_0. \tag{44}$$

Inserting this into (41), we obtain

$$d^2z/d\nu^2 - \pi^2(d\log H_z/d\log r)z = 0. \tag{45}$$

[8] In Section V we shall show that it is very advantageous and, in fact, necessary that the field inhomogeneity be of the order or less than this amount.

[9] In fact, since the magnetic gap is usually considerably larger than the dee height, this approximation will be valid. Direct measurements by R. Wilson (Phys. Rev. **53**, 408 (1938)) show that (42) is justified over the whole region between the dees.

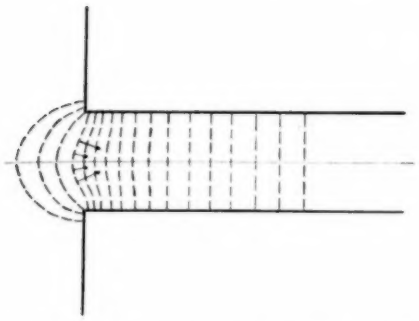

FIG. 3. Schematic representation of magnetic field indicating the focusing forces due to lines of force concave toward the center of the cyclotron chamber.

As in the case of electric focusing, we obtain an oscillation about the median plane if the coefficient of z is positive. This is the case when the magnetic field decreases[10] radially. In the opposite case we shall get an exponential type of solution and therefore strong defocusing. This result can very easily be understood from the shape of the magnetic lines of force. If these lines are concave towards the center of the cyclotron as shown in Fig. 3 the Lorentz force will have a component towards the median plane (besides the main component causing the circular motion of the ions). Concave lines of force are obtained if H_r is negative above the median plane and positive below, which requires $\partial H_r/\partial z<0$ in the median plane and therefore $\partial H_z/\partial r<0$ according to (43). If the magnetic field in the median plane increases radially outwards, the lines of force will be convex toward the center and the Lorentz force will have a component away from the median plane resulting in defocusing.

The actual motion of the ions will be due to the combined action of electric and magnetic focusing. Combining (25) and (45), we obtain

$$\frac{d^2z}{d\nu^2}+\left[\frac{\pi e V_0 \sin\theta}{E}-\pi^2\frac{d\log H_z}{d\log r}\right]z=0. \quad (46)$$

The principal condition for focusing is therefore that the square bracket be positive everywhere. Near the center of the cyclotron where the energy E is small, the first term (electric focusing) will predominate, and in this region it will be allowable to have the second term slightly negative, i.e. to have a slow increase of the magnetic field. In the outer regions (E large), however, the first term becomes negligible so that the whole focusing depends on the gradient of the magnetic field. It is therefore essential for the operation of a cyclotron that the magnetic field decreases with increasing distance r from the center at least in the outer region.

The decrease in intensity due to even a slight amount of defocusing is enormous. Let us assume that H_z decreases everywhere except in a certain region near r_0 of extension δr where it increases with constant gradient. Disregarding the electric focusing, the decrease of the beam intensity will be given by a factor

$$\exp\left[-\pi\int(d\log H_z/d\log r)^{\frac{1}{2}}d\nu\right]$$
$$\approx\exp\left[-2\pi\nu_0(\delta\log H_z)^{\frac{1}{2}}(\delta r/r_0)^{\frac{1}{2}}\right], \quad (47)$$

where ν_0 is the number of accelerations corresponding to the point r_0. Assuming an extension of the defocusing region $\delta r/r_0=1/10$ and an increase of the magnetic field by only one percent, and taking $\nu_0=100$, the intensity is decreased by a factor e^{-20}.

This very great effect of the magnetic focusing explains the extreme sensitivity of the cyclotron operation to the magnetic field (effect of shimming). It can be assumed that the empirical shimming as carried out by the experimenters has tended to avoid a defocusing field. Of course, it is not possible to use a field with too large a gradient, even though this would improve the focusing, because such a field would not give resonance. But we can be reasonably certain that in all practical cases the magnetic field had a negative gradient, and presumably this gradient is in general greatest near the edge of the acceleration chamber. This is the natural shape of the magnetic field produced by cylindrical pole pieces, and it will persist if the field is corrected for greater homogeneity provided care is taken to preserve the focusing character of the field.

If the field is focusing, the amplitude of the oscillations about the median plane is given by

$$z\sim A(r)=\left[\frac{\pi e V_0 \sin\theta}{E}-\pi^2\frac{d\log H_z}{d\log r}\right]^{-\frac{1}{4}}. \quad (48)$$

[10] For convenience we shall assume throughout that $H_z>0$.

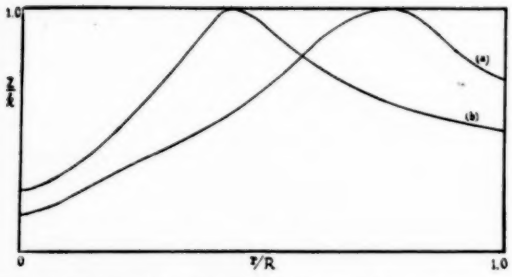

FIG. 4. Curve (*a*): shape of effective beam for electric focusing, $h_N=0.55\times10^{-2}$ for protons. Initial phase sin $\theta_0=1.0$. Maximum displacement at $r=0.71R$. For the minimum initial phase sin $\theta_0=0.9$ the maximum amplitude of the beam is at $r=0.69R$. Curve (*b*): Shape of effective beam for magnetic field of constant energy gradient and sin $\theta_0=0.9C_{\min.}=1.0$. Maximum displacement at $r=0.46R$. For sin $\theta_0=1.0$ the beam maximum is at $r=0.47R$.

In the first part of the path (small energy) the electric focusing will predominate and therefore z will increase as $E^{\frac{1}{4}}$. In the outer part, the magnetic focusing will be the more important, and z will behave as $(|d\log H_z/d\log r|)^{-\frac{1}{2}}$. If the gradient of the magnetic field increases towards the edge, as is usual, the amplitude of the beam will decrease in the region of magnetic focusing. In this case, the amplitude will reach a maximum at the boundary of electric and magnetic region, and the intensity of the beam will depend on the fact that this maximum cannot be larger than half the height of the dees. For the ions which have just this maximum amplitude the envelope of the oscillations is given by

$$Z=kA(r)/A_{\max}, \tag{49}$$

where $A(r)$ is given in (48), and $2k$ is the height of dees. For a given magnetic field the position of the maximum amplitude will depend on the phase at emission, θ_0. Ions of a given phase will leave the source at points below $z_0(\theta_0)$ which is obtained by joining the result (49) to the path near the source obtained by numerical integration. Ions with an initial z larger than $z_0(\theta_0)$ will strike the dees and be lost from the beam. Therefore $z_0(\theta_0)$ gives the effective height of the source for the ions of the given initial phase. Conversely, all ions emitted at $z_0(\theta_0)$ with an initial phase smaller than θ_0 will be able to pass through the cyclotron. For very small phases the focusing is almost entirely due to the magnetic field, *provided the phase remains constant—small energy*. If the magnetic field produces a convergence of the ions at the center of the cyclotron, e.g. field of plane parallel pole faces, ions may be obtained from all parts of the source up to the dees. Thus the effective beam, in this case, will fill the dees up to the point of maximum displacement of the ions emitted at $z=z_0(\pi/2)$ and beyond this point the beam will converge. However, the part of the source near the dees will not be so effective in producing obtainable ions since *only* for small initial phases will the ions clear the dees.

In many cases the beam will diverge in the beginning of the path and the effective height of the source will be limited. Thus for a homogeneous magnetic field and constant phase, the beam diverges over the whole path (Z maximum at the exit slit) and the effective height of the source is about 30 percent of the dee height. For the magnetic fields designed to give high energy ions (Section V) only a limited part of the radiofrequency cycle near $\theta=\pi/2$ can be used and the effective height of source will be between 15 and 30 percent of the dee height (cf. Fig. 4). In any case as long as there is any magnetic focusing the beam in the outer part of the path ($r>\sim$ half the dee radius, say) will be a convergent one. This result is in accord with experiments carried out in the laboratory at Berkeley by R. Wilson (cf. reference 9). The distribution of the radioactivity induced in a copper rod placed vertically at various points in the cyclotron was measured. For the measurements close to the source, the copper rod was covered with carbon because the ion energy would be insufficient to induce radioactivity in Cu. The beam was found to converge from a distance from the source of $r=0.3$ of the dee radius out to the exit slit. The shape of the beam agrees with that expected from the focusing found by inserting the actual field of the Berkeley magnet into (48). Careful measurements of the gradient of this field were carried out by Wilson who also derived theoretically the magnetic part of (48), i.e., the part which alone is important in the outer region.

From the above discussion of the shape of the beam it follows that the cyclotron dees may be constructed so as to just accommodate the effective beam without leaving unnecessary space at top and bottom. This construction which was first suggested by Lawrence has the advantage of materially reducing the capacitance of the

electric oscillating system. The height of the dees must be great only near or up to the maximum of $A(r)$ (cf. (48)) which, in general, will be at r from $\frac{1}{3}$ to $\frac{3}{4}$ the dee radius (cf. Fig. 4). Farther out, the dee height may be chosen considerably smaller.

In this connection, it is essential that the permissible shape of the dees depends very sensitively on the magnetic field. With an exactly homogeneous field, the maximum of the beam amplitude occurs at the exit slit. In order to obtain a larger reduction in capacitance, a somewhat inhomogeneous field is necessary. Such a field has the further advantage of giving a narrower beam at the exit slit which is convenient for scattering experiments, bombarding of small targets, etc. However, for some cases, especially in the high energy region, a homogeneous field may be more desirable for better resonance. It seems likely that for different purposes different constructions will be more advantageous, having more or less magnetic focusing and dees of the corresponding shapes.

IV. The Resonance Requirement

As has been intimated above, the intensity of the emergent beam will depend very much on the phase lag between the angular velocity of the ions and the oscillations of the electric field. Such a phase lag will, of course, occur if the actual magnetic field deviates from the resonance field, defined by (54, 55 cf. below). To maintain accurate resonance would require a homogeneous field, and in fact, taking into account the relativistic change of mass, a slightly increasing field. From the considerations of the preceding section such a field would give a magnetic defocusing which is very strong even for a field which increases slowly. We must therefore be prepared to sacrifice exact resonance. In the following we wish to determine the effect of a deviation from resonance on the beam intensity.

For the phase lag at the νth acceleration we have

$$\Delta\theta_\nu = \omega t_\nu - \nu\pi, \tag{50}$$

where t_ν is the time at which the ion passes through the νth lens. The time required for the passage from the νth to the $(\nu+1)$st lens is

$$dt_\nu/d\nu = t_{\nu+1} - t_\nu = \pi/|\dot{\varphi}|, \tag{51}$$

where the angular velocity $\dot{\varphi}$ is given in (35). Therefore the phase lag for ν accelerations is

$$\Delta\theta_\nu = \pi\int_0^\nu (\omega/|\dot{\varphi}| - 1)d\nu. \tag{52}$$

The total phase change for N accelerations is

$$\Delta\theta_N = \pi\int_0^N (H_{res}/H_z - 1)d\nu, \tag{53}$$

where the resonance field H_{res} is given by

$$H_{res} = H_0(1+E/M_0c^2), \tag{54}$$

$$H_0 = M_0c\omega/e, \tag{55}$$

M_0 being the *rest* mass of the ion. Although the greatest deviation of the magnetic field H_z from the resonance field may be small (of the order of one percent) the total phase change over a *large* number of accelerations ($\sim$200 to 500) may easily be considerably greater than π, which would completely destroy the beam.

Suppose the magnetic field is smaller than the resonance field. If we consider an ion which is emitted when the phase of the electric field is $\theta_0 (0<\theta_0<\pi/2$ for example), then a total phase change $\Delta\theta_N \geqq \pi/2-\theta_0$ will make the phase reach the value $\pi/2$ at some point. The ion then encounters a retarding field and is lost from the beam.

The ion when retarded begins to spiral inwards, undergoing a deceleration at each lens equal to the acceleration received at that same lens on the outward spiral path. The path is then retraced while the phase continues to increase. If the ion should approach the source the phase would approach $\pi-\theta_0$ so that on the entire inward journey the field is a retarding one and the ion cannot return to the beam.

If the field is too large for resonance defocusing by the electric field will result when the phase becomes negative. If the magnetic field provides strong enough focusing to overcome the electric defocusing (cf. reference 12), retardation of the ions results for a total phase change $\Delta\theta_N \leqq -\pi/2 - \theta_0$, i.e., $-\pi<\theta<-\pi/2$.

Therefore we arrive at the conclusion that to obtain a beam of any intensity it is necessary to have a magnetic field which will result in a total phase change of π or less (where electric focusing alone is effective the phase change must

be less than $\pi/2$). The requirement of small phase change is all the more essential insofar as ions which are emitted at a phase near $\pi/2$ will make more revolutions in reaching a given energy. Thus, for these ions the phase changes with *energy* rather rapidly ($\sim$sec. θ).

V. Maximum Energy of the Ions

From the above discussion it is apparent that a magnetic field which accurately maintains resonance ($H_z=H_{res}$) will give magnetic defocusing, the resonance field increasing radially outwards. This opposition between focusing and the requirement of resonance becomes very marked for high energy ions and constitutes a serious barrier in obtaining ions of very much greater energy than obtained in cyclotrons at present.[11] However, sacrificing intensity, it is possible to construct magnetic fields which will give energies appreciably greater than any obtained thus far. The magnetic field must be such that no defocusing of the ions nor phase changes greater than π will take place. The magnetic field which will give the largest energy for a given intensity will be one which is greater than the resonance field near the center of the cyclotron and smaller farther out. With such a field, the phase θ will first decrease and then increase again. The field must be so chosen that θ does not become less than $-\pi/2$ at its minimum, and remains less than $\pi/2$ both at the beginning and at the end of the path.[12] The closer the critical values $-\pi/2$ and $\pi/2$ are approached, the higher will be the energy and the lower the intensity. Our problem is now to determine the best form of the magnetic field which gives maximum energy for prescribed phase changes without defocusing the ions.

The focusing is governed by the quantity (cf. 46)

$$F=(eV_0/E)\sin\theta-2\pi\, d\log H_z/d\log E. \quad (56)$$

The resonance of the ions is determined from the equation (cf. (53))

$$d\theta/d\nu=\pi(H_{res}/H_z-1). \quad (57)$$

We represent the relative inhomogeneity of the field by h, that is

$$H_z=H_0(1+h). \quad (58)$$

Using (54) and (24a) we have from (57)

$$\frac{d\sin\theta}{dE}=\frac{\pi}{2eV_0}\left(\frac{E}{M_0c^2}-h\right). \quad (59)$$

It will be convenient in the following to introduce the abbreviations

$$\epsilon=E/E_N,\quad A=\pi E_N{}^2/2eV_0M_0c^2,$$
$$B=\pi E_Nh_N/2eV_0,\quad C=E_NF/eV_0. \quad (60)$$

Where E_N is the final energy and h_N the value of h at the exit slit. Then the focusing expression (56) becomes

$$C=(\sin\theta)/\epsilon-4B\epsilon\, d(h/h_N)/d\epsilon. \quad (61)$$

This expression must be positive everywhere. The resonance equation (59) becomes

$$d\sin\theta/d\epsilon=A\epsilon-Bh/h_N. \quad (62)$$

As a particularly simple case, and one which should be not too difficult to realize in practice, we consider first a homogeneous magnetic field, $h=h_N$. From (62) we find

$$\sin\theta=\tfrac{1}{2}A\epsilon^2-B\epsilon+\sin\theta_0, \quad (63)$$

where θ_0 is the initial phase. According to our qualitative discussions, B should be positive, i.e., the actual field should be larger than the resonance field at the center. Then $\sin\theta$ as given by (63) will have a minimum at

$$\epsilon_1=B/A. \quad (64)$$

At this point, as may be seen from (59), the magnetic field is equal to the resonance field. The phase of the ions is given by

$$\sin\theta_{min}=\sin\theta_0-B^2/2A. \quad (65)$$

Since for the homogeneous magnetic field we have only electric focusing the minimum θ must be positive. With given values of A and B, $\sin\theta_{min}$ will be zero for a certain value θ_0' of the initial phase θ_0. Only ions having an initial phase between θ_0' and $\pi/2$ will be able to get through the cyclotron (cf. (63)).

In order to lose no *intensity*, the phase at the exit slit, θ_1, must not be greater than θ_0 but it

[11] H. A. Bethe and M. E. Rose, Phys. Rev. **52**, 1254 (1937).

[12] For negative phases the electric field produces defocusing but the magnetic field can always be chosen so that a net focusing action is produced.

is of no advantage at all to make it smaller. For obtaining high *energy*, θ_1 should be as large as possible. Therefore we set $\theta_1=\theta_0$. From (63),

$$\sin\theta_1=\tfrac{1}{2}A-B+\sin\theta_0. \tag{66}$$

Therefore
$$B=\tfrac{1}{2}A. \tag{67}$$

From the definition of θ_0' and (65), we have

$$B^2/2A=\tfrac{1}{8}A=\sin\theta_0'. \tag{68}$$

This determines the maximum obtainable energy E_N in terms of the available part of the radio frequency cycle, $\frac{1}{2}\pi-\theta_0'$. According to (60),

$$E_N=4\pi^{-\frac{1}{2}}(eV_0M_0c^2\sin\theta_0')^{\frac{1}{2}}. \tag{69}$$

If $2V_0$ is the dee voltage in kv, A the atomic weight and Z the atomic number of the ions, the energy in Mev is

$$E_N=1.54(2V_0AZ\sin\theta_0')^{\frac{1}{2}}. \tag{70}$$

For a dee voltage $2V_0=50$ kv and $\theta_0'=\pi/2$, this gives 10.9 Mev protons, 15.4 Mev deuterons and 30 8 Mev α-particles. For $\sin\theta_0'=0.9$, these energies will be reduced by 5 percent. This corresponds to $\theta_0'=64°$, i.e., the usable part of the radiofrequency cycle will be reduced to 30 percent of the part available at low energies.

The rather high energies obtained here are due to the fact that we have made the magnetic field "cross" the resonance field. This crossing is responsible for the minimum of the phase and occurs (cf. (64), (67)) at an energy equal to one-half the final energy, i.e., at a distance from the center equal to 0.7 of the exit slit radius. The value of the magnetic field follows directly from (67) with the help of (60):

$$h_N=\left(\frac{2}{\pi}\right)^{\frac{1}{2}}\left(\frac{2eV_0\sin\theta_0'}{M_0c^2}\right)^{\frac{1}{2}}$$

$$=0.83\times10^{-3}\left(\frac{2V_0Z\sin\theta_0'}{A}\right)^{\frac{1}{2}} \tag{71}$$

with the same notations as in (70). For $2V_0=50$ kv, $\sin\theta_0'=0.9$, we have $h_N=0.55\times10^{-2}$ for protons, and $h_N=0.39\times10^{-2}$ for deuterons and α-particles. Thus the magnetic field must be larger than the resonance field at the center (H_0) by only a fraction of a percent and the resulting energy will be extremely sensitive to its exact value. The condition $\sin\theta_0'<1$ imposes an upper bound on h_N while too low an h_N will result in a small final energy. E.g., for $h_N=0$, the final energy obtainable will be reduced to one-half the above values.

TABLE I. *Proton energy and field characteristics for constant gradient magnetic field (73). Dee voltage = 50 kv.*

A. *Proton energy in Mev*

$\sin\theta_0$ \ $C_{\min}$	0	1	2	4
1.0	14.4	13.8	13.2	11.5
0.9	13.9	13.3	12.6	10.7
0.8	13.4	12.7	11.9	9.7

B. *Excess of field over resonance field at center, $(1+\gamma)h_N$ in percent*

$\sin\theta_0$ \ $C_{\min}$	0	1	2	4
1.0	0.88	0.92	0.96	1.11
0.9	0.87	0.91	0.96	1.13
0.8	0.86	0.90	0.96	1.18

C. *Field inhomogeneity, $h_0-h_N=\gamma h_N$ in percent*

$\sin\theta_0$ \ $C_{\min}$	0	1	2	4
1.0	0.22	0.35	0.51	0.97
0.9	0.24	0.39	0.57	1.10
0.8	0.27	0.43	0.64	1.32

The shape of the effective beam for the homogeneous magnetic field is given in Fig. 4, curve (*a*). It will be noted that in this case the electric field actually produces some convergence of the beam. The reason for this lies in the fact that the phase reaches a minimum. At this point the focusing forces due to the electric field are small. The amplitude of the beam is seen from (61) to be proportional to $(\epsilon/\sin\theta)^{\frac{1}{2}}$ and therefore reaches a maximum.

A simple field which will provide some magnetic focusing and consequently better intensity is one which decreases quadratically with the distance from the center, which means constant gradient with respect to energy. Thus

$$dh/d\epsilon=-\gamma h_N, \tag{72}$$

where γ is constant. This gives

$$h/h_N=1+\gamma(1-\epsilon)=1+\gamma(1-r^2/R^2). \tag{73}$$

From (62) we find

$$\sin\theta=\tfrac{1}{2}(A+B\gamma)\epsilon^2-B(1+\gamma)\epsilon+\sin\theta_0, \tag{74}$$

which is of the same form as (63). As before,

the condition $\sin\theta_1=\sin\theta_0$ gives (cf. (67))

$$\tfrac{1}{2}(A+B\gamma)=B(1+\gamma). \tag{75}$$

The minimum of θ is again reached at $\epsilon=\frac{1}{2}$ and has the value

$$\sin\theta_{\min}=-\tfrac{1}{8}(A+B\gamma)+\sin\theta_0. \tag{76}$$

However, since we now have magnetic focusing, it is no longer necessary to keep the phase θ positive. The condition for net focusing is that the quantity C given in (61) be positive everywhere. With (72), (74), (75) this gives

$$C=\tfrac{1}{2}(A+B\gamma)(\epsilon-1)+(\sin\theta_0)/\epsilon+4B\gamma\epsilon\geqslant 0. \tag{77}$$

The minimum of C is obtained for

$$\epsilon_{\min}{}^2=2\sin\theta_0/(A+9B\gamma), \tag{78}$$

and we find

$$\sin\theta_0=(A+B\gamma+2C_{\min})^2/8(A+9B\gamma). \tag{79}$$

There remains, of course, the condition that $\sin\theta_{\min}\geqslant -1$. Maximum energy will be obtained by taking the equal sign. Then from (76)

$$A+B\gamma=8(1+\sin\theta_0). \tag{80}$$

Combining (79) and (80), we find

$$A=9(1+\sin\theta_0)-(1+\sin\theta_0+\tfrac{1}{4}C_{\min})^2/\sin\theta_0, \tag{81}$$

$$B\gamma=-(1+\sin\theta_0)+(1+\sin\theta_0+\tfrac{1}{4}C_{\min})^2/\sin\theta_0, \tag{82}$$

$$B=5(1+\sin\theta_0)-(1+\sin\theta_0+\tfrac{1}{4}C_{\min})^2/\sin\theta_0. \tag{83}$$

These equations determine the energy and the magnitude and gradient of the magnetic field.

Table IA gives the proton energies obtainable with 50 kv dee voltage for various initial phases θ_0 and various degrees of focusing (determined by $C_{\min}$). For deuterons, the energies are greater by a factor $\sqrt{2}$, for α-particles by $2\sqrt{2}$. In Table IB, we have given $(1+\gamma)h_N$, the excess at the center of the magnetic field above the resonance field, in percent of the latter (H_0), for protons and 50 kv dee voltage. For deuterons and α-particles, these values must be divided by $\sqrt{2}$. Table IC contains the field inhomogeneity γh_N, i.e. the difference between the field at the center and that at the exit slit, also for protons and 50 kv, in percent of the total magnetic field H_0.

It is seen that the maximum energy obtainable is considerably improved (14.4 Mev protons instead of 10.9 Mev) as compared to the homogeneous field case. This is due to the fact that with a magnetic focusing field we can allow the electric field to become defocusing so that greater changes of phase are permissible *viz.* between $\pi/2$ and $-\pi/2$ instead of between $\pi/2$ and 0. The initial phase θ_0 does not have a very great effect on the obtainable energy. On the other hand, the energy will be seriously limited if good focusing (large $C_{\min}$) is required.

The usable part of source is given approximately by

$$[(2eV_0/E_N)nC_{\min}\cot\theta_0]^{\frac{1}{2}}, \tag{84}$$

where n is a number between 1 and 5 representing the first few accelerations during which the path of the ion lies essentially in the acceleration region. For $\sin\theta_0=0.9$, $C_{\min}=1$ and $n=3$, the effective part of the source is 27 percent of the dee height. Fig. 4 curve (*b*) gives the shape of the beam in this case.

The inhomogeneity of this field being only 0.4 percent, we must have the distance between the pole faces change by the same relative amount, the distance being smallest at the center and increasing as const. $+r^2$.[13] This requires extreme

TABLE II.

A. *Proton energies in Mev for 50 kv dee voltage*

$\sin\theta_0$	$C=0$	$C=1$
1	15.7	15.4
0.9		14.9

B. *Percent excess of magnetic field at exit slit over the resonance field at center (H_0). Protons and 50 kv dee voltage.*

$\sin\theta_0$	$C=0$	$C=1$
1	0.85	0.81
0.9		0.785

C. *Diameter of dees (cm) for protons and deuterons (α-particles) for the case $C=1$, $\sin\theta_0=0.9$, $2V_0=50$ kv.*

H_0 (kilogauss)	PROTONS	DEUTERONS α-PARTICLES
15	73	123
18	61	103

[13] We assume that the exit slit lies sufficiently far inside the magnetic poles so that the field from plane parallel poles would be perfectly homogeneous; otherwise, we

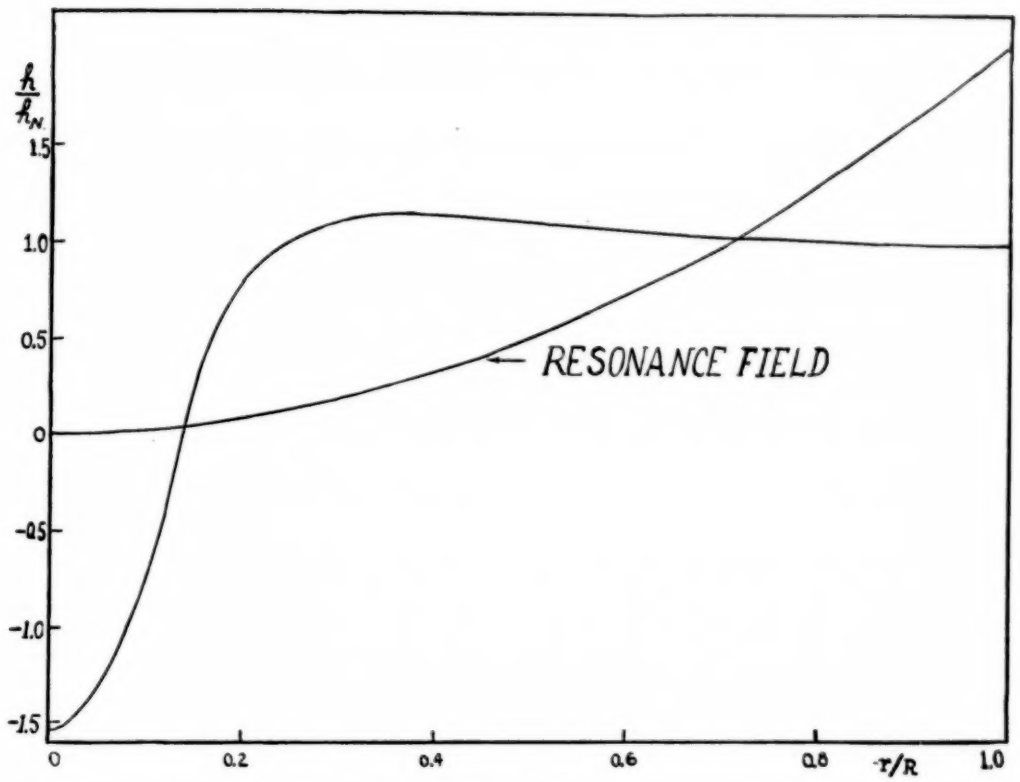

FIG. 5. Magnetic field for high energy ions. $C=1$, $\sin\theta_0=\sin\theta_1=0.9$. $100h_N=0.785$ (protons), $=0.555$ (deuterons and α-particles).

accuracy in the machining of the pole faces or in the shimming, and also extreme homogeneity of the iron (or suitable compensation of inhomogeneities).

In order to obtain the absolute maximum energies without defocusing, we proceed as follows: We choose the magnetic field h as a function of ϵ in such a way that the "focusing force" C (cf. (61)) is constant for all ϵ. This means (cf. (56), (60)) a beam of constant amplitude which improves the intensity. In the limit, we may make $C=0$ in which case there will be no focusing and no defocusing but simply a linear increase of the beam amplitude with the number of accelerations; then about one percent of the ions of correct phase will arrive at the exit slit. Of course, we can only make C constant for ions of a certain initial phase, all other ions will experience a varying focusing force. Furthermore, we shall drop the requirement of constant C very near the origin where it would correspond to a magnetic field of infinite positive gradient (cf. (61)).

Using our assumption $C=$ const., we may eliminate h/h_N from the equations (61) (62) and obtain

$$d^2\sin\theta/d\epsilon^2+\sin\theta/4\epsilon^2=A+C/4\epsilon. \quad (85)$$

The solution of this equation is

$$\sin\theta=4A\epsilon^2/9+C\epsilon+\epsilon^{\frac{1}{2}}(\alpha+\beta\log\epsilon). \quad (86)$$

Since Eq. (85), and therefore its solution (86), are not supposed to hold down to $\epsilon=0$, the integration constants α and β must be determined from the values of $\sin\theta$ and h at $\epsilon=1$. This gives

$$\alpha=\sin\theta_1-4A/9-C, \quad (87)$$

$$\beta=\tfrac{1}{3}A-\tfrac{1}{2}C-\tfrac{1}{2}\sin\theta_1-B. \quad (88)$$

$\sin\theta$ as given in Eq. (86) will in general have a minimum (at ϵ_1, say) and a maximum at a smaller ϵ (ϵ_2, say). The minimum of $\sin\theta$ must again be not smaller than -1, and the highest energies are obtained for $\sin\theta_{\min}=-1$. The

assume that the edge effects have been compensated by suitable shimming.

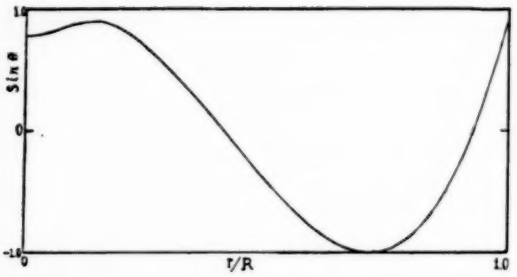

FIG. 6 Sin θ for $C=1$, sin $\theta_0=\sin\theta_1=0.9$.

maximum must be smaller than 1, and will be denoted by sin θ_0. As before it will be most advantageous to take sin $\theta_0=\sin\theta_1$. The available part of the radiofrequency cycle will then be equal to $\pi/2-\theta_0$.

Table IIA gives the proton energies obtainable (with 50 kv dee voltage, IIB the values of h_N for protons. Table IIC gives the diameter of the dees ($2R$) for protons and deuterons (or α-particles) corresponding to the energies found in the case $C=1$ and sin $\theta_0=0.9$. The pole piece diameters may then be larger than these dee diameters by a distance equal to the magnetic gap. The maximum proton energy, obtained for no focusing ($C=0$) and $\theta_0=\pi/2$, is 15.7 Mev; for this energy, the beam intensity will, of course, be negligibly small. With $C=1$ and sin $\theta_0=\sin\theta_1=0.9$, protons of 14.9 Mev can be obtained, or deuterons of 21.1 Mev or α-particles of 42.2 Mev. The intensities in this case would be appreciable, perhaps one-quarter of the intensities obtained at low energies. It seems very probable that the energies mentioned represent the actual upper limit for the cyclotron with the given dee voltage of 50 kv, at least without very radical changes in design.

The magnetic field corresponding to $C=1$, sin $\theta_0=\sin\theta_1=0.9$ is plotted in Fig. 5 as a function of r/R. The curve is seen to cross the curve for the resonance field twice, *viz.* at the positions r_2 and r_1, corresponding to ϵ_2 and ϵ_1, of maximum and minimum phase θ. Inside of the point ϵ_2, the field as computed from (62), (86) was replaced by a field of constant gradient in energy (parabola in r). The two crossing points ϵ_1, ϵ_2 are almost the same in each of the three cases considered in Table II, and the outer one is nearly at the same position as for the homogeneous field and the field of constant gradient discussed above ($\epsilon_1=0.5$, $r_1/R=0.71$). The inhomogeneity of the field, Fig. 5, is very small. Beyond the first crossing point, at $r_2=0.14R$, the maximum inhomogeneity, at $r=0.37R$, is $h=1.16h_N=0.91$ percent. The behavior of the field from the center up to the first crossing point is, of course, not very critical. The only requirement for the field in this region is that the gradient be not so large as to result in a magnetic defocusing larger than the electric focusing. Thus any field with a smaller gradient and smaller inhomogeneity for $r<r_2$ will also be satisfactory. The magnetic fields in the other cases mentioned above are very little different (less than 1 part in 1000) from the field given. This indicates again the sensitivity of the obtainable energy to the magnetic field.

Figure 6 gives the phase sin θ as a function of r/R for the field of Fig. 5.

As has been pointed out repeatedly, high energies can only be obtained from the cyclotron if extreme care is taken to produce the correct magnetic field. Deviations of less than one part in a thousand at any point may completely destroy the desirable characteristics of the field especially since the "best" fields are very close to defocusing fields. Perhaps the first step in obtaining a good field would be to make the field exactly homogeneous. It will not be sufficient to check the homogeneity by direct measurement of the field at various points but sensitive methods for measuring differences and gradients should be applied. If these methods should prove to be not sensitive enough, the performance of the cyclotron itself at a low energy may be taken as a test for the homogeneity. The magnetic field must be so varied that the magnetic part of the focusing disappears, leaving only the electric focusing and therefore resulting in a beam amplitude proportional to $r^{\frac{1}{2}}$. With a source extending over the whole dee height, the beam would in this case fill the whole space within the dees everywhere; if the height of the source is reduced sufficiently, the proportionality of the beam height with $r^{\frac{1}{2}}$ could be tested directly by observing the distribution of radioactivity on a substance placed vertically at various points of the cyclotron. After the homogeneous field has been obtained, the small variations of the field

required by the theory can be achieved by thin shims. The shape and dimensions of these shims will be given in a forthcoming paper.

A further increase of the energy of the ions could, of course, be obtained by increasing the dee voltage. Unfortunately, the maximum energy is only proportional to the square root of this voltage (cf. (60)), and it seems at the moment very difficult to obtain dee voltages higher than, say, 100 kv.

Various possibilities for improving either the focusing or the resonance by changing the design of the cyclotron were considered but there are objections to each of them. As an example an attempt was made to modify the *resonance* condition by considering that the diametral edge of the dees are curved so as to reduce the length of path of the ions between two accelerations but this reduction turns out to be exactly compensated by the ensuing outward deflection of the ions in the acceleration. An improvement of the *focusing* is not possible by merely changing the geometry of the dees or the magnet, but it is necessary to invalidate the Laplace equation for either the electric or magnetic field. The latter could be accomplished in principle by inserting wires carrying currents in the median plane but the necessary currents are large and the scheme seems hardly feasible. The electric focusing could be improved by inserting grids. One arrangement was suggested by Lawrence and consists of a grid in the opening of the dee to which the ions are accelerated. With a plane grid of this type consisting of many (>10) horizontal wires, the energy limit may be increased by 50 percent. Another possibility would be the insertion of a grid into the median plane of each dee. This grid would be at a *static* negative potential of a few kilovolts with respect to top and bottom of the dee. With such an arrangement the energy limit is determined by the electrostatic potential applied, being about 1000 times this potential for protons. In both cases, however, the grid spacing must be very large compared to the diameter of the wires in order to avoid obstruction. Therefore these schemes for improving the cyclotron do not seem of immediate practical value.

The author takes great pleasure in expressing his appreciation to Professor H. A. Bethe for his continued interest in this work and for many valuable discussions.

Appendix

In Eq. (15) it was shown that the deflection of an ion due to the change of energy in passing through a lens depends on the quantity

$$I(z)=\int_{-\infty}^{\infty} V(dU/dx)dx. \tag{1A}$$

From (4b) we have

$$I(z)=-\int_{-\infty}^{\infty} U(dV/dx)dx. \tag{2A}$$

Using the expansion of U as an odd function of z (cf 4a) and the relation

$$\partial^{2n+1}U/\partial z^{2n+1}=(-)^{n+1}\partial^{2n+1}V/\partial x^{2n+1} \tag{3A}$$

which can be derived from (2) and (3) we find

$$I(z)=\sum_{0}^{\infty}\frac{z^{2n+1}}{(2n+1)!}\int_{-\infty}^{\infty}\left[\left(\frac{d}{dx}\right)_{n+1}V\right]^2 dx \tag{4A}$$

where n partial integrations have been performed in the nth term. From this we see that $I(z)$ is a positive monotonic function of z. The evaluation of the integrals in (4A) will depend on the special geometry of the accelerating electrodes. We may, however, obtain a fairly good evaluation of I by considering the behavior near the median plane and near the dees. Near the dees, the electric field is in the z direction ($dV/dx=0$) except between the dees where the field is very nearly parallel to x; so that in the region where dV/dx is not zero U is constant $=U_k$. Therefore

$$I(k)=2U_kV_0. \tag{5A}$$

Near the median plane

$$I=z\int_{-\infty}^{\infty}(dV/dx)^2dx. \tag{6A}$$

To evaluate U_k and the integral in (6) we may use the description of the field given by the Schwarz method.[14] If we denote the dee separation by $2l$ we find

$$U_k=(V_0/\pi)\log(1+a)/(1-a), \tag{7A}$$

where a is defined by

$$\frac{\pi l}{2k}=\frac{(1-a^2)^{\frac{1}{2}}}{a^2}+\log\frac{1+(1-a^2)^{\frac{1}{2}}}{a};\quad a<1. \tag{8A}$$

For the electric field on the median plane we find

$$\left|\frac{dV}{dx}\right|=\frac{a^2V_0}{k}\frac{\sec\pi v/2}{1+a^2\tan^2\pi v/2}, \tag{9A}$$

where $v=V/V_0$. The integral in (6A) becomes

$$\int_{-\infty}^{\infty}(dV/dx)^2dx=2V_0^2\int_0^1(dv/dx)dv$$
$$=\frac{4a^2V_0^2}{\pi k(1-a^2)^{\frac{1}{2}}}\log\frac{1+(1-a^2)^{\frac{1}{2}}}{a}. \tag{10A}$$

From numerical examples we may see that $I(z)$ does not depart very much from linearity. Thus for $l/k=0.64$ ($a=0.9$) the straight line tangent to I at $z=0$ gives $I=1.1V_0^2$ at

[14] Cf. F. Kottler, *Handbuch der Physik*, Vol. 12 p. 480.

$z=k$ while the true value (5A) is $1.9V_0^2$. Therefore a fairly good approximation to I may be obtained by replacing it with a straight line whose slope may be the average of the slope at the origin and $I(k)/k$. That is we write

$$I(z)=\lambda V_0^2 z/k, \tag{11A}$$

where $$2\lambda=2U_k/V_0+k\int_{-\infty}^{\infty}(dv/dx)^2dx.$$

Then the constant b defined in (16) is

$$b=\tfrac{1}{2}\lambda(2eV_0/Mk^2\omega^2)^{\frac{1}{4}}. \tag{12A}$$

The constant b is in general of order unity. For $k=2$ cm, $\omega=10^8$ sec.$^{-1}$, $2V_0=50$ kv and $\lambda=1.5$ ($a=0.9$, $l/k=0.64$) we find $b=0.84$. For a dee separation-height ratio of 0.3 we have $a=0.975$ and $\lambda=2.0$ giving $b=1.12$.

MARCH 1, 1938 PHYSICAL REVIEW VOLUME 53

Magnetic and Electrostatic Focusing in the Cyclotron

ROBERT R. WILSON
Radiation Laboratory, Department of Physics, University of California, Berkeley, California

(Received December 27, 1937)

A quantitative study of the magnetic and electrostatic focusing of ions being accelerated in the cyclotron is made on the basis of electric and magnetic field measurements. The relative importance of the two effects is found to depend on the energy or path radius of the circulating particles. For small energies, only the electrostatic action is effective; and it is found that actually it constitutes a defocusing action which causes the ions to move away from the central plane between the magnet pole faces and so to become lost. At larger energies the electrostatic field becomes a focusing action but also the effect becomes rapidly smaller and, if acting alone, would cause the particles to oscillate back and forth across the central plane with increasing amplitude so that a very diffuse beam would result. On the other hand, at the larger energies, the focusing due to the outward curvature of the magnetic lines of force soon predominates and becomes rapidly larger and causes the ions to oscillate about the central plane, but now with decreasing amplitude so that it is by the magnetic effect that the diffuse starting ions are focused to the concentrated beam which is actually obtained. It is shown that the amplitudes of vertical oscillation due to the electrostatic field increases with $r^{3/4}$, and that the amplitudes due to the magnetic field vary as $(-r\partial H/\partial r)^{-1/4}$ for ions in phase. Calculations of the vertical motion of the ions as they circulate out from the center by means of a step by step process of integration indicate that the electrostatic defocusing action decreases with d/h, the ratio of electrode separation to electrode height. Thus for maximum output currents the electrode height should be as large and the separation as small as possible. The width of the beam and distribution of ions with height was measured at various distances from the center for the case of the cyclotron in use at Berkeley up to August 1937. This was done by measuring the radioactivity induced in a probe which was introduced into the beam. The widths so obtained agree within one or two mm with the widths calculated from the theory presented. Various changes in accelerator electrode design are suggested which would decrease their capacity and so enable larger high frequency input voltages to be obtained.

INTRODUCTION

THAT the cyclotron is a successful method for accelerating ions to high speeds is due in part to a focusing of the ion beam by the action of the magnetic and electric fields. This action not only keeps the circulating particles within the confines of the hollow accelerator electrodes or "dees" but also concentrates them from their initial diffuse distribution to the narrow high energy beam finally obtained. Although the essential nature of the focusing actions has been understood since the inception of the method,[1–3] the knowledge has been qualitative and little has been known of the relative importance or actual resultant effect of the two actions. For example, it was originally thought that the electrostatic focusing was most effective; however, it will be shown that this action can be one of defocusing as well as of focusing, and that it soon becomes negligible in comparison with the magnetic effect. Consequently, the present paper is concerned with an attempt to make a quantitative investigation of these important focusing actions.

The treatment must, in a large part, be of an empirical and graphical nature because of the

[1] Lawrence and Livingston, Phys. Rev. **40**, 19 (1932).
[2] Livingston, Rev. Sci. Inst. **7**, 55 (1936).
[3] Since the completion of this paper, it has come to the author's attention that Rose and Bethe have made a similar analysis and with similar results.

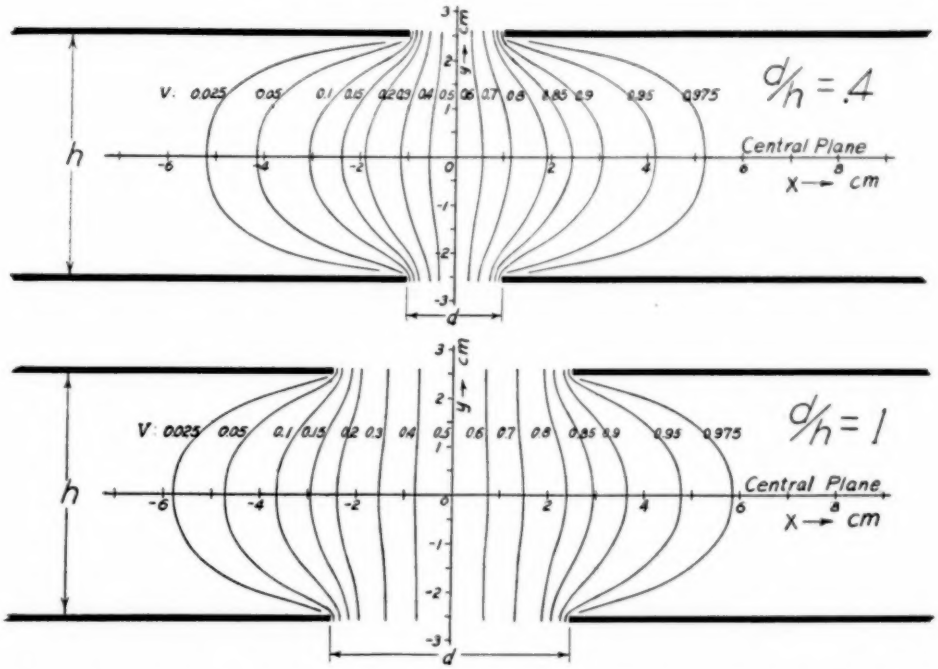

FIG. 1. Distribution of equipotential lines between the accelerating electrodes or dees of the cyclotron. The dees are represented by a cross section perpendicular to the diametral edge.

many variables which enter to complicate the problem. The electrostatic focusing, which is based on electric field measurements, is considered first, to be followed by a treatment of the magnetic focusing based on magnetic field measurements. The two are then compared in the calculation of the vertical motion of ions in the cyclotron. Finally, probe measurements of the height of the beam will be described and correlated to the calculations.

ELECTRIC FIELD

Figure 1 shows the distribution of equipotential lines between the semicircular hollow accelerator electrodes of the cyclotron which are depicted by a cross section of the diametral region. Distributions corresponding to two different ratios of d/h, the electrode separation d to the electrode height h, are given. These, as well as many other plots corresponding to other values of d/h, were obtained experimentally using the standard electrolytic tray method. A comparison of the plots obtained in this way shows that the field between the dees, except in the immediate vicinity of the electrode edges, does not change measurably as d/h becomes less than about 0.4. It is also found that, for d/h less than 0.4, various configurations of metal outside of the space between the dees—such as would correspond to the presence of a filament assembly or to flanging the diametral edges of the electrodes outward—have a negligible effect on the field between the dees. For d/h greater than 0.4, a flat plate placed across and above the gap between the dees causes the equipotential lines to become more vertical and thus the field to become more uniform; the effect of flanging the electrode edge is quite negligible as before.

By a graphical manipulation of the plots of Fig. 1, the curves of Fig. 2 are obtained which show the vertical component of electric field strength E_y plotted against x, the distance into the dees, assuming that $x=0$ midway between the dees. Each curve corresponds to a different value of y, the height above the central plane between the pole faces of the magnet. For purposes of comparison, the horizontal component of electric field strength, as obtained by a method similar to that outlined above for E_y, is also plotted.

The linear dimensions plotted in Figs. 1 and 2 correspond to an $h=5$ cm. This was about the

height of the dees which were used when the probe measurements to be described later were made. In order to obtain the numerical magnitude of E_y from Fig. 2, it is necessary to multiply the scale values by the value of the peak voltage between the dees. The graphs of Figs. 1 and 2 depict the case of a steady voltage applied between the electrodes; actually the voltage alternates at a high frequency so that the field varies rapidly with time. Fortunately, however, because the ions travel around in synchronization with this changing field, the time modified field which an ion actually experiences can be calculated. This will be done in the next section.

Electrostatic Focusing

For a quantitative measure of focusing action, one may consider the change in vertical velocity, Δv_y, that a particle receives in traveling through the field of Fig. 2; if this is known for all positions of a particle within the dees, then the ion paths can be calculated—given initial conditions. A particle which is circulating with a path radius of from 1 to 10 cm—one just getting started—moves through a field that is not only changing rapidly and in a complicated way with its position, as can be seen in Fig. 2, but is also changing with time. This makes an analytical calculation of the Δv_y produced per some fraction of a revolution very difficult so graphical methods will be used later to find this Δv_y when the path radii are small. However, when the radius of path has become larger, the ion moves through all the vertical field after going through only a small fraction of its complete revolution, so that if the particle is in phase (i.e., passes $x=0$ as the voltage reaches a peak value) the variation of the field of Fig. 2 with time need not be considered since the voltage does not change appreciably while the ion is in the field. Then for particles moving with path radii greater than say 10 cm, a calculation can be made of Δv_y per half-revolution, during which the particle crosses the gap once, as follows:

Consider the ion in phase and traveling at an initial height y above the central plane and through a half-revolution such that it goes from $x=-r$ to $x=r+\Delta r$, where r is the initial path radius and Δr the change in r due to the energy acquired in crossing the gap. In going through the first quarter-revolution from $x=-r$ to $x=0$, the particle passes through the negative part of the vertical field and receives a negative Δv_y (i.e., downwards). It is seen in Fig. 2 that the plot of horizontal field has its maximum at $x=0$ where the vertical field is small, so for simplicity assume that all the horizontal acceleration is received at $x=0$. This assumption introduces a considerable error, for although the horizontal field is mostly confined to a region near $x=0$ where the vertical field is very small, some of it extends out farther to where the vertical field is large. The error, which at most is about 20

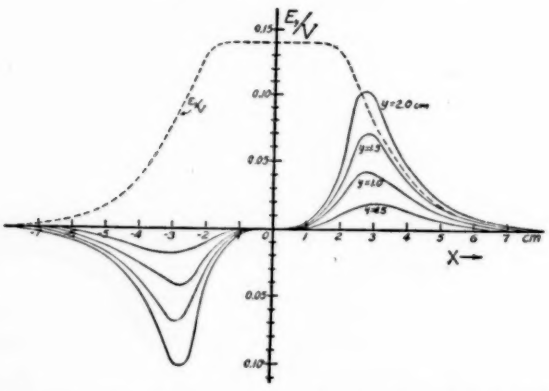

Fig. 2a. The full curves are the vertical electric field divided by the voltage between the dees. The dotted curve represents the horizontal or accelerating field divided by the voltage at a height of 1.5 cm. The case here shown is for $d/h=1$ and $d=5$ cm.

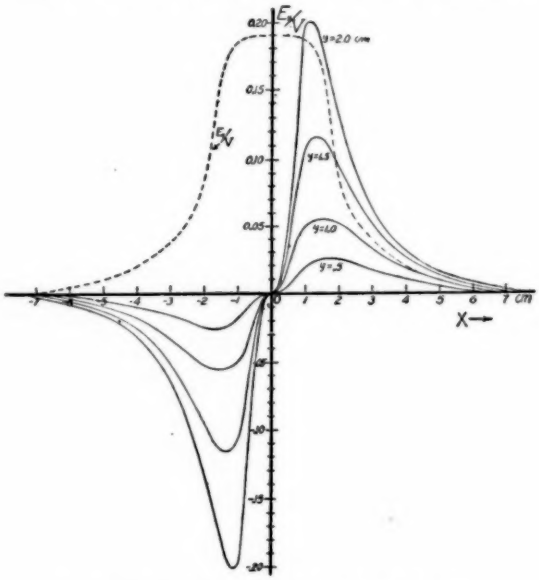

Fig. 2b. Same as Fig. 2a, but for $d/h=0.4$ and with $d=2$ cm.

percent, is such as to make the calculated Δv_y larger than the actual Δv_y and will not seriously affect any of the later calculations, especially as we are interested in showing how small the electrostatic effect is. The ion is given a positive Δv_y (upwards) in the next quarter revolution from $x=0$ to $x=r+\Delta r$, but as the particle is now going faster it remains in the focusing field for a shorter time so that Δv_y is less in magnitude than before. Thus there will be a resultant Δv_y toward the central plane which constitutes the electrostatic focusing action. It is also assumed here that the magnitude of Δv_y in the quarter revolutions is very small in comparison with the horizontal velocity so that the height of the ion will not change appreciably in going through the positive and negative fields. Later calculations will substantiate this assumption.

This can now be considered analytically: The force equation for a particle of mass m and charge e, moving through the vertical field E_y can be written:

$$E_y e = m(dv_y/ds)(ds/dt), \tag{1}$$

where s is measured along the ion path so that ds/dt is simply the horizontal velocity $\mathbf{v}$. While the particle is traveling through the vertical field, it is moving almost parallel to the direction of x, so we may replace s by x. For the first quarter-cycle, $\mathbf{v}$ is constant as the particle is traveling in a field free space, and we may integrate (1) from a relatively large value of x, where the vertical field is zero, to $x=0$ where E_y is again zero to get:

$$\Delta v_y' = \frac{e}{m\mathbf{v}}\int_{-\infty}^{0} E_y dx, \tag{2}$$

where $\Delta v_y'$ is the change in vertical velocity for the quarter-cycle. During the next quarter-cycle from $x=0$ to $x=r+\Delta r$, the horizontal velocity is $\mathbf{v}+\Delta\mathbf{v}$ so Δv_y, the total change of vertical velocity for the half-revolution, is

$$\Delta v_y = \frac{e}{m\mathbf{v}}\int_{-\infty}^{0} E_y dx + \frac{e}{m(\mathbf{v}+\Delta\mathbf{v})}\int_{0}^{\infty} E_y dx; \tag{3}$$

but

$$\int_0^\infty E_y dx = -\int_{-\infty}^{0} E_y dx \tag{4}$$

so that substitution of this and neglecting $\mathbf{v}\Delta\mathbf{v}$ in comparison with $\mathbf{v}^2$ gives:

$$\Delta v_y = -\frac{e}{m}\frac{\Delta\mathbf{v}}{\mathbf{v}^2}\int_0^\infty E_y dx. \tag{5}$$

Now $\int_0^\infty E_y dx$ was evaluated by graphical integration of each of the curves of Fig. 2, and it was found that the integral could be expressed by an empirical equation of the form:

$$\int_0^\infty E_y dx = V_{\max}(a+by)y, \tag{6}$$

where $V_{\max}$ is the maximum voltage between the dees and a and b are constants depending on the ratio d/h. Substitution of (6) and the relations:

$$\mathbf{v} = \frac{e}{m}\frac{Hr}{c} \tag{7}$$

and

$$\Delta\mathbf{v} = \frac{V_{\max} e}{m\mathbf{v}} \tag{8}$$

into (2) gives:

$$\Delta v_y' = -\frac{cV_{\max}}{Hr}(a+by)y \tag{9}$$

for a quarter-cycle, and into (5) gives:

$$\Delta v_y = -\frac{V^2_{\max} c^3 m}{H^3 r^3 e}(a+by)y \tag{10}$$

for the half-revolution or per crossing of the gap.

Typical values of H, $V_{\max}$, and h which correspond to those of the cyclotron in use at Berkeley up to August 1937[4] are $H=16{,}500$ gauss, $V_{\max}=90{,}000$ volts, and $h=5$ cm. For this value of h, $a=0.12$ and $b=0$ if $d/h=1$; while for $d/h=0.4$, $a=0.12$ and $b=0.05$. Substituting these numerical values together with the value of e/m for deuterons, Eqs. (9) and (10) take the form:

$$\Delta v_y' = -66\cdot 10^6 y/r \qquad \Delta v_y = -4.7\cdot 10^8 y/r^3 \qquad \text{for } d/h=1, \tag{11}$$

$$\Delta v_y' = -3.0\cdot 10^6(22+9_y)y/r \qquad \Delta v_y = -2.1\cdot 10^7(22+9_y)y/r^3 \qquad \text{for } d/h=0.4. \tag{12}$$

These equations, of course, hold only where the assumptions are valid, i.e., r greater than 10 cm. The values of Δv_y per crossing of the gap become very small at the large path radii since Δv_y varies inversely with the cube of r. Thus at $r=10$ cm,

[4] Lawrence and Cooksey, Phys. Rev. **50**, 1131 (1936).

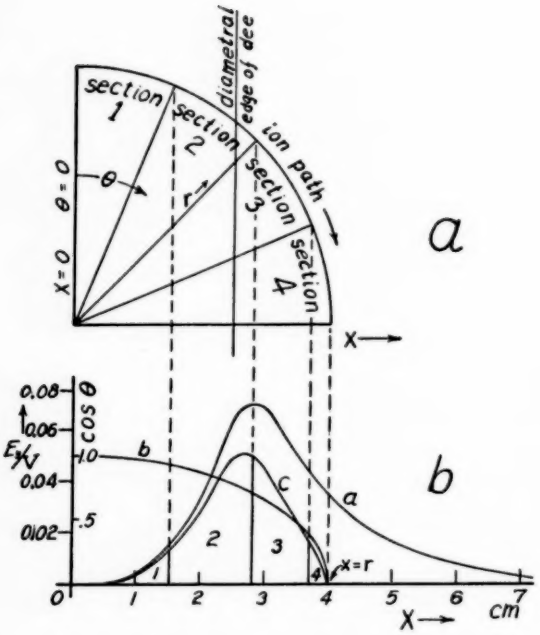

FIG. 3. An ion path is represented in plan view in a. In b, curve a is taken from Fig. 2a for $y=1.0$ cm. To take account of the variation of field with time, curve a must be multiplied by curve b which gives the cos θ corresponding to the position of the ion represented in a. Curve c is the result of this multiplication and represents the vertical electric field which actually acts on a particle in phase and traveling in the path represented in a.

$y=1$ cm and for $d/h=0.4$, $\Delta v_y=0.65\cdot10^6$ cm/sec. per crossing of the gap and the horizontal velocity $\mathbf{v}$ is $6.3\cdot10^8$ cm/sec.; while for $r=30$ cm near where the ions are removed from the chamber, $\Delta v_y=-2.4\cdot10^4$ cm/sec. and $v=2.3\cdot10^9$ cm/sec. The vertical velocity must be greater than 10^6 cm/sec. in order to be appreciable, i.e., cause the particle to move up or down about one mm per revolution. At $r=10$ cm the displacement is of about this magnitude after two revolutions, but at $r=30$ cm the particle would have to make more than 25 revolutions before the Δv_y's add up to an appreciable value. In other words, the electrostatic focusing effect is negligible at large path radii.

In the range of path radii less than 10 cm, the above approximations are no longer valid and the change in vertical velocity must be calculated graphically. Because the particle is going relatively slowly so that its height varies appreciably in one revolution and because the field is changing so rapidly with position and time, we must consider the change in vertical velocity in a smaller fraction of a revolution than a quarter-cycle. Sixteenths of a revolution are chosen as convenient and sufficiently small so the ion path is divided into sections of this size as is depicted in plan view in Fig. 3a. It is only necessary to calculate the change in vertical velocity $\Delta v_y''$ per sixteenth revolution for the four sections shown as $\Delta v_y''$ will be the same in the rest of the sections (for the same value of r and y) except for sign and order.

The $\Delta v_y''$ for these sections are obtained graphically from the curves of Fig. 2 as follows: The vertical field E_y through which a particle of path radius r and height y would pass if a constant voltage of value $V_{\max}$ were maintained between the dees is shown in Fig. 3b, curve a, which is taken from Fig. 2. Now actually the voltage alternates in phase with the revolutions of the particle such that the voltage is equal to $V_{\max}$ as the ion crosses the gap between dees and falls to zero when $x=r$; so to obtain the actual field acting on the particle as it moves around its path we must modify the field of curve a by multiplying by the factor $\cos\theta$ (assuming a sinusoidal wave) which is indicated by curve b of Fig. 3b. The result of the multiplication is shown by curve c. This curve is changed if a different value of r is chosen, so it was necessary to construct the curves for various values of r varying from 1 to 14 cm at intervals of one cm.

Curve c is now broken into sections corresponding to the four one-sixteenth sections of Fig. 3a as is indicated by the dotted line projections. The average field $\bar{E}_y$ experienced by the ion in any section can be found by graphical integration, and from this value we can find $\Delta v_y''$ by the equation:

$$\Delta v_y''=(\bar{E}_y e/m)\Delta t, \tag{13}$$

where Δt is the time which the particle stays in each section and is equal to one-sixteenth of the period of revolution T which is given by

$$T=(2\pi mc)/He. \tag{14}$$

Thus

$$\Delta v_y''=(\pi c/8H)E_y. \tag{15}$$

By this process, $\Delta v_y''$ was obtained for each section, for each value of r, and for each curve of Fig. 2. The resulting curves are plotted in Fig. 4 where $\Delta v_y''$ is plotted as a function of r for each section and for two different values of d/h.

For purposes of comparison with the more theoretically determined $\Delta v_y'$ which is for a quarter-revolution and is given by Eq. (11), the four curves of $\Delta v_y''$ against r shown at the top of Fig. 4 were added to give a $\Delta v_y'$ per quarter-cycle as obtained by this graphical method. These values of $\Delta v_y'$ as well as those given by Eq. (11) are plotted at the bottom of Fig. 4. For r greater than 10 cm the agreement between the two values is remarkable, but as r becomes smaller the graphically obtained values go through a maximum and fall to zero, while the more theoretical $\Delta v_y'$ of Eq. (11) would become infinitely great.

That the two values agree above 10 cm, for which Eq. (11) was derived, indicates that the assumptions made in the derivation are valid for that range. It must be pointed out that these calculations of $\Delta v_y'$ are only true for a particle traveling around in phase with the voltage and centered with respect to the gap. For particles not in phase, $\Delta v_y'$ might be expected to be less since the ions would then travel through the focusing field at lower voltages. However, the total change in vertical velocity Δv_y could be larger or smaller depending on whether the voltage decreases or increases as the ion crosses the gap.[5] The results of this section will be applied to the calculation of ion paths after a consideration of the magnetic focusing action.

Magnetic Field

The magnetic focusing is due to the outward curvature of fringing of the lines of magnetic

[5] Rose and Bethe have considered the electrostatic focusing of ions out of phase. In terms of the present work, to obtain the Δv_y for an ion traveling around out of phase with the voltage by an angle α, one must multiply the Δv_y for ions in phase by $\cos^2\alpha$, and must add to this their "out of phase" term which is given by $V_1 y \sin\alpha/Hr^2$. For the case considered here and at $r=10$ cm, the additive term predominates for ions out of phase as much as 6°; and would become more important as r increases for it decreases with r^2 while the "in phase" term decreases with r^3. Depending on the sign of α, the out of phase term can cause focusing (ions lagging the voltage) or defocusing (ions leading the voltage). In all probability, the term due to Rose and Bethe is the most important in electrostatic focusing as the ions must start behind in phase if they are to get out—due to the falling off of the magnetic field near the edge of the acceleration chamber.

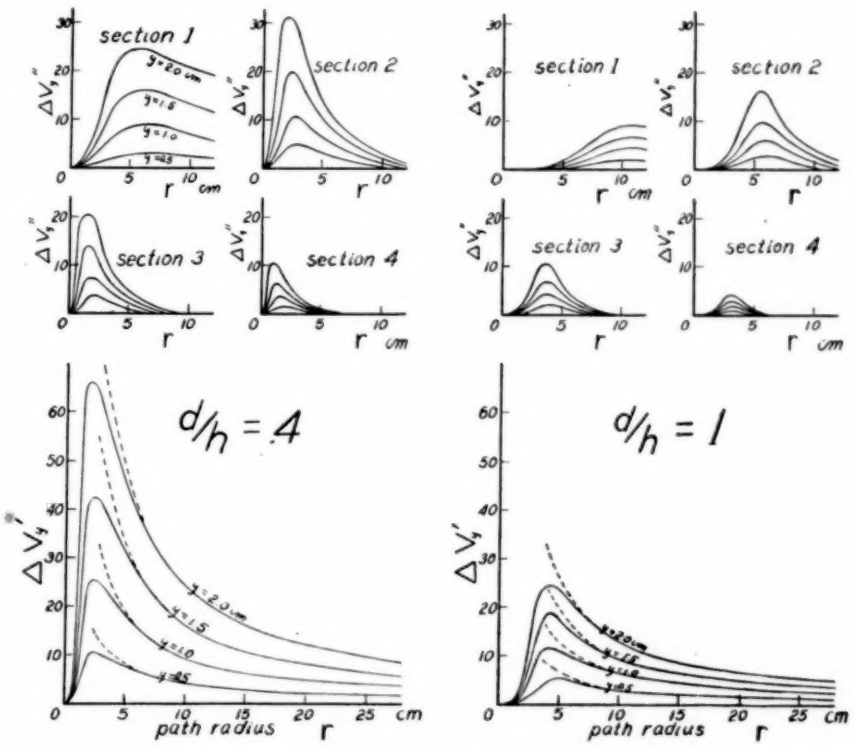

Fig. 4. The upper curves give $\Delta v_y''$, the change in vertical velocity received in a sixteenth section as represented in Fig. 3. The lower curves give $\Delta v_y'$, the change in vertical velocity per quarter revolution, and is the sum of the $\Delta v_y''$ for the four sections as given in the upper curves.

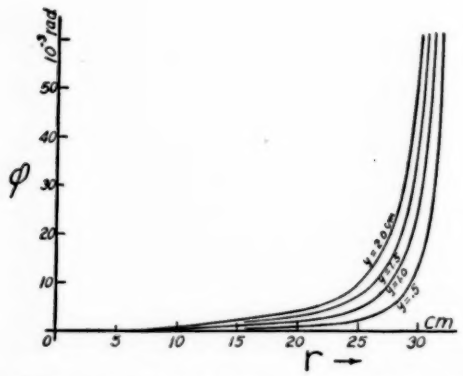

FIG. 5. The angle ϕ which a line of magnetic force makes with the vertical plotted for various heights above the median plane.

force. Accordingly, as a basis for quantitative calculations to determine the nature and importance of this effect, the direction of the magnetic field of the cyclotron at Berkeley was measured by means of a short centrally pivoted iron needle to which was fastened a small mirror. The angle that the needle made with the vertical was measured with an accuracy of one-ten thousandths of a radian by means of a telescope and scale at a distance of one meter. The needle could be moved in and out and up and down in the field by means of a massive brass system of bars and joints. Fig. 5 shows the angle ϕ in radians plotted as a function of the radius r or distance from the center of the pole faces and at various heights above the central plane at which the lines were assumed, due to symmetry, to be vertical. Within the accuracy of the measurements, the lines were symmetrical about the central plane, and ϕ was found to increase linearly with y for any fixed value of r. The angle ϕ becomes measurable about 10 cm from the center of the pole faces and rises rapidly to a magnitude of several degrees in the neighborhood of 30 cm, near where the ions are withdrawn from the cyclotron. The magnitude of H is connected with ϕ by a simple relation: since $\phi=H_r/H$ and curl $H=0$, $(\partial H_y/\partial r)=(\partial H_r/\partial y)$ or, as ϕ is small, $(\partial\phi/\partial y)=(1/H)(\partial H/\partial r)$.

MAGNETIC FOCUSING

The change in vertical velocity due to the magnetic field, which an ion receives per fraction of a revolution, can be calculated quite easily if

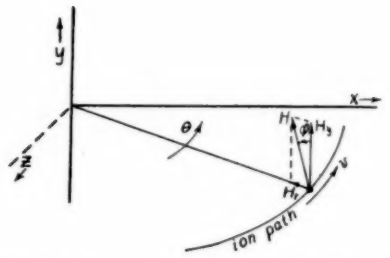

FIG. 6. An ion is represented as traveling in a horizontal path above the median plane and through a magnetic field H.

the particle's path is centered. In Fig. 6 is depicted a particle traveling above the central plane in a horizontal circular path with a velocity $\mathbf{v}$ perpendicular to the magnetic field H which makes a small angle ϕ with the vertical. One can consider H as being broken into two components: a large vertical component H_y which keeps the ion in a circular horizontal path of radius r, and a very small radial component H_r which forces the ion toward the central plane. As the ion—if its path is centered—always moves perpendicular to the small radial component as it travels along its path, there will be a force $-H_r e\mathbf{v}/c$ which will be directed nearly vertically downwards as long as the particle moves in an approximately horizontal direction. Then for the vertical motion

$$m\frac{d^2y}{dt^2}=-\frac{H_r e\mathbf{v}}{c}, \tag{16}$$

and after integration we get the change in vertical velocity received in a time Δt is

$$\Delta v_y=(H_r e/cm)\mathbf{v}\Delta t. \tag{17}$$

We note that $v\Delta t$ is Δs, where s is measured along the ion path, and that $H_r=H_y(\partial\phi/\partial y)$. Substituion gives

$$\Delta v_y=-\frac{He}{cm}y\frac{\partial\phi}{\partial y}\Delta s. \tag{18}$$

In calculating Δv_y in a fraction of a revolution, the distance Δs must be chosen small enough so that ϕ, which varies with height, will remain essentially constant so that its value can be obtained from the curves of Fig. 5. Later it will be seen that the vertical velocity is always so small that Δs can be taken as large as would correspond to from one-eighth to one-half of a

revolution because the particle is displaced at most only a few mm in these distances. Then for a half-revolution $\Delta s = \pi r$, so

$$\Delta v_y = -\frac{e\pi H}{mc} yr\frac{\partial \phi}{\partial y} = -\frac{e\pi}{mc} yr\frac{\partial H}{\partial r}; \tag{19}$$

and for deuterons and a magnetic field of 16,500 gauss:

$$\Delta v_y = -2.5 \cdot 10^8 yr(\partial\phi/\partial y). \tag{20}$$

The value of Δv_y for an ion at any height and with any path radius is then obtained by multiplying $-2.5 \cdot 10^8\, yr$ by the corresponding value of $\partial\phi/\partial y$ which is the value of ϕ at $y=1$ cm as found from the curves of Fig. 5. These values of Δv_y per half-revolution are plotted in Fig. 7. For purposes of comparison, Fig. 7 also shows the values of Δv_y per half-revolution as given by Eq. (12) for the electrostatic case. It is seen that the electrostatic focusing action is the effective one for r less than about 10 cm, but for r greater than this the magnetic focusing becomes predominant while the electrostatic effect becomes rapidly negligible.

Horizontal Ion Paths

Before a calculation of the vertical motion of a particle can be made, it is necessary to know its approximate horizontal path. When the energy of the ions is large, the path simply consists of a series of semi-circles. The radii of these semi-circles can be easily calculated since the particle, if in phase, adds the full value of the peak voltage between the electrodes to its energy each time it passes from one dee to the other. However, when the energy is small so that the path radius is less than 6 cm, the ion adds only a fraction of the peak voltage to its energy at each crossing because the field becomes smaller as the particle goes around due to the variation of voltage with time. A complicated spiral path results, but as far as ensuing calculations are concerned this path can be approximated sufficiently well by a series of semi-circles. The reduced gain in energy for each crossing or semi-circle can be calculated as follows:

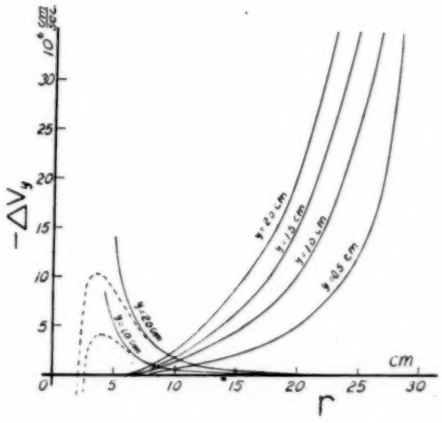

Fig. 7. The relative effect of the magnetic and electric focusing. The curves for which $-\Delta v_y$, the change in velocity per half-revolution, becomes larger with r are for the magnetic effect. The other curves give the change in vertical velocity per half-revolution produced by the electrostatic focusing.

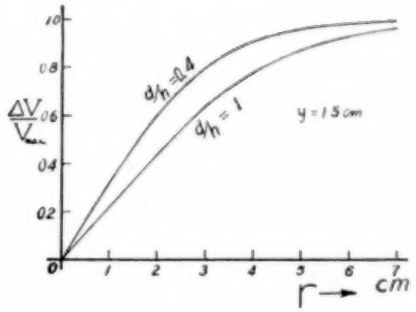

Fig. 8. The fraction of the voltage between the dees that an ion receives at each acceleration plotted as a function of the radius of path.

The semi-circular path is broken into eight sections, each consisting of one-sixteenth of a revolution. The field experienced by a particle in phase with the voltage and a position $x = r \sin\theta$ will be $E_m \cos\theta$, where r and θ describe the position of the particle as in Fig. 3a, and E_m is the value of the horizontal electric field that a steady potential between the dees would give as is shown in Fig. 2. The voltage or energy gained by an ion in going through one of the small sections will be

$$\Delta V = -\int_{\theta_1}^{\theta_2} E_m r \cos^2\theta d\theta, \tag{21}$$

where θ_1 and θ_2 define the section. If we take an average value of E_m for the section, the above will be approximately

$$\Delta V = -\bar{E}_m r[\tfrac{1}{2}\theta + \tfrac{1}{4}\sin 2\theta]_{\theta_1}^{\theta_2}. \tag{22}$$

This was calculated for all the sections and for various values of r. The summation of the ΔV for the eight sections of a semi-circle gives the gain in energy per half-revolution; and the ratio of this gain to the peak voltage is plotted as a function of r in Fig. 8. It is seen that the ratio rises from zero at $r=0$ to unity at about $r=8$ cm. Slightly different curves are obtained for particles revolving at different heights above the central plane and for different values of d/h, but the ratio in all cases essentially reaches unity before $r=8$ cm.

In the calculation of the radii of the successive semi-circles, it is assumed that the ion has already obtained a small amount of energy, and such that it makes a half-revolution with an average path radius r_0. After completing this half-revolution, the particle has gained an amount of energy that can be found approximately by multiplying the ratio, as given by Fig. 8 for r_0, times the voltage between the dees. This energy gain is added to the energy necessary to produce r_0, and thus the radius r_1 of the next semi-circle can be calculated. Continuing this process of adding the energy gains gives the path radii of the successive semi-circles which describe the horizontal motion of the ion. More elaborate calculations do not appreciably change this approximated path which is accurate enough for later calculations.

Vertical Motion

There is now enough information to enable one to calculate the vertical or focusing motion of the ions as they travel out from the center along the horizontal paths just considered. For very small path radius there is no vertical field acting on the ions, as can be seen from Fig. 2, so the procedure is to start with a particle having a small initial path radius r_0, at an initial height y_0, with zero vertical velocity (the velocities of thermal agitation are negligible compared to the electrically produced ones), in phase with the voltage, and at $x=0$, i.e., midway between the dees. The horizontal path is broken into small sections consisting at first of one-sixteenth of a revolution each. The vertical motion is then calculated by following the ion along this horizontal path already calculated; making small changes in the vertical velocity v_y and the height y as it goes through each section. These changes are calculated at each section by a method of successive approximations as follows: The ion enters a section with a vertical velocity v_y which is the sum of the $\Delta v_y''$'s produced in all the preceding sections, and with a height y which is the sum of the initial height y_0 plus all the Δy's produced in the preceding sections. A Δy_0 for the section under consideration is guessed at from the trend of Δy in the preceding sections; then $\Delta v_y''$ is found from the curves of Fig. 4 (the magnetic effect being zero at first) using the value of r as given by the calculation of horizontal path and an average value of y for the section, assuming Δy_0. One-half of this $\Delta v_y''$ added to the total v_y that the ion had as it entered the section gives the average velocity and this multiplied by the time the ion spends in the sections gives Δy_1. If this does not agree with Δy_0, a new $\Delta v_y''$ is found using Δy_1 until two successive values agree. Usually, however, it is found that the initial guess is correct. The time spent in each equal section is the same, and for one-sixteenth of a revolution it is simply one-sixteenth of the period of revolution T which is constant. As the radius of path becomes larger, the size of the sections can be increased as indicated by the calculations until about $r=10$ cm beyond which, when the electrostatic focusing alone is being considered, half-revolutions can be used and Δv_y can be obtained from Eq. (10). When the magnetic action is being considered, half-revolutions can be used at first, the Δv_y being obtained from Fig. 7, but at larger r one must drop to quarter-revolutions and finally one-eigth revolutions as Δv_y becomes larger and larger; Δv_y for the smaller sections being found by decreasing the value given in Fig. 7 by an amount corresponding to the decrease in the size of the section.

Essentially the above procedure amounts to finding an approximate solution of a second order differential equation by a step by step method of integration. The differential equation or better the difference equation for the system being represented graphically by the curves of Figs. 4 and 7 where acceleration (i.e., Δv_y per fraction of a revolution is the same as $\Delta v_y/\Delta t$, as the particle remains an equal time in each equal fraction of a revolution) is plotted as a function of the particle's position.

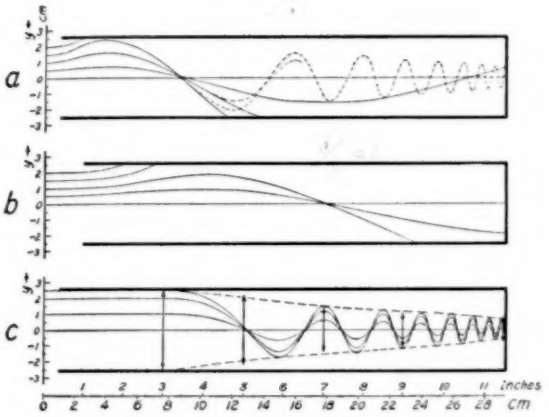

FIG. 9. The vertical motion of ions in the cyclotron. A dee is represented in cross section; and the curves that are plotted are those which will be cut by an ion as it spirals outward. Curve a is for $d/h=0.4$. The full curves are for the case of only the electrostatic focusing acting. The dotted curves illustrate the combined action of the magnetic and electrostatic effects. Curve b is for $d/h=1$ and only the electrostatic effect acting. Curve c is for only the magnetic effect acting. The dotted curves should define the height of the beam theoretically; the vertical lines with arrow point ends indicate the experimentally determined height of the beam.

The results of the calculations of vertical motion are given in Fig. 9 where one dee is represented in cross section by the heavy line and where the position of the ion at its deepest penetration into the dee at each revolution is plotted; the points so obtained are joined by a smooth curve. In other words, the curves plotted are those which will be cut by an ion at each revolution as it spirals outward. In Fig. 9a for the case of $d/h=0.4$, the full curves result if only the electrostatic focusing is considered as acting, while the dotted curves indicate the vertical motion of the ion if both electrostatic and magnetic focusing actions are considered. Fig. 9b is for the case of $d/h=1$ and for only the electrostatic focusing acting; Fig. 9c gives the motion which would result if only the magnetic focusing were to act. In all cases the peak voltage between the dees is taken as 90,000 volts.

The curves are extremely interesting and many conclusions concerning the nature of the focusing can be drawn from a study of them. It is noticed that at first the electrostatic action is one of defocusing so that the particles spiral away from the central plane. Some of them are caught and it is clear that there will be a critical height for each value of d/h such that particles starting above it (above the central plane) will spiral up into the electrode and be lost, while those starting below it will spiral up at first but before striking the dee will be turned back and then will spiral down toward the central plane again. A comparison of Fig. 9a and Fig. 9b shows that this critical height is greater for the smaller value of d/h or for the electrodes closest together. This seems strange as the vertical field in the case of the smaller d/h, as seen in Fig. 2, is much larger than the other. However, there is a defocusing action at first because the ion is penetrating farther into this field with each revolution so the impulse of force on the ion becomes larger as the path radius increases—which makes for defocusing. But after the particle has penetrated all the way through the vertical field the impulse of force on the ion gets less as r increases—because of the increase of v with r—which makes for focusing. Then when d/h is small, the vertical field is more concentrated near the center so the ions penetrate through the vertical field sooner and the defocusing should last for a shorter time, although it may be more powerful while it lasts; an effect which also can be noticed in Fig. 9a and 9b.

The above can also be seen from the curves at the bottom of Fig. 4 which show the $\Delta v_y'$ per quarter of a revolution as a function of r. Here the defocusing will take place when the position of the ion is such that it is to the left of the maxima of the curves. It is seen that these maxima occur roughly at the position corresponding to the diametral edges of the dees, hence the defocusing will last for the shortest time when the electrode separation is least. Since the critical height becomes larger as the defocusing becomes less, one could expect the largest fraction of starting particles to be obtained when the electrode separation or value of d/h is as small as possible without intercepting the ion source beam of electrons coming from the filament. This is in agreement with the increase in current which has actually been observed in various cyclotrons when the dee separation has been decreased.

After the ions are turned back toward the central plane, they will tend to oscillate back and forth across this plane with *increasing amplitude* and period because of electrostatic effects.

If only the electrostatic focusing continued to act many more ions would be lost and at best only a very diffuse beam could be obtained from the cyclotron. This effect is shown in Figs. 9a and 9b where it is seen that many of the ions would be lost after the first crossing of the central plane. Fortunately, however, in this case the magnetic effect becomes appreciable just after the defocusing action ceases, and under the influence of the magnetic field all the remaining ions will now oscillate back and forth across the central plane but with *decreasing amplitude* and periods, as the dotted curve of Fig. 9a indicates. Thus the ions will be focused to the concentrated beam which is observed in practice. Then the eventual focusing of the beam must be ascribed entirely to the magnetic action, although the electrostatic action is important in determining the number of initial ions which can be obtained for this focusing.

The magnetic focusing action is more clearly illustrated in Fig. 9c where it alone is considered as acting. It is noticed that ions starting at different heights cross the central plane at the same places, and that the curves are multiples of one another and in proportions of their initial heights—within the accuracy of the calculations. It is not necessary to carry the tedious point by point calculations through for the whole of each curve. Rather, a curve need only be calculated by this method out to where it has oscillated across the median plane once or twice. We have seen that the ion is acted on by a restoring force directed vertically toward the median plane and proportional to y, i.e.,

$$f=-(H_r e\mathbf{v})/c$$

and from preceding relations:

$$f=-\frac{e^2H^2}{mc^2}ry\frac{\partial\phi}{\partial y} \qquad (23)$$

or

$$=\frac{e^2H}{mc^2}ry\frac{\partial H}{\partial r},$$

i.e., $\partial H/\partial r$ is negative. Then if an ion were to circulate at constant r, it would oscillate about the central plane with simple harmonic motion and with constant amplitude and period. If the force constant changes slowly in comparison with the period of vertical oscillation, as it does in this case, a condition is that the action variable be a constant. In the case of a linear oscillator this requires that UT_v, the energy times the period of vertical oscillation, be a constant. This may be written

$$UT_v=2\pi^2m(A^2/T_v)=\text{constant}, \qquad (24)$$

where A is the amplitude of oscillation. From (24) we find that

$$T_v=2\pi\frac{mc}{eH}\left(\frac{1}{r(\partial\phi/\partial y)}\right)^{\frac{1}{2}} \qquad (25)$$

and on substitution of this into (25) and taking the square root we can write for the amplitude:

$$A=k(r(\partial\phi/\partial y))^{-\frac{1}{2}} \qquad (26)$$

or

$$A=k'(-r(\partial H/\partial r)^{-\frac{1}{2}} \qquad (27)$$

where k and k' are constants depending on e and H. Then if (26) is fitted to the amplitude of the first or second oscillation as calculated by the point by point method, the amplitudes of the succeeding oscillations can be obtained by substitution of values of r and the corresponding $\partial\phi/\partial y$ which can be obtained from Fig. 5. This was done in the case of the curves of Fig. 9c and the succeeding amplitudes as calculated by the two different methods agreed to within ten percent. As a further check the periods of oscillation were calculated from (25), and these agreed to within five percent with the periods as measured from Fig. 9c.

The height of the beam at various r can be found from Fig. 9c. Dotted lines are drawn through the maximum and minimum amplitudes of the curve that starts at the top of the dee. This curve could be for the case of an ion that started at the critical height and was just being turned back toward the median plane at the radius where the magnetic focusing becomes appreciable. Then the dotted curves, the equation of which would be of the form (26) or (27), should define the height of the beam at any radius because particles starting above the critical height would be lost, while ions starting at smaller heights would oscillate with proportionally smaller amplitudes. According to the treatment given above, the height of the beam should be independent of the voltage applied

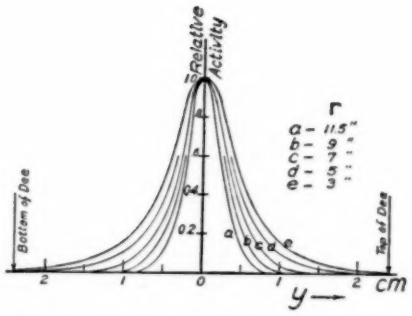

FIG. 10. The distribution of ions with height at various distances from the center.

between the dees. However, a decrease in voltage should produce a corresponding increase in the number of vertical oscillations made because the total number of revolutions made by an ion before getting out is increased. As ions are being accelerated at all voltages less than the peak value (i.e., ions traveling around somewhat out of phase), different ions will have to make a larger or smaller number of vertical oscillations before getting out so that all the space between the dotted curves should be filled with ions.

For the electrostatic focusing at larger path radii where Eq. (10) holds, a sort of restoring force can be obtained by dividing the Δv_y, as given by (10), by $T/2m$. As b in (10) is small, this force will vary approximately with y so, using the same argument as before for the magnetic case, the amplitudes of vertical oscillation would increase with $r^{\frac{1}{2}}$ as in Fig. 9a and 9b if the magnetic focusing did not act.[6]

PROBE MEASUREMENTS

Finally, the distribution of particles with respect to height above and below the central plane at various distances from the center has been measured for the case of the electrode and magnet arrangement for which the above calculations were made (i.e., the Berkeley cyclotron in use up to August 1937[4]). This was done by means of a probe which consisted of a long water-cooled length of copper tubing which was bent double and in such a way that the end where the tubing doubled back on itself could fit in a vertical position between the dees so that it intercepted the ion beam. This tubing was introduced into the electrode chamber through a filament window, and it could be moved to any position by means of a sylphon arrangement.

The ion beam striking the probe caused the copper to become radioactive with emission of electrons and positrons. The strength of the activity along the probe measured the number of particles striking it; assuming all the particles have the same energy. Thus the distribution of particles with height was obtained by measuring the activity of small sections along the probe. This was done by supporting the probe before a lead slit two mm wide which in turn was in front of an ionization chamber and electroscope system. The probe was adjusted in the cyclotron at some measured distance from the center; after bombardment it was removed and the activity was measured at intervals of two mm along its length. The lead slit was then closed and the measurements were repeated to determine the background correction due to the annihilation radiation. The time of each activity measurement was recorded so that, from the known half-life of the radioactive copper (12.8 hr.), all the readings could be referred to one time. At small distances from the center it was necessary to cover the probe with carbon because the energy of the beam was too low to activate the copper. Although the half-life of the radioactive carbon is very short (10 min.), it was possible to extend the measurements over several half-lives because of the prolific activity induced in the carbon.

The results of the measurements are shown in Fig. 10 where the maximum value of all the curves has been adjusted to the same value of activity. It is seen that the curves are broadest, filling out the entire dee height, when the path radius is small and that they become more narrow or more focused as the path radius increases.

The activities near the peak of the curves for small r probably do not represent as many incident ions for a given amount of activity as the activities near the feet of the curves do because the ions do not all start from the same center so that part of them have larger radii and so higher energies than others when they strike the probe. But as these have penetrated farther into the curved magnetic field we would expect them to be more focused; and because of their

[6] In the case of the electrostatic focusing of ions out of phase, the amplitudes would increase with $r^{\frac{1}{2}}$.

higher energy they would induce more activity so a higher peak would result.

The curves are in good agreement with the theory already presented. Thus the widths of the beam at various radii as taken from the base of the curves of Fig. 10 and which are indicated in Fig. 9c by the vertical lines with arrow point ends, are seen to agree with the theoretical values given by the dotted line well within the accuracy of the measurements or calculations.

Certain suggestions concerning accelerator electrode design can be made on the basis of the above material. As has already been found experimentally, the ratio of d/h should be as small as possible in the central region of the dees where the electrostatic effect is large. More important perhaps, the height of the dees farther out from the center could be made smaller without affecting the focusing action or intercepting any of the beam, because the electrostatic action is negligible in this region and, as seen from Fig. 9c, not all of the interior of the dee is filled with circulating ions. In the case considered, it would naturally be suggested that the dees be shaped to conform approximately to the dotted curve of Fig. 9c. Reducing the dee height would decrease the capacity between the dees and so allow larger high frequency voltages to be applied. A further decrease in capacity could be obtained by cutting the dee back so as to make the separation larger; this would, of course, be done at an appreciable distance from the center again where the electrostatic effect is negligible. As only a small amount of bulging of the magnetic field is necessary to produce a focusing which is larger than that due to electrostatic forces, it is conceivable that the focusing near the center could be improved by causing an outward bulging of the field by the placement of suitable circular iron plates or "shims" or by appropriate bevelling of the magnet pole faces.

In conclusion I wish to express my gratitude to Professor E. O. Lawrence for his continued interest and suggestions and for the use of the cyclotron. I also wish to thank Professor E. M. McMillan for discussions and valuable suggestions concerning the theoretical part of the paper, Dr. F. N. D. Kurie who suggested the method that was used in measuring the height of the beam, and the staff of the Radiation Laboratory for their friendly cooperation in making the measurements.

MARCH 1, 1938 PHYSICAL REVIEW VOLUME 53

Nonideal Lloyd's Mirror in Wide-Angle Interference

F. W. DOERMANN
Department of Physics, New York University, University Heights, New York, N. Y.
(Received November 22, 1937)

The paper is an extension of an earlier article on the wide-angle interference of multipole radiation. Nonideal reflections are here taken into account and the theory is applied to the Lloyd's mirror arrangement using a material point source composed of electric or magnetic dipoles, quadrupoles, or octopoles. Qualitatively the earlier results are not appreciably altered; quantitatively it is found that the ideal treatment gives satisfactory results for nonideal metallic mirrors only for divergent beams making an angle greater than about 90°.

I. INTRODUCTION

THAT the sharpness of the fringes produced in wide-angle interference depends upon this angle in a manner characteristic of the constitution of the emitting source is the thesis put forward in a recent article.[1] The argument could be phrased in a very simple and elementary way,[2] independent of the particular type of mechanism employed for bringing the divergent beams to interference. However, in order to give the sim-

[1] O. Halpern and F. W. Doermann, Phys. Rev. **52**, 937 (1937). Throughout the present paper, an extension of this article, the asterisk will (except when employed algebraically to denote the complex conjugate) signify that the quotation to which it is attached is taken from this earlier article.

[2] See, in particular, Section I.*

plest detailed illustrations, certain ideal assumptions were made regarding this mechanism, *viz.*, that in making the divergent beams parallel it produced in them neither diminution in intensity nor polarization. In the numerical examples completely worked out, this part of the mechanism was represented by *ideal* metallic mirrors.

It is our present purpose to extend the detailed theory to embrace a much wider class of mechanism, and to apply this extended theory to the standard arrangement of Lloyd's mirror, using a nonideal[3] reflecting surface but, of course, a material point source. Indeed, the ease with which fringes may be observed with Lloyd's mirror[4] suggests it as a most favorable arrangement for a first experimental approach to our subject.

That for angles of divergence (2θ) in the neighborhood of glancing reflection ($2\theta=0$) the ideal theory cannot be expected even approximately to describe observations made with a nonideal Lloyd's mirror can be seen most readily as follows: Substitution of the values $D_1=D_2=\frac{1}{2}$ (taken from Table I*) into the second of formulas (19)* gives $Q=0$; thus at glancing incidence, without the use of Nicol prisms, no fringes will be found for any order of electric or magnetic multipole. On the other hand, since we are here dealing with zero angle of divergence, we may replace our material point source by an illuminated pinhole, from which the radiation in any *one* direction will be the same as that produced by a properly chosen mixture of multipoles. Thus the *ordinary*[5] Lloyd's mirror should, if the ideal theory were applicable, show no fringes. This is certainly far from being the case: nonideal mirrors, both glass and metal, show perfectly sharp fringes at glancing incidence; indeed, the observed fact that the central fringe is then black constitutes one of the classical demonstrations that such reflections all produce a 180° change of phase in the reflected beam.

We shall at present make no alteration in the general interference arrangement shown in Fig. 1;* we merely make more general the type of mechanism employed for changing the divergent beams I, I' into the parallel interfering beams B, B'. In order to define the class of mechanism to which our present extended theory will be applicable, we shall find it convenient to employ *complex* field vectors[6] $\mathbf{e}$, $\mathbf{h}$, $\mathbf{e}^B$, $\mathbf{h}^B$, associated with the beams I, B, respectively. Our theory may then be applied to any mechanism which may be described by the statement that $\mathbf{h}^B$ is a (complex) linear vector function of $\mathbf{h}$—it being assumed that the medium surrounding the screen does not differ essentially from a vacuum.[7]

II. Complex Interference Parameter Q

In a treatment of the present generality allowance must be made for the fact that points on the interference screen which correspond to zero path[8] difference—the geometric-optical center C of the pattern—will not in general be located at the center of a bright or dark fringe. If, however, we agree to measure δ (by definition proportional to the path difference between the interfering beams) not as heretofore from C but from the center of the *bright* fringe nearest to C, the variation in intensity in the pattern may in this neighborhood still be described by $1+|Q|\cos\delta$. If δ_C designate the value of δ at C, we then have

$$(\mathbf{h}^{B*}\cdot\mathbf{h}^B+\mathbf{h}^{B'*}\cdot\mathbf{h}^{B'})(1+|Q|\cos\delta_C)=(\mathbf{h}^{B*}+\mathbf{h}^{B'*})\cdot(\mathbf{h}^B+\mathbf{h}^{B'}),$$

and since $\delta=0$ corresponds to maximum intensity in the pattern:

$$(\mathbf{h}^{B*}\cdot\mathbf{h}^B+\mathbf{h}^{B'*}\cdot\mathbf{h}^{B'})(1+|Q|)=\max_{\text{varying }\gamma}\{(\mathbf{h}^{B*}+e^{-i\gamma}\mathbf{h}^{B'*})\cdot(\mathbf{h}^B+e^{i\gamma}\mathbf{h}^{B'})\}.$$

From these relations it may now readily be shown that if we set[9]

$$Q=2\mathbf{h}^{B*}\cdot\mathbf{h}^{B'}/(\mathbf{h}^{B*}\cdot\mathbf{h}^B+\mathbf{h}^{B'*}\cdot\mathbf{h}^{B'}) \qquad (1)$$

[3] The ideal Lloyd's mirror has already been discussed in full detail as case C^*.

[4] Cf. R. W. Wood, *Physical Optics*, second edition (1911), p. 130.

[5] I.e., employing an illuminated pinhole as source.

[6] These are connected with the real field vectors as used in the earlier paper by the relations $\mathbf{E}=\Re\{\mathbf{e}\}$, $E_x=\Re\{e_x\}$, etc.

[7] Since in this case $\mathbf{e}^B=-\mathbf{n}^B\times\mathbf{h}^B$ (where $\mathbf{n}^B$ is the unit vector in the direction of B), we shall still find it possible to carry out our mathematical manipulations in terms of the magnetic vectors alone.

[8] By path we here mean *f*nds, no allowance being made for abrupt changes of phase at surfaces of discontinuity.

[9] Since only $|Q|$ and $\cos\delta_C=\Re\{Q\}/|Q|$ have direct physical meaning, this definition of Q might be replaced by its complex conjugate and is therefore not *essentially* asymmetrical in the two beams. It is, of course, here assumed that the radiation is monochromatic, and that $\mathbf{h}^B$ represents

then not only will $|Q|$ have the correct value, but also

$$\delta_C = \text{arc } Q. \tag{2}$$

It is also immediately evident that if, as defined by (1), Q is *real*, it will have the value given by relation (2)* of the more restricted theory. That the restrictions formerly imposed always lead to real Q as here defined will be made clear in footnote 13 below. Thus there is complete identification of the symbol Q as used in the two papers.

III. Evaluation of Q for a Multipole Source

To evaluate Q for a multipole source we may now employ a method entirely analogous to that used in the earlier article. Taking components in directions shown in Fig. 1* we may express the linear vector function in the form:

$$\left.\begin{aligned} h_\xi{}^B &= a_{\xi 1}h_1 + a_{\xi 2}h_2 \\ h_\eta{}^B &= a_{\eta 1}h_1 + a_{\eta 2}h_2 \end{aligned}\right\}, \qquad \left.\begin{aligned} h_1 &= h_{1+} + h_{1-} \\ h_2 &= h_{2+} + h_{2-} \end{aligned}\right\}, \tag{3}$$

$$\left.\begin{aligned} h_\xi{}^{B'} &= a'_{\xi 1'}h'_{1'} + a'_{\xi 2'}h'_{2'} \\ h_\eta{}^{B'} &= a'_{\eta 1'}h'_{1'} + a'_{\eta 2'}h'_{2'} \end{aligned}\right\}, \quad \left.\begin{aligned} h'_{1'} &= h_{1+} - h_{1-} \\ h'_{2'} &= h_{2+} - h_{2-} \end{aligned}\right\}, \tag{3'}$$

where the eight quantities[10] $a_{\xi 1}, \cdots, a'_{\eta 2'}$ may now be *complex* and where the additional subscripts on h_1, h_2 indicate parts even and odd in θ. From relations (13)* we may take for the electrical 2^l pole:

$$\left.\begin{aligned} h_{1\pm} &= -C \csc\theta e^{2\pi i\nu t}\textstyle\sum^{\mp} i a_l{}^m H_z{}^{l,\,m} \\ h_{2\pm} &= \qquad\quad Ce^{2\pi i\nu t}\textstyle\sum^{\mp} a_l{}^m H_y{}^{l,\,m} \end{aligned}\right\}. \tag{4}$$

We substitute these into (3) and (3'), and the resulting relations in turn into (1). We finally average over the constituents of the source, and, on making extensive use[11] of

$$(a_l{}^{m*}a_l{}^{m'})_{Av} = \delta_{mm'}k_l,$$

arrive at our fundamental formula

$$\left.\begin{aligned} Q &= [2/(\rho^2+\rho'^2)][(a^*_{\xi 1}a'_{\xi 1'} + a^*_{\eta 1}a'_{\eta 1'})D_1{}^P \\ &\qquad + (a^*_{\xi 2}a'_{\xi 2'} + a^*_{\eta 2}a'_{\eta 2'})D_2{}^P], \\ \rho^2 &= \tfrac{1}{2}(|a_{\xi 1}|^2 + |a_{\xi 2}|^2 + |a_{\eta 1}|^2 + |a_{\eta 2}|^2) \\ P &= E(\text{electric}),\ M(\text{magnetic}) \end{aligned}\right\}; \tag{5}$$

where ρ' is defined similarly to ρ, and where[12]

$$D_1{}^E = D_2{}^M = D_1, \quad D_2{}^E = D_1{}^M = D_2, \tag{6}$$

D_1 and D_2 being real[13] functions of θ calculable by relations (15)* or by the method given in the Appendix.*

IV. Theory of Lloyd's Mirror

According to the Fresnel-Drude theory of reflection a mirror M may be characterized by two optical constants n, κ such that if we define a complex "angle of refraction" β_r in terms of the angle of incidence β_i by the relation

$$\sin\beta_r = \sin\beta_i/(n - in\kappa), \tag{7}$$

then the formulas of reflection will be given by

$$\left.\begin{aligned} \rho_\perp &\equiv -\sin(\beta_i - \beta_r)/\sin(\beta_i + \beta_r) \\ &\qquad = e_\perp{}^R/e_\perp = h_{||}{}^R/h_{||} \\ \rho_{||} &\equiv \tan(\beta_i - \beta_r)/\tan(\beta_i + \beta_r) \\ &\qquad = e_{||}{}^R/e_{||} = h_\perp{}^R/h_\perp \end{aligned}\right\}, \tag{8}$$

where the subscript $\perp$ on the field vectors indicates a component taken normal to the plane of incidence, and the subscript $\|$ indicates the component taken in that direction which makes with $\perp$ and the direction of propagation of the corresponding beam a right-hand triple.[14] For insulating substances $\kappa = 0$, n is the ordinary refractive index, β_r the ordinary angle of refraction, and the coefficients $\rho_\perp$ and $\rho_{||}$ are real.

---

the *total* field. If, as will be true in the following section, $\mathbf{h}^B$ is taken to represent the field of a single multipole, then the product terms must be averaged over the constituents of the material point source.

[10] In case Nicol prisms are employed these quantities are, of course, functions of the angles at which they are set.

[11] It is convenient to demonstrate first the relations analogous to (6)*, *viz.*:

$$(h_{1+}{}^*h_{1-})_{Av} = (h_{1+}{}^*h_{2-})_{Av} = (h_{2+}{}^*h_{1-})_{Av} = (h_{2+}{}^*h_{2-})_{Av} = (h_{1+}{}^*h_{2+})_{Av} = (h_{1-}{}^*h_{2-}) = 0.$$

The vanishing of the first four of these quantities may be verified by inspection; however, to show that the last two vanish we must employ the properties of the Legendre functions. We find, for example:

$$(h_{1+}{}^*h_{2+})_{Av} = i \csc\theta C^2 k_l \Sigma^- H_z{}^{l,\,m} H_y{}^{l,\,m}.$$

In the summation every pair of terms of equal $|m|$ cancel, as may be shown immediately from their expressions in terms of the $P_{l,\,m}$, together with the fact that $P_{l,\,-m} = (-1)^m P_{l,\,m}$.

[12] Cf. footnote 6.*

[13] According to the earlier restrictions the eight quantities $a_{\xi 1}, \cdots, a'_{\eta 2'}$, are real; hence it follows from (5) that in this case Q also is real.

[14] There is ambiguity among writers on theoretical optics in regard precisely to this point.

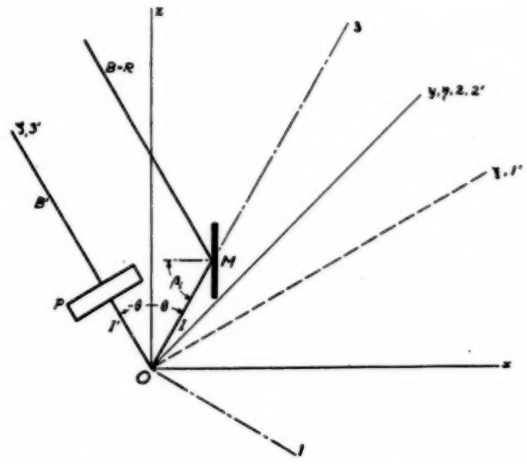

FIG. 1. Diagram showing the experimental arrangement for Lloyd's mirror. Full explanations will be found in the text.

The diagram for the Lloyd's mirror arrangement is shown in Fig. 1. The material point source is located at O; M represents the mirror and P a retarding plane parallel plate which must be placed in beam I' to make the fringe system visible in the neighborhood of its geometrical center. The orientations of the various sets of axes are clearly indicated. We notice that if we choose $\perp = O2 = O\eta$, then $\| = O1$ for the beam I, and $\| = O\xi$ for the beam $B = R$. Thus (8) may be written in the form $h_\xi^B = \rho_\perp h_1$, $h_\eta^B = \rho_{\|} h_2$, which, on comparison with (3), show that

$$a_{\xi 1} = \rho_\perp, \quad a_{\eta 2} = \rho_{\|}, \quad a_{\xi 2} = a_{\eta 1} = 0. \tag{9}$$

The plate P will, of course, produce a fringe system of its own, the effect of which we shall here assume to be negligible. We do not, however, wish to neglect the diminution in intensity which P produces in I'; we suppose this to take place without polarization effects and to be describable by the relation $\mathbf{h}^{B'} = \alpha \mathbf{h}'$ with *real* α. Comparison with (3′) then gives

$$a'_{\xi 1'} = a'_{\eta 2'} = \alpha; \quad a'_{\xi 2'} = a'_{\eta 1'} = 0. \tag{9'}$$

After substituting (9) and (9′) into (5) we find it convenient to write the result in the following form:

$$Q = Fq^*, \quad \begin{cases} F = 2\alpha\rho/(\alpha^2+\rho^2), \\ q = (\rho_\perp/\rho)D_1^P + (\rho_{\|}/\rho)D_2^P. \end{cases} \tag{10}$$

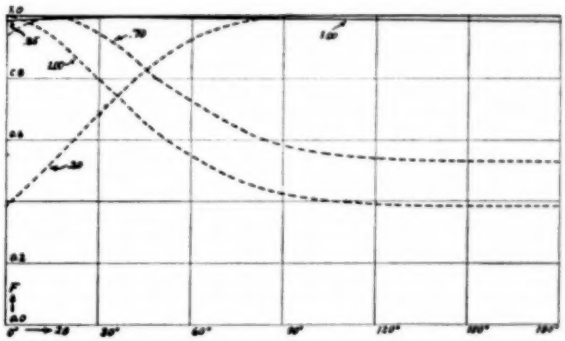

FIG. 2. The adjustable factor F is shown as a function of 2θ for the various constant values of α with which the curves are labeled. The dotted curves are for glass ($n = 1.5$) and the solid curves (almost coincident with $F = 1$) are for metal ($n = 0.35$, $n\kappa = 1.79$).

Here $\rho = +[\frac{1}{2}(|\rho_\perp|^2 + |\rho_{\|}|^2)]^{\frac{1}{2}}$, like α, lies in the interval $0 < \rho \leqq 1$ and its square, analogously to α^2, gives the ratio of the intensity of the reflected beam to the intensity of the unpolarized incident beam; it is, of course, a function of θ calculable by (8), since θ and β_i are complementary. F is thus a positive real quantity which at any particular angle θ_0 can (if, as we shall suppose, α is adjustable) be made to attain its maximum value 1 by making[15] $\alpha = \rho(\theta_0)$. We shall therefore find it convenient to call F the "adjustable factor." Finally, it is clear that

$$|Q| = F|q|, \quad \cos\delta_C = \cos \operatorname{arc} q. \tag{11}$$

V. Discussion of Numerical Results[16]

Detailed calculations have been carried out for glass ($n = 1.50$, $\kappa = 0$) and metal ($n = 0.35$, $n\kappa = 1.79$),[17] and these compared graphically with those previously made for the ideal mirror ($\rho_{\|} = -\rho_\perp = 1$).

Figure 2 shows the adjustable factor F plotted as a function of 2θ for various constant values of α chosen between $\alpha = \rho(\pi/2)$ (perpendicular incidence), and $\alpha = \rho(0) = 1$. For a metallic Lloyd's mirror F is relatively unimportant: for $0.85 \leqslant \alpha \leqslant 1$, F never becomes less than 0.98. For glass,

[15] This, of course, merely means that the two beams B, B' are caused to have the same intensity.

[16] Although only dipoles and electrical quadrupoles could be of significance for optical problems a more complete set of calculations has been made for illustrative purposes.

[17] These are actually the optical constants of Ag for small ν; they interest us here chiefly because they are widely different from those of glass. Cf. W. König, *Handbuch der Physik*, Vol. 20, p. 208.

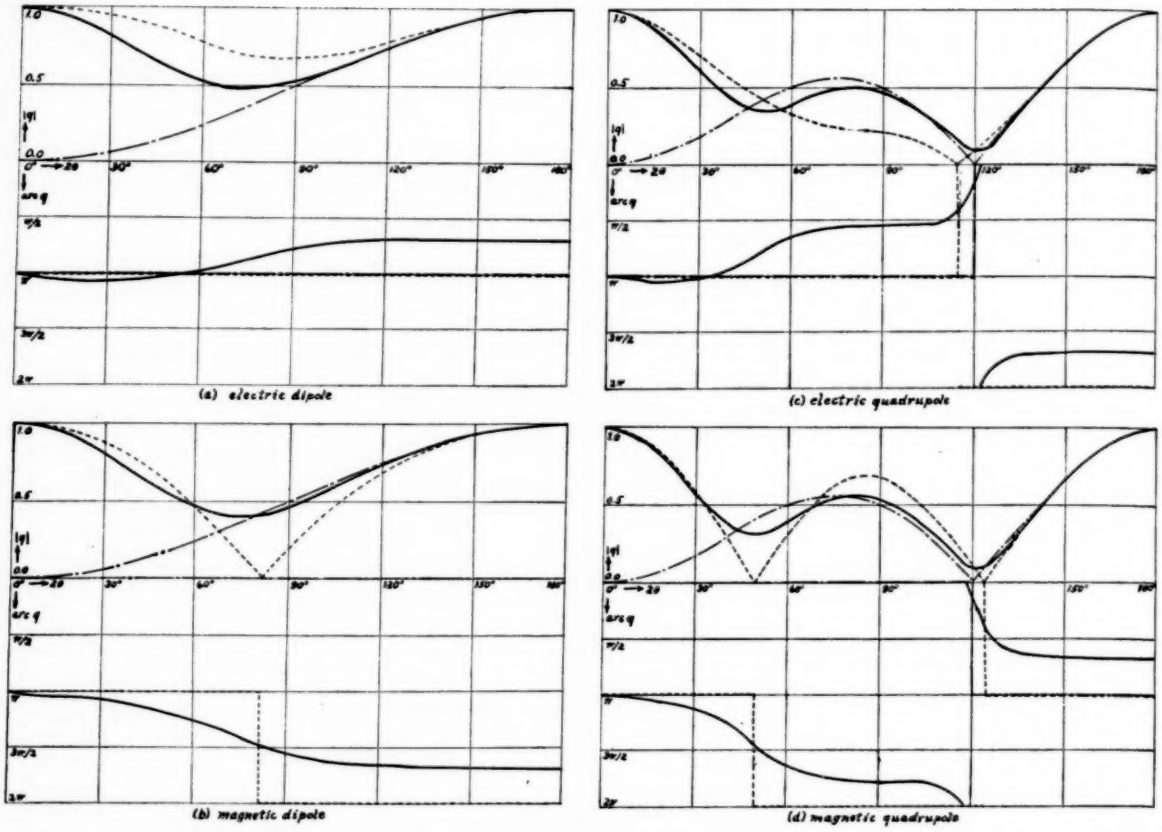

FIG. 3. $|q|$ and arc q are shown as functions of 2θ. The dotted curves are for glass ($n=1.5$), the solid curves for metal ($n=0.35$, $n\kappa=1.79$), and the dot-dash curves for ideal metal ($\rho_{11}=-\rho_{\perp}=1$). As the horizontal lines arc $q=0$, arc $q=2\pi$ are physically identical, the horizontal portions of the step curves have been separated wherever possible.

on the other hand, F can be important, though of course it could theoretically be kept at its maximum value 1 by the constant adjustment of α to maintain the relation $\alpha=\rho(\theta)$.

Far more interesting is the comparison of the curves of Fig. 3, which show $|q|$ and arc q as functions of 2θ for different orders of pole and for glass, metal, and ideal metal mirrors. Although these curves speak fairly well for themselves, a few salient features should, perhaps, be called to attention.

In discussing the curves of $|q|$ we shall assume[18] $F=1$, so that $|q|=|Q|$ is a direct measure of the sharpness of the fringes. If a glass mirror is used, the fringes completely disappear $l-1$ times for the electric 2^l pole and l times for the magnetic 2^l pole ($l=1$, 2, 3). If a nonideal metal mirror is used, on the other hand, the curves for the electric and magnetic multipole of the same order l are closely similar (though not identical) and show no true zeros, but l minima which become sharper and deeper with increasing l and increasing 2θ; indeed for the higher multipoles the last of these minima would be hardly distinguishable from true zeros. For any one multipole the curves for the three mirrors merge as $2\theta\rightarrow 180°$, more rapidly with increasing l, and for the magnetic as against the electric pole; for $2\theta>90°$ the approximation of the nonideal by the ideal curve for metal is very close in all cases.

Among the curves of arc q the general similarity between the step curve for real q and the curve for complex q for the same type and order of pole is at once apparent. It must be observed that arc $q=0$, 2π means that the center C coincides with the center of a bright fringe; arc $q=\pi$ that it coincides with a dark fringe; arc $q=\pi/2$, $3\pi/2$

[18] Since, for constant α, F has no zeros nor sharp minima, this assumption is not necessary for a purely qualitative discussion.

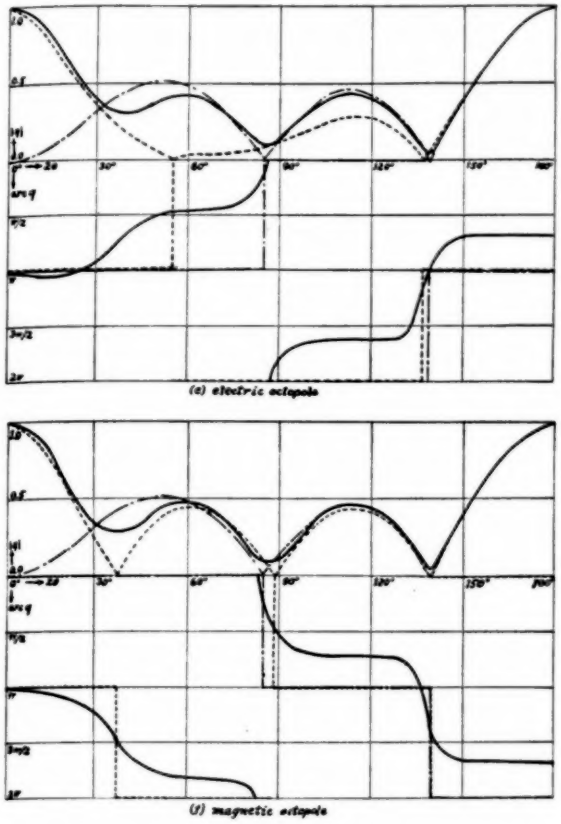

FIG. 3. (*Continued.*)

that it is halfway between, etc. Thus if, when employing a nonideal metal mirror, it is possible to observe fairly accurately the passage of C over the fringe system, it will be possible to determine in this way the type and order of a multipole source.

It may, in conclusion, be pointed out that the curves satisfactorily meet the test of grazing incidence mentioned in Section I; the curves for both nonideal mirrors and for both types and all orders of multipoles merge as 2θ decreases to zero, where q has the common value -1.

Note 1. The Fresnel-Drude formulas (for $\kappa \neq 0$) are famous for the laboriousness of their numerical application; a mere glance at the form into which C. Pfeiffer has thrown them,[19] which has enjoyed considerable favor, is sufficiently explanatory. Now on a modern calculating machine complex numbers can, in their Cartesian form, be manipulated with great ease; hence in calculating points on the curves of Fig. 3 polar forms were assiduously avoided until the very last step. In the first place, β_r was determined for the various values of $\beta_i = \theta - \pi/2$ by solving simultaneously the equations

$$\begin{aligned} &\log \sin \Re\{\beta_r\} + \log \cosh \Im\{\beta_r\} = \log \sin \beta_i + L, \\ &\log \cos \Re\{\beta_r\} + \log \sinh \Im\{\beta_r\} = \log \sin \beta_i + L + \log \kappa \quad (12) \\ &\qquad (L = -\log [n + n\kappa^2]), \end{aligned}$$

which could easily be accomplished to the desired accuracy by interpolations from tables. The rest of the work was then straightforward substitution into (8) and (10).

Note 2. In order to facilitate the derivation of the formulas corresponding to other experimental arrangements involving nonideal reflections, we indicate an easy method for arriving at formulas which correspond to (16)* for ideal reflections. If $\mathbf{n}^I$, $\mathbf{n}^R$ indicate unit vectors in the direction of propagation of the beams I, R respectively, then $c \equiv \mathbf{n}^I \cdot \mathbf{n}^R = -\cos 2\beta_i$ and the relation between $\mathbf{h}^R$ and $\mathbf{h}$ may be written:

$$\begin{aligned} \mathbf{h}^R = \rho_{11}\mathbf{h} - [(\mathbf{n}^R \cdot \mathbf{h})/(1-c^2)] \\ \times [(\rho_{11} - c\rho_\perp)\mathbf{n}^R + (\rho_\perp - c\rho_{11})\mathbf{n}^I]. \end{aligned} \quad (13)$$

If we now set $\mathbf{n}^I = \sin\theta \mathbf{c}_x + \cos\theta \mathbf{c}_z$, $\mathbf{n}^R = \mathbf{c}_\zeta$, $\mathbf{h} = h_1 \cos\theta \mathbf{c}_x + h_2 \mathbf{c}_y - h_1 \sin\theta \mathbf{c}_z$ and then multiply through scalarly by $\mathbf{c}_\xi$ and $\mathbf{c}_\eta$ (the $\mathbf{c}$'s being unit vectors along the corresponding axes), the right-hand sides will appear expressed in terms of h_1, h_2, θ, and the direction cosines relating the $O\xi\eta\zeta$ and $Oxyz$ axes. The coefficients of h_1 and h_2 are then the desired quantities $a_{\xi 1}, \cdots, a_{\eta 2}$.

For the simple arrangements discussed in the earlier paper we find:

$$\begin{aligned} \begin{pmatrix} a_{\xi 1} & a_{\xi 2} \\ a_{\eta 1} & a_{\eta 2} \end{pmatrix} &= \begin{pmatrix} \rho_\perp & 0 \\ 0 & \rho_{11} \end{pmatrix} \text{ (case } A^*\text{)}, \\ &= \begin{pmatrix} \rho_{11}\cos\theta & -\rho_\perp \sin\theta \\ \rho_{11}\sin\theta & \rho_\perp \cos\theta \end{pmatrix} \text{ (case } B^*\text{)}. \end{aligned} \quad (14)$$

The corresponding formulas for the primed quantities are obtained by writing $-\theta$ for θ. If similar mirrors are used for both rays, then, since in these cases β_i is an even function of θ, the ρ's do not need to be primed. Thus we find from (5):

$$\begin{aligned} &\text{Case } A^* \quad Q = \rho^{-2}(|\rho_\perp|^2 {}^2D_1{}^P + |\rho_{11}|^2 {}^2D_2{}^P), \\ &\text{Case } B^* \quad Q = \rho^{-2}(|\rho_{11}|^2 {}^2D_1{}^P + |\rho_\perp|^2 {}^2D_2{}^P)\cos 2\theta. \end{aligned} \quad (15)$$

Since these Q's are *real*, they will show true zeros even for nonideal metallic mirrors.

[19] Quoted by W. König, *Handbuch der Physik*, Vol. 20, p. 242.

Van der Waals Forces in Helium*

CHESTER H. PAGE†
Sloane Physics Laboratory, Yale University, New Haven, Connecticut
(Received December 4, 1937)

A variational method of calculating perturbation energy has been applied to the first two terms of a rapidly converging series expansion of the mutual potential energy of two helium atoms. The result is compared with the much simpler second-order perturbation scheme of Margenau, which it tends to support. The same variational method was then used with the perturbing potential in closed form. This involves the calculation of integrals not previously evaluated. The result validates the previous expansion of the potential. We obtain, for the van der Waals interaction of two unexcited helium atoms:

$$\epsilon=-(A/R^6)\{1+6.26/R^2+51.2/R^4+\cdots\}\text{ ergs},$$

where R is the atomic separation with the first Bohr radius (0.5282 angstrom) as unit distance. The complexity of the integrations requires the use of simple exponential wave functions of the Hartree type; the resulting value of the coefficient A is therefore poor, but this coefficient is well known from other work. It yields a polarization molecule with a dissociation energy of 0.30×10^{-16} erg. The bracketed expression giving the relative contributions of the higher order terms is the chief contribution of the present method of attack.

VAN DER WAALS force is due to secondary polarization; that is, polarization of a neutral atom (or molecule) by another neutral atom. Classically, this occurs only if the second atom has a permanent electric moment. Debye[1] and Keesom[2] found that this force is too small to explain the observed attractions between neutral atoms. In the light of the quantum theory, F. London[3] realized that the relatively strong van der Waals forces arise from the polarization of one molecule by the rapidly changing field due to the instantaneous configuration of the electrons and nuclei of another molecule.

Gropper[4] has recently shown how we may calculate the equation of state on quantum theory, given the interaction corresponding to all separations of molecules. An accurate determination of these forces again becomes an interesting problem, since we are now able to obtain therefrom an accurate equation of state without experimental parameters. Of all gases, helium is most amenable to theoretical calculations, because of its simple structure, and is also the most interesting from a practical point of view, since it is used in standard thermometry.

The repulsive force between helium atoms is known with fair accuracy;[5, 6] the problem in this case reduces to a careful study of the van der Waals attraction.

The most complete theoretical calculation of van der Waals forces in helium has been that made by Margenau[7] by including the effect of dipole-quadrupole and quadrupole-quadrupole forces as well as dipole-dipole forces. The nature of the approximation in his scheme, however, makes the accuracy of these higher order interaction terms somewhat uncertain.

The van der Waals energy in which we are interested is the quantum mechanical average of the perturbing potential due to the proximity of two helium atoms, namely:

$$\epsilon=\frac{\int\psi^*H\psi dT}{\int\psi^*\psi dT}-\frac{\int\psi_0^*H_0\psi_0 dT}{\int\psi_0^*\psi_0 dT},\qquad(1)$$

where ψ is the perturbed state function of the system of two helium atoms, ψ_0 the unperturbed state function, and $H=H_0+v$ the complete Hamiltonian, with

$$v=\frac{8}{\rho_{ab}}+2\left(\frac{1}{\rho_{13}}+\frac{1}{\rho_{14}}+\frac{1}{\rho_{23}}+\frac{1}{\rho_{24}}\right)-4\left(\frac{1}{\rho_{a3}}+\frac{1}{\rho_{a4}}+\frac{1}{\rho_{b1}}+\frac{1}{\rho_{b2}}\right),\qquad(2)$$

the interaction potential in atomic units.

* Part of a dissertation presented to the faculty of the Graduate School of Yale University in candidacy for the degree of Doctor of Philosophy

† Now at Lafayette College, Easton, Penna.

[1] P. Debye, Physik. Zeits. **21**, 178 (1920); **22**, 302 (1921).

[2] W. H. Keesom, Physik. Zeits. **22**, 129, 643 (1921).

[3] F. London, Zeits. f. Physik **63**, 245 (1930).

[4] L. Gropper, Phys. Rev. **50**, 963 (1936). See also: G. E. Uhlenbeck and L. Gropper, Phys. Rev. **41**, 79 (1932); G. E. Uhlenbeck and E. Beth, Physica **3**, 729 (1936).

[5] J. C. Slater, Phys. Rev. **32**, 349 (1928).

[6] N. Rosen, Phys. Rev. **38**, 255 (1931).

[7] H. Margenau, Phys. Rev. **38**, 747 (1931).

The notation here employed is familiar: ρ_{ij} is the distance from the ith particle to the jth; the vector ϱ_{ij} is taken as directed from the ith to the jth particle. The two nuclei are denoted by a and b, having electrons 1 and 2, 3 and 4, respectively.

The usual procedure is to express v as a Taylor series expansion:[7]

$$\begin{aligned} v=&-(2/\rho_{ab}^3)[2x_1x_3-y_1y_3-z_1z_3] \\ &+(3/\rho_{ab}^4)[r_1^2x_3-x_1r_3^2 \\ &+(2y_1y_3+2z_1z_3-3x_1x_3)(x_1-x_3)] \\ &+(3/2\rho_{ab}^5)[r_1^2r_3^2-5r_3^2x_1^2-5r_1^2x_3^2 \\ &-15x_1^2x_3^2+2(4x_1x_3+y_1y_3+z_1z_3)^2]+\cdots, \end{aligned} \tag{3}$$

where $r_1\equiv\rho_{a1}$; $r_3\equiv\rho_{b3}$ with rectangular components x_1, y_1, z_1, x_3, y_3, z_3. We have written the expansion for one electron on each atom. It has been found that, with the use of the symmetric atomic state functions to be used here, the four pairings of electrons simply introduce a factor four in the result.[7]

The terms of the series are known respectively as the dipole-dipole, dipole-quadrupole, quadrupole-quadrupole, etc., interactions.

Margenau's method is an approximate second-order perturbation method which uses the first three terms of the expanded potential. Slater and Kirkwood[8] attacked the problem with a variational calculation, using, however, only the first (dipole-dipole) term of the interaction.

In this paper we shall apply the Slater-Kirkwood method to the first two terms of the series expansion of the potential, and then to the total potential in closed form, given by Eq. (2). In the latter case, the integrations have been carried through in closed form, and the result expanded into a power series for comparison.

I

Briefly, the variation method employed is to consider the perturbed function of the system to be of the form:

$$\psi=\psi_0(1+\varphi), \tag{4}$$

where $\psi_0=\psi_0(1)\psi_0(2)$ is the unperturbed function of two normal helium atoms and $\varphi(r)$ is any convenient parametric function of interparticle distances.

By a simple manipulation we find:[8]

$$\epsilon=\int(1+\varphi)[v\varphi-p(\varphi)]\psi_0^2dT/\int\psi_0^2dT, \tag{5}$$

where

$$p(\varphi)\equiv\nabla^2\varphi+2\nabla\varphi\cdot\nabla\ln\psi_0-v. \tag{6}$$

Now the unperturbed energy

$$E_0=\int\psi_0^*H_0\psi_0dT/\int\psi_0^*\psi_0dT$$

is not a function of φ, so $E=E_0+\epsilon$ can be minimized by minimizing ϵ with respect to the parameters in φ. Although the total energy as calculated by a variational method of the system (E) is greater than or equal to the true total energy, we can make no such statement as to the perturbation energy (ϵ), for the error therein depends upon the relative inaccuracies in the perturbed and unperturbed wave functions.

To make our calculations feasible, we take

$$\psi_0=e^{-Z'(\rho_{a1}+\rho_{a2}+\rho_{b3}+\rho_{b4})}, \tag{7}$$

where Z' is the well-known "screening constant" parameter adjusted to minimize E_0, and

$$\varphi=vf(r)=\lambda ve^{\beta(\rho_{a1}+\rho_{a2}+\rho_{b3}+\rho_{b4})}, \tag{8}$$

where λ and β are the variation parameters of the problem at hand.

The explicit inclusion of the perturbing potential in the variation function is an intuitive scheme which was introduced by Hassé[9] with success. When used with more of the potential than is given by the dipole-dipole term, this type of variation function introduces extreme algebraic complications, but shows very interesting effects.

Substituting Eq. (8) into Eqs. (5) and (6), we have a formal answer for our problem in terms of an integral involving v, v^2, v^3, and derivatives of v. It is found that the contribution of the v^3 terms is negligible, as was to be expected, since these terms occur as $v\varphi^2$, a third-order approximation.

Using for the perturbing potential only the dipole-dipole and dipole-quadrupole interactions, we obtain

$$\epsilon=-A(\beta)\lambda^2+B(\beta)\lambda, \tag{9}$$

so that the minimum with respect to λ is $B^2/4A$. Explicitly:

$$\begin{aligned} B\equiv&\int v^2e^{\beta(r_1+r_3)}\psi_0^2dT_1dT_3, \\ 8A\equiv&\int v^2e^{\beta(r_1+2r_3)}l_1(e^{\beta r_1})\psi_0^2dT_1dT_3 \\ &+\int e^{\beta(r_1+2r_3)}m_1(e^{\beta r_1})\psi_0^2dT_1dT_3 \\ &-\tfrac{1}{2}\int v^3e^{2\beta(r_1+r_3)}\psi_0^2dT_1dT_3, \end{aligned} \tag{10}$$

[8] J. C. Slater and J. G. Kirkwood, Phys. Rev. **37**, 682 (1931).

[9] H. R. Hasse, Proc. Camb. Phil. Soc. **26**, 542 (1930); **27**, 66 (1931).

where
$$l_1(f)=\frac{\partial^2 f}{\partial r_1^2}+\left(\frac{4}{r_1}+2\frac{\partial \ln \psi_0}{\partial r_1}\right)\frac{\partial f}{\partial r_1}+\frac{2}{r_1}\frac{\partial \ln \psi_0}{\partial r_1}f,$$
$$m_1(f)=\frac{18}{R^8}\frac{r_1^4x_3^2-6r_1^2x_1^2x_3^2+x_1^2(4y_1^2y_3^2+4z_1^2z_3^2+9x_1^2x_3^2)}{r_1}\left[\frac{\partial f}{\partial r_1}+f\frac{\partial \ln \psi_0}{\partial r_1}\right], \tag{11}$$

where $R\equiv\rho_{ab}$ is the internuclear distance in terms of the first Bohr radius.

Evaluation of the integrals yields

$$\epsilon=-\frac{(9.2^{26}/R^6)[(z'-\beta)/(2z'-\beta)^2]^{10}z'^6\{1+90/R^2(2z'-\beta)^2\}^2}{12(z'^2-z'\beta+\beta^2)+(15/R^2)\{6+1/2(z'-\beta)^2[30z'^2-18z'\beta+25\beta^2]\}+(1/R^5)243/2(z'-\beta)^4}\text{ergs.} \tag{12}$$

Putting in the value of $z'=27/16$, we find $\epsilon(\beta)$ to be minimized by $\beta=0.23$, giving, after reduction

$$\epsilon=-((0.481\times10^{-10})/R^6)\times\{1+5.88/R^2+\cdots\}\text{ ergs.} \tag{13}$$

If we had used

$$\psi_0=(\rho_{a1}\rho_{a2}\rho_{b3}\rho_{b4})^{-\frac{1}{2}}e^{-z''(\rho_{a1}+\rho_{a2}+\rho_{b3}+\rho_{b4})} \tag{14}$$

instead of our previous choice, we should have obtained:

$$\epsilon=-((0.792\times10^{-10})/R^6)\times\{1+8.30/R^2+\cdots\}\text{ ergs.} \tag{15}$$

Margenau[7] gives

$$\epsilon=-((0.70\times10^{-10})/R^6)\times\{1+7.9/R^2+\cdots\}\text{ ergs} \tag{16}$$

while Slater and Kirkwood[8] give

$$\epsilon=-(0.68\times10^{-10})/R^6\text{ ergs.} \tag{17}$$

for the dipole-dipole energy alone.

We are interested for the moment in the relative strength of dipole-dipole and dipole-quadrupole interactions. It is seen that the variation function which gives a small dipole-dipole energy also gives a small dipole-quadrupole energy, while that which makes the former large also increases the latter. Now the dipole-dipole term is known with considerable accuracy.[8, 10] This suggests the tentative procedure of introducing a scale factor S such that $R'=SR$ makes the dipole-dipole term nearly correct in (15). If this is done, (15) becomes:

$$\epsilon=-((0.70\times10^{-10})/R'^6)\times\{1+7.97/R'^2+\cdots\}\text{ ergs} \tag{18}$$

or

$$\epsilon=-((0.68\times10^{-10})/R'^6)\times\{1+7.89/R'^2+\cdots\}\text{ ergs} \tag{19}$$

tending to justify the relative strengths of Margenau's dipole-dipole and dipole-quadrupole terms.

II

To investigate more adequately the higher order interaction terms, and check the convergence of the Taylor series potential when used with this type of variation function, we repeat this same method of attack using the closed form (Eq. (2)) of the perturbing potential. The use of coordinate systems given in the appendix permits the evaluation of the integrals involved. Even with these coordinates, it is necessary to employ various tricks of integration and very lengthy algebra.

We use the simple ψ_0 of Eq. (7). We shall find that this gives a poor value of the dipole-dipole coefficient, but the simplicity of this function is needed if the higher order terms are to be evaluated. The result is of the form:

$$\epsilon=A(\beta)\lambda^2+B(\beta)\lambda+C(\beta), \tag{20}$$

so that the minimum with respect to λ is $C-B^2/4A$.

The evaluated integrals involve the exponential integral

$$Ei(-x)\equiv\int_\infty^x\frac{e^{-t}}{t}\,dt, \tag{21}$$

[10] H. Margenau, Phys. Rev. **37**, 1425 (1931)..

which has, for large x, the asymptotic expansion:

$$Ei(-x)=\frac{e^{-x}}{-x}\left(1-\frac{1}{x}+\frac{2!}{x^2}-\frac{3!}{x^3}+\cdots\right). \quad (22)$$

This function appears in the results in the combination

$$e^{x}Ei(-x)$$

with x proportional to R, and always large; the expanded combination then becomes an inverse power series in R. A check on the lengthy algebra is provided by the result that all odd power terms eventually add out, as well as all even powers of higher order than $1/R^6$.

Simple exponential terms (e^{-x}) also occur, but are found to be negligible in comparison with the terms in $1/R^{10}$, so the series expansion

$$\epsilon=-((0.467\times10^{-10})/R^6)\{1+6.26/R^2+51.2/R^4+\cdots\} \quad (26)$$

is valid to the number of terms given.

The resulting expression for the perturbation energy is

$$\epsilon=-\frac{3\cdot2^9C_2{}^{16}C_0{}^{12}}{R^6C_1{}^{32}}\times\left\{\frac{1+\dfrac{180}{C_1{}^2R^2}+\dfrac{29100}{C_1{}^4R^4}+\dfrac{1890000}{C_1{}^6R^6}+\dfrac{(10500)^2}{C_1{}^8R^8}+\cdots}{(4\beta^2-2z'\beta+2z'^2)+\dfrac{10}{C_2{}^2R^2}(36\beta^2-21z'\beta+21z'^2)+\dfrac{10}{C_2{}^4R^4}(4200\beta^2-2688z'\beta+2688z'^2)}\right\}\text{ergs}, \quad (23)$$

where we have introduced

$$C_0=2z', \quad C_1=2z'-\beta, \quad C_2=2z'-2\beta. \quad (24)$$

Inserting $z'=27/16$, we find $\epsilon(\beta)$ to be minimized by $\beta=0.14$, giving:

$$\epsilon=-\frac{0.467\times10^{-10}}{R^6}\left\{\frac{1+17.20/R^2+265.7/R^4+\cdots}{1+10.94/R^2+146.0/R^4+\cdots}\right\}\text{ergs} \quad (25)$$

or

$$\epsilon=-((0.467\times10^{-10})/R^6)\{1+6.26/R^2+51.2/R^4+\cdots\}\text{ergs}. \quad (26)$$

Margenau's quadrupole-quadrupole term is $30/R^4$.

As seen before, our dipole-quadrupole energy is lower relative to the dipole-dipole energy than is Margenau's due to our use of a poor unperturbed function. The last, or quadrupole-quadrupole interaction, is considerably higher, and since it would be further raised by improving the initial function, we conclude that his last term is too small.

In the region of the minimum of the combined attraction and repulsion curves ($R^2\doteq30$), this third term is less than 5 percent of the total, and succeeding terms probably less than 1 percent.

Comparing Eq. (26) with Eq. (13) we see that our complete treatment has increased the relative strength of the dipole-quadrupole interaction, but has decreased the absolute strength of the dipole-dipole interaction. This effect is, of course, due to the fact that the variation function contained the perturbing potential explicitly.

We make a numerical comparison of our final result with the previous Eq. (13) in the region of interest; i.e., $R^2=30$. We find, from

(Eq. (13)): $\epsilon=-21.5\times10^{-16}$ ergs,
(Eq. (26)): $\epsilon=-21.9\times10^{-16}$ ergs,

which is an increase of only 2 percent, although the added term (quadrupole-quadrupole) is 6 percent as large as the dipole-dipole term, and the relative strength of the dipole-quadrupole term has increased.

This interesting "self-compensation of the dipole-dipole coefficient may be an indication that an increase in complexity of the perturbation requires a more than proportionate increase in complexity of the variation function, if it is to give noticeable improvement of the calculated perturbation energy. But it is more likely to be a real effect, showing that this type of variation function actually improves an approximation in the perturbation.

To investigate the helium diatomic polarization molecule, we correct our result for the interaction by changing the coefficient of the dipole-dipole term to agree with its known value, thus

$$\epsilon = -((0.68\times10^{-10})/R^6) \times\{1+6.26/R^2+51.2/R^4\} \text{ ergs.} \quad (27)$$

This energy is to be used as the potential energy in the radial vibration equation for the molecule. We take the case of zero angular momentum, and integrate the differential equation by standard numerical methods. The calculation yields a discrete vibrational level with a dissociation energy of 0.30×10^{-16} ergs, or 19 electron microvolts.

The writer takes great pleasure in thanking Professor Henry Margenau for suggesting this problem, and supervising the work with genuine interest.

Appendix

The coordinate systems used are based on the volume element for a single electron in elliptic coordinates. See Fig. 1.

In spherical coordinates:

$$dT=\rho_{b1}^2 \sin\theta d\rho_{b1}d\theta d\varphi.$$

Now $\rho_{a1}^2=\rho_{b1}^2+R^2-2\rho_{b1}R\cos\theta$;

$$\therefore \sin\theta d\theta=\rho_{a1}d\rho_{a1}/R\rho_{b1};$$

$$\therefore dT=(1/R)\rho_{a1}\rho_{b1}d\rho_{a1}d\rho_{b1}d\varphi.$$

The limits of integration are indicated by

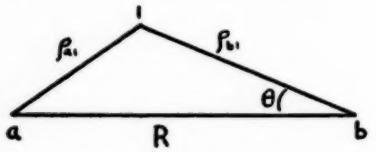

Fig. 1. One-electron coordinates.

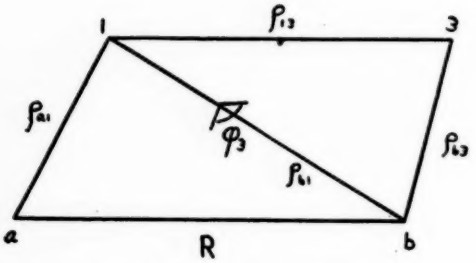

Fig. 2. Two-electron coordinates.

$$T=\frac{1}{R}\int_0^\infty \rho_{b1}d\rho_{b1}\int_{|\rho_{b1}-R|}^{\rho_{b1}+R}\rho_{a1}d\rho_{a1}\int_0^{2\pi}d\varphi.$$

This can easily be extended to two electrons, by considering ρ_{b1} the base line, corresponding to R, for the second electron. See Fig. 2.

As before: $dT_1=(1/R)\rho_{a1}\rho_{b1}d\rho_{a1}d\rho_{b1}d\varphi_1.$

Similarly:

$$dT_3=(1/\rho_{b1})\rho_{b3}\rho_{13}d\rho_{b3}d\rho_{13}d\varphi_3;$$

$$\therefore dT=dT_1dT_3=(1/R)\rho_{a1}d\rho_{a1}\rho_{b3}d\rho_{b3}\rho_{13}d\rho_{13}d\rho_{b1}d\varphi_1d\varphi_3$$

and

$$T=\frac{1}{R}\int_0^\infty d\rho_{b1}\int_{|\rho_{b1}-R|}^{\rho_{b1}+R}\rho_{a1}d\rho_{a1}\int_0^\infty \rho_{b3}d\rho_{b3} \times\int_{|\rho_{b1}-\rho_{b3}|}^{\rho_{b1}+\rho_{b3}}\rho_{13}d\rho_{13}\int_0^{2\pi}d\varphi_1\int_0^{2\pi}d\varphi_3.$$

This process can be applied again to give us a volume element for use in our three electron integrals.

Several two electron integrals involve all five interparticle distances. The volume element given has as variables all the interparticle distances (we exclude R) except ρ_{a3}; in addition, there are two azimuth angles. One of these, φ_3, can be replaced by the introduction of ρ_{a3}. For integrals involving ρ_{a3} in the form ρ_{a3}^2 only, we obtain a simple result after integrating with respect to φ_3, which is perhaps worth indicating here.

Let $\rho_{a1}|\rho_{b1}$ be the projection of ρ_{a1} upon ρ_{b1}, and $\Delta(\rho_{a1}, \rho_{b1}, R)$ the area of the triangle having sides ρ_{a1}, ρ_{b1}, R. By the law of cosines, we find:

$$\rho_{a3}^2=[\rho_{a1}|\rho_{b1}-\rho_{13}|\rho_{b1}]^2+\left[\frac{2\Delta(\rho_{a1},\rho_{b1},R)}{\rho_{b1}}\right]^2 +\left[\frac{2\Delta(\rho_{13},\rho_{b3},\rho_{b1})}{\rho_{b1}}\right]^2-2\frac{2\Delta(\rho_{a1},\rho_{b1},R)}{\rho_{b1}} \times\frac{2\Delta(\rho_{13},\rho_{b3},\rho_{b1})}{\rho_{b1}}\cos\varphi_3,$$

$$\int_0^{2\pi}\rho_{a3}^2d\varphi_3=2\pi\left\{[\rho_{a1}|\rho_{b1}-\rho_{13}|\rho_{b1}]^2+\left[\frac{2\Delta(\rho_{a1},\rho_{b1},R)}{\rho_{b1}}\right]^2 +\left[\frac{2\Delta(\rho_{13},\rho_{b3},\rho_{b1})}{\rho_{b1}}\right]^2\right\}$$

$$=2\pi\left\{\left(\frac{\rho_{a1}^2+\rho_{b1}^2-R^2-\rho_{13}^2-\rho_{b1}^2+\rho_{b3}^2}{2\rho_{b1}}\right)^2 +\frac{(\rho_{a1}+\rho_{b1}+R)(\rho_{a1}+\rho_{b1}-R) \times(\rho_{a1}-\rho_{b1}+R)(-\rho_{a1}+\rho_{b1}+R)}{4\rho_{b1}^2} +\frac{(\rho_{13}+\rho_{b3}+\rho_{b1})(\rho_{13}+\rho_{b3}-\rho_{b1}) \times(\rho_{13}-\rho_{b3}+\rho_{b1})(-\rho_{13}+\rho_{b3}+\rho_{b1})}{4\rho_{b1}^2}\right\}$$

$$=\pi\left\{\frac{(\rho_{a1}^2-R^2)(\rho_{b3}^2-\rho_{13}^2)}{\rho_{b1}^2} +\rho_{a1}^2+\rho_{b3}^2+R^2+\rho_{13}^2-\rho_{b1}^2\right\}.$$

This result will, of course, be multiplied by some function of the four remaining distance coordinates and integrated over the rest of the two-electron volume element.

LETTERS TO THE EDITOR

Prompt publication of brief reports of important discoveries in physics may be secured by addressing them to this department. Closing dates for this department are, for the first issue of the month, the eighteenth of the preceding month, for the second issue, the third of the month. Because of the late closing dates for the section no proof can be shown to authors. The Board of Editors does not hold itself responsible for the opinions expressed by the correspondents.

Communications should not in general exceed 600 words in length.

An Alternative Interpretation of Jauncey's "Heavy Electron" Spectra

In the February first number of *The Physical Review*,[1] Jauncey has shown two photographs of magnetic spectra of electrons, in both of which the main deflected image is taken as evidence of a heavy electron of rest-mass about 3 times normal. Following the suggestion of C. T. Zahn[2] that this image may be caused by scattered electrons, I have calculated that in both of Jauncey's photographs the image in question corresponds with that to be expected from electrons once scattered by the lower plate of his velocity selector.

Jauncey has shown that his velocity selector, with parallel plates 5 cm long and 0.105 cm apart, and with the magnetic and electric fields used in his experiments, will not transmit β-particles coming directly from Ra E, except in the chosen low range of velocities. When these β-rays are however bent by the magnetic field to strike the lower plate, this part of the plate becomes the source of secondaries of only slightly reduced energy. The rays moving forward may then pass through the selector if they do not again strike the plate. Thus for β-rays once scattered, the resolving power is no greater than for a velocity selector of half the length if primary particles only were considered. From the dimensions of Jauncey's apparatus it can thus be shown that while for primary particles the minimum transmissable radius of curvature is 30 cm, the corresponding minimum for particles once scattered is 7.5 cm.

Numerical calculation shows that with the magnetic and electric fields used in Jauncey's experiments any electron with curvature low enough to reach the film will have a radius of curvature of more than 7.5 cm between the plates. That is, the apparatus is not effective in selecting velocities of electrons that have been once scattered. That it does, however, act as an effective velocity selector for the direct β-rays is shown by the sharpness of Jauncey's line *C*, due to electrons with velocities close to the chosen value of $\beta=0.33$.

Calculations of the position of the images to be expected from such once-scattered rays are also in satisfactory agreement with the observed positions of the diffuse images in Jauncey's photographs.

It would thus appear that the heavy electron interpretation of Jauncey's photographs is not required. His new lines may alternatively be ascribed to a kind of "second-order" magnetic spectrum caused by once-scattered particles. Higher order scattering might also, as suggested by Zahn, be supposed to produce detectable effects. The present calculation indicates, however, that only single and not multiple scattering processes need be considered to account for Jauncey's results.

ARTHUR H. COMPTON

University of Chicago,
Chicago, Illinois,
February 16, 1938.

[1] G. E. M. Jauncey, Phys. Rev. **53**, 265 (1938).
[2] Made in discussion of Jauncey's results at the meeting of the American Physical Society, Indianapolis, Dec. 30, 1937, and soon to appear in the *Physical Review*.

Heavy Beta-Particles?

During the past year preliminary cloud-chamber experiments by H. R. Crane, J. J. Turin, D. S. Bayley, and E. R. Gaerttner, on primary beta-particles and Compton recoil electrons, suggested the possibility that beta-particles may be heavier than normal. It was proposed in the above group[1] that the beta-ray paradox might be explained in this way, rather than by the neutrino hypothesis.

Preliminary direct experiments to test this hypothesis were carried out in collaboration with A. H. Spees, and the results[2] were negative. In parallel with this investigation, the continued experiments by Crane's group also finally indicated negative results. Further experiments were performed with a considerably improved apparatus; and the final results, a detailed account of which appears in this issue of the *Physical Review*, indicate agreement with the relativity theory to within the limits of experimental error.

In the course of a mathematical analysis of the instrument it became apparent that the usually accepted simple interpretation of the Bucherer-Neumann experiments might be subject to serious limitations. A similar analysis (to be published in the near future) was then carried out for the *unmodified* Bucherer-Neumann experiment—and it was discovered that the *supposed* velocity filter in Neumann's experiments, even for the case of negligible scattering, must have been completely broken down on the high velocity side, for $\beta>0.7$; and that, even for the lower velocities, the resolution width was approximately as great as that equivalent to the whole relativistic mass effect! Since it is not clear whether Neumann's electron beam was composed largely of scattered radiation, or of direct radiation—and since the effective resolving power de-

creases very rapidly after scattering—it is obvious that the ordinary simple interpretation of experiments of the Bucherer type is not justifiable.

In the meantime (at an unofficial meeting in Indianapolis, December, 1937, and also in a recent Letter to the Editor) this same possibility for dispensing with the neutrino hypothesis was again proposed—by G. E. M. Jauncey, who also described experimental evidence for heavy beta-particles, based on measurements of the Bucherer-Neumann type. The conflicting results obtained here at the University of Michigan were again pointed out by the author at this meeting, and a description was given of the unpublished results of our analysis showing that the Bucherer method is unreliable as regards its simple interpretation.

We believe it quite possible, if not probable, that the radiation photographed by Jauncey was largely scattered radiation, for the following reasons: Jauncey's experiments were performed at a low velocity where the distribution function is small, so that the radium E spectrum was composed almost exclusively of velocities larger than that "observed." When electrons are scattered, their average momentum is reduced, and at the same time the effective resolution width is increased. If the ratio of the condenser separation to the square of the length is near the critical value at which the filter breaks down, then, under the above conditions, the probability for the *leakage* of high velocity scattered radiation becomes relatively large, and one might expect the apparatus to behave rather as a momentum spectrograph for the scattered radiation. Hence one might obtain a spurious peak due to the scattered electrons, and even miss the weak theoretical line altogether.

An examination of the values of Jauncey's geometrical constants in the light of our theory shows that his theoretical resolving power was very near the critical value. We therefore believe it quite possible that his observations correspond to the conditions just outlined. In any case, our results for radium E electrons of $H\rho$ 2000, or $\beta=0.75$, are definitely not consistent with the particular hypothesis discussed here. It is conceivable that *another* type of heavy beta-particle exists, such that the anomaly is inappreciable for $\beta=0.75$ and large for $\beta\sim0.4$; but this does not seem probable in view of the above-mentioned uncertainties.

C. T. ZAHN

Department of Physics,
University of Michigan,
Ann Arbor, Michigan,
February 4, 1938.

[1] See G. Breit, Rev. Sci. Inst. **8**, 141 (1938).
[2] Zahn and Spees, Phys. Rev. **53**, 524 (1937).

Ferromagnetic Impurities

An experimental method has been developed whereby very minute ferromagnetic impurities may be detected in various materials and the magnetic properties of these impurities studied.

The specimen to be tested may have any shape but a short rod of about 0.3 cc volume is most convenient. It is first placed in a field of several thousand oersteds supplied by an electromagnet. This serves to magnetize all ferromagnetic impurities in one direction; the field is then removed and it is assumed that any ferromagnetic impurities present will then be left with a certain remnant magnetization in this direction. This is detected and measured by hanging the specimen from a quartz fiber in the center of a pair of Helmholtz coils, the remnant magnetization being at right angles to the axis of the coils. A field of 40 oersteds or less is applied and the resulting rotation noted by a mirror and scale. The fact that reversing the field reverses the rotation, shows that the effect is a ferromagnetic one. With a strong quartz fiber, whose torsion constant was 0.028 dyne-cm per radian, a magnetic moment per cc, I, of 2×10^{-7} could be detected. A comparison of this with a remnant magnetization of over 500 for pure iron shows the sensitivity attainable.

The values of I found for various materials are given in Table I.

TABLE I.

Brass, commercial	7.5×10^{-7}
Copper, No. 12 D.C.C. wire, insulation removed	1.7×10^{-6}
Bismuth, extruded rod	3.4×10^{-6}
Bismuth, crystallized C.P. analyzed, 0.00% Fe	1.0×10^{-6}
Cadmium, Baker analyzed, 0.003% Fe	6.2×10^{-6}
Tin, Baker analyzed, 0.002% Fe	8.5×10^{-6}
Bakelite	1.0×10^{-6}
Pyrex rod	3×10^{-7}

The surfaces were carefully cleaned and handled only with forceps. Tests failed to show the effect a surface one, unless perhaps for the Pyrex.

Calculations showed that dia- or paramagnetism of a specimen could cause rotation only through (1) different demagnetizing factors in different directions when the specimen is not spherical, or (2) different susceptibilities, K_1 and K_2, in different directions. As (1) depends on K^2H^2 it was too small to be noticeable in the weak fields used, but (2) depends on $(K_1-K_2)H^2$ and so is of a considerably larger order of magnitude. The crystallized Bi sample, which appeared to be a single crystal, gave just such an effect, dependent on H^2 and of just the right magnitude, in addition to the ferromagnetic effect which varies in magnitude and direction with H. We have then also a sensitive method of detecting magnetic anisotropy.

The ferromagnetic impurities could be magnetized in any direction desired or demagnetized by reversals. They would not likely be magnetic in such minute amounts unless they exist as inclusions of aggregates of atoms rather than in a state of diffusion throughout the metal, although the latter may explain the almost null result for Pyrex glass.

The foregoing was prompted by a discussion with F. Bitter at the Cornell Symposium in July, 1937.

F. W. CONSTANT
J. M. FORMWALT

Duke University,
Durham, North Carolina,
February 4, 1938.

Scattering of Cosmic-Ray Particles

The recent experiments of Blackett and Wilson[1] and of Neddermeyer and Anderson[2] show conclusively that the energy lost by cosmic-ray particles ($H\rho \sim 1.0\times10^6$ gauss·cm) in traversing lead plates is on the average considerably less than the theoretical loss for electrons (and also protons). Neddermeyer and Anderson have suggested that this low energy loss may be due to the presence of a new type of particle in cosmic rays, of mass appreciably greater than that of an electron and less than that of a proton. The theoretical energy loss by such a particle in the region of $H\rho$ concerned would be considerably less than that by either electrons or protons. The earlier and alternative hypothesis is that all the particles are ordinary electrons and that the theory of their energy loss breaks down.

The purpose of this note is to draw attention to the important significance of scattering in connection with this problem. The theoretical probability that a particle of mass M, charge E, velocity βc, experiences a collision which deflects it through a small angle θ, in traversing a plate of thickness t containing N nuclei per cm³, nuclear charge Ze, is

$$P(\theta)d\theta=(8\pi Z^2e^2E^2Nt/\xi^2M^2c^4\beta^4)fd\theta/\theta^3.$$

$\xi^{-2}=1-\beta^2$. f is a shielding factor and is a function of $(\hbar/M\beta c\xi\theta R)$ where R is a length depending only on Z, and is of the order of $Z^{-\frac{1}{3}}\times$hydrogen radius. The velocity of the cosmic-ray particles in the experiments concerned is close to that of light so that we may put $\beta=1$. In terms of the value of $H\rho$, which is the quantity actually measured in the experiments, the expression for $P(\theta)$ then becomes

$$P(\theta)=(8\pi Z^2e^2Nt/H^2\rho^2)f(\hbar c/H\rho E\theta R)/\theta^3.$$

This does not involve M—in other words for a given $H\rho$ the scattering is independent of the mass of the particle. Accordingly if the suggestion of Neddermeyer and Anderson for the small energy loss is correct, there should *not* be a corresponding small scattering. The scattering should equal the full theoretical value for electrons. However, if the smallness of the energy loss is due to a breakdown of the theory, all the particles being electrons, we would expect a corresponding small scattering.

The latter statement essentially depends on the circumstance that the distribution of "distance of approach" for the collisions which give rise to the scattering is nearly the same as that for the radiative collisions which cause the energy loss.[3, 4] Actually in both cases the upper limit to the distance of approach in the effective collisions is the same, *viz.*, the "shielding" radius, $R\sim137Z^{-\frac{1}{3}}\hbar/mc$. The lower limit in the radiative effect is $\eta\sim\hbar/mc$, and in the scattering it is somewhat less than $\sigma\sim(137/Z)\times(4\pi Nt)^{-\frac{1}{2}}$. For the scattering by 1 cm of lead $\sigma\sim0.1(\hbar/mc)$, and is therefore not of a very different order from η. The fact that σ is actually less than η means that a breakdown hypothesis would probably reduce the scattering, as represented by the square of the average deflection (α^2), to a greater extent than the energy loss. For instance in the simple type of breakdown hypothesis usually considered, in which the nuclear field within a certain radius b is supposed to have no effect, the radiative loss, if $\eta<b<R$, is reduced in the ratio $\log(R/\eta):\log(R/b)$, and if $\sigma<b<R$ the scattering (α^2) is reduced in the ratio $\log(R/\sigma):\log(R/b)$.[5] The latter is bigger if $\sigma<\eta$. Actually on this simple hypothesis the expected ratio, s, of the observed value of α^2 to its theoretical value, as represented by an approximate formula[6] given previously by the writer,[3] is about $(0.6r)^{\frac{1}{2}}$, where r is the ratio of the observed radiative energy loss to the theoretical value for electrons (if $r<1$). The early experiments of Anderson[7] on the scattering of cosmic-ray particles are roughly in agreement with the theoretical formula mentioned,[3, 4] and do not indicate a failure of the formula to the extent represented by $(0.6r)^{\frac{1}{2}}$. Accordingly insofar as these results go they support the suggestion of Neddermeyer and Anderson that the low observed energy loss is due to the presence of a new particle heavier than an electron.

There seems to be no feasible way of reducing the radiative effect for the high energy electrons under consideration without reducing their scattering. In an earlier discussion[3] the writer pointed out that while the radiative effect depends on the Fourier components of the nuclear force (in the system where the electron is initially at rest) of frequencies of the order of mc^2/h, the scattering may be said to be due to infinitely small frequencies. If therefore instead of saying that the effective nuclear force inside b vanishes (as in the above hypothesis) we supposed that the harmonic components of the force of frequencies mc^2/h are cut out, leaving unaffected lower frequencies, the radiative energy loss would be reduced without reducing the scattering. Such a state of affairs would however mean a time of collision of at least $\hbar/mc^2$, and since in the collisions concerned the time the nuclear field takes to pass over a *point* is small compared with $\hbar/mc^2$, this would require an electron "radius" of at least $\hbar/mc$, which is certainly not the case of ordinary electrons. The proved validity of the Klein-Nishina formula for the scattering of γ-rays of frequency of the order of mc^2/h is sufficient evidence against such a supposition. The radiative energy loss by electrons could also be reduced without reducing the scattering if we supposed the theory to break down not in respect of the force on the electron and its motion, but in the step from its motion to the emitted radiation. However, in the collisions concerned, this again would appear to be ruled out by the validity of the Klein-Nishina formula for hard γ-rays.

E. J. Williams

George Holt Physics Laboratory,
Liverpool, England,
January 24, 1938.

[1] Blackett and Wilson, Proc. Roy. Soc. **160**, 304 (1937).
[2] Neddermeyer and Anderson, Phys. Rev. **51**, 885 (1937).
[3] Williams, Phys. Rev. **47**, 568 (1935).
[4] Williams, Proc. Zurich Physics Conf. (Springer, 1936), p. 123.
[5] If the nuclear field became suddenly ineffective at a sharply defined radius $r=b$, the reduction in the scattering would be somewhat less. Actually of course the "cut-off" would be distributed over a distance not small compared with b, and in that case the result given here is valid.
[6] A correction to this formula to allow for the non-Gaussian part of the scattering, and also to allow more accurately for the shielding of the nuclear field by the atomic electrons (using a Thomas-Fermi model), increases the theoretical value by about 20 percent. s in the text is the ratio of the observed scattering to the uncorrected formula.
[7] Anderson, Phys. Rev. **43**, 381 (1933).

Cosmic Radiation and Electrical Conductivity in the Stratosphere

Korff, Curtiss and Astin published[1] a comparison of observations of cosmic-ray intensity (I) with our measurements[2] of the electrical conductivity of air (λ) for altitudes up to 22 km (their Fig. 3, p. 18) which apparently indicates that $I \doteq a\lambda$ (where a is some constant) at all altitudes. The writers had observed a roughly similar relationship between that conductivity data and Regener's measurements of cosmic-ray intensity but regarded it as of doubtful significance, because if the cosmic radiation is the sole ionizing agent in this portion of the atmosphere then the relation $I \doteq a\lambda$ implies $q = cn$ (where q is number of ion-pairs formed per cm³ per sec. in free air, n is number of ions per cm³, equilibrium assumed, and c is a constant independent of temperature and pressure) whereas the well-known relation $q = \alpha n^2$ (where α is recombination-coefficient, *dependent* upon temperature and pressure) should obtain if the ions are predominantly of the small-ion class. These two relations are reconcilable only when I varies as the inverse square of air-density (assuming α varies directly with pressure and that temperature is constant), a condition that is *roughly* satisfied in the lower eight or nine km of the atmosphere, but obviously not at higher levels. The correspondence at low pressures is considerably exaggerated, owing to some mistake in plotting the points for conductivity in their Fig. 3. If such a correspondence at low pressures is eventually established, that would add to the difficulty of harmonizing these two sets of observed values, as may be seen from the following brief statement of the character and magnitude of the disparity.

The data obtained from registrations of the electrical conductivity of air throughout the flight of the stratosphere balloon Explorer II[2] from Rapid City, South Dakota, geomagnetic latitude 53° north, taken together with measurements of the intensity of cosmic radiation made at Stuttgart, Germany, geomagnetic latitude 50° north, by Professor E. Regener and associates, formed the basis for the first extensive comparison of cosmic radiation and air-conductivity in the free atmosphere. That comparison showed a relation which differed from that to be expected if the cosmic radiation, including its secondary radiation, is the only ionizing agent in the region explored and if the resulting ions are the small type that predominate where air is unpolluted. That cosmic radiation is the predominant ionizing agent in the atmosphere, over the oceans, and everywhere in the troposphere above one or two km, and in the lower stratosphere, has been evident for about three decades. That small ions predominate at altitudes beyond a few km in the free atmosphere has been indicated by indirect evidence which cannot be reviewed here. The expected values are greater than those observed and the ratio of the former to the latter varies unmistakably as a simple function of pressure, namely, as $p^{-0.36}$ (where p is pressure in atmospheres), throughout the altitude-range, 5 to 19 km. That ratio rises to the large value 2.6 at 19 km. No simple relationship was expected below five or six km because complicating factors are known to be present there. From 19 to 22 km the ratio increased irregularly but in the average much faster than in the altitude-range from 5 to 19 km.

By mere inspection of the graphs for the several sets of cosmic-radiation data, such as were shown in Fig. 7, p. 28 of a paper by Curtiss, Astin, Stockman, Brown, and Korff,[3] it may be seen that a detailed comparison with more recent measurements of cosmic radiation would not modify any important features or conclusions, except as to magnitudes, derived from our initial comparison. Although in these graphs the cosmic-radiation intensity is expressed in percent of the value at the surface in each case, yet that is not of account here since the comparison with Regener's data showed that no adjustment of the constant factor, amounting in the aggregate to more than seven percent, would improve the agreement. In that exhibit the difference between the more recent data and those of Regener is not consistently greater the lower the pressure in the range from 600 to 70 millibars as would be required. The required difference is not small. It should be nearly 80 percent, or the intensity should be 20 percent, of Regener's value at 70 millibars. The values reported by Bowen, Millikan and Neher[4] for geomagnetic latitude 53° north are about 70 percent *greater* than those of Regener.

Furthermore it appears, especially from observations made at Washington, D. C.,[3] geomagnetic latitude 50° north, that for pressures below 70 millibars the cosmic-ray intensity is directly proportional to atmospheric pressure, or density, within the error of measurement. For that condition the electrical conductivity, insofar as it is dependent upon the cosmic radiation, should continue to increase down to the lowest pressure, so that the decrease in conductivity at pressures below 70 millibars cannot be attributed to the observed decrease in cosmic-ray intensity.

Thus a comparison of the more recent cosmic-ray data with the air-conductivity data shows a disparity of the same character but of even greater magnitude than that which appeared in the initial comparison. Some factors to which this disparity may perhaps be attributed are discussed in our report.[2]

O. H. GISH
K. L. SHERMAN

Department of Terrestrial Magnetism,
Carnegie Institution of Washington,
Washington, D. C.,
February 9, 1938.

[1] Korff, Curtiss and Astin, Phys. Rev. **53**, 14–22 (1938).
[2] O. H. Gish and K. L. Sherman, Nat. Geog. Soc., Contrib. Tech. Papers, Stratosphere Ser., No. 2, 94–116 (1936).
[3] Curtiss, Astin, Stockman, Brown and Korff, Phys. Rev. **53**, 23–29 (1938).
[4] Bowen, Millikan and Neher, Phys. Rev. **52**, 80–88 (1937).

Effect of Chemical Combination on the $K\alpha_{1,2}$ Line of Sodium

The $K\alpha_{1,2}$ doublet from the elements 12 (Mg) to 17 (Cl) belonging to the second horizontal line in the periodic system is influenced by chemical combination, apparent through the displacement of the doublet. It is to be expected that an analogous effect on the $K\alpha_{1,2}$ line of 11 (Na) must be very small indeed and earlier measurements on the $K\alpha_{1,2}$ line of sodium in compounds[1, 2] have given no conclusive evidence of any displacement of the line. How-

ever, a closer investigation has now shown the existence of such effects. This was proved by using a tube for secondary fluorescence x-rays, the distance between the target and the fluorescence-ray plate being rather (great) —about 18 mm. The tube was connected with a high vacuum spectrograph with a concave grating (principle of Johann), which consisted of a gypsum crystal bent to a radius of 500 mm. The dispersion was about 18 X.E./mm.

The results of measurements are given in Table I. The displacements of the $K\alpha_{1,2}$ line of the compounds in relation to the line of the metallic sodium are shown in the third column. The lines are all displaced towards shorter wave-lengths, as always when the emitting atom has the character of a positive ion. Because of the low atomic number of sodium which has only one valence electron outside the L shell, the $K\alpha_{1,2}$ line appears as an unresolved doublet, as a line with diffuse broadening. The wave-lengths cannot therefore be measured with very great accuracy. However, the measurements of displacement of the same compound differ at most by 0.04 volt and all the displacements, possibly except those of NaN_3, NaP_3 and Na_2C_2, must be considered as real.

TABLE I. *Displacements of $K\alpha_{1,2}$ line of compounds.*

COMPOUND	WAVE-LENGTH X.E.	DISPLACEMENT VOLTS
Na	11885.8	—
NaF	11885.0	0.07
NaCl	11884.5	0.11
NaBr	11884.7	0.10
NaI	11884.8	0.09
NaOH	11884.9	0.08
Na_2SiO_3	11884.8	0.09
Na_3PO_4	11884.6	0.10
Na_2SO_4	11884.4	0.12
$NaClO_4$	11883.9	0.17
Na_2S	11884.8	0.09
NaN_3	11885.3	0.04
NaP_3	11885.2	0.05
Na_2C_2	11885.3	0.04

From the results it is evident that the binding of sodium to oxygen does not give the same effect in the various oxygen compounds. Thus we get for the perchlorate a displacement—that is twice as great as the displacement of the hydroxide.

N. G. JOHNSON

Physical Institute,
University, Lund, Sweden,
January 21, 1938.

[1] V. Kunzl, Zeits. f. Physik **99**, 481 (1936).
[2] N. G. Johnson, Nature **138**, 1056 (1936).